

DISSERTATION

DISTINGUISHING HOMOGENEOUS AND HETEROGENEOUS WATER OXIDATION
CATALYSIS WHEN BEGINNING WITH COBALT POLYOXOMETALATES

Submitted by

Jordan J. Stracke

Department of Chemistry

In partial fulfillment of the requirements

For the Degree of Doctor of Philosophy

Colorado State University

Fort Collins, Colorado

Fall 2013

Doctoral Committee:

Advisor: Richard G. Finke

Eugene Y.-X. Chen

C. Michael Elliott

Eric M. Ferreira

James R. Sites

ABSTRACT

DISTINGUISHING HOMOGENEOUS AND HETEROGENEOUS WATER OXIDATION CATALYSIS WHEN BEGINNING WITH COBALT POLYOXOMETALATES

Development of energy storage technologies is required prior to broad implementation of renewable energy sources such as wind or solar power. One of the leading proposals is to store this energy by splitting water into hydrogen and oxygen—that is, to store energy in chemical bonds. A major obstacle en route to this overall goal is the development of efficient, cost-effective water oxidation catalysts (WOCs). Due to the highly oxidizing environment needed to drive this reaction, one question which has arisen when dealing with homogeneous precatalysts is whether these precursors remain as intact, homogeneous WOCs, or whether they are transformed into heterogeneous metal-oxide catalysts. This problem, reviewed in Chapter II, addresses the methods and literature studies related to distinguishing homogeneous and heterogeneous water oxidation catalysts.

Chapters III through V further develop the methodology for distinguishing homogeneous and heterogeneous water oxidation catalysis when beginning with the cobalt polyoxometalate $[\text{Co}_4(\text{H}_2\text{O})_2(\text{PW}_9\text{O}_{34})_2]^{10-}$ (Co_4POM). In Chapter III, the investigation of Co_4POM using electrochemical oxidation at a glassy carbon electrode reveals that under the conditions therein, an in-situ formed, heterogeneous cobalt-oxo-hydroxo (CoO_x) material is the dominant catalyst and is formed from Co^{2+} leached from the Co_4POM . In Chapter IV, investigation of whether the intact Co_4POM could be a catalyst under other, more forcing conditions of higher electrochemical potentials and lower Co_4POM concentrations is reported. Although the Co_4POM

shows different electrochemical properties relative to CoO_x controls, the possibility that the Co_4POM is being transformed into a meta-stable heterogeneous catalyst cannot be ruled out since the Co_4POM degrades during the experiment. Lastly, Chapter V presents a kinetic and mechanistic study of the Co_4POM when using a ruthenium(III)tris(2,2'-bipyridine) ($\text{Ru(III)(bpy)}_3^{3+}$) chemical oxidant to drive the water oxidation reaction (i.e., rather than electrochemically driven oxidation). In this study, it was found that Co_4POM catalyzes the oxidation of water as well as oxidation of the 2,2'-bipyridine ligand. In contrast, controls with in-situ formed CoO_x catalysts more selectively promote the catalytic oxidation of water. The difference in reactivity and kinetics between the Co_4POM and CoO_x systems indicates that the active catalysts are fundamentally different when a chemical oxidant is employed. Overall, these studies demonstrate the need for careful experimental controls and highlight the importance which reaction conditions—in particular the source and electrochemical potential of the oxidant—can play in determining the active oxidation catalyst in water oxidation reactions.

DEDICATION

This work is dedicated to my wife Katie, the fire that brings light into my life.

TABLE OF CONTENTS

ABSTRACT	ii
DEDICATION	iv
I. INTRODUCTION	1
II. POLYOXOMETALATES IN WATER OXIDATION CATALYSIS: DISTINGUISHING HOMOGENEOUS FROM HETEROGENEOUS CATALYSTS	4
Overview	4
Introduction	5
Methods for distinguishing homogeneous and heterogeneous water oxidation catalysts	8
Water oxidation catalysis studies beginning with polyoxometalates	26
Summary	62
III. ELECTROCATALYTIC WATER OXIDATION BEGINNING WITH THE COBALT POLYOXOMETALATE $[\text{Co}_4(\text{H}_2\text{O})_2(\text{PW}_9\text{O}_{34})_2]^{10-}$: IDENTIFICATION OF HETEROGENEOUS CoO_x AS THE DOMINANT CATALYST	80
Overview	80
Introduction	80
Results and Discussion	82
Supporting Information	90
IV. WATER OXIDATION CATALYSIS BEGINNING WITH $2.5 \mu\text{m}$ $[\text{Co}_4(\text{H}_2\text{O})_2(\text{PW}_9\text{O}_{34})_2]^{10-}$: INVESTIGATION OF THE TRUE ELECTROCHEMICALLY DRIVEN CATALYST AT $\geq 600 \text{ mV}$ OVERPOTENTIAL AT A GLASSY CARBON ELECTRODE	109
Overview	109
Introduction	110
Experimental Section	113
Results and Discussion	118
Conclusions	133
Supporting Information	136
V. WATER OXIDATION CATALYSIS BEGINNING WITH $[\text{Co}_4(\text{H}_2\text{O})_2(\text{PW}_9\text{O}_{34})_2]^{10-}$ WHEN DRIVEN BY THE CHEMICAL OXIDANT RUTHENIUM(III)TRIS(2,2'-BIPYRIDINE): STOICHIOMETRY, KINETIC, AND MECHANISTIC STUDIES EN ROUTE TO IDENTIFYING THE TRUE CATALYST	151
Overview	151
Introduction	152
Experimental Section	157
Results and Discussion	160
Conclusions	175
Supporting Information	178

VI. SUMMARY193

I. INTRODUCTION

The goal of this dissertation is to address the experimental methodology for distinguishing homogeneous and heterogeneous water oxidation catalysts (WOCs) when beginning with polyoxometalates (POMs). This dissertation follows a “journal’s format” where each chapter is a manuscript which has been prepared for or accepted for publication in a scientific journal and, therefore, follows the formatting guidelines for those journals. To create a cohesive dissertation from these manuscripts, the following pieces are included: (i) an introduction, (ii) connecting paragraphs at the beginning of Chapters II-V, and (iii) a summary (Chapter VI). A brief description of Chapters II-VI is given below.

Chapter II provides a comprehensive review of the literature for distinguishing homogeneous and heterogeneous water oxidation catalysts when beginning with POMs. This manuscript has been prepared and formatted for submission to the *Journal of Molecular Catalysis A: Chemistry* (Elsevier). This review consists of: (i) an overview of the methodology needed to identify the true WOC when starting with POMs, (ii) a comprehensive description of POM WOC precatalysts and the specific experiments used therein to distinguish homogeneous and heterogeneous catalysis, and (iii) a comparison of the POM literature to non-POM, homogeneous WOC precatalysts. Of particular relevance to this dissertation is the discussion of the seven reports which investigate $[\text{Co}_4(\text{H}_2\text{O})_2(\text{PW}_9\text{O}_{34})_2]^{10-}$ as a WOC precatalyst.

Chapter III examines the cobalt polyoxometalate, $[\text{Co}_4(\text{H}_2\text{O})_2(\text{PW}_9\text{O}_{34})_2]^{10-}$, as a water oxidation catalyst precursor when using electrochemical oxidation to drive the reaction. This chapter was published in the *Journal of the American Chemical Society* (Stracke, J.J., Finke, R.G., *J. Am. Chem. Soc.* **2011**, *133*, 14872). In this study, decomposition of the

$[\text{Co}_4(\text{H}_2\text{O})_2(\text{PW}_9\text{O}_{34})_2]^{10-}$ precursor occurs concomitantly with formation of a more active WOC. Multiple physical methods and controls indicate the dominant WOC is a heterogeneous cobalt-oxo-hydroxo (CoO_x) film which forms on the glassy carbon working electrode during the electrolysis reaction.

Chapter IV, a report published in *ACS Catalysis* (Stracke, J. J.; Finke, R. G. *ACS Catal.* **2013**, 3, 1209), then addresses whether $[\text{Co}_4(\text{H}_2\text{O})_2(\text{PW}_9\text{O}_{34})_2]^{10-}$ could be a WOC under different conditions. Therefore, the cobalt POM was tested at lower concentrations and larger electrochemical driving forces, conditions chosen to ostensibly favor the intact $[\text{Co}_4(\text{H}_2\text{O})_2(\text{PW}_9\text{O}_{34})_2]^{10-}$ as a WOC. Multiple control and stability measurements do not yet allow distinguishing homogeneous and heterogeneous catalysis in that case and under those conditions. However, these experiments do provide evidence against an aqueous Co(II) to heterogeneous CoO_x WOC mechanism (i.e., the WOC formation mechanism found under the conditions described in Chapter III). That is, reaction conditions matter for production of, and when determining, the true WOC.

Chapter V investigates the stoichiometry, kinetics, and mechanism of water oxidation when using $[\text{Co}_4(\text{H}_2\text{O})_2(\text{PW}_9\text{O}_{34})_2]^{10-}$ in combination with a ruthenium(III)tris(2,2'-bipyridine) ($\text{Ru}(\text{bpy})_3^{3+}$) chemical oxidant. This manuscript has been submitted to *ACS Catalysis* (and has been tentatively accepted pending the usual revisions for the referees comments). In this study, both water oxidation and bpy ligand oxidation reactions occur in parallel. Therefore, the O_2 evolution and $\text{Ru}(\text{bpy})_3^{3+}$ reduction rates were measured independently which allowed the generation of an empirical rate law. Comparison of the O_2 evolution and bpy ligand oxidation kinetics, when starting with either $[\text{Co}_4(\text{H}_2\text{O})_2(\text{PW}_9\text{O}_{34})_2]^{10-}$ or CoO_x controls, provide evidence that the dominant WOC is different in these two systems.

Chapter VI gives a summary of the work in this dissertation. An overview of these studies provides insights into the factors controlling WOC identity and the methods needed to distinguish a true POM WOC from the alternative heterogeneous, CoO_x catalyst.

II. POLYOXOMETALATES IN WATER OXIDATION CATALYSIS: DISTINGUISHING HOMOGENEOUS FROM HETEROGENEOUS CATALYSTSⁱ

Overview

Polyoxometalates (POMs) have been proposed to be excellent homogeneous water oxidation catalysts (WOCs) due to their oxidative stability and activity. However, recent literature indicates that even these relatively robust compounds can be transformed into heterogeneous, metal-oxide WOCs under the oxidizing reaction conditions needed to drive O₂ evolution. This review covers the experimental methodology for distinguishing homogeneous and heterogeneous WOCs ; it then addresses the “who is the true catalyst?” problem for POMs used as precatalysts in the oxidation of water to O₂. These results are also compared to the broader WOC literature. The primary findings in this review are: (1) Multiple, complimentary experiments are needed to determine the true catalyst including determination of catalyst stability, speciation, and kinetics under operating conditions; (2) Controls with hypothetical heterogeneous metal-oxide catalysts are required to determine their kinetic competence in the reaction and support the conclusion of either a homogeneous or heterogeneous catalyst; (3) Although many studies observe qualitative stability of the starting POM under the reaction conditions, there is a serious lack of quantitative stability studies; if one doesn’t know where the (pre)catalyst mass lies, then it is very difficult to rule out the possibility of an alternative species

ⁱ This dissertation chapter has been prepared for submission to the *Journal of Molecular Catalysis A: Chemistry*, and provides a review of the literature using polyoxometalates as water oxidation catalyst (WOC) precursors. Included in this review is a discussion of the methods needed to distinguish homogeneous and heterogeneous WOCs and a description of how these methods have been applied to the POM WOC literature. Particularly relevant to the remainder of this dissertation is the extensive discussion of cobalt WOC precursors including the cobalt POM [Co(H₂O)₂(PW₉O₃₄)₂]¹⁰⁻. Overall, this review promotes a disproof-based method for distinguishing homogeneous vs heterogeneous catalysts, one which relies on stability, characterization, kinetic, and control measurements.

as the true catalyst; (4) The stability of POMs is dependent on the metal center and reaction conditions; and, (5) As a result of the variable stability of POMs under different reaction conditions, those conditions can influence the dominant catalyst identity. Overall, knowledge of which POMs (or other starting materials) tend to transform into heterogeneous WOCs, and how they do so, is therefore critical to developing the next generation of higher stability, higher activity POM and other water oxidation catalysts.

Introduction

Catalysis is as important a discipline as any in the chemical sciences. It is directly involved in the production of numerous chemicals and materials. Recent estimates indicate catalysis is involved in 80% of chemical industrial processes.¹

Due to the economic and fundamental scientific impact of catalysis, knowledge of the true catalyst is of utmost importance in catalysis science. Restated, since all catalytic properties are derived directly from the identity of the active catalyst—including activity, selectivity, lifetime, poisoning, isolability, and catalyst regeneration—one must first identify the active catalyst in order to optimize and improve it. A sub-topic of the catalyst identification problem is distinguishing homogeneous from heterogeneous catalysts. This topic has been reviewed both generally^{2,3} and in a variety of specific areas, including cross coupling,⁴ hydrogenation,⁵ water splitting,⁶ and water oxidation⁷ reactions.

Recently, the problem of identifying the true catalyst has come to a head in the water oxidation literature, where a number of systems which begin with discrete precursors are transformed into heterogeneous metal oxide catalysts under the highly oxidizing environments needed for catalytic water oxidation. Current interest in water oxidation derives from the potential importance this reaction promises to play in sustainable energy storage schemes such as

water splitting^{8,9,10,11,12,13,14,15,16,17,18,19} and the reduction of CO₂ to fuels^{20,21,22,23,24,25} such as methanol. The water oxidation half-reaction is often cited as a bottle-neck in these fuel forming cycles due to the complexity of this net four electron, four proton transfer reaction along with the requirements of high activity, long lifetime, and affordability of the catalyst. Numerous reports of water oxidation and solar water splitting devices have begun addressing these challenges and have been reviewed extensively.^{26,27,28,29,30,31,32,33,34,35,36,37}

However, and despite the explosion of research in the area of water oxidation by discrete precursors, only recently has the problem of distinguishing homogeneous and heterogeneous catalysis become a priority. Recent reviews have addressed this problem in a broad manner for water oxidation catalysis.^{6,7} The first of these provides a general discussion of determining water oxidation catalysts by focusing on a handful of case studies.⁷ The second review⁶ discusses water splitting with discussion of WOCs as well as on H⁺ reduction catalysts—an area which had been reviewed previously³ although not in the specific area of H₂ evolution. The main conclusions of the prior reviews in the area of distinguishing homogeneous and heterogeneous WOCs are: (i) conditions are important in determining the true catalyst; (ii) organic ligands decompose under the highly oxidizing conditions; and, (iii) multiple techniques are needed to characterize the catalysts. Overall, these reviews cover some of the methods and literature relevant to determining the true WOC.^{6,7}

One primary, current hypothesis for overcoming the instability of organic ligands under oxidizing conditions is to use non-oxidizable complexes such as polyoxometalates (POMs).^{38,39,40,41} This class of compounds, which were first synthesized in 1826,⁴² possesses many properties desirable in oxidation catalysis,^{43,44,45,46,47,48,49} namely oxidative stability and the ability to adopt a wide variety of structures while incorporating single or multi-metallic catalytic

centers. The synthetic and structural aspects of this broad class of compounds has been extensively reviewed by others and will, therefore, not be addressed directly herein.^{50,51,52,53,54} Additionally, these compounds can sometimes act as discrete metal-oxide mimics,^{55,56} and are therefore relevant to the study of both homogeneous and heterogeneous WOCs.

The scope of the current review is to comprehensively address the question of distinguishing homogeneous and heterogeneous water oxidation catalysis when beginning with discrete polyoxometalate precursors. This review will address the methodology and characterization methods needed to fully answer this question, describe how this methodology has been applied to the polyoxometalate WOC literature, and discuss how these results fit into the broader field of homogeneous WOCs. Note, the terms “homogeneous” and “heterogeneous” are used throughout to indicate the type of active site and *not the phase* of the catalyst, as first proposed by Schwartz,⁵⁷ that is, a homogeneous catalyst contains a single type of active site whereas a heterogeneous catalyst has multiple types of active sites. An alternative nomenclature of “homotopic” and “heterotopic” has been proposed by Crabtree to indicate the type of active site.² Hence, for the purposes of this review “homogeneous” means “homotopic” and “heterogeneous” means “heterotopic”. Although the present review focuses on polyoxometalate WOC precursors, the general methodology for distinguishing homogeneous and heterogeneous catalysis, which has been developed in our lab for over 20 years,^{3,5} is applicable to all WOCs as well as other catalytic transformations. That is, the methods and discussions which follow, for determining the true catalysts, are broadly applicable.

Methods for distinguishing homogeneous and heterogeneous water oxidation catalysts

The methodology to distinguish homogeneous and heterogeneous catalysts developed previously^{3,5} is given in Figure 2.1. Rigorous identification of the true catalyst via this method

consists of five basic steps: (1) Generation of all possible hypotheses for the true catalyst; (2) Determination of the stability of the precursor ideally *in operando* (i.e., under the operating conditions); (3) Isolation and characterization of all detectable forms of the (pre)catalyst where possible; (4) Measurement of the kinetics of the reaction including controls with alternative precatalysts; and, (5) Conducting additional phenomenological tests, controls, and so on as required. Lastly, one must use the data in steps 2-5 to rule out all alternative forms of the catalyst en route to a final conclusion of either homogeneous or heterogeneous catalysis. Ultimately, this method is as simple or as difficult as *(i) determining where the mass of the precursor lies under the reaction conditions, and then (ii) quantifying the contribution of those possible catalyst forms to the observed activity.*

Generation of Hypotheses for the True Catalyst.

The central intellectual tool for identification of the active WOC is the disproof of multiple alternative hypotheses. This method, described by Platt⁵⁸ and which dates back to Chamberlain's classic 1890 paper,⁵⁹ emphasizes the need to consider any and all reasonable explanations for experimental data. In the present case of WOCs starting from POMs, the three primary competing hypotheses are: (1) that the catalyst is the starting discrete polyoxometalate precursor; (2) that the POM precursor transforms into a heterogeneous catalyst such as the corresponding metal oxide; or (3) that an unknown, possibly insidious, material is the catalyst (e.g., insidious Co^{2+} as a counter-cation in a cobalt POM, where cobalt(II) should only be within the POM structure). It is also possible that the true catalyst is some combination of these three hypotheses—or another, not yet conceived hypothesis for the true catalyst.

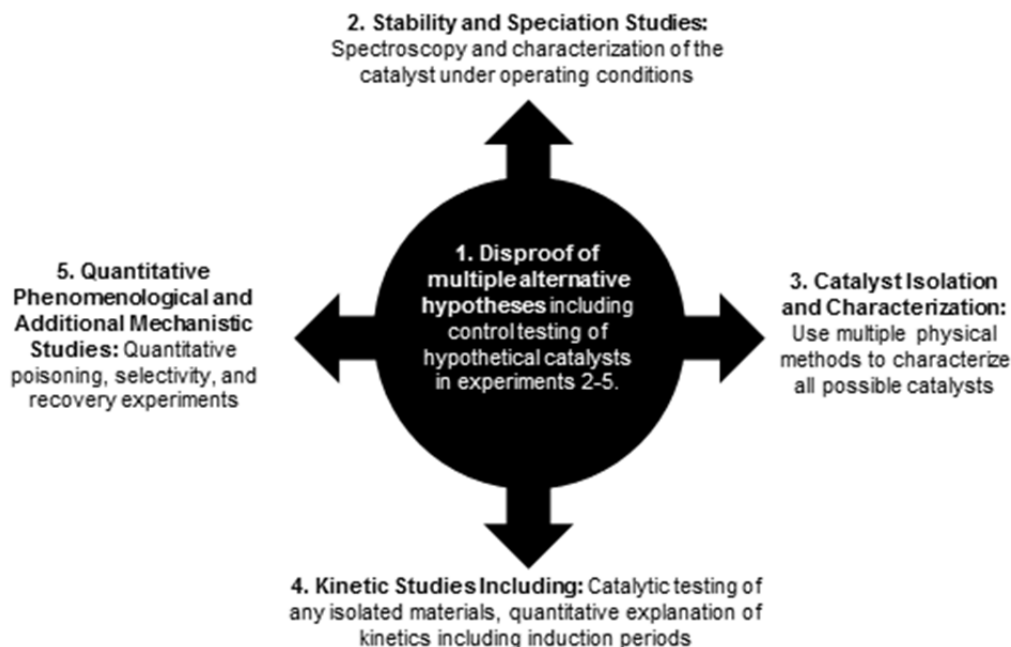


Figure 2.1. A general methodology for distinguishing homogeneous from heterogeneous catalysts, including water oxidation catalysts. This is an updated version of the method which has been developed by our group^{3,5} for identifying the true catalyst in other reactions.

Proper application of Platt's method requires careful experimental design of control experiments. These control experiments are crucial to ruling out alternative hypotheses and/or determining the limits of particular methods employed. In particular, control experiments are needed when investigating the reaction kinetics since different catalysts will, by definition, have different mechanisms. A caveat here is that one must know what the alternative catalytic material might be in order to run the correct control experiment.³ Overall, rigorously distinguishing homogeneous and heterogeneous WOCs must rely on a method which directly attempts to disprove any alternative forms of the catalytic species in each step of the process. The following sections address these steps and the specific methods which can be applied to these catalyst identification problems with POM starting materials. Unfortunately, we will see that too often in the literature, a disproof-based method is not employed.

In Operando and In Situ Stability and Speciation Studies

A first step in identifying the true WOC is determining the stability and speciation of the precursor under the reaction conditions. Although characterization of the fate of the (pre)catalyst may seem obvious, it is frequently a challenging task due to the low precatalyst concentrations (frequently in the low micromolar range for POMs) and the even lower possible concentrations of hypothetical alternative catalysts derived from the precatalyst. Polyoxometalates have the additional complication of ion-pairing with cations and/or limited solubility under many reaction conditions; because these complexes have large anionic charges, they interact strongly with cations derived from their precursor salts, the electrolyte/buffer, and especially polycations which sometimes include the oxidant (e.g., $\text{Ru}(\text{bpy})_3^{3+}$). To combat these difficulties, a variety of techniques are often needed to discover the speciation of POMs under the reaction conditions. It should be noted here that although *in operando* characterization is best,^{60,61} *in operando* spectroscopic methods have not yet been applied to any POM under standard reaction conditions. Instead, characterization typically takes place under conditions which are in-situ but take place either before or after the reaction. Hence, the use of *in operando* spectroscopies with POM and other WOCs is an important area for future studies.

UV-vis spectroscopy

UV-vis spectroscopy can be a useful initial method for determining the stability of polyoxometalates. Contant has used UV-visible spectroscopy to measure the association constants for numerous metal-substituted, lacunary POMs.^{62,63} Only one example exists in the literature where UV-vis spectroscopy has been used to characterize a POM derived catalyst under the presence of excess oxidant.⁶⁴ Others, ourselves included, have used the visible absorption bands to measure the solution stability of POMs in-situ (but, again, not *in*

operando).^{65,66,67,68,69,70,71,72,73,74,75,76,77,78} For these experiments, the identity of the incorporated metal largely determines the utility of this method. For example, most cobalt-POMs have relatively weak d-d transitions in the visible region, thereby making this method useful only at high (usually millimolar) POM concentrations, as done by Galan-Mascaros in electrochemical studies where the loss in $\{\text{Co}_9(\text{H}_2\text{O})_6(\text{OH})_3(\text{HPO}_4)_2(\text{PW}_9\text{O}_{34})_3\}^{16-}$ was determined after bulk electrolysis.⁷⁹ In comparison, absorption coefficients of ruthenium POMs are larger,^{72,73,74,75,76} allowing them to be measured accurately using conditions more relevant to catalysis.

POMs also have strong absorption bands in the UV region. These bands are broad and occur in all POMs and, therefore, are not a definitive characterization method. However, the large absorption coefficients for these bands have been useful in quantifying POMs which have been separated by HPLC (*vide infra*),⁸⁰ as was done to determine the oxidative stability of $[\text{Co}_4(\text{H}_2\text{O})_2(\text{PW}_9\text{O}_{34})_2]^{10-}$ at $\sim 1.25\text{-}5.0\ \mu\text{M}$ concentrations.⁸¹

Electrochemistry

Polyoxometalates have a rich electrochemistry associated with both reduction of tungsten or molybdenum and oxidation of heteroatoms (i.e., the incorporated cobalt, ruthenium, iridium, or nickel atoms, metals of special interest for WOCs^{13,16,17}). These characteristic peaks can be used to identify POMs, especially when used in conjunction with other physical methods. Electrochemical methods can also be used to characterize possible intermediates in the water oxidation reaction, as is common for ruthenium-based POMs.^{82,83,84} In addition to direct measurements of the POMs, electrochemical methods have also been used to quantify decomposition products, including aqueous Co^{2+} , and CoO_x or MnO_x films which form under oxidizing conditions.^{66,81,85,86,87,88,89} This ability to electrodeposit metal-oxide films, if present, is

advantageous since it allows one to easily isolate and then characterize these films, which are often very active WOCs.^{19,66,79,81}

Conversely, the electrode can make it difficult to identify homogeneous catalysts since electrodeposition of heterogeneous metal oxides will concentrate/enhance the effect of the film over relatively dilute solution species, thereby obscuring any homogeneous activity. Note however, this concentrating effect can be observed for any adsorbed material, including adsorbed polyoxometalates.^{90,91,92} This phenomenon has been followed by electrochemical quartz crystal microbalance studies for water oxidation studies with $[(\text{Mn(III)}(\text{H}_2\text{O}))_3(\text{SbW}_9\text{O}_{33})_2]^{9-}$.⁸⁷ In our own studies, we also have electrochemical evidence that $[\text{Co}_4(\text{H}_2\text{O})_2(\text{PW}_9\text{O}_{34})_2]^{10-}$ may be adsorbing to glassy carbon electrodes in both pH 5.8 and 8.0 sodium phosphate solutions.⁸¹ One caveat in electrochemical studies is that sometimes the redox activity of transition-metal substituted POMs is absent, depending on the specific POM, the electrode material, or the pH, thereby making electrochemical methods useful in only some cases.

One electrochemical method which has found wide use in studies of WOCs is the measurement of a current-overpotentialⁱⁱ relationship. In this method, the log of the current is plotted versus the log of the overpotential which results in a straight line for well-behaved systems; this is also known as a Tafel plot.⁹³ The slope of the fitted line is ultimately related to the catalytic mechanism. For example, a slope of 60 mV/decade (i.e., the current changes by an order of magnitude when the overpotential is increased by 60 mV) is consistent with a reversible one-electron transfer followed by a chemically turnover-limiting step whereas a 120 mV/decade slope could be consistent with a turnover-limiting electron transfer step. Others have used these

ⁱⁱ The overpotential, or electrochemical driving force, is defined as the difference between the electrode potential and the reversible potential for the reaction of interest. For the water oxidation reaction, the overpotential can be calculated using the equation: $\eta = E - (1.23 - 0.059 \cdot \text{pH}) \text{ V}$, where E is the potential of the electrode versus NHE and $(1.23 - 0.059 \cdot \text{pH}) \text{ V}$ is the reversible potential for water oxidation.

plots as a qualitative method to differentiate between catalysts. Additional discussion of current-overpotential relationships can be found elsewhere.⁹³

In short, electrochemical methods allow one to both measure catalyst activity as a function of driving force and characterize redox active reaction intermediates and their stability en route to identifying the true WOC.

NMR/EPR

Since POMs typically have no organic ligands (unless intentionally functionalized), NMR characterization typically relies on ³¹P, ¹⁸³W, ⁵¹V, ⁹⁵Mo, and ¹⁷O nuclei, the last of which must be intentionally incorporated in most applications.^{94,95,96} A primary benefit of NMR, is that it can directly follow the stability and speciation of POMs since the number and chemical shift of peaks are often definitive fingerprints for POMs. For example Contant and Zhu et al. have used NMR (among other methods) to study the pH dependent speciation of phosphotungstates.^{97,98} Despite the utility of NMR spectroscopy, it has been used relatively infrequently for POM WOC studies since many of the species are paramagnetic, thereby broadening and shifting peaks while requiring higher catalyst concentrations for detection.⁹⁹ However, Hill and co-workers have successfully used ³¹P-NMR to qualitatively demonstrate the presence of a $[\text{Co}_4(\text{H}_2\text{O})_2(\text{PW}_9\text{O}_{34})_2]^{10-}$ species at the end of water oxidation reaction using a $\text{Ru}(\text{bpy})_3^{3+}$ oxidant.⁶⁵ In other, non-catalytic studies, Ohlin et al. have used ¹⁷O-NMR to measure the rate of water ligand exchange on $[\text{Co}_4(\text{H}_2\text{O})_2(\text{PW}_9\text{O}_{34})_2]^{10-}$ and found a fast $1.5 \times 10^6 \text{ s}^{-1}$ water exchange rate constant—a necessary requirement for highly active WOCs.¹⁰⁰ Overall, NMR is potentially useful in quantitating POM stability under reaction conditions, but has found limited application due to low magnetic receptivity of ¹⁸³W and ⁹⁵Mo, solubility and concentration issues (vide infra), and the presence of paramagnetic metal centers.

The presence of paramagnetic redox centers open up the possibility of EPR spectroscopic characterization. Ruthenium POMs have been characterized by EPR including, $[\text{Ru}_4(\mu\text{-O})_4(\mu\text{-OH})_2(\text{H}_2\text{O})_4(\gamma\text{-SiW}_{10}\text{O}_{36})_2]^{10-}$ and $[\text{Ru}(\text{H}_2\text{O})\text{SiW}_{11}\text{O}_{39}]^{5-}$ and their higher oxidation state analogs.^{64,76} EPR has also been used to determine the solution stability of $[\text{Co}_4(\text{H}_2\text{O})_2(\text{PW}_9\text{O}_{34})_2]^{10-}$ and $[\text{Co}_4(\text{H}_2\text{O})_2(\text{P}_2\text{W}_{15}\text{O}_{56})_2]^{16-}$, where aqueous, leached Co^{2+} is also EPR active.¹⁰⁰ Although this method can illuminate possible paramagnetic solution species, kinetic studies are needed to connect the observed species to water oxidation activity.

IR, Raman, and Resonance Raman

Due to the large number of vibrational bands, IR spectra are often used as diagnostic fingerprints. In general, IR characterization is used to either identify a particular compound, or to verify the presence of the hypothesized catalyst after it has been isolated from the post-reaction solution.^{65,69,72,78,79,101} However, since water interferes with collection of IR, this method is generally not applicable to *in-situ* or *in operando* characterization of water oxidation catalysts.

Raman and resonance Raman (rRaman) have proven to be more useful than IR when characterizing POMs under water oxidation reaction conditions.¹⁰² Resonance Raman is especially useful since it allows the catalyst/pre-catalyst to be selectively excited thereby enhancing the signal to noise ratio and allowing lower concentrations of catalyst to be investigated. This method has been used to investigate the reaction intermediates in ruthenium WOCs where the conversion of Ru-OH₂ into Ru=O bonds occurs upon oxidation.^{64,76} Regions of particular relevance to water oxidation catalysis are the M-OH, and M-OH₂ which appear from 330 to 550 cm⁻¹ for $[\text{Ru}_4(\mu\text{-O})_4(\mu\text{-OH})_2(\text{H}_2\text{O})_4(\gamma\text{-SiW}_{10}\text{O}_{36})_2]^{10-}$ (and its oxidized products) and the M=O at ~800 cm⁻¹ for $[\text{Ru}(\text{O})\text{SiW}_{11}\text{O}_{39}]^{5-}$.^{64,76} The strength of Raman spectroscopy

ultimately derives from its potential ability to characterize WOCs *in operando*, and is a potentially powerful, underutilized method at present.

XAFS/XANES

Extended x-ray absorption fine structure (EXAFS) and x-ray absorption near edge structure (XANES) are valuable techniques to probe both the local coordination environment and the oxidation state of either solution or solid-state materials. Despite the potentially powerful nature of these experiments, characterization of $[\text{Ru}_4(\mu\text{-O})_4(\mu\text{-OH})_2(\text{H}_2\text{O})_4(\gamma\text{-SiW}_{10}\text{O}_{36})_2]^{10-}$ reaction intermediates is presently the only example of EXAFS/XANES in the POM WOC literature.¹⁰³ Unfortunately, in the case of $[\text{Ru}_4(\mu\text{-O})_4(\mu\text{-OH})_2(\text{H}_2\text{O})_4(\gamma\text{-SiW}_{10}\text{O}_{36})_2]^{10-}$, the ruthenium EXAFS/XANES is nearly identical to a heterogeneous RuO_2 material, thereby obfuscating the ability to distinguish a homogeneous vs heterogeneous catalyst during catalytic water oxidation (which was not pursued in this example,¹⁰³ since prior evidence is consistent with a homogeneous POM catalyst⁷²). In addition, the optimum use of these X-ray absorption methods requires accurate models which may or may not be available for hypothetical heterogeneous MO_x WOCs. Pure materials or knowledge of the catalyst speciation is also needed since EXAFS is a bulk technique which measures the average absorption. Therefore, EXAFS/XANES provide strong evidence for the active catalyst under the reaction conditions, but only if the speciation and kinetics have been measured by other techniques.

Dynamic Light Scattering and Small Angle X-Ray Scattering

This last set of characterization techniques, namely dynamic light scattering (DLS) and small angle x-ray scattering (SAXS), are aimed at determining whether particles are formed in solutions and, if present, their size. Of these methods, DLS has found the broadest usage due to the wide availability and the ability to measure particles *in-situ*.^{68,74,78,104,105} Throughout the POM

WOC literature the putative absence of particles in a post-reaction solution has been used as evidence to rule out heterogeneous WOCs. *However*, this conclusion follows only if the underlying assumption, that all heterogeneous materials can be detected, is true—a potentially difficult analytical problem since the sensitivity of DLS decreases with the particle radius and concentration.^{106,107} That is, the lack of observed particles only guarantees that there are no particles above the detection limit of the method, not that lower concentrations of potentially very catalytically active particles are not there. Conversely, the presence of particles does not guarantee a heterogeneous metal-oxide material is the catalyst since POMs can also precipitate under the reaction conditions, especially when cationic oxidants such as Ru(bpy)₃³⁺ are used.^{65,69,70} In summary of DLS and SAXS methodology in the WOC area, these methods can provide evidence for particles, in which case additional experiments are needed to characterize these materials and demonstrate the catalytic competence (or not) of the particles. Additionally, when no particles are observed, controls are critical to determining the detection limit of these methods in order to rule out (or support) the possibility of highly active, heterogeneous WOCs.

Catalyst Isolation and Ex-Situ Characterization, Where Possible

Once the speciation of the POM starting material is known, a third, useful step in distinguishing homogeneous and heterogeneous catalysis is isolation and *ex-situ* characterization of any detected forms of the catalyst. This step is closely tied to the second since it involves determining where the catalyst mass lies and its precise composition. However, caution must be taken when interpreting *ex-situ* characterization results since isolation processes can alter the material. In addition, *ex-situ* methods also tend to be more qualitative and overall less definitive than *in operando* methods. IR and NMR are often utilized on the resultant isolated materials, but these methods have been addressed above and, therefore, will not be discussed further here.

Since isolation of POM and/or heterogeneous MO_x materials is required prior to any *ex-situ* characterization, isolation methods that have proven useful are provided first.

Extraction

Due to the large anionic charge of most POMs, they interact strongly with a variety of organic solvent soluble cations such as tetra-alkyl ammoniums. Strong cation^{m+}-POMⁿ⁻ interactions allow one to extract POMs from aqueous solutions into organic solvents which contain alkyl-ammonium cations.¹⁰⁸ In addition to isolation of the POM, an extraction can leave behind cationic decomposition products. Hill and co-workers elegantly leveraged this technique to determine the hydrolytic stability of $[\text{Co}_4(\text{H}_2\text{O})_2(\text{PW}_9\text{O}_{34})_2]^{10-}$; the POM was extracted from aqueous solution using toluene/tetra-*n*-heptylammonium nitrate and then the remaining aqueous Co^{2+} was quantified by ICP-MS.⁶⁷ One complicating factor of extraction is that although the POM has been separated from the aqueous solution, additional isolation methods, such as recrystallization, are needed to recover the POM which is dissolved in the organic solvent.

Precipitation/Filtration/Centrifugation

Perhaps the easiest way to isolate POMs from solution is via precipitation upon addition of an excess of cations.^{65,68,69,72,79} For this purpose, large cations such as Cs^+ or $\text{Ru}(\text{bpy})_3^{2+}$ are most effective due to size matching effects resulting in good solid-lattice energies. Indeed, when chemical/photochemical oxidants are used to drive the water oxidation reaction, POMs often precipitate prior to or during the reaction (a factor which also complicates the observed kinetics as discussed in that section). Once the POM has been precipitated, it can easily be collected by filtration or centrifugation. The filtrate or supernatant can also be tested for residual catalytic activity to help determine the phase of the catalyst.

HPLC

Separation of multiple POM or other species is difficult to achieve if the species possess similar solubility, charge, and/or size characteristics. One of the few methods capable of this separation is reverse-phase, ion-pair HPLC where the combination of (alkyl-cation)-POM plus (alkyl-stationary-phase)-(alkyl-cation) interactions allow POMs to be separated based primarily on their charge.⁸⁰ Application of this HPLC method has allowed the stability of $[\text{Co}_4(\text{H}_2\text{O})_2(\text{PW}_9\text{O}_{34})_2]^{10-}$ to be quantified using post-electrocatalytic reaction solutions.⁸¹ Controls using pre-established UV-vis extinction coefficients are also useful to verify whether or not the POM of interest is soluble in the eluting solvents and is stable on the column.^{80,81} Two limitations of this method are that MO_x materials have not yet been successfully separated by HPLC, and precipitated POM materials will not be observable. Overall, in favorable cases HPLC can put a lower limit on the POM stability, but is an indirect method where controls plus caution are needed in interpreting the results, especially since conditions on the HPLC column are typically far different than the catalytic conditions. HPLC is, however and in our experience, not able to identify where any missing (pre)catalyst mass lies.

Electrodeposition/Electrode Rinsing

When a positively biased electrode is the oxidant source, the electrode material can easily be removed from the polyoxometalate solution and rinsed with water to remove residual electrolyte or soluble catalyst.^{66,79,81} The resultant electrode can then be subjected to a battery of tests to characterize its surface; it can also be placed in POM-free solution and tested for residual catalytic activity. This simple experiment can be very telling if a heterogeneous metal-oxide catalyst is present on the electrode surface and especially if that solid oxide is the dominant WOC. However, caution should be exercised when interpreting these rinsing experiments since

some MO_x catalysts are not stable under the highly oxidizing conditions needed for water oxidation— CoO_x instability at 1.4 V vs Ag/AgCl in pH 8 sodium phosphate is a case in point.⁸¹ A variety of POMs, including Co or Mo containing POMs, are known to adsorb strongly to glassy carbon and mercury electrodes.^{81,87,90,91,92} Hence, a significant caveat here is that the absence of a metal-oxide film cannot rule out heterogeneous catalysis and residual activity after rinsing cannot definitively rule out homogeneous POM catalysis.

Post-electrolysis surface characterization (SEM, EDX, WDS, XPS)

To visualize and characterize an electrode used for electrochemically driven water oxidation, scanning electron microscopy (SEM) with energy dispersive x-ray spectroscopy (EDX) (or wavelength dispersive x-ray spectroscopy, WDS) analysis is a useful first step.^{66,79,81,109} This technique requires that a catalytically active material remains on the electrode surface. When a deposited catalyst is present, EDX or WDS can provide qualitative identification of, and ratios for, the elemental components of the material. This information can then be used to provide evidence for or against the starting POM being deposited on the electrode, within the detection limit of the method.¹¹⁰ However, care should be taken in interpreting these results since the incident electron beam, which ultimately results in the element specific x-ray emission, penetrates to depths of microns and therefore is relatively surface insensitive.¹¹⁰ For nanometer thick films or monolayer coverage of electrodes, surface-sensitive techniques are more appropriate.

X-ray photoelectron spectroscopy (XPS) is one technique which is more surface sensitive than EDX, but which provides similar information on the elemental makeup of a post-electrolysis electrode.⁸¹ Since this technique relies on the detection of relatively low-energy (<1 keV) emitted electrons, only the surface 1-20 nm allow a significant portion of these

electrons to escape.¹¹¹ XPS has the benefit of providing additional characterization data since the measured binding energy (i.e., the energy of the ejected electrons) depends on the oxidation state and chemical environment of each element. Controls examining known materials are therefore powerful in distinguishing between different materials/compounds, even when the same elements are present (e.g., distinguishing between Co_3O_4 and CoO). Overall, ex-situ characterization of post-reaction electrodes can lead to critical information when a catalytic material remains deposited or adsorbed. That said, the lack of a detectable catalytic material provides little insight into the true WOC.

TEM

Technological advancement and broadening availability of transmission electron microscopy (TEM) has led to the widespread use of this primarily ex-situ method in visualizing nanometer and sub-nanometer particles which can form during water oxidation reactions.¹¹² Unlike SEM, which is primarily for analysis of electrochemically driven reactions, TEM can be used to analyze the post-reaction solution components regardless of the oxidant source. As noted in our 2003 review on distinguishing homogeneous from heterogeneous catalysts,³ several limitations of TEM should be considered when using *ex-situ* microscopy evidence in support of a homogeneous vs a heterogeneous catalyst hypothesis. First, TEM does not provide direct evidence for catalysts, but rather indicates the presence or absence of materials which *might* be catalysts; stoichiometry (i.e., how much of the starting material is converted into possible catalytic materials under, ideally, *in operando* conditions) and *kinetics* are needed to provide supporting evidence for the true catalyst. Second, beam damage can occur when using electron microscopy where nanoparticles are formed within the electron beam.¹¹³ Controls are therefore needed to verify the stability of starting materials under irradiation.¹¹³ Third, most water

oxidation systems (and POMs in particular) have the added difficulty of a low concentration of pre-catalyst in the presence of a very large excess of non-volatile buffer (e.g., a pre-catalyst:buffer ratio of up to 1:10⁴).⁶⁷ That is, finding and detecting the presence of nanoparticle catalysts (if they are present) can become exceedingly difficult under such dilute conditions. Therefore, if TEM is invoked as evidence against a heterogeneous catalyst, one should also demonstrate that *control experiments can easily detect the amount of heterogeneous material needed to account for the observed catalytic activity*. Due to the limitations expounded above, TEM has been used much less frequently in identifying heterogeneous WOCs than in metal(0) nanoparticle literature where reducing conditions are typically used.³

MS and ICP/MS

Mass spectrometry (MS) is another characterization method which lends itself to both speciation and *ex-situ* characterization studies; MS is classified as a latter, *ex-situ* method for the purposes of this review. To our knowledge, MS has not yet been used to characterize POMs under catalysis conditions, even though MS can provide very strong evidence for the presence of specific species due to the high molecular weights and characteristic isotopic peak ratios, as reviewed by Cronin and co-workers.¹¹⁴ Of course, MS has the disadvantage that only species which are soluble and small enough to desorb/“fly” will be observed. Hence, only with extensive controls on authentic, possible heterogeneous and other catalysts can MS accurately report on the presence, or absence, of such materials.

POMs also lend themselves to tandem isolation-ICP/MS (inductively couple plasma-MS) methods which can be used to infer the solution speciation. For example, Hill and co-workers have used POM-extraction plus ICP/MS of the resultant aqueous solution to quantify the dissociation of Co²⁺ from a [Co₄(H₂O)₂(PW₉O₃₄)₂]¹⁰⁻ starting material.⁶⁷ Others have used

HPLC/ICP/MS (in conjunction with ^{31}P -NMR) to determine the speciation of phosphotungstates as a function of pH (although these POMs were not studied for their catalytic activity).⁹⁸ Hence, MS and ICP/MS can provide speciation and characterization data which is complementary to in-situ spectroscopies such as NMR, Raman, X-ray absorption, and UV-vis. Although isolation and *ex-situ* characterization is, again, less desirable than *in operando* characterization due to the possibility of sample alteration during the experiment, all of the *ex-situ* methods described in the above section can provide visual and elemental analysis evidence necessary for correct identification of catalytic species.

Kinetics

Distinguishing homogeneous and heterogeneous WOCs *requires* kinetic studies since, in the words of Jack Halpern, “catalysis is, by definition, purely a kinetic phenomenon”.¹¹⁵ Every catalyst has a characteristic mechanism which determines the observed kinetics. Therefore, understanding the kinetic dependence of the reaction variables is absolutely required for unequivocal identification of the true catalyst.

Dioxygen (O_2) evolution kinetics are one of the most relevant metrics, since the desired product of 4e^- water oxidation is O_2 (and 4H^+). Oxygen evolution can be measured using several different methods, including electrochemically (e.g. a Clark-type electrode), fluorescence quenching probes, gas chromatography, or a pressure transducer, the latter along with independent verification that O_2 is the gaseous product being measured.^{72,74,76,81,116,117,118} Alternatively, one can measure oxidant consumption¹¹⁹ or oxidation current as a *proxy* for O_2 evolution, if the overall efficiency for the reaction is near 100 %. In other words, one must verify that the oxidant is being quantitatively used for the O_2 evolution reaction in order to be able to correlate the rate of oxidant loss directly to the rate of O_2 evolution (the latter divided by the

stoichiometric factor of 4, i.e., $-d[1e^- \text{ oxidant }]/dt = \frac{1}{4} d[O_2]/dt$). This point is especially relevant since stoichiometric conversion of the oxidant into O_2 is rarely observed since side-reactions are possible, such as 2,2'-bipyridine ligand oxidation when $Ru(bpy)_3^{3+}$ is used as the oxidant.^{120,121} When a chemical oxidant is used the efficiency is usually referred to as the “ O_2 yield”, whereas when electrochemical oxidation is used the term “faradaic efficiency” is most common. In general, faradaic efficiencies tend to be higher than chemically driven O_2 yields conducted under otherwise similar conditions since fewer side oxidation reactions are observed, at least to date, when electrochemical oxidation is used.

An additional complicating factor observed in O_2 evolution kinetics is the presence of sigmoidal or S-shaped kinetic curves. Sigmoidal curves and other curves with induction periods have been observed in the literature when the starting material is converted into a more active catalytic material (i.e., the starting material is not the catalyst and is frequently converted into a heterogeneous catalyst).³ Increasing catalytic activity with time is *prima facie* evidence that the starting material is not the best catalytic material—and, hence, an indication that additional characterization (ideally *in operando*) is needed to determine the actual catalyst that is being formed.

However, the other possible explanation for sigmoidal kinetics is that the S-shape is only an artifact and is caused by (1) a slow response time for the O_2 quantification method, or (2) slow solution-to-gas transfer when the method samples the reaction vessel headspace. Both of these complications are likely prevalent in the WOC literature since solution-based probes often have response times of 8-30 s (e.g. with a widely used FOXY or a commercially available Clark electrode),^{81,116} and since pressure transducers and GC methods rely on headspace analysis.

Hence, faster, reliable O₂ quantification methods will be needed to understand the increasingly active homogeneous and heterogeneous WOCs currently being developed.

Controls

Kinetic controls are a critical experiment type for accurate identification of the true WOC. As noted above, the catalytic mechanism is ultimately played out, and leaves its most definitive fingerprint, in the kinetics. Therefore, one can provide strong evidence for or against a homogeneous POM WOC by comparing the kinetics of the POM *to kinetics of heterogeneous WOCs* (which could hypothetically be derived from the starting POM).^{67,76,84,122,123} For example, Hill and co-workers tested the activity of RuCl₃ and RuO₂ en route to concluding that [Ru₄(μ-O)₄(μ-OH)₂(H₂O)₄(γ-SiW₁₀O₃₆)₂]¹⁰⁻ is a WOC.¹¹⁸ Galán-Mascarós and co-workers have used Co²⁺ and Co₃O₄ materials in attempts to distinguish {Co₉(H₂O)₆(OH)₃(HPO₄)₂(PW₉O₃₄)₃}¹⁶⁻ and CoO_x catalysts.¹⁰¹ We used Co²⁺ and CoO_x controls to determine the relative stability and activity of these precursors compared to [Co₄(H₂O)₂(PW₉O₃₄)₂]¹⁰⁻.⁸¹ The caveat to all of these control studies is that the precise catalyst may not be known and it is therefore not possible to conduct the best, most telling control experiments. Also, if a heterogeneous catalyst is being tested, the number of active sites needs to be taken into account but is typically not known and often difficult to determine. In short, the full rate law, plus several controls with multiple precursors, are necessary to provide compelling evidence for (or against) the final conclusion of a homogeneous (or heterogeneous) WOC.

Phenomenological Studies: Ligand or Poison Additions

The last set of experiments for distinguishing homogeneous and heterogeneous WOCs involves phenomenological tests. These experiments involving the addition of exogenous ligands or poisons are often basically kinetic experiments, although as presently performed they

are frequently more qualitative in nature—despite the fact that quantitative poisoning studies can be one of the single most powerful means to distinguish homogeneous from heterogeneous catalysts.¹²⁴ For example, Hill and co-workers⁶⁵ and Goberna-Ferrón et al.⁷⁹ removed excess aqueous Co^{2+} by adding 2,2'-bipyridine (bpy) to their $[\text{Co}_4(\text{H}_2\text{O})_2(\text{PW}_9\text{O}_{34})_2]^{10-}$ and $\{\text{Co}_9(\text{H}_2\text{O})_6(\text{OH})_3(\text{HPO}_4)_2(\text{PW}_9\text{O}_{34})_3\}^{16-}$ solutions, respectively; the authors conclude that the remaining water oxidation activity is therefore due to the starting POM since controls with Co^{2+} plus 2,2'-bipyridine show no O_2 evolution activity. Although this bpy addition experiment argues against a Co^{2+} to CoO_x catalyst formation pathway, one must also know the stability of the POM under the reaction conditions to rule out a POM to CoO_x WOC formation pathway. Other phenomenological tests include addition of different counter cations and anions, changes in buffer, and changes in oxidant; as with bpy addition, changing any one of these variables might provide insight into the active catalyst *or* it could potentially change the true catalyst identity.

Summary of the Methodology

The methodology described herein is meant as a general guide to the reader as well as a practical guide for the practitioner. As with many areas of chemical science, the ability to identify the true WOC will continue to evolve as analytical methods are improved. Overall, the problem of distinguishing homogeneous and heterogeneous catalysis is as simple or as complex as (i) identifying any and all possible catalytic materials, and then (ii) obtaining the catalytic water oxidation activity (and rate laws) of those observed materials and comparing and correlating that data with the observed water oxidation reaction kinetics.

The next section will describe specific studies of water oxidation catalysis when beginning with POM starting materials and the experiments reported therein to distinguish homogeneous and heterogeneous catalysis.

Water Oxidation Catalysis Studies Beginning with Polyoxometalates

Presently, there are 38 literature examples of water oxidation catalysis studies which use 28 different polyoxometalates as the starting materials. These reports include cobalt, ruthenium, manganese, molybdenum, iridium and nickel based POMs, in order of decreasing prevalence. The following sections are separated according the (hypothetically) active metal center. Each metal is then divided into two subsections: (1) precedent in terms of examples of non-POM studies with that metal which provide evidence for conversion of homogeneous starting materials into heterogeneous WOCs, and then (2) WOC studies which start with polyoxometalates containing that same metal. The first subsection is needed to put the POM studies into broader perspective within the WOC literature as well as to suggest metal-specific experiments which have been used to successfully to distinguish homogeneous and heterogeneous WOCs. The second subsection for each metal then addresses the specific studies of POMs while critically analyzing the experimental data relevant to identifying the true catalyst.

Cobalt

Non-POM Cobalt Precatalysts

Determining the true catalyst in cobalt-based water oxidation systems has been addressed beginning with some of the earliest studies which used cobalt(II) salts as starting materials. In these cases, distinguishing homogeneous and heterogeneous catalysis has proved to be challenging in part due to the possible formation of potentially low amounts of *hard-to-detect, ostensibly high-activity, colloidal CoO_x*. Despite these difficulties, Parmon and co-workers have made significant progress on this problem, starting back as early as 1981, by studying both homogeneous cobalt precursors (e.g. CoCl₂) and heterogeneous colloidal cobalt(III) hydroxide in the presence of chemical oxidants (e.g. Ru(bpy)₃³⁺).^{125,126,127,128,129,130,131,132} Ultimately, they

concluded that the true catalyst is the same when beginning with either aqueous cobalt salts or heterogeneous cobalt(III) hydroxide since the catalytic O₂ generation rate and yields are identical for both starting materials, even when the conditions are varied (e.g. the pH, the catalyst-to-oxidant ratio, and when additional cations are provided).¹³⁰

More recently, Shevchenko et al. reported in 2011 that aqueous cobalt [Co(ClO₄)₂] plus methylenediphosphonate solutions will transform into catalytically active CoO_x colloidal solutions using photochemical (hv + Ru(bpy)₃²⁺ + Na₂S₂O₈) or chemical (Ru(bpy)₃³⁺) oxidants.^{133,134} Interestingly, by including or excluding the methylenediphosphonate, the authors were able to control the size of the CoO_x colloids (10-60 nm in the presence of and 50-2500 nm in the absence of methylenediphosphonate), thereby exhibiting some control over the catalytic activity of the colloids. Shevchenko et al.'s paper is of additional importance in that it provides evidence consistent with the existence of anion-stabilized CoO_x colloids—a possibility which is not addressed in the current POM WOC literature.

In a related study, Fukuzumi and co-workers have investigated CoO_x WOCs derived from homogeneous cobalt precursors such as [Co(Cp*)(bpy)(OH₂)]²⁺ and [Co(tris(N,N'-dimethylaminoethyl)amine)(OH₂)]²⁺.¹³⁵ When these precursors were illuminated in the presence of Ru(bpy)₃²⁺ and Na₂S₂O₈, the formation of 20±10 nm and 200±100 nm particles were observed by dynamic light scattering and TEM. The resultant O₂ evolution total turnovers (TTO) was also measured and is higher for the smaller vs larger particles, 420 vs 320 mols O₂/mols Co, respectively. The authors conclude that organic ligands appear to stabilize *in-situ* formed CoO_x particles during photo-driven water oxidation, but direct evidence for CoO_x-ligand bonds, nor the Co:ligand ratio(s) involved, was provided.

Water oxidation catalysis when beginning with cobalt salts and electrochemical oxidation has been studied as well.¹³⁶ Although several papers reported that aqueous Co(II) solutions form a heterogeneous cobalt-oxy-hydroxy material, the activity of these in-situ formed oxides was not studied in the presence of the Co(II) precursor until Nocera and co-workers began investigations of these systems in 2008.^{137,138} Therein, Nocera and co-workers demonstrate that when aqueous Co(II) is electrolyzed above 1.05 V vs NHE in neutral to slightly basic solution, a CoO_x material forms which is composed of cobalt, oxygen, and adventitious electrolyte cations and anions.^{137,138} Additional studies of CoO_x have shown that these materials are self-healing, contain cobalt in primarily the Co(III) and Co(IV) oxidation states, and are composed of cobalt-oxo cubane domains which are more or less ordered depending on the deposition conditions.^{139,140,141,142,143,144}

In a related study, attempts to make a homogeneous Co(III)F₃ water oxidation catalyst by Gerken and Stahl also resulted in the formation of a heterogeneous CoO_x material. Under their conditions they observed by EDX a material which consisted of Co:O:F in a ratio of 1:6:0.3.¹⁴⁵ In addition, by electrodepositing several different CoO_x materials (including the CoPi-type CoO_x of Nocera and co-workers, *op. cit.*), Gerken and Stahl showed that all of the CoO_x had similar activity and equilibrated with the reaction solution to form nearly identical materials after bulk electrolysis.

A subsequent, pivotal study by Stahl and co-workers elaborated upon their initial results by investigating aqueous Co(II) precursors from pH 1-14.¹⁴⁶ Therein, it was found that three pH regimes were found: (i) at pH > 5.5, stable CoO_x films were formed on the electrode; (ii) at 5.5 > pH > 3, a CoO_x film could be formed on the electrode, but was oxidatively unstable and would dissolve during electrolysis if excess Co(II) was not present in the solution, (iii) at pH < 3, no

film was observed on the electrode and the dependence of activity on aqueous Co(II) followed an adsorption isotherm—evidence which is consistent with the active catalyst precursor being the dissolved cobalt(II) species. This important result demonstrates that the stability of heterogeneous CoO_x catalysts can vary with reaction conditions, and that CoO_x films are unstable at $\text{pH} < 3$. Restated, the absence of an observed heterogeneous material at the *end* of a reaction does not guarantee it was not present and active *during* the reaction, depending on the pH and other conditions to start and at the end of the reaction— H^+ being a product of the oxidation of water. Furthermore, by comparing the kinetics and products of the water oxidation reaction, these authors were able to differentiate between the homogeneous and heterogeneous catalyst systems which differ only in the pH employed.

Cobalt POM Precatalysts

Perhaps the most intensely studied complex in the recent water oxidation literature is the cobalt polyoxometalate $[\text{Co}_4(\text{H}_2\text{O})_2(\text{PW}_9\text{O}_{34})_2]^{10-}$ (Co_4POM) (Figure 2.2). This compound was first reported to be a WOC in a 2010 *Science* paper by Hill and co-workers with a high turnover frequency ($\text{TOF} = 5 \text{ s}^{-1}$, albeit for an unknown rate law¹¹⁶) when using a $\text{Ru(III)(bpy)}_3^{3+}$ oxidant at pH 8.⁶⁵ Therein, the authors provided several experiments consistent with their hypothesis that Co_4POM is the true catalyst. First, the Co_4POM was reported to be stable by UV-vis and ^{31}P -NMR spectroscopy at pH 8 over 1 month, consistent with at least some hydrolytic stability of the complex, although the claimed stability was not quantitated, nor were error bars given. Second, 2,2'-bipyridine was added to the solution in order to complex any adventitious aqueous Co(II), which would form a CoO_x catalyst in-situ, if present; this caused the O_2 yield to decrease from 67% to 48% for the 3.2 μM Co_4POM solution in the absence and presence of the 2,2'-bipyridine. In contrast, controls beginning with 13 μM $\text{Co}(\text{NO}_3)_2$ showed O_2 yields of 80% and 0% when

2,2'-bipyridine was absent or present. These results suggest that at least CoO_x formed solely from aqueous Co(II) is not the dominant catalyst in the Co_4POM system.

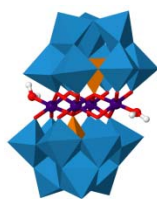


Figure 2.2. Mixed polyhedral/ball-and-stick model of $[\text{Co}_4(\text{H}_2\text{O})_2(\text{PW}_9\text{O}_{34})_2]^{10-}$ where blue polyhedral = WO_6 , orange polyhedral = XO_4 (X = P or Si), purple = Co, red = O, white = H.

Qualitative evidence that the Co_4POM is largely (i.e., but, again, not quantitatively) stable during the reaction was demonstrated by observation of the ^{31}P -NMR signal for the polyoxometalate in the post-reaction solution which had been treated with sodium tetraphenylborate to precipitate $\text{Ru(II)(bpy)}_3^{2+}$. Additionally, the Co_4POM could be precipitated from the post-reaction solution by addition of excess $\text{Ru(II)(bpy)}_3^{2+}$ and showed IR signals consistent with the starting POM. This precipitated $[\text{Co}_4(\text{H}_2\text{O})_2(\text{PW}_9\text{O}_{34})_2]^{10-}:\text{Ru(II)(bpy)}_3^{2+}$ material was then dissolved and tested for water oxidation activity by addition of $\text{Ru(III)(bpy)}_3^{3+}$ oxidant, resulting in an O_2 yield of 49 %. Although these results are all consistent with the authors' hypothesis/conclusion that the Co_4POM is the true catalyst, they did not rule out the possibility that a portion of the starting Co_4POM is transformed into either a different POM fragment or a heterogeneous CoO_x catalyst under the reaction conditions. That is, in order to rule out this possible formation of a highly active derivative material, additional studies were required.

Subsequently, Hill, Lian, and co-workers also reported the Co_4POM as a photochemically driven WOC where the oxidizing equivalents were derived from the common $\text{Ru(II)(bpy)}_3^{2+}$, Na_2SO_8 , plus $h\nu$ system with a maximum O_2 yield of 45 %.¹⁰⁴ Therein, the authors reported that no evidence for particle formation was observed by dynamic light

scattering and Tyndall effects under conditions of 1 mM Ru(bpy)₃²⁺, 160 mM NaBi, pH 8, 5 μM Co₄POM, 5 mM Na₂S₂O₈. This is an interesting result since the prior report⁶⁵ by the same group said that supersaturated solutions of Co₄POM were formed when as few as 40 equivalents of Ru(bpy)₃²⁺ were present (i.e., which would translate to 200 μM Ru(bpy)₃²⁺ in the photo-chemical system). Although the absence of detectable CoO_x colloids is a relevant result, one must also know what concentration and size of CoO_x colloids would account for the observed activity and then determine whether that amount and size of colloid can be detected via dynamic light scattering (or any other measurement of suspended colloids).

Reinvestigation of the photochemically driven Ru(bpy)₃²⁺ plus Co₄POM was conducted by Natali et al.⁸⁵ In this study, the Co₄POM was aged and then subjected to flash photolysis—an experiment wherein Ru(III)(bpy)₃³⁺ is photochemically generated by quenching of the Ru(II)(bpy)₃²⁺ excited state by sodium persulfate and then the rate of Ru(II)(bpy)₃²⁺ recovery is observed as a function of time. In these experiments, it was found that the amount of Ru(II)(bpy)₃²⁺ recovered during the first 100 μs increased with increasing Co₄POM aging time. The Ru(II)(bpy)₃²⁺ recovery plateaued for Co₄POM solutions aged 90 minutes or more when the initial conditions were [Ru(II)(bpy)₃²⁺] = [Co₄POM] = 50 μM, 5 mM Na₂S₂O₈, pH 8, and 80 mM sodium phosphate. Controls with Co(NO₃)₂ were also reported to quench the Ru(III)(bpy)₃³⁺ more slowly than the Co₄POM solution, although no details for these experiments were given. The authors claim⁸⁵ that this evidence shows the starting Co₄POM *cannot* be the true WOC and instead favor a POM fragment or decomposition product as a likely WOC when Ru(III)(bpy)₃³⁺ is used as an oxidant. Although this flash photolysis study highlights some potential complexities of working with Co₄POM, a follow-up study by Hill and co-workers⁶⁷ show that under the conditions used for flash photolysis, no measurable O₂ is generated. The lesson here is that the

proper interpretation of kinetic data requires that the reaction stoichiometry be known—and, ideally, the O₂ evolution kinetics also measured, but this can be problematic to nearly impossible on fast (μs) timescales.

Following the initial work of Hill and co-workers, Stracke and Finke began studies attempting to incorporate the Co₄POM into a hybrid semiconductor-catalyst device for light-driven water oxidation.¹⁴⁷ However, those initial studies of Co₄POM, quickly led, instead, to an electrochemical investigation of whether the Co₄POM is a homogeneous WOC or whether it is a precursor for a heterogeneous CoO_x material.⁶⁶ In this investigation, it was found that linear sweep voltammetry of a 500 μM Co₄POM solutions shows an anodic wave at ~1.05 V vs Ag/AgCl which increases more than 10-fold in magnitude during three hours of aging in pH 8, sodium phosphate buffer. This increasing current occurs concomitantly with a 4.3±0.6 % decrease in the 580 nm absorbance of Co₄POM—two results which by themselves, pretty much demand that the Co₄POM is evolving to a significantly more active, true WOC. Aging of Co₄POM also results in a 58±2 μM increase in the apparent aqueous [Co²⁺], which was measured by two complementary methods—by comparing the anodic wave current to Co(NO₃)₂ controls and also by cathodic stripping voltammetry.⁶⁶ Bulk electrolysis of the Co₄POM solution at 1.1 V vs Ag/AgCl (without aging) results in an increasing catalytic current with time and the deposition of a catalytically active film, that proved to be CoO_x. When this film was removed from the Co₄POM solution and placed into a POM-free solution, the film maintains all of its water oxidation activity. The elemental makeup of this film is consistent with other heterogeneous CoO_x catalysts, containing Co, P, Na, and O as determined by XPS. Importantly, no tungsten was observed in the film, as would be expected if the [Co₄(H₂O)₂(PW₉O₃₄)₂]¹⁰⁻ was present. Lastly, catalytic controls with a 500 μM Co₄POM solution (aged for 3 hours) and a 58

$\mu\text{M Co(NO}_3)_2$ solution (i.e., the amount of aqueous cobalt quantitated in the aged Co_4POM solution) showed quantitatively identical water oxidation activity during a 5 minute bulk electrolysis at 1.1 V vs Ag/AgCl, within experimental error, Figure 2.3. Together, these results all indicate that when a glassy carbon electrode is used as the oxidant source in 500 $\mu\text{M Co}_4\text{POM}$ solutions, and under the specific conditions cited earlier, the dominant WOC is an in-situ formed CoO_x and not the starting polyoxometalate to $101\pm 12\%$.⁶⁶

The observation that Co_4POM could be a viable precursor for heterogeneous CoO_x prompted Stracke and Finke to investigate the interesting Co_4POM system under conditions which would favor homogeneous Co_4POM catalysis, if it were present. Their next study therefore looked at the Co_4POM at much lower concentrations and higher electrochemical potentials of 2.5 μM and >1.3 V vs Ag/AgCl, conditions chosen to ostensibly favor water oxidation catalysis by the discrete Co_4POM .⁸¹ Under those new conditions, an irreversible oxidation wave was observed above potentials of 1.25 V vs Ag/AgCl, one which saturated at Co_4POM concentrations of ~ 5 μM . Comparison to $\text{Co(NO}_3)_2$ controls revealed that the anodic wave in Co_4POM solutions occurred at about 200 mV more positive potential than $\text{Co(NO}_3)_2$ solutions. Furthermore, the Co_4POM wave shifts by -32 mV/pH unit, whereas the $\text{Co(NO}_3)_2$ wave has a -66 mV/pH unit dependence. In addition, the aqueous $[\text{Co}^{2+}]$ in 2.5 $\mu\text{M Co}_4\text{POM}$ solution was found to be an average 170 nM during a one hour aging experiment. Controls using 200 nM Co^{2+} (added via $\text{Co(NO}_3)_2$) demonstrated that this amount of aqueous cobalt(II) *cannot* account for the water oxidation activity observed in the Co_4POM solution during bulk electrolysis at 1.4 V vs Ag/AgCl (Figure 2.4). That is, the differing electrochemical features for the Co_4POM and $\text{Co(NO}_3)_2$, plus the controls using the independently measured amount of Co^{2+} , provide strong evidence that CoO_x formed *at least solely from* Co^{2+} is not the dominant WOC at

these micromolar concentrations of Co₄POM—a conclusion which differs from their first electrochemical study, and a conclusion which highlights the importance reaction conditions can play in determining the true WOC as others also stress.^{6,7,67,81}

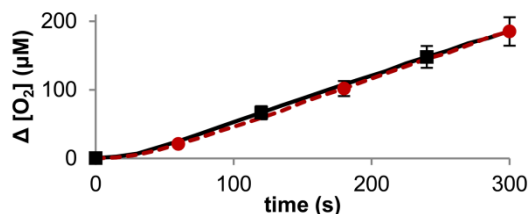


Figure 2.3. Measured change in dissolved O₂ during bulk electrolysis of either a 500 μM Co₄POM which had been aged for 3 hours (red circles) or a 58 μM Co(NO₃)₂ control (i.e., the amount of Co²⁺ determined to dissociated from the starting Co₄POM during the 3 hour aging) in pH 8, 0.1 M sodium phosphate buffer. Electrolysis was conducted at 1.1 V vs Ag/AgCl at a glassy carbon plate and O₂ was measured using a fluorescence-based probe from Ocean Optics. Under these conditions, all of the O₂ producing activity (100±12 %) in the Co₄POM solution is accounted for by the in-situ formed CoO_x catalytic film. The O₂ concentration was recorded every 15 s; the symbols and error bars are given at 60 s intervals for clarity. Reproduced with permission from Ref 66.

An additional question, relevant to the electrochemically driven Co₄POM system, is whether the polyoxometalate could transform into a heterogeneous CoO_x catalyst under the oxidative reaction conditions? To answer this question Stracke and Finke started by measuring the Co₄POM concentration via HPLC both before, and after, bulk electrolysis at 1.4 V vs Ag/AgCl. They found that the Co₄POM concentration decreased by 2.7±7.3 and 9.4±5.1 % during a 60 second electrolysis in pH 8.0 and 5.8 sodium phosphate solutions.⁸¹ At pH 8, quantification of the post-reaction solution [Co²⁺] shows an increase of 50±34 nM relative to the pre-reaction solution. Meanwhile, controls with pre-deposited CoO_x catalysts revealed that if only 3.4 or 8.3 % of the Co₄POM were converted into a CoO_x catalyst, then that would account for all of the observed catalytic activity at pH 8.0 and 5.8. That is, the observed instability of the Co₄POM at 1.4 V vs Ag/AgCl and the high activity of the CoO_x controls do not yet allow one to distinguish between an authentic Co₄POM and a heterogeneous CoO_x catalyst under the reaction

conditions of that study designed to favor Co₄POM-based, electrochemically driven water oxidation catalysis.

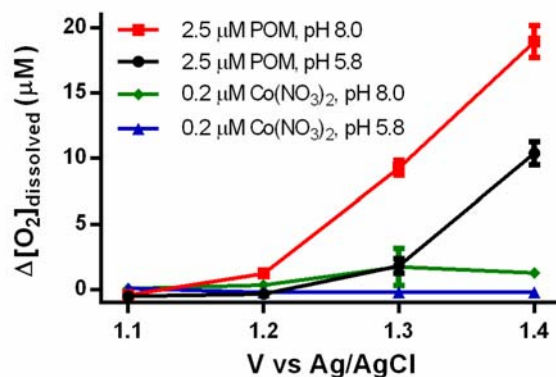


Figure 2.4. Quantification of O₂ produced during a 60s bulk electrolysis using a glassy carbon electrode at 1.4 V vs Ag/AgCl under the catalyst and pH conditions indicated in the legend (POM = [Co₄(H₂O)₂(PW₉O₃₄)₂]¹⁰⁻). The controls using 200 nM Co(NO₃)₂ were chosen since this is the average [Co²⁺] in Co₄POM solutions measured over a 1 hour aging period in pH 8, 0.1 M sodium phosphate buffer. These data contrast with Figure 2.3 in that a Co²⁺ to CoO_x WOC is not supported by the data under the different 2.5 μM Co₄POM, 1.4 V oxidation conditions. Reproduced with permission from ref 81.

In a 2013 study by Hill and co-workers, additional evidence is provided which is consistent with the Co₄POM being an active WOC when using chemical and photochemical oxidation by Ru(III)(bpy)₃³⁺.⁶⁷ First, the stability of Co₄POM was measured under non-catalytic conditions of 2 μM Co₄POM, pH 8, and 80 mM sodium borate, where 70 nM Co²⁺ dissociated from the parent POM over 3 hours. Measurement of the Ru(bpy)₃³⁺ loss kinetics using either 2 μM Co₄POM or 2 μM Co₄POM plus 0.1 μM Co(NO₃)₂ in the presence of ~ 1 mM Ru(bpy)₃³⁺ resulted in oxidant-loss rates which were within 5% of one another. Other kinetic controls with 0.5 μM Co(NO₃)₂ showed sigmoidal Ru(bpy)₃³⁺ reduction kinetics and reduction rates which were comparable, or slower, than 2 μM Co₄POM. Although these results are consistent with a POM catalyst, one cannot rigorously compare Ru(bpy)₃³⁺ reduction rates with O₂ evolution activity since a significant portion of the reduction rate corresponds to unproductive ligand oxidation reactions.

More direct evidence for a Co₄POM catalyst was provided by Hill and co-workers in photochemical experiments where controls using 0.15 μM Co(NO₃)₂ produced O₂ in the same (negligible) amount as controls with no catalyst.⁶⁷ Photochemical experiments with 2 μM Co₄POM under the same conditions resulted in 24.2±0.1% O₂ yields. However, multiple other photochemical controls with Co(NO₃)₂ showed O₂ yields which were comparable or greater than Co₄POM experiments when equivalent amounts were used; for example when 2 μM Co(NO₃)₂ was used, 40.8±0.5% O₂ yields were seen. That is, the Co₄POM stability under the reaction conditions must still be quantified to rule out the possibility of an in-situ formed CoO_x material contributing to the activity.

Another line of evidence for Co₄POM catalysis provided by the Hill et al. involves a series of extraction experiments and controls.⁶⁷ First, a standard 2 μM Co₄POM photochemical reaction was run which produced the expected amount of O₂. Following the reaction, the POM was extracted using a toluene/tetra-*n*-heptylammonium nitrate (THpANO₃) procedure. When fresh Ru(bpy)₃²⁺ and S₂O₈²⁻ were added to the solution, a subsequent photochemical reaction produced no O₂. To ensure the residual toluene and THpANO₃ do not influence the reaction, a control was conducted where an aqueous solution of the sodium borate buffer was subjected to the extraction procedure, followed by addition of 2 μM Co₄POM, Ru(bpy)₃²⁺ and S₂O₈²⁻; when this solution was illuminated, it produced the same amount of O₂ as a standard (unextracted) reaction. A photochemical control using a 2 μM Co(NO₃)₂ solution which had undergone extraction showed that this method does not interfere with Co²⁺ catalyst precursors. Although the authors also claim that the extraction procedure does not interfere with a CoO_x catalyst, no data was provided to support this claim. Overall, the pre-catalytic Co₄POM stability measurement,

controls with the measured amount of dissociated Co^{2+} , and extraction experiments are all consistent with a homogeneous POM catalyst.

Most recently, Stracke and Finke have conducted a kinetic and mechanistic analysis of the Co_4POM plus $\text{Ru}(\text{bpy})_3^{3+}$ water oxidation system.¹¹⁶ Under initial conditions of 0.5-2.0 μM Co_4POM , 500-1500 μM $\text{Ru}(\text{bpy})_3^{3+}$, 50-200 μM $\text{Ru}(\text{bpy})_3^{2+}$, pH 6.8-7.8, and 0.3 M sodium phosphate, they measured both the O_2 evolution kinetics and $\text{Ru}(\text{bpy})_3^{3+}$ reduction kinetics en route to determining the empirical rate law in eq. (1):

$$\frac{-d[\text{Ru(III)(bpy)}_3^{3+}]}{dt} = (k_1 + k_2) \frac{[\text{Ru(III)(bpy)}_3^{3+}][\text{Co}_4\text{POM}]_{\text{soluble}}}{[\text{H}^+]} \quad (1)$$

Parameters k_1 and k_2 correspond to the observed rate constants for the parallel O_2 evolution and bpy ligand oxidation reactions and $[\text{Co}_4\text{POM}]_{\text{soluble}}$ is the amount of soluble POM. In comparison, Co^{2+} controls showed a first-order dependence of the O_2 evolution rate on $[\text{Co}^{2+}]$, a zero-order dependence for the bpy ligand oxidation rate on $[\text{Co}^{2+}]$, and a zero order dependence of the O_2 evolution rate on $[\text{Ru}(\text{bpy})_3^{3+}]$. That is, the ligand oxidation rate shows different dependences of the [precatalyst] for Co_4POM and Co^{2+} (which generates CoO_x *in-situ*) and the O_2 evolution rate shows different dependences on $[\text{Ru}(\text{bpy})_3^{3+}]$ for Co_4POM and Co^{2+} precatalysts. Overall, this kinetic contrast argues strongly that the true catalyst is different in these two systems, although the precise identity and atomic composition of the true catalyst remains unknown.

In other cobalt POM studies, Song et al. looked at a variety of cobalt substituted Keggin type POMs (Figure 2.5) and found the $\text{Co(III)Co(II)W}_{11}\text{O}_{39}^{7-}$ showed a water oxidation TOF of 0.5 s^{-1} (for an unknown rate law) and a 30% O_2 yield when using photochemically generated $\text{Ru(III)(bpy)}_3^{3+}$.⁶⁸ These authors provided evidence that the active catalyst is homogeneous, including the absence of any at least detectable particles by dynamic light scattering after 10

minutes of illumination. However and curiously, when only 0.1 mol % of Co^{2+} was added to the $\text{Co(III)Co(II)W}_{11}\text{O}_{39}^{7-}$ reaction solution (where $[\text{Co}^{2+}] + [\text{Co(III)Co(II)W}_{11}\text{O}_{39}^{7-}] = 15 \mu\text{M}$), particles were observable *both before and after photolysis*—that is, it is not clear why such a small amount of Co^{2+} plus the $\text{Co(III)Co(II)W}_{11}\text{O}_{39}^{7-}$ forms particles prior to irradiation, but 1 mM $\text{Ru(II)(bpy)}_3^{2+}$ plus the polyoxometalate does not? Also, a control with 45 nM $\text{Co(NO}_3)_2$ showed no observable water oxidation activity. UV-vis spectroscopy and flash photolysis of aged $\text{Co(III)Co(II)W}_{11}\text{O}_{39}^{7-}$ solutions further attest to the hydrolytic stability of this POM. Cyclic voltammetry of the $\text{Co(III)Co(II)W}_{11}\text{O}_{39}^{7-}$ in comparison with $\text{Co(NO}_3)_2$ controls is also consistent with Co^{2+} not being present in the solution before the photolysis reaction. Interestingly, the $\text{Co(II)Co(II)W}_{11}\text{O}_{39}^{8-}$ oxidation state of the POM is not hydrolytically stable in solution, but instead forms bulk Co(OH)_2 over a 1 hour aging experiment in the pH 9 sodium borate buffer. This result is intriguing because it possible, if not likely, that the $\text{Co(III)Co(II)W}_{11}\text{O}_{39}^{7-}$ goes through this lower oxidation state during water oxidation catalysis.

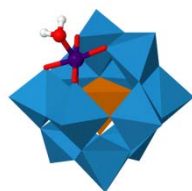


Figure 2.5. A general structural model for $[\text{XYW}_{11}\text{O}_{39}]^{n-}$ where blue polyhedral are WO_6 , red = O, and white = H. For $\text{Co(III)Co(II)W}_{11}\text{O}_{39}^{7-}$, orange = CoO_4 , purple = Co. For ruthenium analogs $[\text{Ru(H}_2\text{O)SiW}_{11}\text{O}_{39}]^{5-}$, $[\text{Ru(H}_2\text{O)GeW}_{11}\text{O}_{39}]^{5-}$ and $[\text{Ru(H}_2\text{O)PW}_{11}\text{O}_{39}]^{4-}$, purple = Ru and orange = SiO_4 , GeO_4 , and PO_4 .

Experiments consistent with $\text{Co(III)Co(II)W}_{11}\text{O}_{39}^{7-}$ stability under reaction conditions include precipitation of the POM from post-photolysis solutions with subsequent characterization by IR and EDX.⁶⁸ Also, after precipitation and centrifugation, no residual particles were observed in the reaction solution by DLS. Redissolution of the precipitated POM also showed no observable particles by DLS and subsequent photocatalytic testing showed similar, ~10% lower,

activity for the redissolved $\text{Co(III)Co(II)W}_{11}\text{O}_{39}^{7-}$ compared to the initial $\text{Co(III)Co(II)W}_{11}\text{O}_{39}^{7-}$ solution. As noted previously, although these types of phenomenological tests are consistent with the starting material being a WOC, quantitative knowledge of the speciation *during* the reaction is needed to unequivocally identify the active catalyst. Hence, the true catalyst in the case of the $\text{Co(III)Co(II)W}_{11}\text{O}_{39}^{7-}$ precatalyst remains uncertain.

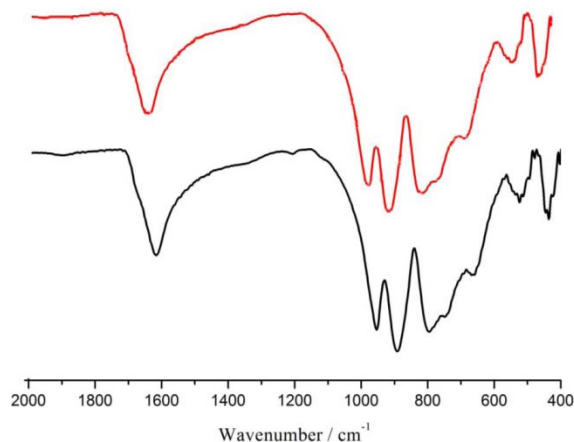


Figure 2.6. Comparison of fresh $\text{Co(III)Co(II)W}_{11}\text{O}_{39}^{7-}$ (top) and the material isolated from a post-photocatalytic reaction (bottom) via acetone addition and centrifugation. The similarity between the spectra indicates the starting POM remains qualitatively intact during the reaction. Additional controls using authentic CoO_x are needed to help determine if CoO_x can be observed via this isolation/characterization method. Reproduced with permission from Ref 68.

Another interesting cobalt polyoxometalate system is

$\{\text{Co}_9(\text{H}_2\text{O})_6(\text{OH})_3(\text{HPO}_4)_2(\text{PW}_9\text{O}_{34})_3\}^{16-}$ (Co_9POM , which is shown in Figure 2.7) since it is a trimeric analog of the Co_4POM dimer. In a study by Galán-Mascarós and co-workers, bulk electrolysis of the Co_9POM at 1.41 V vs NHE resulted in the formation of a catalytic film on the electrode in pH 7 sodium phosphate buffer.⁷⁹ This film, which contains cobalt and phosphorus by EDX, maintains its activity when it is transferred to a POM-free solution—similar to other in-situ formed, heterogeneous CoO_x catalysts. In order to help distinguish whether any of the activity was due to authentic Co_9POM water oxidation catalysis, 2,2'-bipyridine was added to the electrolysis solution which resulted in a 40-fold decrease in the oxidation current at 1.41 V vs

NHE; no CoO_x film was observed post the 2,2'-bipyridine addition on the post-electrolysis FTO electrode by SEM or EDX. Concurrent with electrolysis, a $[\text{Co(III)(bpy)}_3]_4\text{K}_{4-x}\text{Na}_x[\text{Co}_9\text{POM}]$ precipitates from the solution and the dissolved $[\text{Co}_9\text{POM}]$ decreases by 30 %, as determined by UV-vis spectroscopy. Cyclic voltammetry was also used to characterize Co_9POM which shows a peak at 0.75 V and a catalytic wave at 1.10 V; when 2,2'-bipyridine is added only a 1.10 V catalytic wave onset is seen—evidence which the authors claim rules out CoO_x when bpy is present. However, due to the observed instability of the Co_9POM under oxidizing conditions and the similar onset potential for the catalytic current, it is also possible that the Co_9POM is simply being converted into a transiently stable CoO_x catalyst. Controls with authentic CoO_x are needed to rule out, or support, this possibility.

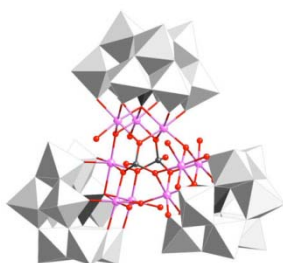


Figure 2.7. Mixed polyhedral/ball-and-stick model of $\{\text{Co}_9(\text{H}_2\text{O})_6(\text{OH})_3(\text{HPO}_4)_2(\text{PW}_9\text{O}_{34})_3\}^{16-}$ where white polyhedral = WO_6 , black = PO_4 or P, pink = Co, and red = O. Hydrogen atoms are not shown for clarity. Reproduced with permission from Ref 79.

Stronger evidence for homogeneous catalysis was found for Co_9POM when NaClO was used as an oxidant at pH 8.⁷⁹ For these NaClO oxidation experiments, no change in the UV-vis spectrum of the Co_9POM was observed, dynamic light scattering showed the same size particles of $\sim 1\text{nm}$ before and after the experiment (i.e., the approximate size of the Co_9POM), and addition of bipyridine does not significantly change the O_2 yields or kinetics. The POM can also be recovered from the solution by addition of excess alkali cation and was the same as the initial, unreacted Co_9POM sample (as judged by IR and XRD). The only possible evidence that

Co₉POM transforms into a more active WOC during the reaction is the slightly sigmoidal shape of the O₂ versus time plot when the pH is 7 or at 15 °C ([Co₉POM] = 1.0 mM, [NaClO] = 100 mM). Alternatively, and as noted in the introduction, a sigmoidal O₂ evolution plot could be due to the slow O₂ solution-to-gas transfer. This remaining question could be resolved by measuring the O₂ generation rate in solution with a faster sensor or by increasing the stirring rate to accelerate the O₂ solution/gas equilibration.

In 2012, Car et al. studied photochemical water oxidation with [Co₄(H₂O)₂(SiW₉O₃₄)₂]¹²⁻, which is the silicon(IV) core analog of [Co₄(H₂O)₂(PW₉O₃₄)₂]¹⁰⁻ (Figure 2.2).⁶⁹ Initial UV-vis stability measurements indicate that up to 25% of the POM decomposes during a 2.5 hour period in pH 5.8 NaSiF₆ buffer. Despite this decomposition, the authors claim catalytic activity resides in a precipitated [Co₄(H₂O)₂(SiW₉O₃₄)₂]¹²⁻: [Ru(bpy)₃]²⁺ material which forms immediately upon combining the cobalt POM and the photosensitizer. FTIR of the pre- and post-catalytic precipitate indicate the presence of [Co₄(H₂O)₂(SiW₉O₃₄)₂]¹²⁻; this precipitate can also be reused with moderate, ~50% loss in O₂ evolution activity. Controls with Co²⁺ showed higher activity compared with the [Co₄(H₂O)₂(SiW₉O₃₄)₂]¹²⁻ starting material. Additional speciation data, and characterization of the precipitate's surface, may provide further evidence for the true WOC.

Zhu et al. used [Co₄(μ-OH)(H₂O)₃(Si₂W₁₉O₇₀)]¹¹⁻ under typical Ru(bpy)₃²⁺ plus S₂O₈²⁻ photochemical conditions to generate O₂ from water as shown in Figure 2.8.^{70,71} This POM starting material was found to be even less stable than other tetra-cobalt POMs, such as [Co₄(H₂O)₂(PW₉O₃₄)₂]¹⁰⁻, under non-catalytic conditions. UV-vis spectroscopy showed the [Co₄(μ-OH)(H₂O)₃(Si₂W₁₉O₇₀)]¹¹⁻ transforming into other species over a period of hours to days. From these aged solutions, Zhu recovered K₁₀Na[{Co(H₂O)}(μ-H₂O)₂K {Co(H₂O)₄}(Si₂W₁₈O₆₆)] and [Co(H₂O)SiW₁₁O₃₉]⁶⁻. Stoichiometric

analysis and UV-vis data indicate that aqueous Co^{2+} is also released during this process. To probe whether the decomposition products are contributing to catalysis, controls were completed with both $\text{K}_{10}\text{Na}[\{\text{Co}(\text{H}_2\text{O})\}(\mu\text{-H}_2\text{O})_2\text{K}\{\text{Co}(\text{H}_2\text{O})_4\}(\text{Si}_2\text{W}_{18}\text{O}_{66})]$ and $[\text{Co}(\text{H}_2\text{O})\text{SiW}_{11}\text{O}_{39}]^{6-}$ under photochemical conditions where three times less activity, and no O_2 evolution activity, were observed, respectively. Aging the $[\text{Co}_4(\mu\text{-OH})(\text{H}_2\text{O})_3(\text{Si}_2\text{W}_{19}\text{O}_{70})]^{11-}$ solution for 3-4 weeks followed by catalytic testing results in 20-30% lower O_2 yields compared to the fresh POM precursor. Although the authors claim that $[\text{Co}_4(\mu\text{-OH})(\text{H}_2\text{O})_3(\text{Si}_2\text{W}_{19}\text{O}_{70})]^{11-}$ could be the active WOC, they acknowledge the possibility that dissociated aqueous Co^{2+} (i.e., in-situ formed CoO_x) contributes to catalysis. Until the catalytic contribution of heterogeneous CoO_x is known, the claim of a homogeneous POM catalyst remains uncertain for this case as well.

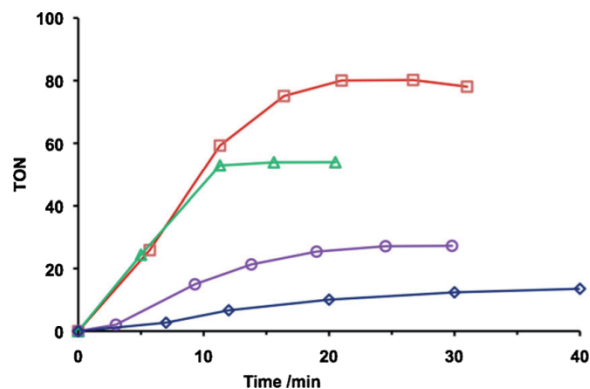


Figure 2.8. Calculated turnover number (TON = mols O_2 generated per mol $[\text{Co}_4(\mu\text{-OH})(\text{H}_2\text{O})_3(\text{Si}_2\text{W}_{19}\text{O}_{70})]^{11-}$) for a photocatalytic reaction containing 1.0 mM $\text{Ru}(\text{bpy})_3^{2+}$, 5 mM $\text{S}_2\text{O}_8^{2-}$, 25 mM buffer, and 10 μM $[\text{Co}_4(\mu\text{-OH})(\text{H}_2\text{O})_3(\text{Si}_2\text{W}_{19}\text{O}_{70})]^{11-}$. The buffers used are: pH 9 sodium borate (red squares), pH 8 sodium borate (green triangles), pH 8 equi-molar sodium phosphate:sodium borate (purple circles), and pH 7.2 sodium phosphate (blue diamonds). Note the slightly sigmoidal kinetics seen in the bottom two curves; additional *in operando* speciation and O_2 experiments are therefore needed to determine whether the induction period is due to slow solution-to-gas transfer of the O_2 (as suggested by the authors) or whether the POM is evolving into a faster WOC. Alternatively, one could simply measure the solution concentration of O_2 to determine whether the induction period is real or an artifact. Reproduced with permission from Ref 70.

Another set of Keggin dimers with di-cobalt, di-bismuth bridges were studied by Guo et al.⁸⁶ When 5.6 μM $\text{Na}_9\text{H}_5[\text{Co}_2\text{Bi}_2(\alpha\text{-B-CoW}_9\text{O}_{34})_2]$ or $\text{Na}_9\text{H}_5[\text{Co}_2\text{Bi}_2(\beta\text{-B-CoW}_9\text{O}_{34})_2]$ were

illuminated with a 300 W xenon lamp in the presence of 1.0 mM Ru(bpy)₃²⁺ and 5.0 mM S₂O₈²⁻ in pH 7.4 sodium phosphate buffer, up to 18 μmol of O₂ (TON = ~32) was produced. Stability of these POMs under non-catalytic conditions was examined by measuring the cyclic voltammetry response over a three hours aging period. Since no change in the CV was observed, the authors conclude that the POMs are stable. Unfortunately, no other data speaks to the speciation or stability of the POMs under the reaction conditions. Hence, the true catalyst is unknown in this case.

Others have observed instability of cobalt POMs under electrocatalytic conditions. Lai et al. drop cast cobalt-polyoxotitanates, [Ti₁₂O₁₅(OⁱPr)₁₇]⁺[(CoBr)₆Ti₁₅O₂₄(OⁱPr)₁₈(Br)]⁻ and [(CoI)Ti₁₁O₁₄(OⁱPr)₁₇], onto FTO electrodes and then biased the electrodes at 1.35 V vs NHE where catalytic oxidation was observed.¹⁰⁹ Before electrolysis, SEM/EDX of the drop cast film shows islands which contain cobalt but no phosphorus islands. In contrast, the post-catalysis electrode shows islands with a Co:P of 1:9 plus a new film between the islands which has a Co:P of 2:1—evidence that POMs can transform into heterogeneous CoO_x WOCs under oxidizing conditions. Although a CoO_x material likely contributes to the overall electrocatalytic activity of the system, following the decomposition of the [Ti₁₂O₁₅(OⁱPr)₁₇]⁺[(CoBr)₆Ti₁₅O₂₄(OⁱPr)₁₈(Br)]⁻ and [(CoI)Ti₁₁O₁₄(OⁱPr)₁₇] POMs over time and determining whether this corresponds to increasing or decreasing activity may help distinguish whether the starting POM might also be contributing to the activity.

A final cobalt-based example of electrocatalytic water oxidation uses a carbon-paste supported [Hpy]₂{[Co(4,4'-Hbpy)₂(H₂O)₂][SiCoW₁₁O₃₉]}.¹⁴⁸ The starting POM was characterized by x-ray crystallography, IR spectroscopy, and elemental analysis. Although the

authors claim catalytic water oxidation by the POM, the only evidence provided is cyclic voltammetry showing an irreversible oxidation wave at ~1300 mV vs Ag/AgCl.

In summary of this section on cobalt POMs, when beginning with cobalt POMs, a wide variety of characterization techniques have been used to examine these materials for their *qualitative* stability under water oxidation reaction conditions. However, there is a lack of *quantitative stability measurements*, with the exception of electrochemical studies of Co₄POM and Co₉POM.^{81,79} It seems possible that this dearth of information may be a result of using Ru(bpy)₃³⁺ as an oxidant and the resulting complications of POMⁿ⁻:Ru(bpy)₃^{3+/2+} formation and precipitation, or the need to work at low micromolar concentrations to minimize such precipitates. Study of cobalt POMs and determination of the true catalysts therein would therefore benefit greatly from the development of either a neutral or anionic terminal oxidant, or continued use of electrochemical oxidation methods.

Ruthenium

Non-POM Ruthenium Precatalysts

Ruthenium has been reported as a homogeneous WOC active site more than any other metal.^{12,15,16,17} Despite the widespread use of ruthenium in homogeneous WOC precursors, we have found only one literature example which provides substantial evidence that a homogeneous ruthenium complex (ruthenium red, [(NH₃)₅RuORu(NH₃)₄ORu(NH₃)₅]⁶⁺) irreversibly decomposes into a possibly polymeric ruthenium material upon oxidation by cerium(IV) ammonium nitrate (Ce(IV)).¹⁴⁹ This study relies primarily on UV-vis spectroscopy to characterize the transformation and to demonstrate that decomposition occurs prior to chemically driven water oxidation catalysis. Studies by Collin and Sauvage also observe the formation of brown and/or black precipitates when starting with Ce(IV) and a variety of ruthenium precursors

including RuCl_3 , $\text{Ru}(\text{bpy})_2(\text{CO}_3)$, or $[(\text{bpy})_2(\text{H}_2\text{O})\text{RuORu}(\text{OH}_2)(\text{bpy})_2]^{4+}$; these authors therefore conclude that bulk RuO_2 (or other decomposition products) may be contributing to the observed catalysis in these cases.¹⁵⁰ Liu et al. suggest in their WOC review that the difficulty in identifying a heterogeneous RuO_2 catalyst might have to do with the non-descript visible absorption spectrum associated with ruthenium oxide. Alternatively, the relative strength of ruthenium metal-ligand bonds may account for the observed robustness under water oxidation conditions. Regardless of whether homogeneous ruthenium WOC stability is real or perceived, more thorough study of ruthenium-based precatalysts in water oxidation catalysis should continue.

Ruthenium POM Precatalysts

In 2008, Hill and co-workers⁷³ and Sartorel and co-workers⁷² independently reported catalytic water oxidation using a tetra-ruthenium POM, $[\text{Ru}_4(\mu\text{-O})_4(\mu\text{-OH})_2(\text{H}_2\text{O})_4(\gamma\text{-SiW}_{10}\text{O}_{36})_2]^{10-}$ shown in Figure 2.9, in conjunction with either a $\text{Ru}(\text{bpy})_3^{3+}$ oxidant (pH 7.2) or a $\text{Ce}(\text{IV})$ oxidant (pH 0.6). Evidence for POM stability was collected by characterizing the different oxidation/protonation states of the ruthenium POM.^{64,74} These complexes were generated either electrochemically via bulk electrolysis or by addition of 1-4 equivalents of oxidant. Characterization was accomplished by electrochemical methods,⁸² EPR, resonance Raman, and EXAFS/XANES¹⁰³. The $[\text{Ru}_4(\mu\text{-O})_4(\mu\text{-OH})_2(\text{H}_2\text{O})_4(\gamma\text{-SiW}_{10}\text{O}_{36})_2]^{10-}$ could also be recovered from a reaction solution after 8 equivalents of $\text{Ce}(\text{IV})$ were added followed by a one hour aging time and precipitation of the POM as the Cs^+ salt.⁷² FTIR and resonance Raman of the precipitate appear qualitatively the same as the pre-reaction $[\text{Ru}_4(\mu\text{-O})_4(\mu\text{-OH})_2(\text{H}_2\text{O})_4(\gamma\text{-SiW}_{10}\text{O}_{36})_2]^{10-}$ —evidence that at least some of the POM remains intact.⁷² However, UV-vis spectroscopy indicates slow decomposition of the starting POM below pH 1.⁷² When 7000 to

2.4×10^5 equivalents of Ce(IV) were used, O_2 evolution kinetics are first-order in $[Ru_4(\mu-O)_4(\mu-OH)_2(H_2O)_4(\gamma-SiW_{10}O_{36})_2]^{10-}$ (initial [POM] = 4.5-145 μ M).⁷² Additional evidence in support of a homogeneous POM WOC includes controls using $K_4Ru_2OCl_{10}$ (i.e., the ruthenium precursor used in the $[Ru_4(\mu-O)_4(\mu-OH)_2(H_2O)_4(\gamma-SiW_{10}O_{36})_2]^{10-}$ synthesis) which show a significant induction period and an approximately 10-fold slower O_2 evolution rate compared to $[Ru_4(\mu-O)_4(\mu-OH)_2(H_2O)_4(\gamma-SiW_{10}O_{36})_2]^{10-}$.⁷²

Complementary tests and controls done by Hill and co-workers using $RuCl_3$ in the presence and absence of the $[\gamma-SiW_{10}O_{36}]^{8-}$ POM building block reveal $Ru(bpy)_3^{3+}$ reduction rates 100 times slower than with $[Ru_4(\mu-O)_4(\mu-OH)_2(H_2O)_4(\gamma-SiW_{10}O_{36})_2]^{10-}$ and which produce <11% O_2 yields.⁷³ Kinetic experiments, using 1-8 μ M $[Ru_4(\mu-O)_4(\mu-OH)_2(H_2O)_4(\gamma-SiW_{10}O_{36})_2]^{10-}$ plus 0.6-2.3 mM $Ru(bpy)_3^{3+}$ at pH 7.2, resulted in an empirical rate law which is first-order in POM and first-order in the $Ru(bpy)_3^{3+}:Ru(bpy)_3^{2+}$ ratio.⁷⁴ Additionally, consistent with the absence of observable heterogeneous catalyst, no particles were detected by DLS or SAXS techniques in the post reaction $[Ru_4(\mu-O)_4(\mu-OH)_2(H_2O)_4(\gamma-SiW_{10}O_{36})_2]^{10-}$ solutions, although particle detection limits for these methods were not reported.

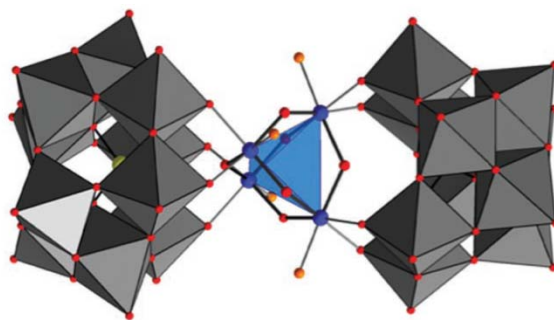


Figure 2.9. Mixed polyhedral/ball-and-stick structure of $[Ru_4(\mu-O)_4(\mu-OH)_2(H_2O)_4(\gamma-SiW_{10}O_{36})_2]^{10-}$ where grey polyhedra = WO_6 , blue = Ru, red = O(H), orange = OH_2 . Reproduced with permission from Ref 73.

Subsequently, other studies of the $[Ru_4(\mu-O)_4(\mu-OH)_2(H_2O)_4(\gamma-SiW_{10}O_{36})_2]^{10-}$ complex have investigated incorporation into photochemically driven systems including the common $h\nu +$

photosensitizer + $\text{S}_2\text{O}_8^{2-}$ setup where the photosensitizer can be $\text{Ru}(\text{bpy})_3^{2+}$ or related derivatives such as $[\text{Ru}(\text{II})\{(\mu\text{-dpp})\text{Ru}(\text{II})(\text{bpy})_2\}_3]^{8+}$ (dpp = 2,3-bis(2'-pyridyl)pyrazine).^{117,118,119} Studies using the 1.0 mM $\text{Ru}(\text{bpy})_3^{2+}$ photosensitizer formed a precipitate with the starting POM when $[\text{Ru}_4(\mu\text{-O})_4(\mu\text{-OH})_2(\text{H}_2\text{O})_4(\gamma\text{-SiW}_{10}\text{O}_{36})_2]^{10-}$ concentrations were above 5 μM ;¹¹⁸ concomitant with this precipitation, O_2 evolution rates did not increase when the POM concentration was above 2.5 μM . That is, O_2 evolution kinetics appear to scale with the amount of soluble ruthenium polyoxometalate. Importantly, and consistent with the $\text{Ru}(\text{bpy})_3^{3+}$ and Ce(IV) oxidant studies, photochemical RuCl_3 controls showed no O_2 and RuO_2 controls resulted in O_2 evolution rates which were 10-20 times slower than when starting with the $[\text{Ru}_4(\mu\text{-O})_4(\mu\text{-OH})_2(\text{H}_2\text{O})_4(\gamma\text{-SiW}_{10}\text{O}_{36})_2]^{10-}$ complex.¹¹⁸ Although these observations are *consistent* with a POM catalyst, the RuO_2 controls should, if possible, be corrected for the number of active sites so that a more direct comparison of the per-site activity can be made. Overall, however, the multiple studies, extensive characterization of $[\text{Ru}_4(\mu\text{-O})_4(\mu\text{-OH})_2(\text{H}_2\text{O})_4(\gamma\text{-SiW}_{10}\text{O}_{36})_2]^{10-}$, and multiple kinetic controls suggests that this complex is a homogeneous WOC when using chemically and photochemically driven oxidation.

The tetra-ruthenium POM $[\text{Ru}_4(\mu\text{-O})_4(\mu\text{-OH})_2(\text{H}_2\text{O})_4(\gamma\text{-SiW}_{10}\text{O}_{36})_2]^{10-}$ has also been studied using electrochemically driven oxidation. Toma et al. prepared and tested $[\text{Ru}_4(\mu\text{-O})_4(\mu\text{-OH})_2(\text{H}_2\text{O})_4(\gamma\text{-SiW}_{10}\text{O}_{36})_2]^{10-}$ which had been loaded onto polyamidoamine-functionalized multi-walled carbon nanotubes.⁸³ These functionalized electrodes can be cycled at least nine times up to 1.6 V vs Ag/AgCl without significant changes in the observed oxidation current. Although impressive pre-catalysis characterization of the electrode via HRTEM, STEM, EDX, SAXS and Raman spectroscopy indicate the presence of the intact POM, no post-catalysis characterization was reported. Without knowledge of the $[\text{Ru}_4(\mu\text{-O})_4(\mu\text{-OH})_2(\text{H}_2\text{O})_4(\gamma\text{-SiW}_{10}\text{O}_{36})_2]^{10-}$ stability

under the reaction conditions and without catalytic controls (e.g., RuO₂), it is difficult to make any firm conclusions about the active catalyst in this interesting, but complex, electrochemical water oxidation system.

Another tetra-ruthenium POM, $[(\gamma\text{-PW}_{10}\text{O}_{36})_2\text{Ru}_4\text{O}_5(\text{OH})(\text{H}_2\text{O})_4]^{9-}$ which incorporates a phosphotungate backbone, was also reported as a photochemically driven WOC.⁷⁵ Observation of two reversible protonation equilibria, and seven reversible cyclic voltammetry waves, indicate the initial stability of the POM in solution. Also, consistent with the $[\text{Ru}_4(\mu\text{-O})_4(\mu\text{-OH})_2(\text{H}_2\text{O})_4(\gamma\text{-SiW}_{10}\text{O}_{36})_2]^{10-}$ analog studies, the O₂ evolution rate depends only weakly on the initial $[(\gamma\text{-PW}_{10}\text{O}_{36})_2\text{Ru}_4\text{O}_5(\text{OH})(\text{H}_2\text{O})_4]^{9-}$ concentration. That is, the primary evidence $[(\gamma\text{-PW}_{10}\text{O}_{36})_2\text{Ru}_4\text{O}_5(\text{OH})(\text{H}_2\text{O})_4]^{9-}$ might be homogeneous is that it behaves similar to $[\text{Ru}_4(\mu\text{-O})_4(\mu\text{-OH})_2(\text{H}_2\text{O})_4(\gamma\text{-SiW}_{10}\text{O}_{36})_2]^{10-}$ where evidence for homogeneous catalysis is stronger. Further studies addressing the true catalyst when beginning with $[(\gamma\text{-PW}_{10}\text{O}_{36})_2\text{Ru}_4\text{O}_5(\text{OH})(\text{H}_2\text{O})_4]^{9-}$ would be welcome, however.

An interesting tri-ruthenium substituted Keggin silicotungstate, $[\{\text{Ru}_3\text{O}_3(\text{H}_2\text{O})\text{Cl}_2\}(\text{SiW}_9\text{O}_{34})]^{7-}$, was used as a starting material in a 1.0 mM Ru(bpy)₃²⁺ plus 5.0 mM S₂O₈²⁻ photochemically driven system (Figure 2.10).⁶⁹ Contrary to most other POM WOC studies, Car et al. hypothesize that precipitated $([\{\text{Ru}_3\text{O}_3(\text{H}_2\text{O})\text{Cl}_2\}(\text{SiW}_9\text{O}_{34})]^{7-}:\text{Ru}(\text{bpy})_3^{2+})$ is the active catalytic species. Consistent with this assertion, a precipitate forms upon combining the tri-ruthenium POM and the Ru(bpy)₃²⁺ photosensitizer. This precipitate contains IR bands characteristic of the intact POM at approximately 976, 948, and 873 cm⁻¹ in both the initial POM and also after a catalytic run with isolation by centrifugation. The supernatant of the centrifuged post-catalysis solution contains no residual activity even when fresh Ru(bpy)₃²⁺ and S₂O₈²⁻ were added—evidence that the true catalyst resides primarily in the solid state.

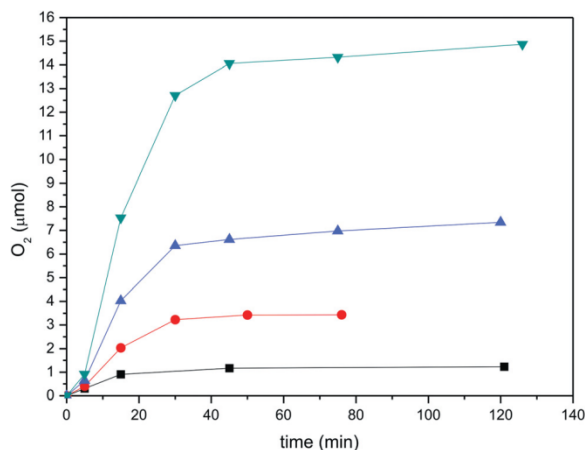


Figure 2.10. O₂ evolution kinetics for [$\{\text{Ru}_3\text{O}_3(\text{H}_2\text{O})\text{Cl}_2\}(\text{SiW}_9\text{O}_{34})\}^{7-}$] in the presence of 1 mM Ru(bpy)₃²⁺, 5 mM S₂O₈²⁻, 20 mM Na₂SiF₆ buffer (pH 5.8), and 465 nm illumination. [POM] = 16 μM (black squares), 21 μM (red circles), 31 μM (blue triangles), and 50 μM (green inverted triangles). O₂ was measured by GC of the reaction headspace. The sigmoidal shape of these kinetic curves indicate the need for experiments aimed at identifying whether the shape is determined by solution-to-gas transfer limitations or by changes in the active catalyst, as discussed above. Reproduced with permission from Ref. 69.

Stability of the starting [$\{\text{Ru}_3\text{O}_3(\text{H}_2\text{O})\text{Cl}_2\}(\text{SiW}_9\text{O}_{34})\}^{7-}$] under non-catalytic conditions was investigated by UV-vis where a 3.5% decrease in the 440 nm absorbance over 3 hours is observed; no additional decomposition is seen for the POM in the presence of S₂O₈²⁻ and illumination over 2.5 hours.⁶⁹ Photochemical controls with RuCl₃ under otherwise standard conditions did not result in O₂ formation. Further evidence of the true catalyst could include determining the fate of the 3.5% unstable fraction of the POM and looking into whether that form of ruthenium possesses any catalytic activity. XPS of the pre- and post-catalysis ([$\{\text{Ru}_3\text{O}_3(\text{H}_2\text{O})\text{Cl}_2\}(\text{SiW}_9\text{O}_{34})\}^{7-}$):[Ru(bpy)₃²⁺] solid could also potentially help determine whether the surface of the material changes during catalysis or not.

In a different ruthenium POM dimer, Howells et al. claimed electrocatalytic water oxidation when starting with what is believed to be¹⁵¹ [Ru(III)₂Zn₂(H₂O)₂(ZnW₉O₃₄)₂]¹⁴⁻ and using a gold electrode in pH 8 phosphate buffer.¹²² Oxygen evolution was observed to be potential dependent for the [Ru(III)₂Zn₂(H₂O)₂(ZnW₉O₃₄)₂]¹⁴⁻, whereas controls using a di-Zn

POM (whose structure was not specified) or $[\text{Ru}(\text{H}_2\text{O})\text{PW}_{11}\text{O}_{39}]^{4-}$ showed no O_2 evolution activity up to 1.05 V vs NHE. The current-overpotential (Tafel) relationship was also measured to be 120 mV/decade for $[\text{Ru}(\text{III})_2\text{Zn}_2(\text{H}_2\text{O})_2(\text{ZnW}_9\text{O}_{34})_2]^{14-}$; heterogeneous RuO_2 and perovskite materials typically exhibit slopes of 60 or 120 mV/decade. That is, a pure RuO_2 WOC is most likely *not* present in this POM system, but the possibility of a catalytic contribution from a different, unknown heterogeneous material has not been ruled out.

If the active catalyst is indeed the starting $[\text{Ru}(\text{III})_2\text{Zn}_2(\text{H}_2\text{O})_2(\text{ZnW}_9\text{O}_{34})_2]^{14-}$, it is also not clear what the active site might be since the ruthenium atoms are on the interior of the complex and are not coordinated to terminal aquo, hydroxo, or oxo ligands. This problem is further complicated by the observation of only ~ 1.24 equivalents of Ruthenium incorporated into the two central positions according to XRD refinement where the other 0.76 equivalents correspond to tungsten; the XRD calculation also contrasts with the elemental analysis which indicates the presence of ~ 1.94 equivalents of ruthenium per POM.¹²² That is, the authors have not ruled out the possibility that ruthenium is acting as an outer sphere/non-coordinated counter-cation in the isolated “ $\text{Na}_{14}[\text{Ru}(\text{III})_2\text{Zn}_2(\text{H}_2\text{O})_2(\text{ZnW}_9\text{O}_{34})_2]$ ” complex and also do not know if this adventitious ruthenium could be contributing to the catalytic activity. Quite possibly relevant here is literature showing that Ru(III) incorporation into a $[\text{WZn}_3(\text{H}_2\text{O})_2(\text{ZnW}_9\text{O}_{34})_2]^{12-}$ precursor—as the Howell et al.¹²² paper uses—can be problematic. For example, such syntheses are known to lead, in the case of what was claimed to be “ $[\text{WZnRu}^{\text{III}}_2(\text{H}_2\text{O})(\text{OH})(\text{ZnW}_9\text{O}_{34})_2]^{11-}$ ”, to what is actually a physical mixture of the $\text{Ru}(\text{II})(\text{DMSO})_4\text{Cl}_2$ and $\text{WZn}_3(\text{H}_2\text{O})_2(\text{ZnW}_9\text{O}_{34})^{12-}$ starting materials.¹⁵¹ Therefore, additional characterization and stability studies are needed to provide stronger evidence for both the purity and precise nature of the starting complex, as well as for the true catalyst.

In addition to the multi-Ru POMs described above, single-site ruthenium POMs have also been studied as water oxidation precatalysts. One of the most thorough investigations of a mono-ruthenium POM starting materials was completed by Murakami et al. where 0.3 mM $[\text{Ru}(\text{H}_2\text{O})\text{SiW}_{11}\text{O}_{39}]^{5-}$ or $[\text{Ru}(\text{H}_2\text{O})\text{GeW}_{11}\text{O}_{39}]^{5-}$ (Figure 2.5, vide supra for their structure) was combined with 6.0 mM Ce(IV) oxidant to produce O_2 in up to 90 % yields.⁷⁶ Characterization of Ru(III), Ru(IV), and Ru(V)-POM intermediates included pH dependent electrochemical studies, EPR, resonance Raman, and UV-vis spectroscopy (Figure 2.11). Significantly, addition of two or more Ce(IV) equivalents to the starting POM resulted in the formation of a proposed $[\text{Ru}(\text{O})\text{GeW}_{11}\text{O}_{39}]^{5-}$ species. Kinetic analyses were also conducted and indicate that O_2 evolution kinetics: (i) are first order in the Ru(V)=O species (i.e., the proposed catalyst resting state under oxidizing conditions), (ii) saturate in $[\text{Ce}(\text{IV})]$, and (iii) are nearly zero order in $[\text{H}^+]$ (although a slight inverse dependence is observed). Multiple controls also support the conclusion of a homogeneous POM WOC, including a lack of O_2 evolution activity when RuCl_3 , $\text{Ru}(\text{acac})_3$ or $[\text{SiW}_{11}\text{O}_{39}]^{8-}$ were tested as precatalysts. Perhaps the only remaining experiment still needed is to quantify the stability of $[\text{Ru}(\text{H}_2\text{O})\text{SiW}_{11}\text{O}_{39}]^{5-}$ and $[\text{Ru}(\text{H}_2\text{O})\text{GeW}_{11}\text{O}_{39}]^{5-}$ during and after the catalytic run.

Sadakane and co-workers also investigated $[\text{Ru}(\text{H}_2\text{O})\text{SiW}_{11}\text{O}_{39}]^{5-}$ and $[\text{Ru}(\text{H}_2\text{O})\text{GeW}_{11}\text{O}_{39}]^{5-}$ as well as $[\text{Ru}(\text{H}_2\text{O})\text{PW}_{11}\text{O}_{39}]^{4-}$ ($[\text{POM}] = 0.3 \text{ mM}$) with 30 mM Ce(IV) oxidation in 0.1 M HNO_3 ;^{84,123} approximately quantitative conversion of Ce(IV) into O_2 was observed over 2 hours. These authors did not observe significant O_2 production in control experiments with a variety of precursors, including $[\text{Ru}(\text{benzene})\text{Cl}_2]_2$, $[\text{PW}_{11}\text{O}_{39}\{\text{Ru}(\text{II})(\text{benzene})(\text{H}_2\text{O})\}]^{5-}$, or $[\text{K}_7\text{PW}_{11}\text{O}_{39}]$ plus $[\text{Ru}(\text{benzene})\text{Cl}_2]_2$. Controls with $\text{RuCl}_2(\text{DMSO})_4$, $[\text{K}_7\text{PW}_{11}\text{O}_{39}]$ or $\text{RuCl}_2(\text{DMSO})_4$ plus $[\text{K}_7\text{PW}_{11}\text{O}_{39}]$ had O_2 evolution induction

periods of a half-hour and produced approximately three times less O₂ than [Ru(H₂O)PW₁₁O₃₉]⁴⁻. Although the studies of Sadakane did not report any other experiments directly relevant to identifying the true catalyst in their ruthenium POM solutions, it seems plausible that the catalyst is homogeneous since these authors used similar HNO₃ electrolyte and Ce(IV) oxidant conditions comparable to the more extensive studies of Murakami et al.⁷⁶

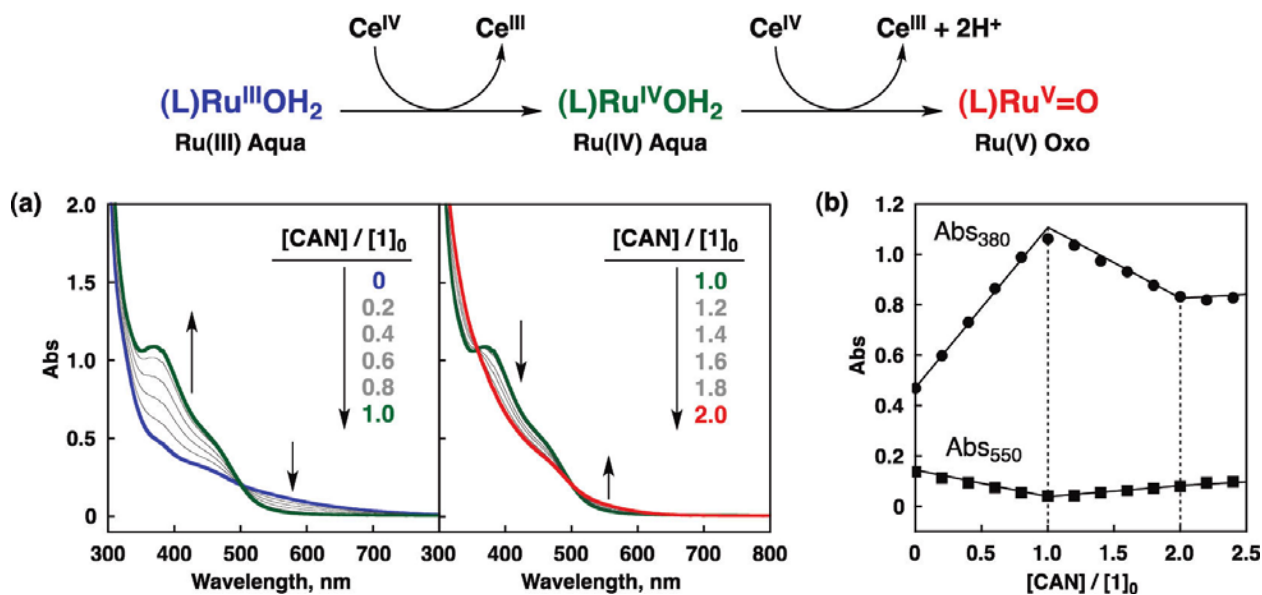


Figure 2.11. (a) UV-vis spectroscopy of 0.3 mM [Ru(H₂O)SiW₁₁O₃₉]⁵⁻ upon addition of 0 to 2.5 equivalents of Ce(IV) (i.e., CAN) oxidant. (b) Absorbance changes at 380 nm and 550 nm plotted as a function of added Ce(IV) equivalents. Coupled with the complementary methods of EPR, resonance Raman, and electrochemical techniques, this example data provides good evidence for a homogeneous POM WOC. This figure is reproduced with permission from Ref 76.

In summary of this section, Ru-POM water oxidation precatalysts have been studied relatively thoroughly compared to other transition-metal-based POM precursors. Two traits have contributed to this improved understanding. First, ruthenium POMs appear to be more stable than first row transition metal analogs. This increased stability has allowed the ruthenium POMs to be examined using Ce(IV) oxidation in acidic (pH 1 or less) solution; Ce(IV) supplied generally as [Ce(NO₃)₆](NH₄)₂, also appears to cause less problems with precipitation compared to a Ru(bpy)₃³⁺ oxidant as one might expect from their respective charges. This makes *in-situ*

and even *in operando* characterization of ruthenium POMs feasible. The second characteristic which makes ruthenium POMs easier to study is the rich redox chemistry of the active site. Because multiple, reversible electron/proton transfers occur prior to onset of catalytic activity, these reaction intermediates can be studied and characterized in detail. Despite these advantages, there is clearly a shift in the recent literature toward studying catalysts which incorporate earth abundant elements—one important trait which ruthenium does not possess.

Manganese

Non-POM Manganese Precatalysts

Homogeneous complexes containing manganese have been studied extensively due to their potential relationship with the biological water oxidation catalyst of photosystem II which contains a Mn_4 active site. An $L_6Mn_4O_4$ complex ($L =$ diphenylphosphate anion) is one of the few complexes which has been reported to be both a structural and catalytic mimic of the photosystem II active site.^{152,153} Subsequently, Hocking et al. used a combination of EXAFS/XANES, multiple Mn^{2+} starting material controls, and HRTEM to provide strong evidence that a heterogeneous manganese(III/IV) oxide catalyst is formed within the Nafion membrane upon oxidation of the $L_6Mn_4O_4$ starting material.¹⁵⁴ Interestingly, reduction of the heterogeneous MnO_x results in the disappearance of the nanoparticles that are formed concomitant with what appears to be homogeneous $[Mn(OH_2)_6]^{2+}$. In other words, manganese WOCs can cycle between heterogeneous catalysts and homogeneous resting states.

Decomposition of homogeneous manganese coordination complexes, including $(bpy)_2Mn(\mu-O)_2Mn(bpy)_2$ and $Mn(phen)_3^{2+}$ has also been described when using Ce(IV) oxidation. When the manganese complexes were combined with Ce(IV) in aqueous solution, a mixture of soluble Mn(III), soluble MnO_4^- , and heterogeneous MnO_x were formed although no

O₂ was detected.¹⁵⁵ The colloidal MnO_x was characterized by XPS, IR, DLS, TEM, and UV-vis. However, when (bpy)₂Mn(μ-O)₂Mn(bpy)₂ was supported on clay followed by Ce(IV) addition, O₂ evolution was observed; post-reaction IR, XPS, SEM and XRD characterization indicated the formation of heterogeneous MnO₂ and MnO materials concomitant with loss of the organic bpy ligands. These studies indicate the potentially high instability of manganese complexes to oxidizing conditions.

Manganese POM Precatalysts

All three of the manganese polyoxometalate studies which report water oxidation catalysis are electrochemically driven. It should also be noted that none of these studies quantify O₂ production since this was not the primary focus of these reports; therefore, the reaction being studied is not known definitively for these Mn-POMs. Despite this shortcoming, the techniques used in these studies are relevant to distinguishing between homogeneous and heterogeneous electrocatalysts and are therefore included in the present review.

In 2007, Keita et al. reported the synthesis and electrochemical activity of a [(Mn(III)(H₂O))₃(SbW₉O₃₃)₂]⁹⁻ complex.⁸⁷ Cyclic voltammetry studies at a glassy carbon electrode show a reversible Mn(III/IV) redox process followed by an irreversible wave at 1.345 V vs SCE which is attributed to catalytic water oxidation by a Mn(V) complex. Scan rate dependent voltammetry suggests that some of the Mn(III/IV) oxidation is due to adsorbed [(Mn(III)(H₂O))₃(SbW₉O₃₃)₂]⁹⁻. Multiple scans of the POM up to 1.5 V results in a continually increasing catalytic wave, while the Mn(III/IV) waves increase only slightly and stabilize after three scans. Due to the complexity of the electrochemical response, the authors used electrochemical quartz crystal microbalance (EQCM) experiments to gain insights into the possibility of MnO_x formation under oxidizing conditions. Consistent with their cyclic

voltammetry results, the POM in the Mn(IV) oxidation state adsorbs to the electrode while reduction to the Mn(II) state results in desorption in the majority, but not all, of the electrode-bound film. The authors suggest this residual film may correspond to MnO_x and is likely responsible for the water oxidation activity. Additional surface characterization was not conducted, however. Even though the identity of the true WOC remains unknown in the case of $[(\text{Mn(III)(H}_2\text{O)})_3(\text{SbW}_9\text{O}_{33})_2]^{9-}$, the use of EQCM should prove to be a very useful technique for detecting heterogeneous electrocatalysts.

Two other electrocatalytic water oxidation studies have been reported when starting with manganese POMs. Cyclic voltammetry of $[\text{Mn(III)}_3(\text{H}_2\text{O})_5(\text{A-}\alpha\text{-PW}_9\text{O}_{er})_2]^{9-}$,⁸⁸ which is structurally similar to $[(\text{Mn(III)(H}_2\text{O)})_3(\text{SbW}_9\text{O}_{33})_2]^{9-}$, shows an apparently catalytic oxidation wave at ~ 1.1 V vs SCE, proposed by the authors to be water oxidation, but was not investigated further. A catalytic oxidation wave is also observed in $[\text{Mn}_{19}(\text{OH})_{12}(\text{SiW}_{10}\text{O}_{37})_6]^{34-}$ solutions and exhibits a current-overpotential slope of 135 mV/decade with as little as 330 mV of overpotential.⁸⁹ Oxidation of $[\text{Mn}_{19}(\text{OH})_{12}(\text{SiW}_{10}\text{O}_{37})_6]^{34-}$ also results in the formation of a thin film on the electrode.

In summary of this section, an important feature of these Mn POMs is that they operate at moderate to low overpotentials and they incorporate earth abundant catalytic centers. Hence, further characterization of both the POM stability, as well as any in-situ formed films, is of interest for all of these manganese POMs.

Molybdenum

There are no other proposed homogeneous (or to our knowledge heterogeneous) molybdenum WOCs. This is not surprising since molybdenum oxide or polyoxomolybdates typically contain the metal in its highest oxidation state (VI) and the (VI/V) reduction potentials

are well below the reversible water oxidation potential. In other words, there is no obvious mechanism for oxidizing water when starting with a molybdenum(VI)-oxo species.

Given the lack of (non-POM-based) Mo WOCs, the cases and claims of molybdenum POMs acting as water oxidation catalysts is something of a curiosity. Hence, there is an additional burden of proof for researchers claiming Mn POM, or for that matter any Mo-based WOC, be it potentially homogeneous or heterogeneous catalysis.

Molybdenum POM Precatalysts

One study which claims Mo-POM WOCs begins with insoluble POM-Ru(phen)₃²⁺ salts including [Ru(II)(phen)₃(CH₃OH)(Mo₆O₁₉)], [Ru(II)(phen)₃(C₂H₈N₂)(C₃H₇NO)(Mo₅S₂O₂₃)], and [(Ru(II)(phen)₃)₂(CH₃CN)₂(Mo₈O₂₆)].¹⁵⁶ In the presence of light and 10 mM S₂O₈²⁻, 10 μM POM:photosensitizer suspensions produce O₂ for up to 12 hours without significant changes in activity. PXRD of the materials before and after photocatalysis provide evidence that no significant changes to the bulk of the material occur, although this method would not detect amorphous surface catalysts. To test their hypothesis of a HO• radical-based reaction mechanism, the authors added hydroquinone which is a radical scavenger. In the presence of hydroquinone, [Ru(II)(phen)₃(CH₃OH)(Mo₆O₁₉)] produces no O₂ under an otherwise standard photochemical reaction. Although the lack of O₂ in this experiment is consistent with a radical mechanism, it is also possible that hydroquinone is simply easier to oxidize than water and therefore reacts preferentially. Additionally, if a radical mechanism involving HO• is invoked, the authors should also rule out the possibility that the sulfate radical anion (SO₄•⁻)—a byproduct of this particular photochemical system—is not involved directly in the reaction. This problem could be addressed by using ¹⁸O labeled water to verify the source of oxygen in the product O₂. Due to the unprecedented nature of molybdenum WOCs, the most likely WOC involves the Ru(phen)₃³⁺.

Lay et al. and Creutz and Sutin have proposed water oxidation mechanisms when starting solely with ruthenium polypyridyl complexes to account for O₂ evolved in the absence of other WOCs.^{157,158} Determining the catalyst in this case should therefore rely on understanding the stability and speciation of both the POM and photosensitizer materials under the reaction conditions.

Another study of water oxidation catalysis beginning with molybdenum POMs, which arguably could also be classified as a cobalt POMs, uses [Co(III)Mo₆O₂₄H₆]³⁻ and [Co(III)₂Mo₁₀O₃₈H₄]⁶⁻.¹⁰⁵ These POMs are considered molybdenum POMs for the purposes of this review because the cobalt atoms are internal, core cobalts and contain no terminal aquo, hydroxo, or oxo ligands. Hence, if these intact POMs are indeed homogeneous WOCs, then the oxygen atoms in the O₂ product should not have been coordinated to the cobalt. Photochemical water oxidation with 1-20 μM [CoMo₆O₂₄H₆]³⁻ and [Co₂Mo₁₀O₃₈H₄]⁶⁻ was investigated in the presence of 0.06 mM Ru(bpy)₃²⁺, 3.0 mM S₂O₈²⁻, and illumination from a 300 W xenon lamp; yields of up to 25% and 20% conversion of persulfate into O₂ are observed. As with other POMs, evidence for POM:Ru(bpy)₃²⁺ precipitation includes saturation kinetics in the O₂ evolution rate beginning at ~10 μM [CoMo₆O₂₄H₆]³⁻ and 5 μM [Co₂Mo₁₀O₃₈H₄]⁶⁻. DLS also showed the presence of particles when 40 μM [Co₂Mo₁₀O₃₈H₄]⁶⁻ was combined with 60 μM [Co₂Mo₁₀O₃₈H₄]⁶⁻, but not at lower concentrations. Other DLS experiments did not detect particles in standard post-reaction solutions of [CoMo₆O₂₄H₆]³⁻ or [Co₂Mo₁₀O₃₈H₄]⁶⁻ which had been illuminated for 30 s (i.e., ~1/20th the length of normal photochemical reactions). A control using 10 μM Co(NO₃)₂ under otherwise standard photochemical conditions resulted in the formation of 10-100 nm particles, which were characterized by DLS after 30 s of illumination. No other characterization of these nanoparticles was reported, although literature precedent

suggests they are likely CoO_x materials.^{133,134} In another control experiment $20 \mu\text{M Co(NO}_3)_2$ evolved 7-8 times less O_2 than $[\text{CoMo}_6\text{O}_{24}\text{H}_6]^{3-}$ or $[\text{Co}_2\text{Mo}_{10}\text{O}_{38}\text{H}_4]^{6-}$ during a standard 30 minute photolysis. It would be interesting to test other, lower concentrations of $\text{Co(NO}_3)_2$ in this system since others have observed an O_2 evolution activity *which can depend inversely on the precursor Co^{2+} concentration*.¹²¹ Determining the correct $\text{Co(NO}_3)_2$ control in this and other systems ultimately relies on knowing the stability/speciation of the $[\text{CoMo}_6\text{O}_{24}\text{H}_6]^{3-}$ or $[\text{Co}_2\text{Mo}_{10}\text{O}_{38}\text{H}_4]^{6-}$ materials *in operando*, something missing from the above, intriguing system.

Iridium

Non-POM Iridium Precatalysts

The current iridium WOC literature is divided as to whether homogeneous iridium complexes are active WOCs or whether they decompose into heterogeneous IrO_x . Initially, a number of IrCp and IrCp^* complexes were reported as homogeneous WOCs.^{159,160,161,162} Then, in 2010 Grotjahn and co-workers published a pivotal study which found that many of these iridium complexes are initially not active WOCs;¹⁶³ instead, greater than 5 equivalents of Ce(IV) are needed to form an active WOC. *In operando* UV-vis of the Ir complexes plus Ce(IV) is also consistent with the evolution of catalytically active IrO_x materials during the reaction. Lastly, ex-situ STEM/EDX revealed the presence of Ir-rich nanoparticles contained in a ceria matrix. Although the true catalyst continues to be debated in iridium plus Ce(IV) systems,^{164,165} the study of Grotjahn et al. provides excellent precedent for the in-situ formation of IrO_x nanoparticles in at least certain cases.

Electrochemical studies by Crabtree and co-workers have also investigated distinguishing homogeneous and heterogeneous iridium water oxidation catalysis.^{166,167} Investigation of $[\text{Cp}^*\text{Ir(H}_2\text{O)}_3]^{2+}$ and $[\text{Cp}^*\text{Ir(2-(2'-pyridyl)-2-proponolate)Cl}]$ using an electrochemical quartz

crystal nanobalance (EQCN) showed that at oxidizing potentials (up to 1.5 V vs NHE) the $[\text{Cp}^*\text{Ir}(\text{H}_2\text{O})_3]^{2+}$ complex electrodeposited a catalytically active, amorphous IrO_x film onto the electrode which contains ~9% carbon (by EDX); no measureable iridium oxide was deposited onto the electrode for the other iridium complex.^{166,167} Therefore, the authors concluded that this EQCN technique can distinguish homogeneous and heterogeneous iridium catalysts, a conclusion with which we concur.

$[(\text{IrCl}_4)\text{KP}_2\text{W}_{20}\text{O}_{72}]^{7-}$ Precatalyst

The only example of an iridium polyoxometalate precursor in water oxidation catalysis was reported by Cao et al. in 2009.⁷⁷ When 0.02 mM $[(\text{IrCl}_4)\text{KP}_2\text{W}_{20}\text{O}_{72}]^{7-}$ is combined with 1.4 mM $\text{Ru}(\text{bpy})_3^{3+}$ oxidant at pH 7.2, O_2 yields of up to 30% were observed. In comparison, a control with an equivalent amount of IrCl_3 yielded 38% O_2 under otherwise identical conditions. Instability of the starting POM was also observed in the pH 7.2 electrolyte by UV-vis spectroscopy, the iridium dissociating completely from $[(\text{IrCl}_4)\text{KP}_2\text{W}_{20}\text{O}_{72}]^{7-}$ within 24 hours. Stability of the complex under the reaction conditions was not reported, however. The authors conclude that although the starting POM could be a catalyst, they cannot disprove the possibility of *in-situ* formation of heterogeneous IrO_2 nanoparticle catalysis. Indeed, the combination of $[(\text{IrCl}_4)\text{KP}_2\text{W}_{20}\text{O}_{72}]^{7-}$ instability and kinetic competence of the IrCl_3 control is most consistent with an *in-situ* formed IrO_x WOC.

Nickel

Non-POM Nickel Precatalysts

Oxidative conversion of aqueous nickel(II) salts and nickel coordination complexes into heterogeneous NiO_x WOCs has been reported by Spiccia and co-workers.^{168,169} These studies use a variety of starting materials including $\text{Ni}(\text{en})_3^{2+}$, $\text{Ni}(\text{NH}_3)_6^{2+}$, $\text{Ni}(\text{tacn})_2^{2+}$, $\text{Ni}(\text{tacn})(\text{OH}_2)_3^{2+}$, and

Ni(cyclen)(OH₂)₂²⁺ which were oxidized at FTO electrodes to form the nickel oxide films when the potential is scanned up to 1.3 V vs Ag/AgCl in pH 9.2 sodium borate buffer.

EXAFS/XANES, SEM, Raman, and EDX characterization of the films indicate the NiO_x materials were similar to other NiOOH catalytic materials. Interestingly, if the electrode potential is scanned only up to 0.85 V vs NHE (i.e., past the first oxidation wave, but prior to catalytic water oxidation) no measurable NiO_x is formed for any of the complexes (except for controls with Ni(OH₂)₆²⁺). *This result indicates that stability of a complex prior to catalysis does not guarantee its stability under more oxidizing conditions—a point which is frequently overlooked in the POM WOC literature.* Another relevant finding in these studies is the observation of increasing electrocatalytic activity with increasing electroactive surface area of the NiO_x films. Although surface-area-dependent activity is well known in heterogeneous catalysis, this result reinforces the need to consider and account for the effect of solid catalyst's surface area and numbers of active sites in control experiments aimed at ruling out, or supporting, the presence of heterogeneous WOCs.

[Ni₅(OH)₆(OH₂)₃(Si₂W₁₈O₆₆)]¹²⁻ Precatalyst

A 2010 report by Zhu et al. describes the synthesis of the penta-nickel POM, [Ni₅(OH)₆(OH₂)₃(Si₂W₁₈O₆₆)]¹²⁻, and tests it as a WOC starting material.⁷⁸ As was observed for several other POMs, DLS shows the formation of 700-1300 nm particulate precipitate when [Ni₅(OH)₆(OH₂)₃(Si₂W₁₈O₆₆)]¹²⁻ and Ru(bpy)₃²⁺ are combined. If this POM:Ru(bpy)₃²⁺ is filtered from the solution, the filtrate produces no O₂ when testing under standard photochemical conditions (455 nm light, 1.0 mM Ru(bpy)₃²⁺, and 5.0 mM S₂O₈²⁻). Controls using Ni(NO₃)₂ showed that filtration followed by standard photochemical testing did result in O₂ evolution—evidence against Ni²⁺ leaching from the Ni-POM prior to catalysis. The pre-catalytic stability of

$[\text{Ni}_5(\text{OH})_6(\text{OH}_2)_3(\text{Si}_2\text{W}_{18}\text{O}_{66})]^{12-}$ was also followed by UV-vis spectroscopy, DLS, and IR (after crystallization from pH 8 solution) and showed no apparent changes upon aging in pH 8 borate buffer in experiments which lasted up to 12 hours or 2 years.

Evidence consistent with the $\{[\text{Ni}_5(\text{OH})_6(\text{OH}_2)_3(\text{Si}_2\text{W}_{18}\text{O}_{66})]^{12-}\}:[\text{Ru}(\text{bpy})_3^{2+}]$ precipitate stability under the photochemical reaction conditions includes three FTIR experiments:⁷⁸ (1) characteristic POM IR peaks are present both before and after photo-catalysis; (2) nickel hydroxide controls show IR bands at 525 and 3640 cm^{-1} both as an isolated material and when mixed with the Ni-POM in a 9:1 molar ratio; (3) the post reaction IR shows no evidence of the nickel hydroxide bands. Although these experiments are good initial tests, it is not clear whether the nickel hydroxide ($\text{Ni}(\text{OH})_2$) control (which was prepared by precipitation of aqueous nickel(II) using KOH) would show the same IR stretches of oxidatively prepared Ni(III)OOH. The authors also assumed that if a NiOOH-containing nanoparticle was formed, that it would be isolated by the centrifugation isolation method and therefore observable in the FTIR spectrum. An alternative explanation is that the catalyst remains in the supernatant.

The authors final argument for a homogeneous nickel POM WOC is that the kinetic traces for photochemical O_2 evolution and dark $\text{Ru}(\text{bpy})_3^{3+}$ reduction (i.e., where the reaction is driven by addition of the ruthenium(III) oxidant in the dark) are similar and the O_2 yields have the same trend for light-driven and dark reactions.⁷⁸ Unfortunately there are at least two possible gaps in this argument. First, O_2 evolution and oxidant loss kinetics can only be rigorously compared when the O_2 yield is near 100% since one cannot know what portion of the oxidant loss corresponds to O_2 evolution, and what portion corresponds to side-oxidation reactions. Second, an observation of increasing O_2 yields with increasing [Ni-POM] for both light and dark reactions only requires that the amount of catalyst increases for both these systems when more

starting material is used; that is, increasing O₂ evolution rates do not indicate the true catalyst unless they can be correlated with a precise compound/species under the reaction conditions.

Summary

Analysis of the WOC literature which uses POM precatalysts reveals several important insights:

- The majority of studies examine the stability of the starting POM prior to catalysis and then infer the stability of the catalyst under the reaction conditions. *In operando* quantitative stability, with error limits, and speciation studies are badly needed.
- With two exceptions,^{79,81} the studies which do address whether the POM is present at the end of the reaction do not quantify the stability; instead these studies rely on FTIR, ³¹P-NMR, and PXRD to show the qualitative stability of the POM. Thus, the hypothesized superior stability of POMs under water oxidation conditions has yet to be supported by concrete evidence since the two quantitative studies available at present^{79,81} actually report POM *instability*.
- Although *in-situ* tests for particles such as DLS and SAXS are useful, one should also be aware of and report the detection limit of the particles one is attempting to detect when these techniques are used to provide evidence against nanoparticles in the solution.
- *Control experiments are critical to distinguishing homogeneous and heterogeneous WOCs and are greatly underutilized at present.* In order to compare a heterogeneous control to a homogeneous precursor, one should also know the approximate number of active sites/surface area of the heterogeneous control catalyst as well as its concentration dependence in the observed kinetics.

- Understanding the water oxidation kinetics of all possible forms of the catalyst is crucial to determining which catalyst is active in a particular system.
- Reaction conditions can play an important role in determining the identity of the dominant WOC especially when working with only quasi-stable POMs.
- Electrochemical studies have several advantages over chemical/photochemical oxidation methods including:
 - Many of the solubility issues associated with $\text{Ru}(\text{bpy})_3^{3+}$ or $\text{Ce}(\text{IV})$ oxidants can be avoided since the concentration and identity of the electrolyte can be chosen to maximize POM solubility.
 - Fewer side oxidation reactions are observed in electrochemical systems relative to the common ligand oxidation reactions associated with the $\text{Ru}(\text{bpy})_3^{3+}$ oxidant.
 - If heterogeneous materials are deposited onto the electrode during the reaction, they can be easily isolated from the starting POM solution and can be characterized by a variety of methods including SEM/EDX, XPS, IR.
 - The electrochemical potential/driving force for the reaction can be easily varied in order to determine kinetic parameters and compare different catalysts/controls.
- Chemical oxidation methods have the benefit of interacting with the entire solution instead of only the portion that reaches the electrode/solution interface. That said, there is a pressing need for an uncharged or anionic oxidant that yields a stable, readily identified and quantitated, reduced-oxidant product.
- In comparison to the broader WOC literature, knowledge of the true catalyst when beginning with POMs is lagging and can be quite challenging in part due to the solubility/stability problems associated with the use of chemical oxidation methods.

Again, either new, non-cationic oxidants are needed, or electrochemical oxidation methods should be utilized.

- Conceptually solving the “is it homogeneous or heterogeneous catalysis?” question is as simple or as complex as (i) having complete speciation of the precatalyst under the reaction conditions, and then (ii) knowing the kinetic contribution of each species formed. Practically, however, this is much harder than it sounds, especially when micromolar to nanomolar amount of leached metal can form competent catalysts.^{66,67,81}
- Finally, “catalysis is [...] a kinetic phenomenon”. This, in turn, means that rigorous, unequivocal identification of the true catalyst for any catalytic reaction is impossible without the requisite kinetic studies. An important corollary here is that a comparison of TOFs, without knowledge of the underlying rate laws, will tend to be a comparison of mechanisms, conditions, and terms in the rate law, or worse, both.^{170,171} A summary of the POM WOC precatalyst studies is provided in Table 2.1.

Due to the challenges associated with determining the homogeneity or heterogeneity of water oxidation catalysts, development of methods aimed at answering this fundamentally important problem will continue to be highly relevant. Understanding the fundamental properties that control catalyst activity, stability, and lifetime, will assist in developing future water oxidation catalysts capable of the stringent requirements needed for sustainable energy storage.

Table 2.1. Summary of experiments relevant to distinguishing homogeneous and heterogeneous WOCs when using POM precatalysts.

POM	Oxidant, Electrolyte ^a	Experiments Relevant to Distinguishing Homogeneous and Heterogeneous Catalysis	Ref.
[Co ₄ (H ₂ O) ₂ (PW ₉ O ₃₄) ₂] ¹⁰⁻	hv, Ru(II)(bpy) ₃ ²⁺ , Na ₂ S ₂ O ₈ in pH 8, NaBi	No particles observed by dynamic lights scattering or Tyndall effects, under conditions of 1 mM Ru(bpy) ₃ ²⁺ , 160 mM NaBi, pH 8, 5 μM Co ₄ POM, 5 mM Na ₂ S ₂ O ₈ . Sequential photochemical runs, where additional Na ₂ S ₂ O ₈ was added between runs, showed a ~20% decrease in O ₂ yield.	104

POM	Oxidant, Electrolyte ^a	Experiments Relevant to Distinguishing Homogeneous and Heterogeneous Catalysis	Ref.
$[\text{Co}_4(\text{H}_2\text{O})_2(\text{PW}_9\text{O}_{34})_2]^{10-}$	Ru(III)(bpy) ₃ ³⁺ in pH 8.0, NaPi and NaBi	No UV-vis or ³¹ P-NMR changes observed over 1 month at pH 8. Aging Co ₄ POM for 3 days did not decrease the O ₂ yield whereas controls with aged Co(NO ₃) ₂ decreased to 33.6 % O ₂ yield. In postreaction solution (where Ru(bpy) ₃ ²⁺ had been precipitated by addition of sodium tetraphenylborate), the ³¹ P-NMR spectrum showed the presence of the Co ₄ POM. CV of Co ₄ POM plus Ru(bpy) ₃ ²⁺ both before and after reaction with Ru(bpy) ₃ ³⁺ shows a oxidative wave which changes only slightly; controls with Co(NO ₃) ₂ showed a decrease in the post-reaction CV (which likely contained CoO _x plus the Ru(bpy) ₃ ²⁺) compared to the pre-reaction CV. When Co ₄ POM is precipitated from the post-reaction solution by addition of Ru(bpy) ₃ ²⁺ , the IR is consistent with the Co ₄ POM being present in the precipitate. Addition of 2,2'-bipyridine to the 3.2 μM Co ₄ POM decreased the O ₂ yield from 67 to 48% and decreased the O ₂ yield for 13 μM Co(NO ₃) ₂ controls from 80 to 0%. No O ₂ was observed for Co ₄ POM at pH 6.2 but Co(NO ₃) ₂ showed a yield of 35%. Redissolution of the Ru(bpy) ₃ ²⁺ -Co ₄ POM precipitate and addition of Ru(bpy) ₃ ³⁺ showed an O ₂ yield of 49%.	65
$[\text{Co}_4(\text{H}_2\text{O})_2(\text{PW}_9\text{O}_{34})_2]^{10-}$	hv, Ru(II)(bpy) ₃ ²⁺ , Na ₂ S ₂ O ₈ in pH 8, NaPi	Co(NO ₃) ₂ flash photolysis controls reportedly do not show any observed particles by light scattering. CV of Co ₄ POM solutions show an anodic peak at ~1.2 V vs Ag/AgCl which increases with aging time and an irreversible wave is observed above ~1.3 V. Flash photolysis showed increasing activity of Ru(bpy) ₃ ³⁺ quenching by Co ₄ POM solutions with aging of the Co ₄ POM solutions—the maximum activity corresponds to ~20% of the initial [Co ₄ POM] which is reached in about 90 minutes of aging. Controls with Co(NO ₃) ₂ were reported to consume the photo-generated Ru(bpy) ₃ ³⁺ on a longer timescale.	85
$[\text{Co}_4(\text{H}_2\text{O})_2(\text{PW}_9\text{O}_{34})_2]^{10-}$	Electrochem. 1.14 V vs Ag/AgCl, Glassy Carbon in pH 8, NaPi	Linear sweep voltammetry shows increasing anodic wave at ~1.05 V with aging over 3 hours. This increasing current occurs concomitantly with a 4.3±0.6 % decrease in the 580 nm absorbance of Co ₄ POM and a 58±2 μM increase in the apparent aqueous [Co ²⁺] which was measured by two methods. Bulk electrolysis of the Co ₄ POM solution at 1.14 V vs Ag/AgCl (without aging) results in the deposition of a catalytically active film. The electrodeposited film was removed from the Co ₄ POM solution and placed into a POM-free solution and maintains all its water oxidation activity. Also, this film contains Co, P, Na, and O as determined by EDX (i.e., no W as would be expected if the film contained the Co ₄ POM). Bulk electrolysis of the Co ₄ POM solution at 1.14 V vs Ag/AgCl (without aging) results in an increasing catalytic current with time. Catalytic controls with a 500 μM Co ₄ POM solution (aged for 3 hours) and a 58 μM Co(NO ₃) ₂ solution showed quantitatively identical water oxidation activity (101±12%) during a 5 minute bulk electrolysis at 1.14 V vs Ag/AgCl.	66
$[\text{Co}_4(\text{H}_2\text{O})_2(\text{PW}_9\text{O}_{34})_2]^{10-}$	Electrochem. 1.4 V vs Ag/AgCl, Glassy Carbon in pH 5.8-8.0 NaPi	Co ₄ POM cyclic voltammograms show onset of an oxidation wave above ~1.25 V vs Ag/AgCl, whereas controls with CoO _x show a catalytic wave onset of ~1.05 V. The Co ₄ POM wave saturates at concentration of ~5 μM Co ₄ POM. The [Co ²⁺] _{apparent} in 2.5 μM Co ₄ POM solutions increases to 0.25 μM during a 1 hour aging experiment at pH 8. The [Co ²⁺] also increases by 50±34 μM during the electrolysis. Repeated bulk electrolysis (for 60s at 1.4 V vs Ag/AgCl, repeated three times on the same solution) resulted in a [Co ²⁺] = 825 nM. Comparison of the pre- and post-reaction Co ₄ POM solutions revealed that during a 60 s bulk electrolysis, the [Co ₄ POM] decreases by 2.7±7.3% and 9.4±5.1% at pH 8.0 and 5.8. The Co ₄ POM solutions and CoO _x -coated electrodes show a pH-oxidation wave dependence of -36 and -66 mV/pH unit (i.e., for each pH unit increase, the oxidation wave moves by 36 and 66 mV to a more negative potential, respectively). Bulk electrolysis controls at 1.4 V vs Ag/AgCl using the predetermined amount of Co ²⁺ (i.e., 0.2 μM) do not account for the observed water oxidation activity in Co ₄ POM solutions. Controls with deposited CoO _x reveal that 0.45-0.58 nmols and 1.0-1.5 nmols of CoO _x , at pH 8.0 and 5.8, could account for observed activity in Co ₄ POM solutions.	81

POM	Oxidant, Electrolyte ^a	Experiments Relevant to Distinguishing Homogeneous and Heterogeneous Catalysis	Ref.
$[\text{Co}_4(\text{H}_2\text{O})_2(\text{PW}_9\text{O}_{34})_2]^{10-}$	Ru(III)(bpy) ₃ ³⁺ and hv, Ru(II)(bpy) ₃ ²⁺ , Na ₂ S ₂ O ₈ in NaPi and NaBi pH 6.2-9	The dissociated $[\text{Co}^{2+}] = 0.07 \mu\text{M}$ starting with $2 \mu\text{M}$ Co ₄ POM in pH 8 sodium borate, as determined by stripping voltammetry and ICP-MS. UV-vis showed Co ₄ POM has lower stability in phosphate buffer compared to borate buffer. DLS of post-photocatalytic Co ₄ POM reactions showed no observable particles whereas controls using Co(NO ₃) ₂ precursors did show particles. Extraction of the post-photocatalytic POM solution with toluene/THpANO ₃ resulted in complete loss of activity. Control extractions showed that extraction before POM addition and photocatalysis did not affect O ₂ evolution. Control with Co ²⁺ did not extract the Co ²⁺ or affect subsequent photocatalysis. Kinetics using either $2 \mu\text{M}$ Co ₄ POM or $0.1 \mu\text{M}$ Co(NO ₃) ₂ plus $2 \mu\text{M}$ Co ₄ POM showed the same Ru(bpy) ₃ ³⁺ loss rate within 5%. A control with $0.5 \mu\text{M}$ showed the same or slower Ru(bpy) ₃ ³⁺ loss rate compared to $2 \mu\text{M}$ Co ₄ POM. A photocatalytic control with $0.15 \mu\text{M}$ Co(NO ₃) ₂ produced the same amount of O ₂ as a control with no catalyst. A photocatalytic control with $2 \mu\text{M}$ Co(NO ₃) ₂ gave an O ₂ yield = $40.8 \pm 0.5\%$ compared to $2 \mu\text{M}$ Co ₄ POM which gave a $24.2 \pm 0.1\%$ yield. Multiple other Co(NO ₃) ₂ and CoO _x controls were conducted.	67
$[\text{Co}_4(\text{H}_2\text{O})_2(\text{PW}_9\text{O}_{34})_2]^{10-}$	Ru(III)(bpy) ₃ ³⁺ in pH 7.2, NaPi	A $[\text{Ru}(\text{bpy})_3^{2+}]_3[\text{Co}_4(\text{H}_2\text{O})_2(\text{PW}_9\text{O}_{34})_2]^{10-}$ precipitate is formed with a $K_{sp} = (8 \pm 7) \times 10^{-25} \text{ M}^5$. Co(NO ₃) ₂ controls show a first order dependence on precursor concentration while Co ₄ POM shows $[\text{Co}_4\text{POM}]^{1-9}$ kinetics with respect to the initial POM concentration; this behavior is consistent with Co ₄ POM being removed from solution via a $[\text{Ru}(\text{bpy})_3^{2+}]_3[\text{Co}_4(\text{H}_2\text{O})_2(\text{PW}_9\text{O}_{34})_2]^{10-}$ precipitate. The initial rate of 2,2'-bipyridine ligand oxidation followed the same trends as the initial water oxidation rate for Co ₄ POM solutions, but was independent of the initial $[\text{Co}(\text{NO}_3)_2]$ in control experiments. That is, Co ₄ POM solutions appear to catalyze ligand oxidation whereas Co(NO ₃) ₂ solution do not. Controls with Co(NO ₃) ₂ showed decreasing yields with increasing Ru(bpy) ₃ ³⁺ :Co ²⁺ (54-18%) whereas the Co ₄ POM shows increasing O ₂ yields with increasing Ru(bpy) ₃ ³⁺ :Co ₄ POM ratios which peaks at a ratio of 500 : 1 and 22 % yield.	116
$[\text{Co}^{\text{III}}\text{Co}^{\text{II}}(\text{H}_2\text{O})\text{W}_{11}\text{O}_{39}]^{7-}$	hv, Ru(II)(bpy) ₃ ²⁺ , Na ₂ S ₂ O ₈ , and Ru(III)(bpy) ₃ ³⁺ in pH 8.0-10.0, NaBi, NaPi, NaCi	$[\text{Co}^{\text{II}}\text{Co}^{\text{II}}(\text{H}_2\text{O})\text{W}_{11}\text{O}_{39}]^{8-}$ (i.e. the one electron reduction product of the starting POM) decomposes rapidly at the pH of the reactions. No observed particles in $[\text{Co}^{\text{III}}\text{Co}^{\text{II}}(\text{H}_2\text{O})\text{W}_{11}\text{O}_{39}]^{7-}$ solutions by DLS after 10 minutes of reaction (conditions not given) whereas reactions containing 0.1 to 1 mol% Co(NO ₃) ₂ ($[\text{Co}(\text{NO}_3)_2] + [\text{Co}_2\text{POM}] = 15 \mu\text{M}$) produced observable particle both before and after photochemical reactions. The authors noted differences in the CVs between the POM and Co(NO ₃) ₂ , although the catalytic wave onset is very similar. UV-vis band is stable over 10 minutes at pH 9.0 although no error bars were given. Reaction solutions of $[\text{Co}^{\text{II}}\text{Co}^{\text{II}}(\text{H}_2\text{O})\text{W}_{11}\text{O}_{39}]^{8-}$ are also active in the water oxidation reaction. Control with 45 nM Co(NO ₃) ₂ showed no observable photo-oxidation activity. Hole scavenging kinetics did not vary with aging the POM solution (1-60 minutes aging time). Only ~40% of initial activity is observed when the POM is isolated and retested. Isolation is achieved by precipitating with acetone followed by centrifugation.	68

POM	Oxidant, Electrolyte ^a	Experiments Relevant to Distinguishing Homogeneous and Heterogeneous Catalysis	Ref.
$\{\text{Co}_9(\text{H}_2\text{O})_6(\text{OH})_3(\text{HPO}_4)_2(\text{PW}_9\text{O}_{34})_3\}^{16-}$	Electrochem., 1.41 V vs NHE, FTO and NaClO in pH 7 and 8, NaPi	During electrolysis, the POM concentration decreases by ~15% and 30% in the absence and presence of bipyridine, as judged by UV-vis spectroscopy. In the presence of bipyridine, a pink precipitate forms during bulk electrolysis of the POM. For NaClO oxidation experiments, no change in the UV-vis spectrum was observed, dynamic light scattering showed the same result before and after the experiment. Bulk electrolysis of 1 mM POM for 1 hour resulted in formation of a catalytic film which contained cobalt and phosphate, as determined by SEM/EDX. The pink precipitate formed during bulk electrolysis of the POM in the presence of bpy was reported to be a $[\text{Co}(\text{bpy})_3]^{3+}[\text{POM}]$ salt and was characterized by IR. In NaClO oxidation experiments, the POM can be recovered from the solution by crystallization or precipitation (as judged by IR and XRD). At 15 °C, the NaClO plus POM reaction appears slightly sigmoidal. Repeated additions of NaClO to the POM shows the TOF and yield after each addition (for five additions) is the same within experimental error. If 2,2'-bipyridine was added to the POM solution before electrolysis, the oxidation current decreases by ~50-fold, and no film was visible by SEM/EDX and no residual activity was observed on the electrode. The electrochemical onset of oxidation occurs at 0.75 V and 1.10 V in the absence and presence of bipyridine. Addition of 10 equivalents of bipyridine to the POM plus NaClO oxidation does not significantly change the O ₂ yields or kinetics with additions of NaClO occurring at 0, 84, 108, and 131 hours.	79
$\text{Cs}_{15}\text{K}[\text{Co}_9(\text{H}_2\text{O})_6(\text{OH})_3(\text{HPO}_4)_2(\text{PW}_9\text{O}_{34})_3]$ -Carbon Paste	Electrochem. 1.5 V vs NHE Carbon Paste in pH 7.0, NaPi	IR spectroscopy and XRD shows same peaks for Co ₉ -POM before and after 8 hour 1.5 V electrolysis. Controls conducted with Co ₃ O ₄ at a variety of loading. 20x the molar amount of cobalt in the form of Co ₃ O ₄ has about half the current of the Co ₉ -POM. At pH 1, Co ₃ O ₄ show the same current as carbon paste background; Co(NO ₃) ₂ controls show decreasing activity with increasing amounts of 17.5-52.5 μmols.	101
$[\{\text{Ru}_3\text{O}_3(\text{H}_2\text{O})\text{Cl}_2\}(\text{SiW}_9\text{O}_{34})]^{7-}$ and $[\text{Co}_4(\text{H}_2\text{O})_2(\text{SiW}_9\text{O}_{34})]^{12-}$	hv, Ru(II)(bpy) ₃ ²⁺ , Na ₂ S ₂ O ₈ in pH 5.8, Na ₂ SiF ₆ buffer	A 3.5% and 25% decrease in the UV-vis absorbance bands of $[\{\text{Ru}_3\text{O}_3(\text{H}_2\text{O})\text{Cl}_2\}(\text{SiW}_9\text{O}_{34})]^{7-}$ and $[\text{Co}_4(\text{H}_2\text{O})_2(\text{SiW}_9\text{O}_{34})]^{12-}$ were observed over 150-180 minutes at pH 5.8. $[\{\text{Ru}_3\text{O}_3(\text{H}_2\text{O})\text{Cl}_2\}(\text{SiW}_9\text{O}_{34})]^{7-}$ is stable under illumination (but no catalysis) for 3 hours. The Ru ₃ POM-Ru(bpy) ₃ ²⁺ and Co ₄ POM complexes precipitate, can be isolated from the solution by centrifugation and maintain the characteristic IR bands of the Ru ₃ POM and Co ₄ POM. O ₂ evolution kinetics appear slightly sigmoidal. Control experiments with RuCl ₃ gave no observed O ₂ . Controls with Co ²⁺ salts were conducted. After centrifugation of the Ru(bpy) ₃ ²⁺ -Ru ₃ POM solution, the supernatant contains no residual water oxidation activity. Both the precipitated Ru(bpy) ₃ ²⁺ - Ru ₃ POM and Ru(bpy) ₃ ²⁺ - Co ₄ POM can be resuspended in solution while maintaining water oxidation activity.	69
$[\text{Co}_4(\mu\text{-OH})(\text{H}_2\text{O})_3(\text{Si}_2\text{W}_{19}\text{O}_{70})]^{11-}$	hv, Ru(II)(bpy) ₃ ²⁺ , Na ₂ S ₂ O ₈ in pH 7.2-9.0, NaPi and NaBi	Estimated 5.5 equiv. of aqueous Co ²⁺ dissociates over 40 days (UV-vis). POM decomposes to $[\text{Co}(\text{H}_2\text{O})\text{SiW}_{11}\text{O}_{39}]^{6-}$. Sigmoidal O ₂ evolution kinetics at pH 7.2. TON decreases with aging (3-4 weeks)	70, 71
$\text{Na}_9\text{H}_5[\text{Co}_2\text{Bi}_2(\alpha\text{-B-CoW}_9\text{O}_{34})_2]$ and $\text{Na}_9\text{H}_5[\text{Co}_2\text{Bi}_2(\beta\text{-B-CoW}_9\text{O}_{34})_2]$	Electrochem., Glassy Carbon and hv, Ru(II)(bpy) ₃ ²⁺ , Na ₂ S ₂ O ₈ in pH 7.4, NaPi	A 0.25 mM solution of either POM does not show an electrochemical oxidation wave during 3 hours of aging at pH 7.4.	86
$[\text{Ti}_{12}\text{O}_{15}(\text{O}^i\text{Pr})_{17}]^{+}$ $[(\text{CoBr})_6\text{Ti}_{15}\text{O}_{24}(\text{O}^i\text{Pr})_{18}(\text{Br})]^{-}$ and $[(\text{CoI})\text{Ti}_{11}\text{O}_{14}(\text{O}^i\text{Pr})_{17}]^{+}$	Electrochem. 1.35 V vs NHE, FTO in pH 7.0, Pi buffer	SEM/EDX shows the presence of porous islands of the precursor before bulk electrolysis composed of 5.8% cobalt and 0% phosphorus. After catalysis the islands contain 1.1 % and 9.0 % cobalt and phosphorus and the interstitial space between the island contains 8.24 % and 4.81 %—consistent with in-situ formed CoO _x .	109

POM	Oxidant, Electrolyte ^a	Experiments Relevant to Distinguishing Homogeneous and Heterogeneous Catalysis	Ref.
[Hpy] ₂ {[Co(4,4'-Hbpy) ₂ (H ₂ O) ₂][SiCoW ₁₁ O ₃₉]}	Electrochem. Carbon Paste in pH 4.5, NaOAc	N/A	148
[Ru ₄ (μ-O) ₄ (μ-OH) ₂ (H ₂ O) ₄ (γ-SiW ₁₀ O ₃₆) ₂] ¹⁰⁻	Ce(IV) in pH 0.6	UV-vis shows reversible protonation of POM over pH range of 0.6-2.0 (pK _a = 3.62). This protonation/deprotonation is concentration independent and the FTIR spectrum is unchanged during this titration. The 443 nm absorption band changes only slightly over 4 days at pH 0.6. 8 equiv. of Ce(IV) were added to the POM, allowed to sit for 1 hour, the POM was precipitated by Cs ⁺ addition, and collected by filtration; the IR and resonance Raman spectra appear qualitatively the same as the unreacted sample. (Note: Most catalytic reactions were run with ~500-1000 equiv. Ce(IV)). O ₂ evolution is first-order in [POM]. Control with K ₄ Ru ₂ OCl ₁₀ showed 20 minute induction period, ~10x slower O ₂ evolution, and 8x lower O ₂ yield.	72
[Ru ₄ (μ-O) ₄ (μ-OH) ₂ (H ₂ O) ₄ (γ-SiW ₁₀ O ₃₆) ₂] ¹⁰⁻	Ce(IV) and Electrochem (Glassy Carbon or Pt) 1.15 V vs SSCE	Characterized POM WOC intermediates by CV, UV-vis, EPR, and resonance Raman; data are consistent with oxidation states for the tetra-ruthenium core ranging from Ru(IV) ₄ to Ru(V) ₄ . Ru ₄ -POM has nearly identical XANES Ru K-edge and Ru-O bond distance (1.98 Å) compared to RuO ₂ .	64, 103
[Ru ₄ (μ-O) ₄ (μ-OH) ₂ (H ₂ O) ₄ (γ-SiW ₁₀ O ₃₆) ₂] ¹⁰⁻	Ru(bpy) ₃ ³⁺ in pH 7.2, NaPi	UV-vis shows two reversible protonation equilibria between pH 2.5-7.5. The electrochemical response of the POM was reported at pH 1.0 and showed several reversible ruthenium redox waves. At pH 7, an electrocatalytic wave is observed above 900 mV vs Ag/AgCl; when the POM and Ru(bpy) ₃ ²⁺ are combined, the Ru(III/II)(bpy) ₃ ^{3+/2+} couple becomes less chemically reversible as the [POM] increases. Controls with Ru(III)Cl ₃ in the presence and absence of [γ-SiW ₁₀ O ₃₆] ⁸⁻ showed Ru(bpy) ₃ ³⁺ reduction rates which were 100 times slower than in the presence of the POM.	73
[Ru ₄ (μ-O) ₄ (μ-OH) ₂ (H ₂ O) ₄ (γ-SiW ₁₀ O ₃₆) ₂] ¹⁰⁻	Ru(bpy) ₃ ³⁺ in pH 7.2, NaPi	Reversible oxidation/reduction between core oxidation states of (Ru(IV) ₂ Ru(V) ₂) and (Ru(IV) ₂ Ru(III) ₂) using both electrochemical and chemical (Ce(IV) and Sn(II)) oxidants/reductants. UV-vis and CV does not change over several months at room temperature and pH 3-4; slow decomposition is seen in 0.1 M HCl solution. No particles are seen in post-reaction solution by SAXS and DLS. Proposed rate law for oxidant consumption: -d(Ru(bpy) ₃ ³⁺)/dt = 4k _{cat} [POM]/(1 + [Ru(bpy) ₃ ²⁺]/(K[Ru(bpy) ₃ ³⁺])). Reaction depends on Ru(bpy) ₃ ^{3+/2+} / Ru(bpy) ₃ ²⁺ ratio, but not on initial [Ru(bpy) ₃ ³⁺]. Control with RuCl ₃ gave O ₂ yield of <11 % which is about 5 times less than for the POM. Addition of bpy does not change the O ₂ yield within experimental error. Addition of potassium decreases O ₂ yield by 50%.	74
[Ru ₄ (μ-O) ₄ (μ-OH) ₂ (H ₂ O) ₄ (γ-SiW ₁₀ O ₃₆) ₂] ¹⁰⁻	Electrochem., Glassy Carbon in 0.1 M HCl or 0.05 M H ₂ SO ₄	Measured ten electrochemical redox potentials for the POM by AC voltammetry. Ru(IV,IV,V,V)/Ru(IV,V,V,V) and Ru(IV,V,V,V)/Ru(V,V,V,V) potentials were measured to be 1.15 and 1.32 V vs Ag/AgCl in 0.05 M H ₂ SO ₄ . Electron-transfer rates were reported for most of the redox processes. Potassium cations increase the electron transfer rates.	82
[Ru ₄ (μ-O) ₄ (μ-OH) ₂ (H ₂ O) ₄ (γ-SiW ₁₀ O ₃₆) ₂] ¹⁰⁻	hv, Ru(II)(bpy) ₃ ²⁺ , Na ₂ S ₂ O ₈ or hv, TiO ₂ /Ru(4,4'-diphosphonate-2,2'-bipyridine)(bpy) ₂ ²⁺ in pH 7, Pi	Flash photolysis experiments yield a bimolecular rate constant of (2.1±0.4)×10 ⁹ M ⁻¹ s ⁻¹ for the Ru(bpy) ₃ ³⁺ + POM reaction. Caveat: No O ₂ .	119
[Ru ₄ (μ-O) ₄ (μ-OH) ₂ (H ₂ O) ₄ (γ-SiW ₁₀ O ₃₆) ₂] ¹⁰⁻	hv, [Ru(II){(μ-dpp)Ru(II)(bpy) ₂ } ₃] ⁸⁺ , Na ₂ S ₂ O ₈ in pH 7.2, KPi	Reaction is zero order in photosensitizer and persulfate for up to 80% of reaction. System also active in pH 5.8 Na ₂ SiF ₆ /Na ₂ B ₄ O ₇ buffer.	117

POM	Oxidant, Electrolyte ^a	Experiments Relevant to Distinguishing Homogeneous and Heterogeneous Catalysis	Ref.
$[\text{Ru}_4(\mu\text{-O})_4(\mu\text{-OH})_2(\text{H}_2\text{O})_4(\gamma\text{-SiW}_{10}\text{O}_{36})_2]^{10-}$	hv, Ru(II)(bpy) ₃ ²⁺ , Na ₂ S ₂ O ₈ in pH 7.2, NaPi	At concentrations above 5 μM POM, a POM-Ru(bpy) ₃ ²⁺ precipitate formed. Increasing [POM] from 2.5 to 5.0 μM resulted in no increase in O ₂ production. O ₂ evolution rate scales approximately with initial [Ru(bpy) ₃ ²⁺] and [Na ₂ S ₂ O ₈]. A control with RuCl ₃ yielded no measurable O ₂ . A RuO ₂ control yielded O ₂ evolution rates which were 10-20x lower than the POM.	118
MWCNT/PAMAM/[Ru ₄ (H ₂ O) ₄ (μ-O) ₄ (μ-OH) ₂ (γ-SiW ₁₀ O ₃₆) ₂] ¹⁰⁻ , where MWCNT/PAMAM are polyamidoamine functionalized multiwalled carbon nanotubes	Electrochem. 1.1-1.6 V vs Ag/AgCl on ITO in pH 7, Pi	Electrodes could be cycled at least 9 times between 1 and 1.6 V vs Ag/AgCl without significant changes in response.	83
$[(\gamma\text{-PW}_{10}\text{O}_{36})_2\text{Ru}_4\text{O}_5(\text{OH})(\text{H}_2\text{O})_4]^{9-}$	hv, Ru(II)(bpy) ₃ ²⁺ , Na ₂ S ₂ O ₈ in pH 5.8, Na ₂ SiF ₆	Two reversible protonation equilibria occur at ~pH 3. Seven reversible ruthenium redox waves are observed for core oxidation states of (Ru(IV) ₂ Ru(V) ₂) to (Ru(II)Ru(III) ₃) over pH 0 to 7. O ₂ evolution rate does not appear to depend strongly on initial [POM] although the overall O ₂ yield does depend on the initial [POM]. O ₂ evolution kinetics look slightly sigmoidal at 5.1 μM POM. [Ru ₄ (μ-O) ₄ (μ-OH) ₂ (H ₂ O) ₄ (γ-SiW ₁₀ O ₃₆) ₂] ¹⁰⁻ gave an O ₂ yield = 40 % compared to 25 % for $[(\gamma\text{-PW}_{10}\text{O}_{36})_2\text{Ru}_4\text{O}_5(\text{OH})(\text{H}_2\text{O})_4]^{9-}$.	75
$[\text{Ru}(\text{III})_2\text{Zn}_2(\text{H}_2\text{O})_2(\text{ZnW}_9\text{O}_{34})_2]^{14-}$	Electrochem. 0.5-1.05 V vs SHE on Au in pH 8, Pi	Controls with di-ZnPOM and [PW ₁₁ O ₃₉ Ru(III)(H ₂ O)] ⁴⁺ showed no O ₂ evolution activity. Tafel analysis gives a 120 mV/decade slope (i.e. twice that typical of RuO ₂).	122
[Ru(H ₂ O)SiW ₁₁ O ₃₉] ⁵⁻ and [Ru(H ₂ O)GeW ₁₁ O ₃₉] ⁵⁻	Ce(IV) in 0.1-0.55 M HNO ₃	Pourbaix diagrams characterize the ruthenium POM redox potentials as a function of potential and pH. the Ru(IV) and Ru(V) POM oxidation states were also characterized by UV-vis, EPR, and resonance Raman (note that only UV-vis was in operando). O ₂ was not evolved in controls using RuCl ₃ , Ru(acac) ₃ , or [SiW ₁₁ O ₃₉] ⁸⁻ . O ₂ yield of up to 90 % were reported for the POM. Ce(IV) loss kinetics was reported as a function [Catalyst], pH, and [CAN]; reaction is first-order in POM, approximately zero order in [H ⁺], and shows saturation kinetics for Ce(IV).	76
$[\text{PW}_{11}\text{O}_{39}\text{Ru}(\text{III})(\text{H}_2\text{O})]^{4-}$, $[\text{SiW}_{11}\text{O}_{39}\text{Ru}(\text{III})(\text{H}_2\text{O})]^{5-}$, $[\text{GeW}_{11}\text{O}_{39}\text{Ru}(\text{III})(\text{H}_2\text{O})]^{5-}$	Ce(IV) in pH 1, HNO ₃	Pourbaix diagram indicates that the Ru(V/VI) couple occurs near the reversible water oxidation potential. Controls with [Ru(benzene)Cl ₂] ₂ , [PW ₁₁ O ₃₉ {Ru(II)(benzene)(H ₂ O)}] ⁵⁻ , and [K ₇ PW ₁₁ O ₃₉] + [Ru(benzene)Cl ₂] ₂ , did not show significant amounts of O ₂ evolution. O ₂ evolution kinetics are slightly sigmoidal for [PW ₁₁ O ₃₉ Ru(III)(H ₂ O)] ⁴⁻ and [SiW ₁₁ O ₃₉ Ru(III)(H ₂ O)] ⁵⁻ .	84
$[\text{PW}_{11}\text{O}_{39}\text{Ru}(\text{III}/\text{II})(\text{DMSO})]^{4-}$	Ce(IV) in pH 1, HNO ₃	Controls with RuCl ₂ (DMSO) ₄ , [K ₇ PW ₁₁ O ₃₉], and RuCl ₂ (DMSO) ₄ plus [K ₇ PW ₁₁ O ₃₉], showed induction periods of ~0.5 hours, and O ₂ yields which were ~3 times less than [PW ₁₁ O ₃₉ Ru(II)(DMSO)] ⁵⁻ .	123
$[(\text{Mn}(\text{III})(\text{H}_2\text{O}))_3(\text{SbW}_9\text{O}_{33})_2]^{9-}$	Electrochem. 1.345V vs SCE, Glassy Carbon in pH 6, NaOAc	CV shows oxidation peak at 1.345V which is attributed to Mn(V) and electrocatalytic water oxidation; the Mn(IV/III) reduction wave remains chemically reversible. CV indicates adsorption of the POM to the electrode. The oxidation peak currents become larger and the peaks shift to more negative potentials upon cycling the electrode from -0.9 to 1.5 V vs SCE. Bulk electrolysis of the Mn(II) ₃ POM at 0.8 V results in 6.3 electrons passed concomitant with solution color becoming brown. EQCM indicates deposition of a film at the same potential as the Mn(IV/III) oxidation wave. This film can be removed by reversing the potential negative of the Mn(IV/III) redox potential. Repeated cycling indicates that a small portion of the deposited film remains attached to the electrode; the authors suggest this could be a MnO _x film. Mn(V) oxidation wave was also observed in NaPi buffer at pH 6.	87

POM	Oxidant, Electrolyte ^a	Experiments Relevant to Distinguishing Homogeneous and Heterogeneous Catalysis	Ref.
[Mn(III) ₃ (H ₂ O) ₅ (A- α -PW ₉ O _{er}) ₂] ⁹⁻	Electrochem. 1.1-1.3 V vs SCE, Glassy Carbon in pH 5, NaPi	CV shows two oxidation peaks (0.55 and 0.78 vs SCE). The peaks become shaper and shift to slightly more negative potentials when the electrode is cycled four times between -0.6 and 1.0 V; authors suggest this is due to MnO _x deposition.	88
[Mn ₁₉ (OH) ₁₂ (SiW ₁₀ O ₃₇) ₆] ³⁴⁻	Electrochem. ~0.9-1.25V vs SCE, Glassy Carbon in pH 5, NaOAc	CV shows two reversible waves at 0.5 and 0.74 V. Bulk electrolysis at 0.83 V results in passage of 2.00±0.005 electrons per Mn. The electrode can be subjected to hundreds of cycles without deactivation. A film deposits on the electrode surface during water oxidation electrolysis and cycling experiments. Tafel slope of 135 ± 10 mV/decade	89
[Ru(II)(phen) ₃ (CH ₃ OH)(Mo ₆ O ₁₉)] [Ru(II)(phen) ₃ (C ₂ H ₈ N ₂)(C ₃ H ₇ NO)(Mo ₅ S ₂ O ₂₃)] [Ru(II)(phen) ₃ (CH ₃ CN) ₂ (Mo ₈ O ₂₆)]	hv, Na ₂ S ₂ O ₈	PXRD does not show significant changes when comparing pre- and post- photocatalysis POM samples.	156
[CoMo ₆ O ₂₄ H ₆] ³⁻ and [Co ₂ Mo ₁₀ O ₃₈ H ₄] ⁶⁻	hv, Ru(II)(bpy) ₃ ²⁺ , Na ₂ S ₂ O ₈ in pH 8.0, NaBi	POMs showed no particles by DLS after reaction. Control with 10µM Co(NO ₃) ₂ showed particles by DLS post reaction. Single control with 20µM Co(NO ₃) ₂ which showed ~8x lower activity than POMs.	105
[(IrCl ₄)KP ₂ W ₂₀ O ₇₂] ⁷⁻	Ru(bpy) ₃ ³⁺ in pH 7.2, NaPi	Complete dissociation (> 99%) of an [IrCl ₄ (H ₂ O) ₂] ⁻ unit from the POM occurs over 24 hours at pH 6.5 or 7.2, as determined by UV-vis and ³¹ P-NMR. Control with IrCl ₃ gave slightly higher O ₂ yield (38 %) compared to the POM (30 %).	77
[Ni ₅ (OH) ₆ (OH ₂) ₃ (Si ₂ W ₁₈ O ₆₆)] ¹²⁻	hv, Ru(II)(bpy) ₃ ²⁺ , Na ₂ S ₂ O ₈	DLS shows 700-1300 nm particles prior to the reaction. Prior to addition of Ru(bpy) ₃ ²⁺ , the POM UV-vis spectrum is stable for at least 12 hours in pH 8 solution, and can be recrystallized after two years in solution. A nickel-borate film forms on electrode surfaces above 1.1 V. FTIR of the pre- and post-reaction POM-Ru(bpy) ₃ ²⁺ material appeared nearly identical (note, the reaction was run at 25x larger scale). An FTIR peak observed at 3640 cm ⁻¹ for a Ni(OH ₂) ₂ material was not observed in the post-reaction POM solution. Reported O ₂ evolution kinetics for light driven experiments and Ru(bpy) ₃ ³⁺ reduction kinetics for dark experiments. Filtration of the pre-catalysis solution followed by irradiation yields no O ₂ . A control with 1 µM Ni(NO ₃) ₂ + Ru(bpy) ₃ ²⁺ with filtration, did yield O ₂ upon illumination.	78

^a NaPi, NaBi, NaCi, and NaOAc are sodium phosphate, sodium borate, sodium carbonate, and sodium acetate buffers.

REFERENCES

- ¹ *Chem. Indust.* 2002, Jan 21., p. 22.
- ² R.H. Crabtree, *Chem. Rev.* 112 (2012) 1536-1554.
- ³ J.A. Widegren, R.G. Finke, *J. Mol. Catal. A: Chem.* 198 (2003) 317-341.
- ⁴ N.T.S. Phan, M. Van Der Sluys, C.W. Jones, *Adv. Synth. Catal.* 348 (2006) 609-679.
- ⁵ W.M. Alley, I.K. Hamdemir, K.A. Johnson, R.G. Finke, *J. Mol. Catal. A: Chem.* 315 (2010) 1-27.
- ⁶ V. Artero, M. Fontecave, *Chem. Soc. Rev.* 42 (2013) 2338-2356.
- ⁷ S. Fukuzumi, D. Hong, *Eur. J. Inorg. Chem.* DOI: 10.1002/ejic.201300684.
- ⁸ N.S. Lewis, D.G. Nocera, *Proc. Natl. Acad. Sci.* 103 (2006) 15729-15735.
- ⁹ T.R. Cook, D.K. Dogutan, S.Y. Reece, Y. Surendranath, T.S. Teets, D.G. Nocera, *Chem. Rev.* 110 (2010) 6474-6502.
- ¹⁰ W. Ruttiger, G.C. Dismukes, *Chem. Rev.* 97 (1997) 1-24.
- ¹¹ T.A. Betley, Q. Wu, T. Van Voorhis, D.G. Nocera, *Inorg. Chem.* 47 (2008) 1849-1861.
- ¹² F. Liu, J.J. Concepcion, J.W. Jurss, T. Cardolaccia, J.L. Templeton, T.J. Meyer, *Inorg. Chem.* 47 (2008) 1727-1752.
- ¹³ H. Dau, C. Limberg, T. Reier, M. Risch, S. Roggan, P. Strasser, *ChemCatChem* 2 (2010) 724-761.
- ¹⁴ C.W. Cady, R.H. Crabtree, G.W. Brudvig, *Coord. Chem. Rev.* 252 (2008) 444-455.
- ¹⁵ X. Sala, I. Romero, M. Rodriguez, L. Escriche, A. Llobet, *Angew. Chem. Int. Ed.* 48 (2009) 2842-2852.
- ¹⁶ M. Yagi, M. Kaneko, *Chem. Rev.* 101 (2001) 21-35.
- ¹⁷ X. Liu, F. Wang, *Coord. Chem. Rev.* 256 (2012) 1115-1136.
- ¹⁸ D.J. Wasylenko, R.D. Palmer, C.P. Berlinguette, *Chem. Commun.* 49 (2013) 218-227.
- ¹⁹ P. Du, R. Eisenberg, *Energy Environ. Sci.* 5 (2012) 6012-6021.
- ²⁰ N.D. McDaniel, S. Bernhard, *Dalton Trans.* 39 (2010) 10021-10030.
- ²¹ C. Song, *Catal. Today* 115 (2006) 2-32.

- ²² A.J. Morris, G.J. Meyer, E. Fujita, *Acc. Chem. Res.* 42 (2009) 1983-1994.
- ²³ M.R. Dubois, D.L. Dubois, *Acc. Chem. Res.* 42 (2009) 1974-1982.
- ²⁴ E.E. Benson, C.P. Kubiak, A.J. Sathrum, J.M. Smieja, *Chem. Soc. Rev.* 38 (2009) 89-99.
- ²⁵ G.A. Olah, A. Goeppert, G.K. Surya Prakash, *J. Org. Chem.* 74 (2009) 487-498.
- ²⁶ C. Herrero, A. Quaranta, W. Leibl, A.W. Rutherford, A. Aukauloo, *Energy Environ. Sci.* 4 (2011) 2353-2365.
- ²⁷ L.L. Tinker, N.D. McDaniel, S. Bernhard, *J. Mater. Chem.* 19 (2009) 3328-3337.
- ²⁸ P.D. Tran, V. Artero, M. Fontecave, *Energy Environ. Sci.* 3 (2010) 727-747.
- ²⁹ R. Brimblecombe, G.C. Dismukes, G.F. Swiegers, L. Spiccia, *Dalton Trans.* (2009) 9374-9384.
- ³⁰ M. Yagi, A. Syouji, S. Yamada, M. Komi, H. Yamazaki, S. Tajima, *Photochem. Photobiol. Sci.* 8 (2009) 139-147.
- ³¹ E.S. Andreiadis, M. Chavarot-Kerlidou, M. Fontecave, V. Artero, *Photochem. Photobiol.* 87 (2011) 946-964.
- ³² K.J. Young, L.A. Martini, R.L. Milot, R.C. Snoeberger III, V.S. Batista, C.A. Schmuttenmaer, R.H. Crabtree, G.W. Brudvig, *Coord. Chem. Rev.* 256 (2012) 2503-2520.
- ³³ J.R. Swierk, T.E. Mallouk, *Chem. Soc. Rev.* 42 (2013) 2357-2387.
- ³⁴ M.G. Walter, E.L. Warren, J.R. McKone, S.W. Boettcher, Q. Mi, E.A. Santori, N.S. Lewis, *Chem. Rev.* 110 (2010) 6446-6473.
- ³⁵ V. Balzani, L. Moggi, M.F. Manfrin, F. Bolletta, M. Gleria, *Science* 189 (1975) 852-856.
- ³⁶ A.J. Bard, M.A. Fox, *Acc. Chem. Res.* 28 (1995) 141-145.
- ³⁷ D. Gust, T.A. Moore, A.L. Moore, *Faraday Discuss.* 155 (2012) 9-26.
- ³⁸ Y.V. Geletii, Q. Yin, Y. Hou, Z. Huang, H. Ma, J. Song, C. Besson, Z. Luo, R. Cao, K.P. O'Halloran, G. Zhu, C. Zhao, J.W. Vickers, Y. Ding, S. Mohebbi, A.E. Kuznetsov, D.G. Musaev, T. Lian, C.L. Hill, *Isr. J. Chem.* 51 (2011) 238-246.
- ³⁹ Z.G. Han, A.M. Bond, C. Zhao, *Sci. China*, 54 (2011) 1877-1887.
- ⁴⁰ H. Lv, Y.V. Geletii, C. Zhao, J.W. Vickers, G. Zhu, Z. Luo, J. Song, T. Lian, D.G. Musaev, C.L. Hill, *Chem. Soc. Rev.* 41 (2012) 7572-7589.
- ⁴¹ A. Sartorel, M. Bonchio, S. Campagna, F. Scandola, *Chem. Soc. Rev.* 42 (2013) 2262-2280.

- ⁴² M.T. Pope, *Heteropoly and Isopoly Oxometalates*, Springer, Berlin, 1983.
- ⁴³ S. Nlate, C. Jahier, *Eur. J. Inorg. Chem.* (2013) 1606-1619.
- ⁴⁴ A. Dolbecq, P. Mialane, B. Keita, L. Nadjjo, *J. Mater. Chem.* 22 (2012) 24509-24521.
- ⁴⁵ N. Mizuno, K. Kamata, K. Yamaguchi, *Top. Organomet. Chem.* 37 (2011) 127-160.
- ⁴⁶ N. Mizuno, K. Yamaguchi, K. Kamata, *Catal. Surv. Asia* 15 (2011) 68-79.
- ⁴⁷ S. Berardi, M. Carraro, A. Sartorel, G. Modugno, M. Bonchio, *Isr. J. Chem.* 51 (2011) 259-274.
- ⁴⁸ J.-M. Brégeault, M. Vennat, L. Salles, J.-Y. Piquemal, Y. Mahha, E. Briot, P.C. Bakala, A. Atlamsani, R. Thouvenot, *J. Mol. Catal. A: Chem.* 250 (2006) 177-189.
- ⁴⁹ B. Keita, L. Nadjjo, *J. Mol Catal. A: Chem.* 262 (2007) 190-215.
- ⁵⁰ S.-T. Zheng, G.-Y. Yang, *Chem. Soc. Rev.* 41 (2012) 7623-7646.
- ⁵¹ O. Oms, A. Dolbecq, P. Mialane, *Chem. Soc. Rev.* 41 (2012) 7497-7536.
- ⁵² N.V. Izarova, M.T. Pope, U. Kortz, *Angew. Chem. Int. Ed.* 51 (2012) 9492-9510.
- ⁵³ P. Putaj, F. Lefebvre, *Coord. Chem. Rev.* 255 (2011) 1642-1685.
- ⁵⁴ M. Hutin, D.-L. Long, L. Cronin, *Isr. J. Chem.* 51 (2011) 205-214.
- ⁵⁵ R.G. Finke, M.W. Droege, *J. Am. Chem. Soc.* 106 (1984) 7274-7277.
- ⁵⁶ R.G. Finke, B. Rapko, R.J. Saxton, P.J. Domaille, *J. Am. Chem. Soc.* 108 (1986) 2947-2960.
- ⁵⁷ J. Schwartz, *Acc. Chem. Res.* 18 (1985) 302-308.
- ⁵⁸ J.R. Platt, *Science* 146 (1964) 347-353.
- ⁵⁹ T.C. Chamberlain, *Science* 148 (1965) 754-759.
- ⁶⁰ F. Meunier, M. Daturi, *Catal. Today* 113 (2006) 1-2.
- ⁶¹ S.J. Tinnemans, J.G. Mesu, K. Kervinen, T. Visser, T.A. Nijhuis, A.M. Beale, D.E. Keller, A.M.J. van der Eerden, B. M. Weckhuysen, *Catal. Today* 113 (2006) 3-15.
- ⁶² R. Contant, J.-P. Ciabrini, *J. Chem. Res. Synop.* (1982) 50-51.
- ⁶³ R. Contant, *J. Chem. Res. Synop.* (1984) 120-121.

- ⁶⁴ A. Sartorel, P. Miró, E. Salvadori, S. Romain, M. Carraro, G. Scorrano, M. Di Valentin, A. Llobet, C. Bo, M. Bonchio, *J. Am. Chem. Soc.* 131 (2009) 16051-16053.
- ⁶⁵ Q. Yin, J.M. Tan, C. Besson, Y.V. Geletii, D.G. Musaev, A.E. Kuznetsov, Z. Luo, K.I. Hardcastle, C.L. Hill, *Science* 328 (2010) 342-345.
- ⁶⁶ J.J. Stracke, R.G. Finke, *J. Am. Chem. Soc.* 133 (2011) 14872-14875.
- ⁶⁷ J.W. Vickers, H. Lv, J.M. Sumliner, G. Zhu, Z. Luo, D.G. Musaev, Y.V. Geletii, C.L. Hill, *J. Am. Chem. Soc.* 135 (2013) 14110-14118.
- ⁶⁸ F. Song, Y. Ding, B. Ma, C. Wang, Q. Wang, X. Du, S. Fu, J. Song, *Energy Environ. Sci.* 6 (2013) 1170-1184.
- ⁶⁹ P.-E. Car, M. Guttentag, K.K. Baldrige, R. Alberto, G.R. Patzke, *Green Chem.* 14 (2012) 1680-1688.
- ⁷⁰ G. Zhu, Y.V. Geletii, P. Kögerler, H. Schilder, J. Song, S. Lense, C. Zhao, K.I. Hardcastle, D.G. Musaev, C.L. Hill, *Dalton Trans.* 41 (2012) 2084-2090.
- ⁷¹ G. Zhu, H. Lv, J.W. Vickers, Y.V. Geletii, Z. Luo, J. Song, Z. Huang, D.G. Musaev, C.L. Hill, *Proc. SPIE* 8109 (2011) 81090A.
- ⁷² A. Sartorel, M. Carraro, G. Scorrano, R. De Zorzi, S. Geremia, N.D. McDaniel, S. Bernhard, M. Bonchio, *J. Am. Chem. Soc.* 130 (2008) 5006-5007.
- ⁷³ Y.V. Geletii, B. Botar, P. Kögerler, D.A. Hillesheim, D.G. Musaev, C.L. Hill, *Angew. Chem. Int. Ed.* 47 (2008) 3896-3899.
- ⁷⁴ Y.V. Geletii, C. Besson, Y. Hou, Q. Yin, D.G. Musaev, D. Quiñonero, R. Cao, K.I. Hardcastle, A. Proust, P. Kögerler, C.L. Hill, *J. Am. Chem. Soc.* 131 (2009) 17360-17370.
- ⁷⁵ C. Besson, Z. Huang, Y.V. Geletii, S. Lense, K.I. Hardcastle, D.G. Musaev, T. Lian, A. Proust, C.L. Hill, *Chem. Commun.* 46 (2010) 2784-2786.
- ⁷⁶ M. Murakami, D. Hong, T. Suenobu, S. Yamaguchi, T. Ogura, S. Fukuzumi, *J. Am. Chem. Soc.* 133 (2011) 11605-11613.
- ⁷⁷ R. Cao, H. Ma, Y.V. Geletii, K.I. Hardcastle, C.L. Hill, *Inorg. Chem.* 48 (2009) 5596-5598.
- ⁷⁸ G. Zhu, E.N. Glass, C. Zhao, H. Lv, J.W. Vickers, Y.V. Geletii, D.G. Musaev, J. Song, C.L. Hill, *Dalton Trans.* 41 (2012) 13043-13049.
- ⁷⁹ S. Goberna-Ferrón, L. Vigara, J. Soriano-López, J.R. Galán-Mascarós, 51 (2012) 11707-11715.
- ⁸⁰ A.D. Kirk, W. Riske, D.K. Lyon, B. Rapko, R.G. Finke, *Inorg. Chem.* 28 (1989) 792-797.

- ⁸¹ J.J. Stracke, R.G. Finke, *ACS Catal.* 3 (2013) 1209-1219.
- ⁸² C.-Y. Lee, S.-X. Guo, A.F. Murphy, T. McCormac, J. Zhang, A.M. Bond, G. Zhu, C.L. Hill, Y.V. Geletii, *Inorg. Chem.* 51 (2012) 11521-11532.
- ⁸³ F.M. Toma, A. Sartorel, M. Iurlo, M. Carraro, P. Parisse, C. Maccato, S. Rapino, B.R. Gonzalez, H. Amenitsch, T.D. Ros, L. Casalis, A. Goldoni, M. Marcaccio, G. Scorrano, G. Scoles, F. Paolucci, M. Prato, M. Bonchio, *Nature Chem.* 2 (2010) 826-831.
- ⁸⁴ S. Ogo, M. Miyamoto, Y. Ide, T. Sano, M. Sadakane, *Dalton Trans.* 41 (2012) 9901-9907.
- ⁸⁵ M. Natali, S. Berardi, A. Sartorel, M. Bonchio, S. Campagna, F. Scandola, *Chem. Commun.* 48 (2012) 8808-8810.
- ⁸⁶ D. Guo, S. Teng, Z. Liu, W. You, L. Zhang, *J. Clust. Sci.* 24 (2013) 549-558.
- ⁸⁷ B. Keita, P. Mialane, F. Sécheresse, P. de Oliveira, L. Nadjo, *Electrochem. Commun.* 9 (2007) 164-172.
- ⁸⁸ R. Al-Oweini, B.S. Bassil, T. Palden, B. Keita, Y. Lan, A.K. Powell, U. Kortz, *Polyhedron* 52 (2013) 461-466.
- ⁸⁹ B.S. Bassil, M. Ibrahim, R. Al-Oweini, M. Asano, Z. Wang, J. van Tol, N.S. Dalal, K.-Y. Choi, R.N. Biboum, B. Keita, L. Nadjo, U. Kortz, *Angew. Chem. Int. Ed.* 50 (2011) 5961-5964.
- ⁹⁰ C. Rong, F.C. Anson, *Anal. Chem.* 66 (1994) 3124-3130.
- ⁹¹ B. Keita, R. Contant, E. Abdeljalil, F. Girard, L. Nadjo, *Electrochem. Commun.* 2 (2000) 295-300.
- ⁹² B. Keita, E. Abdeljalil, L. Nadjo, R. Contant, R. Belghiche, *Langmuir* 22 (2006) 10416-10425.
- ⁹³ E. Gileadi, *Electrode Kinetics for Chemists, Chemical Engineers, and Materials Scientists*, Wiley-VCH, New York, 1993.
- ⁹⁴ M.A. Fedotov, R.I. Maksimovskaya, *J. Struct. Chem.* 47 (2006) 952-978.
- ⁹⁵ Y.-G. Chen, J. Gong, L.-Y. Qu, *Coord. Chem. Rev.* 248 (2004) 245-260.
- ⁹⁶ O.W. Howarth, *Mol. Eng.* 3 (1993) 131-140.
- ⁹⁷ R. Contant, *Can. J. Chem.* 65 (1987) 568-573.
- ⁹⁸ Z. Zhu, R. Tain, C. Rhodes, *Can. J. Chem.* 81 (2003) 1044-1050.
- ⁹⁹ T.L. Jorris, M. Kozik, N. Casan-Pastor, P.J. Domaille, R.G. Finke, W.K. Miller, L.C.W. Baker, *J. Am. Chem. Soc.* 109 (1987) 7402-7408.

- ¹⁰⁰ C.A. Ohlin, S.J. Harley, J.G. McAlpin, R.K. Hocking, B.Q. Mercado, R.L. Johnson, E.M. Villa, M.K. Fidler, M.M. Olmstead, L. Spiccia, R.D. Britt, W.H. Casey, *Chem. Eur. J.* 17 (2011) 4408-4417.
- ¹⁰¹ J. Soriano-López, S. Goberna-Ferrón, L. Vígara, J.J. Carbó, J.M. Poblet, J.R. Galán-Mascarós, *Inorg. Chem.* 52 (2013) 4753-4755.
- ¹⁰² I.E. Wachs, C.A. Roberts, *Chem. Soc. Rev.* 39 (2010) 5002-5017.
- ¹⁰³ S. Piccinin, A. Sartorel, G. Aquilanti, A. Goldoni, M. Bonchio, S. Fabris, *Proc. Natl. Acad. Sci.* 110 (2013) 4917-4922.
- ¹⁰⁴ Z. Huang, Z. Luo, Y.V. Geletii, J.W. Vickers, Q. Yin, D. Wu, Y. Hou, Y. Ding, J. Song, D.G. Musaev, C.L. Hill, T. Lian, *J. Am. Chem. Soc.* 133 (2011) 2068-2071.
- ¹⁰⁵ S. Tanaka, M. Annaka, K. Sakai, *Chem. Commun.* 48 (2012) 1653-1655.
- ¹⁰⁶ K. Kaxauba, D. McKnight, M.T. Connah, F.K. McNeil-Watson, U. Nobbmann, *J. Nanopart. Res.* 10 (2008) 823-829.
- ¹⁰⁷ P.J. Wyatt, *Anal. Chim. Acta* 272 (1993) 1-40.
- ¹⁰⁸ D.E. Katsoulis, M.T. Pope, *J. Am. Chem. Soc.* 106 (1984) 2737-2738.
- ¹⁰⁹ Y.-H. Lai, C.-Y. Lin, Y. Lv, T.C. King, A. Steiner, N.M. Muresan, L. Gan, D.S. Wright, E. Reisner, *Chem. Commun.* 49 (2013) 4331-4333.
- ¹¹⁰ J.I. Goldstein, D.E. Newbury, D.C. Joy, C.E. Lyman, P. Echlin, E. Lifshin, L. Sawyer, J.R. Michael, *Scanning Electron Microscopy and X-Ray Microanalysis*, third ed., Kluwer, New York, 2003.
- ¹¹¹ D.R. Baer, M.H. Engelhard, *J. Electron. Spectrosc. Relat. Phenom.* 178-179 (2010) 415-432.
- ¹¹² Y. Wang, I.A. Weinstock, *Chem. Soc. Rev.* 41 (2012) 7479-7496.
- ¹¹³ C.M. Hagen, J.A. Widegren, P.M. Maitlis, R.G. Finke, *J. Am. Chem. Soc.* 127 (2005) 4423-4432.
- ¹¹⁴ H.N. Miras, E.F. Wilson, L. Cronin, *Chem. Commun.* (2009) 1297-1311.
- ¹¹⁵ J. Halpern, *Inorg. Chim. Acta* 50 (1981) 11-19.
- ¹¹⁶ J.J. Stracke, R.G. Finke, *ACS Catal.* (2013) submitted.
- ¹¹⁷ F. Puntoriero, G. La Ganga, A. Sartorel, M. Carraro, G. Scorrano, M. Bonchio, S. Campagna, *Chem. Commun.* 46 (2010) 4725-4727.

- ¹¹⁸ Y.V. Geletii, Z. Huang, Y. Hou, D.G. Musaev, T. Lian, C.L. Hill, *J. Am. Chem. Soc.* 131 (2009) 7522-7523.
- ¹¹⁹ M. Orlandi, R. Argazzi, A. Sartorel, M. Carraro, G. Scorrano, M. Bonchio, F. Scandola, *Chem. Commun.* 46 (2010) 3152-3154.
- ¹²⁰ B.S. Brunshwig, M.H. Chou, C. Creutz, N. Sutin, *J. Am. Chem. Soc.* 105 (1983) 4832-4833.
- ¹²¹ P. Ghosh, B.S. Brunshwig, M. Chou, C. Creutz, N. Sutin, *J. Am. Chem. Soc.* 106 (1984) 4772-4783.
- ¹²² A.R. Howells, A. Sankarraj, C. Shannon, *J. Am. Chem. Soc.* 126 (2004) 12258-12259.
- ¹²³ M. Sadakane, N. Rinn, S. Moroi, H. Kitatomi, T. Ozeki, M. Kurasawa, M. Itakura, S. Hayakawa, K. Kato, M. Miyamoto, S. Ogo, Y. Ide, T. Sano, *Z. Anorg. Allg. Chem.* 637 (2011) 1467-1474.
- ¹²⁴ E. Bayram, J.C. Linehan, J.L. Fulton, J.A.S. Roberts, N.K. Szymczak, T.D. Smurthwaite, S. Ozkar, M. Balasubramanian, R.G. Finke, *J. Am. Chem. Soc.* 133 (2011) 18889-18902.
- ¹²⁵ G.L. Elizarova, L.G. Matvienko, N.V. Lozhkina, V.N. Parmon, K.I. Zamarev, *React. Kinet. Catal. Lett.* 16 (1981) 191-194.
- ¹²⁶ G.L. Elizarova, L.G. Matvienko, N.V. Lozhkina, V.N. Parmon, *React. Kinet. Catal. Lett.* 22 (1983) 49-53.
- ¹²⁷ T.V. Kim, G.L. Elizarova, V.N. Parmon, *React. Kinet. Catal. Lett.* 26 (1984) 57-60.
- ¹²⁸ G.L. Elizarova, L.G. Matvienko, N.V. Lozhkina, V.N. Parmon, *React. Kinet. Catal. Lett.* 26 (1984) 62-72.
- ¹²⁹ G.L. Elizarova, T.V. Kim, L.G. Matvienko, V.N. Parmon, V.I. Nkitin, *React. Kinet. Catal. Lett.* 31 (1986) 455-459.
- ¹³⁰ G.L. Elizarova, L.G. Matvienko, V.N. Parmon, *J. Mol. Catal.* 43 (1987) 171-181.
- ¹³¹ O.P. Pestunova, G.L. Elizarova, V.N. Parmon, *Kinet. and Catal.* 41 (2000) 375-384.
- ¹³² G.L. Elizarova, G.M. Zhidomirov, V.N. Parmon, *Catal. Today* 58 (2000) 71-88.
- ¹³³ D. Shevchenko, M.F. Anderlund, A. Thapper, S. Styring, *Energy Environ. Sci.* 4 (2011) 1284-1287.
- ¹³⁴ M. Risch, D. Shevchenko, M.F. Anderlund, S. Styring, J. Heidkamp, K.M. Lange, A. Thapper, I. Zaharieva, *Int. J. Hydrog. Energy* 37 (2012) 8878-8888.
- ¹³⁵ D. Hong, J. Jung, J. Park, Y. Yamada, T. Suenobu, Y.-M. Lee, W. Nam, S. Fukuzumi, *Energy Environ. Sci.* 5 (2012) 7606-7616.

- ¹³⁶ V.Y. Shafirovich, V.V. Strelets, *New. J. Chem.* 2 (1978) 199-201.
- ¹³⁷ M.W. Kanan, D.G. Nocera, *Science* 321 (2008) 1072-1075.
- ¹³⁸ M.W. Kanan, Y. Surendranath, D.G. Nocera, *Chem. Soc. Rev.* 38 (2009) 109-114.
- ¹³⁹ D.A. Lutterman, Y. Surendranth, D.G. Nocera, *J. Am. Chem. Soc.* 131 (2009) 3838-3839.
- ¹⁴⁰ Y. Surendranth, M. Dinca, D.G. Nocera, *J. Am. Chem. Soc.* 131 (2009) 2615-2620.
- ¹⁴¹ M.W. Kanan, J. Yano, Y Surendranath, M. Dinca, V.K. Yachandra, D.G. Nocera, *J. Am. Chem. Soc.* 132 (2010) 13692-13701.
- ¹⁴² J.G. McAlpin, Y. Surendranath, M. Dinca, T.A. Stich, S.A. Stoian, W.H. Casey, D.G. Nocera, R.D. Britt, *J. Am. Chem. Soc.* 132 (2010) 6882-6883.
- ¹⁴³ Y. Surendranath, M.W. Kanan, D.G. Nocera, *J. Am. Chem. Soc.* 132 (2010) 16501-16509.
- ¹⁴⁴ M. Risch, V. Khare, I. Zaharieva, L. Gerencser, P. Chernev, H. Dau, *J. Am. Chem. Soc.* 131 (2009) 6936-6937.
- ¹⁴⁵ J.B. Gerken, E.C. Landis, R.J. Hamers, S.S. Stahl, *ChemSusChem* 3 (2010) 1176-1179.
- ¹⁴⁶ J.B. Gerken, J.G. McAlpin, J.Y.C. Chen, M.L. Rigsby, W.H. Casey, R.D. Britt, S.S. Stahl, *J. Am. Chem. Soc.* 133 (2011) 14431-14442.
- ¹⁴⁷ J.T. Kirner, J.J. Stracke, B.A. Gregg, R.G. Finke, Manuscript in preparation.
- ¹⁴⁸ H. Wang, W. You, B. Meng, X. Sun, H. Cheng, W. Shan, *J. Clust. Sci.* 21 (2010) 857-865.
- ¹⁴⁹ A. Mills, T. Russel, *J. Chem. Soc. Faraday Trans.* 87 (1991) 313-318.
- ¹⁵⁰ J.P. Collin, J.P. Sauvage, *Inorg. Chem.* 25 (1986) 135-141.
- ¹⁵¹ A.M. Morris, O.P. Anderson, R.G. Finke, *Inorg. Chem.* 48 (2009) 4411-4420.
- ¹⁵² R. Brimblecombe, D.R.J. Kolling, A.M. Bond, G.C. Dismukes, G.F. Swiegers, L. Spiccia, *Inorg. Chem.* 48 (2009) 7269-7279.
- ¹⁵³ R. Brimblecombe, A. Koo, G.C. Dismukes, G.F. Swiegers, L. Spiccia, *J. Am. Chem. Soc.* 132 (2010) 2892-2894.
- ¹⁵⁴ R.K. Hocking, R. Brimblecombe, L.-Y. Chang, A. Singh, M.H. Cheah, C. Glover, W.H. Casey, L. Spiccia, *Nature Chem.* 3 (2011) 491-466.
- ¹⁵⁵ M.M. Najafpour, A.N. Moghaddam, *Dalton Trans.* 41 (2012) 10292-10297.

- ¹⁵⁶ J. Gao, S. Cao, Q. Tay, Y. Liu, L. Yu, K. Ye, P.C.S. Mun, Y. Li, G. Rakesh, S.C.J. Loo, Z. Chen, Y. Zhao, C. Xue, Q. Zhang, *Sci. Rep.* 3 (2013) 1853.
- ¹⁵⁷ P.A. Lay, W.H.F. Sasse, *Inorg. Chem.* 24 (1985) 4707-4710.
- ¹⁵⁸ C. Creutz, N. Sutin, *Proc. Nat. Acad. Sci. USA* 72 (1975) 2858-2862.
- ¹⁵⁹ N.D. McDaniel, F.J. Coughlin, L.L. Tinker, S. Bernhard, *J. Am. Chem. Soc.* 130 (2008) 210-217.
- ¹⁶⁰ J.F. Hull, D. Balcells, J.D. Blakemore, C.D. Incarvito, O. Eisenstein, G.W. Brudvig, R.H. Crabtree, *J. Am. Chem. Soc.* 131 (2009) 8730-8731.
- ¹⁶¹ J.D. Blakemore, N.D. Schley, D. Balcells, J.F. Hull, G.W. Olack, C.D. Incarvito, O. Eisenstein, G.W. Brudvig, R.H. Crabtree, *J. Am. Chem. Soc.* 132 (2010) 16017-16029.
- ¹⁶² A. Savini, G. Bellachioma, G. Ciancaleoni, C. Zuccaccia, D. Zuccaccia, A. Macchioni, *Chem. Commun.* 46 (2010) 9218-9219.
- ¹⁶³ D.B. Grotjahn, D.B. Brown, J.K. Martin, D.C. Marelus, M.-C. Abadjian, H.N. Tran, G. Kalyuzhny, K.S. Vecchio, Z.G. Sp, echt, S.A. Cortes-Llamas, V. Mirando-Soto, C. van Niekerk, C.E. Moore, A.L. Rheingold, *J. Am. Chem. Soc.* 133 (2011) 19024-19027.
- ¹⁶⁴ A. Savini, A. Bucci, G. Bellachioma, L. Rocchigiani, C. Zuccaccia, A. Llobet, A. Macchioni, *Eur. J. Inorg. Chem.* (2013) In Press, DOI: 10.1002/ejic.201300530.
- ¹⁶⁵ U. Hintemair, S.W. Sheehan, A.R. Parent, D.H. Ess, D.T. Richens, P.H. Vaccaro, G.W. Brudvig, R.H. Crabtree, *J. Am. Chem. Soc.* 135 (2013) 10837-10851.
- ¹⁶⁶ N.D. Schley, J.D. Blakemore, N.K. Subbaiyan, C.D. Incarvito, F. D'Souza, R.H. Crabtree, G.W. Brudvig, *J. Am. Chem. Soc.* 133 (2011) 10473-10481.
- ¹⁶⁷ J.D. Blakemore, N.D. Schley, G.W. Olack, C.D. Incarvito, G.W. Brudvig, R.H. Crabtree, *Chem. Sci.* 2 (2011) 94-98.
- ¹⁶⁸ A. Singh, S.L.Y. Chang, R.K. Hocking, U. Bach, L. Spiccia, *Catal. Sci. Technol.* 3 (2013) 1725-1732.
- ¹⁶⁹ A. Singh, S.L.Y. Chang, R.K. Hocking, U. Bach, L. Spiccia, *Energy Environ. Sci.* 6 (2013) 579-586.
- ¹⁷⁰ S. Kozuch, J.M. Martin, *ACS Catal.* 2 (2012) 2787-2794.
- ¹⁷¹ G. Lente, *ACS Catal.* 3 (2013) 381-382.

III. ELECTROCATALYTIC WATER OXIDATION BEGINNING WITH THE COBALT POLYOXOMETALATE $[\text{Co}_4(\text{H}_2\text{O})_2(\text{PW}_9\text{O}_{34})_2]^{10-}$: IDENTIFICATION OF HETEROGENEOUS CoO_x AS THE DOMINANT CATALYSTⁱ

Overview

The question of “what is the true catalyst?” when beginning with the cobalt polyoxometalate (POM) $[\text{Co}_4(\text{H}_2\text{O})_2(\text{PW}_9\text{O}_{34})_2]^{10-}$ in electrochemical water oxidation catalysis is examined in pH 8.0 sodium phosphate buffer at a glassy carbon electrode—is $[\text{Co}_4(\text{H}_2\text{O})_2(\text{PW}_9\text{O}_{34})_2]^{10-}$ a true water oxidation catalyst (WOC), or just a precatalyst? Electrochemical, kinetic, UV-vis, SEM, EDX, and other data provide four main lines of compelling evidence that, under the conditions used herein, the dominant water oxidation catalyst is actually heterogeneous CoO_x and not homogeneous $[\text{Co}_4(\text{H}_2\text{O})_2(\text{PW}_9\text{O}_{34})_2]^{10-}$.

Introduction

Efficient storage of energy is requisite for the broad implementation of solar energy technologies, since photon energy input is available only while the sun is shining.¹ The storage of energy in chemical bonds is one arguably superior solution to the energy storage problem.¹ Conversion of solar to chemical energy can be achieved by oxidation of water to oxygen and protons with simultaneous reduction of protons to hydrogen fuel.² Of these two half-reactions, the oxidation of water is more demanding because it encompasses the transfer of four electrons

ⁱ This chapter contains a manuscript published in the Journal of the American Chemical Society (Stracke, J. J.; Finke, R. G. *J. Am. Chem. Soc.* **2011**, *133*, 14872). As addressed in Chapter II of this dissertation, the cobalt polyoxometalate, $[\text{Co}_4(\text{H}_2\text{O})_2(\text{PW}_9\text{O}_{34})_2]^{10-}$, has been reported as an active, stable, homogeneous WOC (Yin et al., *Science* **2010**, *328*, 342). The current chapter describes our investigation into whether $[\text{Co}_4(\text{H}_2\text{O})_2(\text{PW}_9\text{O}_{34})_2]^{10-}$ is a homogeneous WOC or is transformed into a heterogeneous WOC when the water oxidation reaction is driven electrochemically.

and four protons and often requires large electrochemical overpotentials in order to drive the reaction at an appreciable rate.³

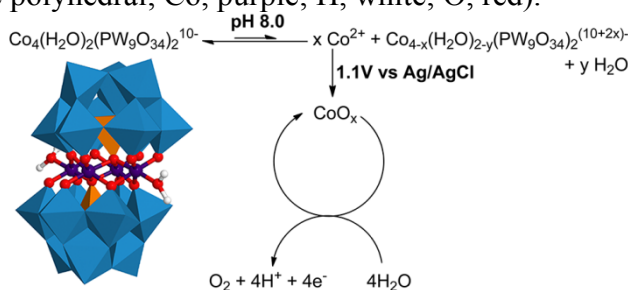
In-situ-formed CoO_x water oxidation catalysts (WOCs) have been reported by Nocera and co-workers and others;^{4,5} these catalysts are formed under oxidizing conditions from aqueous Co(II) salts, operate at moderate overpotentials, and are oxidatively stable.⁴ The CoO_x formula is used herein to indicate a cobalt-oxo/hydroxo-based solid that can incorporate additional counterions and anions (e.g., we observed herein a CoO_x catalyst with the empirically observed formula $\text{Co}_a\text{O}_b\text{Na}_c\text{P}_d$, see below).

A 2010 *Science* paper and a 2011 *JACS* paper reported that the cobalt containing polyoxometalate (POM) $[\text{Co}_4(\text{H}_2\text{O})_2(\text{PW}_9\text{O}_{34})_2]^{10-}$ is an extremely active, stable, homogeneous water oxidation catalyst (WOC) when using either chemical or photochemical oxidants.^{6,7} However, no detailed study of this cobalt POM as an electrochemical WOC has previously appeared. Two standard electrochemical studies of $[\text{Co}_4(\text{H}_2\text{O})_2(\text{PW}_9\text{O}_{34})_2]^{10-}$ round out what is known about the redox activity of this POM^{8,9} work which did not report any type of nor any WOC.

We report herein experimental results providing compelling evidence that CoO_x , and not the $[\text{Co}_4(\text{H}_2\text{O})_2(\text{PW}_9\text{O}_{34})_2]^{10-}$ POM precatalyst, is the dominant WOC when the oxidizing equivalents are supplied by a glassy carbon electrode in 0.1 M sodium phosphate buffer at pH 8.0 under air (Scheme 3.1). This conclusion is supported by the following four primary lines of evidence: (1) $[\text{Co}_4(\text{H}_2\text{O})_2(\text{PW}_9\text{O}_{34})_2]^{10-}$ degrades in pH 8.0 sodium phosphate buffer, as determined by UV-vis spectroscopy and by electrochemical measurement of the aqueous, leached Co(II) concentration; (2) a CoO_x WOC film is formed in situ from $[\text{Co}_4(\text{H}_2\text{O})_2(\text{PW}_9\text{O}_{34})_2]^{10-}$ solutions on a glassy carbon working electrode under oxidizing

conditions (1.1 V vs Ag/AgCl) by electrochemical, UV-vis, SEM and EDX methods ; (3) 58 μM Co(II) (or its functional equivalent, hereafter noted as *apparent Co(II)*, *vide infra*) is detectable in solution by 2 independent methods; and (4) authentic $\text{Co}(\text{NO}_3)_2$, at the 58 μM level leached into solution from the $[\text{Co}_4(\text{H}_2\text{O})_2(\text{PW}_9\text{O}_{34})_2]^{10-}$, *quantitatively* accounts for all of the water oxidation activity within experimental error.

Scheme 3.1. Proposed heterogeneous CoO_x catalyst formation pathway. On the left is a polyhedral plus ball-and-stick model of the cobalt polyoxometalate starting material (WO_6 , blue polyhedral; PO_4 , orange polyhedral; Co, purple; H, white; O, red).



Results and Discussion

The $\text{Na}_{10}[\text{Co}_4(\text{H}_2\text{O})_2(\text{PW}_9\text{O}_{34})_2]$ POM was synthesized according to the procedure of Weakley¹⁰ as modified by Hill and co-workers.⁶ The POM was recrystallized twice from water. Its basic structure confirmed by IR spectroscopy [see the Supporting Information (SI)]. The purity of the cobalt POM—especially the absence of any detectable, excess Co(II) present as a simple counteranion—was confirmed by elemental analysis as detailed in the Supporting Information.

Initial investigations of the catalytic activity of $[\text{Co}_4(\text{H}_2\text{O})_2(\text{PW}_9\text{O}_{34})_2]^{10-}$ solutions were conducted using a standard three-electrode electrochemical setup; unless otherwise noted, the solutions were in contact with air and a glassy carbon working electrode ($A = 0.071 \text{ cm}^2$), Ag/AgCl reference electrode, and a platinum wire counter electrode were used for all electrochemical measurements which follow (full experimental details are available in the SI). One minute after $[\text{Co}_4(\text{H}_2\text{O})_2(\text{PW}_9\text{O}_{34})_2]^{10-}$ (500 μM) was dissolved in 0.1 M sodium phosphate

buffer at pH 8.0, linear sweep voltammetry showed an oxidation wave (onset at 1.05 V); as this solution was aged over a 3 h period, the oxidation wave *increased by greater than 10-fold in magnitude and shifted to lower onset potentials* (Figure 3.1). Since the catalytic oxidation wave increased over time, the most active catalyst cannot be the initially present $[\text{Co}_4(\text{H}_2\text{O})_2(\text{PW}_9\text{O}_{34})_2]^{10-}$; the most active catalyst must instead be a derivative of the cobalt POM. Restated, $[\text{Co}_4(\text{H}_2\text{O})_2(\text{PW}_9\text{O}_{34})_2]^{10-}$ is a precatalyst of the most active WOC.

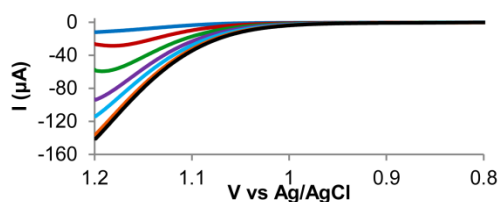


Figure 3.1. Linear sweep voltammetry of 500 μM $[\text{Co}_4(\text{H}_2\text{O})_2(\text{PW}_9\text{O}_{34})_2]^{10-}$ in pH 8.0 sodium phosphate buffer monitored for the first three hours after dissolving in the electrolyte; scans were taken at $t = 0.02$ (blue), 0.5 (red), 1.0 (green), 1.5 (purple), 2.0 (light-blue), 2.5 (orange), and 3.0 (black) hours.

Cyclic voltammetry of a 500 μM $[\text{Co}_4(\text{H}_2\text{O})_2(\text{PW}_9\text{O}_{34})_2]^{10-}$ solution initially showed a small quasi-irreversible oxidation wave at ~ 1.1 V with a maximum anodic current of 11 μA (Figure 3.2(a); an expanded view is shown in Figure S3.1 in the SI). When a constant potential of 1.1V vs Ag/AgCl was applied to the cell, the oxidation current increased rapidly and bubbles (O_2 ; see below) formed at the working electrode. Concomitant with the increase in current, a film (identified as CoO_x by UV-vis, SEM, and EDX, see below) was deposited onto the glassy carbon electrode. If the electrode was then removed from solution, rinsed with water, and placed into a solution containing only 0.1 M sodium phosphate buffer at pH 8.0 (i.e., no $[\text{Co}_4(\text{H}_2\text{O})_2(\text{PW}_9\text{O}_{34})_2]^{10-}$), the catalytic activity was maintained at the previously observed levels in both cyclic voltammetry and controlled-potential electrolysis experiments (Figure 3.2a,b). The slow decrease in catalytic activity of the film is attributed to poor adhesion of the film to glassy

carbon, resulting in dissolution of the film in pH 8.0 sodium phosphate buffer; that poor film adhesion also prevented longer electrodeposition times.

SEM of the electrodeposited catalytic film on a glassy carbon plate showed complete coverage of the substrate plus sporadic nodules that measured ~100 nm in diameter (Figure S3.2). EDX revealed that these catalytic films contained oxygen, cobalt, sodium, and phosphorus (with an approximate Co:Na:P ratio of 4:1:1) as well as carbon from the substrate (Figure S3.3). In comparison, for their authentic CoO_x catalyst films, Nocera and co-workers observed a similar Co:P ratio ranging from 2:1 to 3:1 for films deposited from 1 mM $\text{Co}(\text{NO}_3)_2$ in 0.1 M potassium phosphate buffer (pH 7.0).⁴

Notably, *no tungsten* was observed in our CoO_x film (i.e., no detectable W-containing cobalt POM). As a control, SEM of a drop-coated $\text{Na}_{10}[\text{Co}_4(\text{H}_2\text{O})_2(\text{PW}_9\text{O}_{34})_2]$ film showed micrometer-sized, block-like crystallites (Figure S3.2). EDX analysis showed a film composed of oxygen, tungsten, sodium, and cobalt (although phosphorus was presumably present, it could not be identified because the tungsten $M\gamma$ line overlaps with the phosphorus $K\alpha, \beta$ lines shown in Figure S3.4). This control confirmed that the cobalt POM would have been observed by SEM/EDX in our hands had it been present. Comparison of the $\text{Na}_{10}[\text{Co}_4(\text{H}_2\text{O})_2(\text{PW}_9\text{O}_{34})_2]$ and CoO_x films in Figure S3.2 demonstrates that the electrodeposited heterogeneous catalyst is fundamentally different than the cobalt POM starting material.

The CoO_x film could also be deposited onto a transparent indium tin oxide (ITO) electrode under the conditions given above. UV-vis of the resultant CoO_x film on ITO showed no evidence of the $[\text{Co}_4(\text{H}_2\text{O})_2(\text{PW}_9\text{O}_{34})_2]^{10-}$ POM (Figure S3.6). Since $[\text{Co}_4(\text{H}_2\text{O})_2(\text{PW}_9\text{O}_{34})_2]^{10-}$ could not be observed in the catalytic film by EDX or UV-vis spectroscopy and the catalytic film was more active than the initial $[\text{Co}_4(\text{H}_2\text{O})_2(\text{PW}_9\text{O}_{34})_2]^{10-}$ solution, the evidence again implies

that CoO_x and not the $[\text{Co}_4(\text{H}_2\text{O})_2(\text{PW}_9\text{O}_{34})_2]^{10-}$ is the dominant catalytic species. A caveat here is because ITO was used as an electrode, the system is not rigorously comparable to studies using glassy carbon.

An important question is how is the $[\text{Co}_4(\text{H}_2\text{O})_2(\text{PW}_9\text{O}_{34})_2]^{10-}$ being transformed into CoO_x under the reaction conditions? Is the POM converting directly to the CoO_x catalyst, or does it release freely diffusing Co(II) [or its functional equivalent, denoted *apparent* Co(II) , *vide infra*], which in turn, is transformed/oxidized into the heterogeneous catalyst? Relevant here is the fact that the Co(II) dissociation constants of several cobalt-substituted POMs have been measured by Contant and Hamlaoui et al. and found to be both non-zero and in a range that could yield catalytically viable amounts of Co(II) , *vide infra*. Specifically, the dissociative equilibrium constants for Co(II) -substituted $\alpha_1\text{-P}_2\text{W}_{17}\text{O}_{61}^{10-}$, $\alpha_2\text{-P}_2\text{W}_{17}\text{O}_{61}^{10-}$, and $\alpha\text{-PW}_{11}\text{O}_{39}^{7-}$ are approximately $10^{-7.5}$, $10^{-5.5}$, and $10^{-4.5}$ in 1 M LiClO_4 ¹¹ and $10^{-5.6}$ in 1 M NaClO_4 for $\alpha_2\text{-P}_2\text{W}_{17}\text{O}_{61}^{10-}$.¹² This in turn means that leaching of Co(II) from the $[\text{Co}_4(\text{H}_2\text{O})_2(\text{PW}_9\text{O}_{34})_2]^{10-}$ POM in aqueous solution is a plausible and arguably the simplest (i.e., Ockham's razor) *hypothesis* en route to the observed CoO_x .

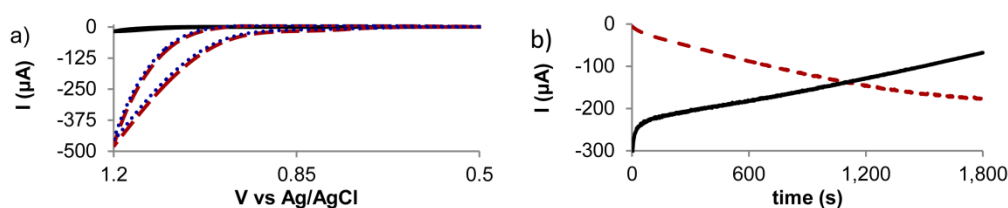


Figure 3.2. (a) Cyclic voltammograms of 500 μM $[\text{Co}_4(\text{H}_2\text{O})_2(\text{PW}_9\text{O}_{34})_2]^{10-}$ immediately after dissolving (black solid curve) and after 30 minutes electrolysis at 1.1 V vs Ag/AgCl (red dashed curve); CV of the catalytic film formed during the 30 minute electrolysis, but after washing with water and placing the working electrode into a pure sodium phosphate electrolyte (i.e. no added $[\text{Co}_4(\text{H}_2\text{O})_2(\text{PW}_9\text{O}_{34})_2]^{10-}$) (blue dotted curve). The scan rate was 100mV/s. (b) Controlled potential electrolysis of 500 μM $[\text{Co}_4(\text{H}_2\text{O})_2(\text{PW}_9\text{O}_{34})_2]^{10-}$ (red dashed curve) and of the catalytic film in sodium phosphate electrolyte without added POM (black solid curve). Electrolysis experiments were stirred at 600 rpm. Supporting electrolyte is 0.1M sodium phosphate buffer (pH 8.0) for all experiments.

Hence, the solution stability of $[\text{Co}_4(\text{H}_2\text{O})_2(\text{PW}_9\text{O}_{34})_2]^{10-}$ was determined next by UV-vis spectroscopy and electrochemical methods. Upon dissolution of 500 μM $[\text{Co}_4(\text{H}_2\text{O})_2(\text{PW}_9\text{O}_{34})_2]^{10-}$ in 0.1 M sodium phosphate buffer at pH 8.0 in air, the absorbance band at 580 nm decreased by $4.3(\pm 0.6)\%$ over the course of a 3 h period (Figure 3.3). This decrease in the absorbance corresponds to degradation ca. 21.5 μM of $[\text{Co}_4(\text{H}_2\text{O})_2(\text{PW}_9\text{O}_{34})_2]^{10-}$ ($\leq 86 \mu\text{M}$ Co(II), or $\sim 64 \mu\text{M}$ Co(II) for $x = 3$, Scheme 3.1 and Figure S3.11).¹³

In contrast, the aforementioned 2010 *Science* paper reported that 0.75-1.0 mM $[\text{Co}_4(\text{H}_2\text{O})_2(\text{PW}_9\text{O}_{34})_2]^{10-}$ solutions did not vary with age or pH when the electrolyte was sodium acetate (50 mM, pH 3.5, 1 day), sodium phosphate (11 mM, pH 8.0, 1 month), or sodium borate (50 mM, pH 9.0, 1 month).⁶ In a separate study, Ohlin et al. found that decreasing the pH from 7.2 to 4.0 in 1.1 mM $[\text{Co}_4(\text{H}_2\text{O})_2(\text{PW}_9\text{O}_{34})_2]^{10-}$ solutions yielded a decrease in the 580 nm absorption band and an increase in the absorption below ~ 475 nm; however, Co(II) EPR measurements did not detect any POM decomposition over this pH range, albeit over an unspecified time scale.¹⁴ In short, and as is already known,¹⁵ these types of inorganic POM ligands are *not* immune to hydrolytic degradation under acidic ($\text{pH} < 4$) or basic ($\text{pH} \geq 8$) conditions. Indeed, the expected hydrolytic instability of $[\text{Co}_4(\text{H}_2\text{O})_2(\text{PW}_9\text{O}_{34})_2]^{10-}$, with which we have worked before,¹⁶ was one primary reason we were drawn to examine the question “who is the true WOC catalyst?” for this cobalt POM.

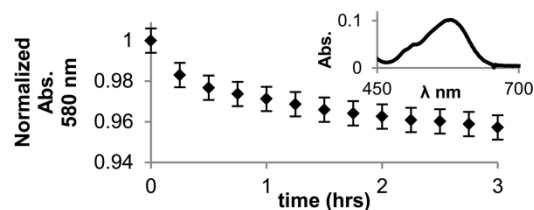


Figure 3.3. Normalized peak absorbance at 580 nm for a 500 μM $[\text{Co}_4(\text{H}_2\text{O})_2(\text{PW}_9\text{O}_{34})_2]^{10-}$ in 0.1 M sodium phosphate solution (pH 8.0). Inset: absorption spectrum ~ 1 minute after dissolution of the POM, which is defined as $t = 0$. The decrease over 3 hours was $4.3(\pm 0.6)\%$.

In order to determine whether cobalt was being released by $[\text{Co}_4(\text{H}_2\text{O})_2(\text{PW}_9\text{O}_{34})_2]^{10-}$ in pH 8.0 solutions, the *apparent* $[\text{Co}^{2+}]$ was determined via catalytic oxidative linear-sweep voltammetry [the *apparent Co(II)* was determined, since we do not know unequivocally whether it is just aqueous Co^{2+} , a Co(II)-POM fragment, or conceivably some other Co(II)-containing species, see below). A Co(II) calibration curve was constructed using $\text{Co}(\text{NO}_3)_2$ as a standard precursor for a CoO_x catalyst (Figure S3.8); linear sweep voltammetry of $\text{Co}(\text{NO}_3)_2$ solutions showed that the oxidation wave current was directly proportional to $[\text{Co}^{2+}]$ over the range ~1.0-1.1 V; the resultant calibration curve was linear over the concentration range and scan rates used herein ($[\text{Co}^{2+}] \leq 75 \mu\text{M}$; $20\text{mV/s} \leq \text{scan rate} \leq 100 \text{mV/s}$). Noteworthy here is the fact that the oxidation wave (~1.0 V onset vs Ag/AgCl) in these scans corresponds to catalytic water oxidation by the CoO_x film, as was reported previously by Nocera and co-workers and as reproduced herein, *vide supra*.^{4a}

Using the authentic $[\text{Co}^{2+}]$ calibration curve in Figure S3.8 in conjunction with linear sweep voltammetry of $[\text{Co}_4(\text{H}_2\text{O})_2(\text{PW}_9\text{O}_{34})_2]^{10-}$ (Figure 3.1) allowed calculation of the apparent $[\text{Co}^{2+}]$ versus time curve for a 500 μM cobalt POM solution, Figure 3.4. Over the course of 3 hours, the calculated apparent $[\text{Co}^{2+}]$ increased from 1 ± 1 to $58 \pm 2 \mu\text{M}$. In order to verify that the oxidation wave is caused by a Co(II) species, the apparent $[\text{Co}^{2+}]$ was confirmed by a modified procedure for cathodic stripping voltammetry reported by Krolicka et al. (experimental details are given in the SI);¹⁷ this complementary method showed that after 3 h of aging, an initially 500 μM $[\text{Co}_4(\text{H}_2\text{O})_2(\text{PW}_9\text{O}_{34})_2]^{10-}$ solution contained an apparent $[\text{Co}^{2+}]$ of $56(\pm 2) \mu\text{M}$. The *excellent agreement* between the apparent $[\text{Co}^{2+}]$ values obtained from the two methods, along with the observed decrease in the 580 nm absorption band of the POM, provides compelling evidence that

the starting $[\text{Co}_4(\text{H}_2\text{O})_2(\text{PW}_9\text{O}_{34})_2]^{10-}$ slowly degrades in 0.1 M phosphate buffer solution at pH 8.0.

Direct comparison of the catalytic activities of authentic $\text{Co}(\text{NO}_3)_2$ and $[\text{Co}_4(\text{H}_2\text{O})_2(\text{PW}_9\text{O}_{34})_2]^{10-}$ solutions was made next in order to quantify how much of the catalytic water oxidation reaction could be attributed to the $\text{Co}(\text{II})$ or its functional equivalent available in aged cobalt POM solutions. Significantly, and to verify that WOC activity was being measured, the WOC product O_2 was measured in the solution during catalytic controlled-potential electrolysis by using a fluorescence based O_2 sensor (Neofox/FOXY phase-measurement system).

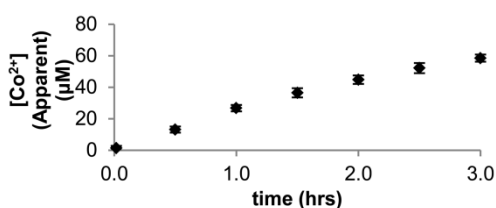


Figure 3.4. Increasing apparent $[\text{Co}^{2+}]$ in $[\text{Co}_4(\text{H}_2\text{O})_2(\text{PW}_9\text{O}_{34})_2]^{10-}$ solution vs time based on the anodic current at 1.1 V for a 500 μM $[\text{Co}_4(\text{H}_2\text{O})_2(\text{PW}_9\text{O}_{34})_2]^{10-}$ solution and the $[\text{Co}^{2+}]$ calibration curve (Figure S3.8). The supporting electrolyte was 0.1 M sodium phosphate (pH 8.0).

As shown in Figure 3.5, the O_2 generated over a 5 min period during controlled-potential electrolysis (1.1 V vs Ag/AgCl) of a 500 μM $[\text{Co}_4(\text{H}_2\text{O})_2(\text{PW}_9\text{O}_{34})_2]^{10-}$ solution aged for 3 h is identical within experimental error to the O_2 generated by the amount of leached, apparent $\text{Co}(\text{II})$ independently determined above, that is, by a 58 μM $\text{Co}(\text{NO}_3)_2$ solution (1.09 ± 0.13 versus 1.10 ± 0.12 μmol of O_2). The theoretical O_2 yields (i.e., the moles of electrons passed during electrolysis divided by the stoichiometric factor of 4) are 1.05 ± 0.14 and 1.06 ± 0.03 μmol O_2 for solutions containing 500 μM $[\text{Co}_4(\text{H}_2\text{O})_2(\text{PW}_9\text{O}_{34})_2]^{10-}$ and 58 μM $\text{Co}(\text{NO}_3)_2$, respectively. This result indicates that the low (58 μM) apparent concentrations of $\text{Co}(\text{II})$ present in

$[\text{Co}_4(\text{H}_2\text{O})_2(\text{PW}_9\text{O}_{34})_2]^{10-}$ solutions in pH 8.0 sodium phosphate buffer *quantitatively account for all of the observed catalytic water oxidation activity within the stated $\pm 12\%$ experimental error.*

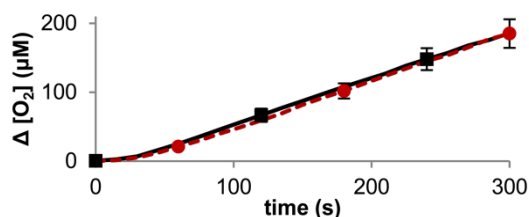


Figure 3.5. Change in O_2 solution concentration ($\Delta[\text{O}_2] = [\text{O}_2]_{(t)} - [\text{O}_2]_{(t=0)}$) produced during controlled potential electrolysis at 1.1V for a $500 \mu\text{M}$ $[\text{Co}_4(\text{H}_2\text{O})_2(\text{PW}_9\text{O}_{34})_2]^{10-}$ solution aged for 3 h (red ●) and a $58 \mu\text{M}$ $\text{Co}(\text{NO}_3)_2$ solution (■). The supporting electrolyte was 0.1 M sodium phosphate buffer (pH 8.0). $[\text{O}_2]$ was recorded every 15 s; for clarity, only the points at 60 s intervals are displayed. The solid and dashed lines are provided solely as guides for the eye (i.e., no curve fitting was done). The glassy carbon working electrode ($A = 1.92 \pm 0.07 \text{ cm}^2$) and Ag/AgCl reference electrodes were separated from the platinum auxiliary electrode via a fine frit; the working compartment was stirred at 600 rpm. The short induction period at the start of the experiment is due to both a slow response of the O_2 sensor and initially slower water oxidation (the CoO_x film activity increases as more material is electrodeposited).

In conclusion, we have provided four main lines of compelling evidence that *under the conditions used in this study*, the Co-containing POM in $[\text{Co}_4(\text{H}_2\text{O})_2(\text{PW}_9\text{O}_{34})_2]^{10-}$ solutions at pH 8.0 partially decomposes to release Co(II) or its functional equivalent, which in turn forms a well-precedented active CoO_x WOC under oxidizing conditions. Our results reveal the important insight that $[\text{Co}_4(\text{H}_2\text{O})_2(\text{PW}_9\text{O}_{34})_2]^{10-}$ is *not* the most active WOC under the conditions examined herein.¹⁸ Our results are also consistent with a growing trend in the literature that claims of water oxidation by homogeneous molecular complexes must attempt to disprove the often facile catalysis by what can be low levels of the corresponding known M_xO_y WOCs.¹⁹ Such mechanistic studies are central to a better understanding and rational improvement of both the present, as well as all other, WOCs since catalyst activity, stability, selectivity, isolability, and regeneration of these—indeed of all—catalysts depend on the identity of the true catalyst.²⁰

Supporting Information

Experimental Section

Materials

$\text{Na}_{10}[\text{Co}_4(\text{H}_2\text{O})_2(\text{PW}_9\text{O}_{34})_2]\cdot 27\text{H}_2\text{O}$ was synthesized and purified according to the procedure of Yin et al.⁶ Specifically, it was recrystallized twice from water. Purity was verified by IR spectroscopy in comparison to the literature and cobalt elemental analysis to ensure the absence of Co(II) as a counter-ion within experimental error (Calculated: 4.33% Found: 4.50%). All other chemicals were obtained from Sigma Aldrich or Fisher and used without further purification. Aqueous solutions were made with 18 M Ω water from a Barnstead Nanopure water purification system. Glassy carbon plates were obtained from Alfa Aesar. Glassy carbon (3mm diameter) and Ag/AgCl reference electrodes were obtained from CH Instruments. Indium tin oxide coated glass slides (ITO substrates) with 8-12 Ω /square resistance were obtained from Delta Technologies.

Electrochemical Measurements

A CH Instruments 630D potentiostat was used for all electrochemical measurements. Unless otherwise noted, all electrochemical experiments used the following standard conditions: glassy carbon (3mm diameter) working, Ag/AgCl reference, and platinum wire auxiliary electrodes; sodium phosphate buffer (0.1 M, pH 8.0) supporting electrolyte. Solutions were *not* purged with Argon and were open to an air atmosphere unless otherwise noted. Glassy carbon electrodes were cleaned between experiments by polishing for 60 seconds with 0.05 μm polishing powder (CH Instruments), rinsing with water, and sonicating in water for 30 seconds, despite the manufacturer's recommendation not to use ultrasonic cleaning. Note that when sonication was not used, residual polishing powder was left on the glassy carbon surface which

led to lower and irregular electrochemical currents relative to sonicated electrodes, consistent with established literature.²¹ Experiments using the 3 mm diameter glassy carbon electrode were also pre-conditioned by holding the potential at 1.2 V in 0.1 M sodium phosphate buffer (pH 8.0) for 30 seconds. Stirring rates were measured using a Monarch tachometer.

Electrochemical Deposition of CoO_x Film from [Co₄(H₂O)₂(PW₉O₃₄)₂]¹⁰⁻ Solution and Subsequent Testing in Pure Supporting Electrolyte

5.4 mg of Na₁₀[Co₄(H₂O)₂(PW₉O₃₄)₂]·27H₂O were weighed into a 2 dram vial and dissolved in 2.00 mL of sodium phosphate electrolyte. Immediately after dissolving the polyoxometalate, the solution was stirred (600 rpm) while the working electrode was held at 1.1V vs Ag/AgCl for 30-60 minutes. Electrochemical water oxidation activity of the resultant, deposited film was then tested in the [Co₄(H₂O)₂(PW₉O₃₄)₂]¹⁰⁻ solution by cyclic voltammetry from 0.5-1.2V with a scan rate = 20 mV/s. The electrode was rinsed with water and placed into pure 0.1 M sodium phosphate electrolyte (i.e., no added [Co₄(H₂O)₂(PW₉O₃₄)₂]¹⁰⁻). Electrochemical activity of the CoO_x film was tested by cyclic voltammetry (0.5-1.2V, scan rate = 10 mV/s) and controlled potential electrolysis with stirring at 1.1V for 30 minutes.

Linear Sweep Voltammetry of Co(NO₃)₂

Linear sweep voltammetry of Co(NO₃)₂ solutions were conducted by scanning from 0.5-1.2V vs Ag/AgCl at 20 mV/s and for [Co²⁺] = 0, 25, 50, and 75 μM. [Co²⁺] was plotted versus the catalytic anodic current at 1.1V in order to generate a cobalt(II) calibration curve Figure S3.8(a). Linear sweep voltammetry of standard cobalt solutions were also recorded at a 100 mV/s scan rate; however, the anodic current at 1.1V was less linear at the faster scan rate. Each measurement was repeated three times.

Linear Sweep Voltammetry of $[\text{Co}_4(\text{H}_2\text{O})_2(\text{PW}_9\text{O}_{34})_2]^{10-}$

5.4 mg of $\text{Na}_{10}[\text{Co}_4(\text{H}_2\text{O})_2(\text{PW}_9\text{O}_{34})_2] \cdot 27\text{H}_2\text{O}$ was dissolved in 2.00 mL of sodium phosphate electrolyte. Immediately after the polyoxometalate dissolved, the linear sweep voltammogram was recorded from 0.5 to 1.2V at 20 mV/s. Subsequent linear sweep voltammetry scans were taken every 30 minutes for 3 hours. This procedure was repeated three times.

Control Experiment of Linear Sweep Voltammetry Under an Argon Atmosphere: 5.4 mg of $\text{Na}_{10}[\text{Co}_4(\text{H}_2\text{O})_2(\text{PW}_9\text{O}_{34})_2] \cdot 27\text{H}_2\text{O}$ was dissolved in 2.00 mL of sodium phosphate electrolyte which had been purged with argon for ~30 minutes. Immediately after the polyoxometalate dissolved, the linear sweep voltammogram was recorded from 0.5 to 1.2V at 20 mV/s. After a period of 3 hours, another linear sweep voltammogram was recorded from 0.5 to 1.2V at 20 mV/s. The cobalt polyoxometalate solution was kept under a flow of argon during the electrochemical and aging processes. This data is shown and discussed in Figure S3.14.

Cathodic Adsorptive Stripping Analysis

The procedure used here is a modification of a previous method reported by Krolicka et al.¹⁷ As noted above, the following experiments were performed in air.

Electrode Preparation: The glassy carbon electrode (3 mm diameter) was plated with bismuth by controlled potential electrolysis at -0.25V vs Ag/AgCl for 45 seconds in an aqueous solution containing 0.02 M $\text{Bi}(\text{NO}_3)_3$, 0.5 M LiBr, and HCl (1 M). The bismuth coated working electrode was then washed with water. The coated electrode was then placed into the cobalt analyte solution (containing either $\text{Co}(\text{NO}_3)_2$ or $\text{Na}_{10}[\text{Co}_4(\text{H}_2\text{O})_2(\text{PW}_9\text{O}_{34})_2] \cdot 27\text{H}_2\text{O}$, as detailed below) and was preconditioned by scanning from -0.7 to -1.3V at 10 mV/s.

Calibration Curve using $\text{Co}(\text{NO}_3)_2$: Following electrode preconditioning, a linear sweep voltammogram was obtained for $\text{Co}(\text{NO}_3)_2$ solutions by scanning from -0.7 to -1.3V at 10 mV/s.

A sample scan is shown in Figure S3.9. Standard solutions contained $[\text{Co}^{2+}] = 1, 5, 10, \text{ and } 20$ μM dissolved in sodium phosphate electrolyte (0.1 M, pH 8.0). The area of the cathodic peak at approximately -1.05V was measured using the analysis software included with the CH Instruments potentiostat; this area was then plotted versus $[\text{Co}^{2+}]$ to generate a calibration curve (Figure S3.10).

Measurement of $[\text{Co}^{2+}]$ in $\text{Na}_{10}[\text{Co}_4(\text{H}_2\text{O})_2(\text{PW}_9\text{O}_{34})_2]$ Solutions: 2.7 mg

$\text{Na}_{10}[\text{Co}_4(\text{H}_2\text{O})_2(\text{PW}_9\text{O}_{34})_2]$ was dissolved in 1.00 mL of sodium phosphate electrolyte. After aging for 3 hours, 0.50 mL of this solution was added to 1.5 mL of a mixture containing sodium phosphate electrolyte (0.1 M, pH 8.0) and dimethylglyoxime (100 μM). Following preconditioning of the bismuth electrode (see above), linear sweep voltammetry was conducted by scanning from -0.7 to -1.3 V at 10 mV/s. The area of the cathodic peak at ~ 1.05 V was used in combination with the previously described calibration curve (S10) in order to determine the $[\text{Co}^{2+}]$ in solution; this $[\text{Co}^{2+}]$ was then multiplied by 4 in order to account for dilution made during the experiment.

Oxygen Measurements

Oxygen measurements were made using an Ocean Optics Neoflex Phase Measurement System with a FOXY-R probe. The probe was calibrated using a two point curve (0 and 20.9%). Oxygen concentrations were measured in solution during controlled potential electrolysis at 1.1 V vs Ag/AgCl using a glassy carbon plate working electrode ($A = 1.91 \pm 0.07 \text{ cm}^2$). A two compartment H-cell separated by a fine frit was used for these experiments; each compartment in the cell has a total volume of ~ 15 mL. The working compartment of the electrochemical cell contained the glassy carbon plate working electrode, the Ag/AgCl reference electrode, and the O₂ FOXY-R probe and was stirred at 600 rpm. This compartment was filled (6 mL) with either

58 μM $\text{Co}(\text{NO}_3)_2$ plus sodium phosphate electrolyte (0.1 M, pH 8.0) or 500 μM $[\text{Co}_4(\text{H}_2\text{O})_2(\text{PW}_9\text{O}_{34})_2]^{10-}$ plus sodium phosphate electrolyte (0.1 M, pH 8.0) with 3 hour aging. The second compartment of the electrochemical cell contained the platinum wire auxiliary electrode and was filled with 6 mL of sodium phosphate buffer (0.1 M, pH 8.0). The electrolyte solution was in contact with air during these experiments.

A control experiment was conducted where the working compartment contained no cobalt catalyst and only sodium phosphate electrolyte (0.1 M, pH 8.0); during the 5 minute bulk electrolysis (1.1 V vs Ag/AgCl) of this solution a current of $\sim 30 \mu\text{A}$ was observed and an O_2 increase of 10 (± 18) nmoles was detected (i.e. no O_2 is produced in this no-cobalt-catalyst control experiment).

UV-Visible Spectroscopy

UV-Visible spectra were recorded on an HP 8452A Diode Array Spectrophotometer.

Under an air atmosphere: 5.4 mg of $\text{Na}_{10}[\text{Co}_4(\text{H}_2\text{O})_2(\text{PW}_9\text{O}_{34})_2] \cdot 27\text{H}_2\text{O}$ was dissolved in 2.00 mL of sodium phosphate electrolyte and spectra were recorded every 15 min. in a quartz cuvette (1 cm path length). Spectra were corrected by subtracting the average absorbance between 700-800 nm. This experiment was also conducted using 5.4 mg of $\text{Na}_{10}[\text{Co}_4(\text{H}_2\text{O})_2(\text{PW}_9\text{O}_{34})_2] \cdot 27\text{H}_2\text{O}$ dissolved in 2.00 mL of 0.1 M lithium perchlorate (Figure S3.7). When the 500 μM $\text{Na}_{10}[\text{Co}_4(\text{H}_2\text{O})_2(\text{PW}_9\text{O}_{34})_2] \cdot 27\text{H}_2\text{O}$ solutions in sodium phosphate buffer were aged for longer periods (e.g., one week), a small amount of pink precipitate forms and the absorbance of the 580 nm band decreases by $>20\%$ relative to the initial spectrum.

Under an argon atmosphere: 5.4 mg of $\text{Na}_{10}[\text{Co}_4(\text{H}_2\text{O})_2(\text{PW}_9\text{O}_{34})_2] \cdot 27\text{H}_2\text{O}$ was dissolved in 2.00 mL of sodium phosphate electrolyte (which had been purged with Ar for ~ 30 minutes) and spectra were recorded every 15 min. in an air free, glass cuvette (1 cm path length). Spectra

were corrected by subtracting the average absorbance between 700-800 nm. As shown in Figure S3.13, the normalized absorbance at 580 nm decreases by $8.8(\pm 2.0)\%$ during the 3 hour experiment.

IR Spectroscopy

IR spectra were made on a Nicolet 380 FT-IR in transmission mode and the spectra were processed using OMNIC software. For $\text{Na}_{10}[\text{Co}_4(\text{H}_2\text{O})_2(\text{PW}_9\text{O}_{34})_2] \cdot 27\text{H}_2\text{O}$, IR spectra were made in a KBr pellet with the background corrected using a blank KBr pellet.

SEM/EDX

A JEOL JSM-6500F was used for SEM analysis. EDX was measured using a Thermo Electron EDX System. Glassy carbon substrates were cleaned by polishing for 60 seconds with $0.05 \mu\text{m}$ polishing powder (CH Instruments), rinsing with water, and sonicating in water for 30 seconds.

CoO_x film preparation for SEM/EDX. A glassy carbon plate was covered with the CoO_x film by electrodeposition at 1.1V for 1 hour from a solution containing 5.4 mg $[\text{Co}_4(\text{H}_2\text{O})_2(\text{PW}_9\text{O}_{34})_2]^{10-}$ in 2 mL sodium phosphate electrolyte in contact with air as described above.

Na₁₀[Co₄(H₂O)₂(PW₉O₃₄)₂] film preparation for SEM/EDX. A sample of 2.7 mg $\text{Na}_{10}[\text{Co}_4(\text{H}_2\text{O})_2(\text{PW}_9\text{O}_{34})_2]$ was dissolved in 1.0 mL water. Approximately 4 drops of this solution was dropped onto a clean glassy carbon plate and was dried in air.

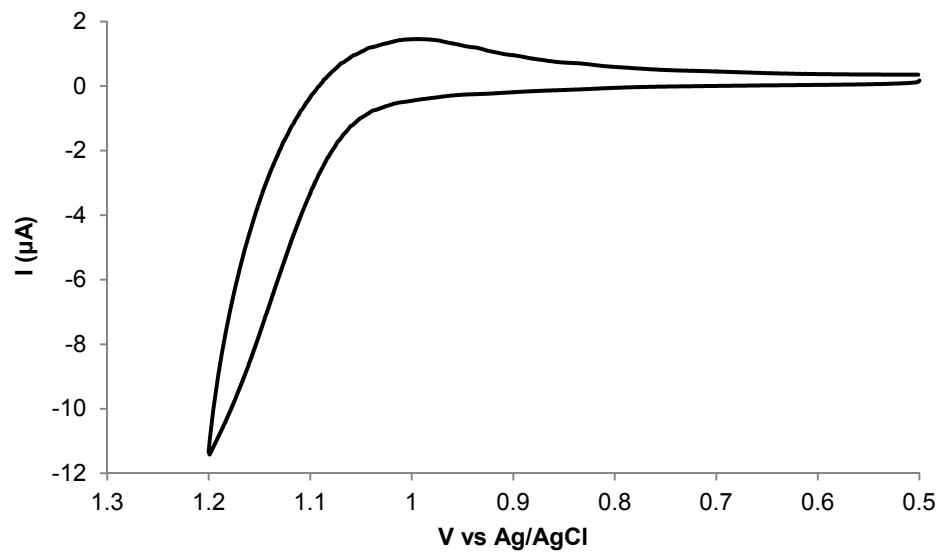


Figure S3.1. Cyclic voltammogram of a 500 μM $[\text{Co}_4(\text{H}_2\text{O})_2(\text{PW}_9\text{O}_{34})_2]^{10-}$ approximately 1 minute after dissolving in sodium phosphate buffer (0.1 M, pH 8.0). The working electrode is a 3mm diameter glassy carbon electrode. The scan rate is 20 mV/s.

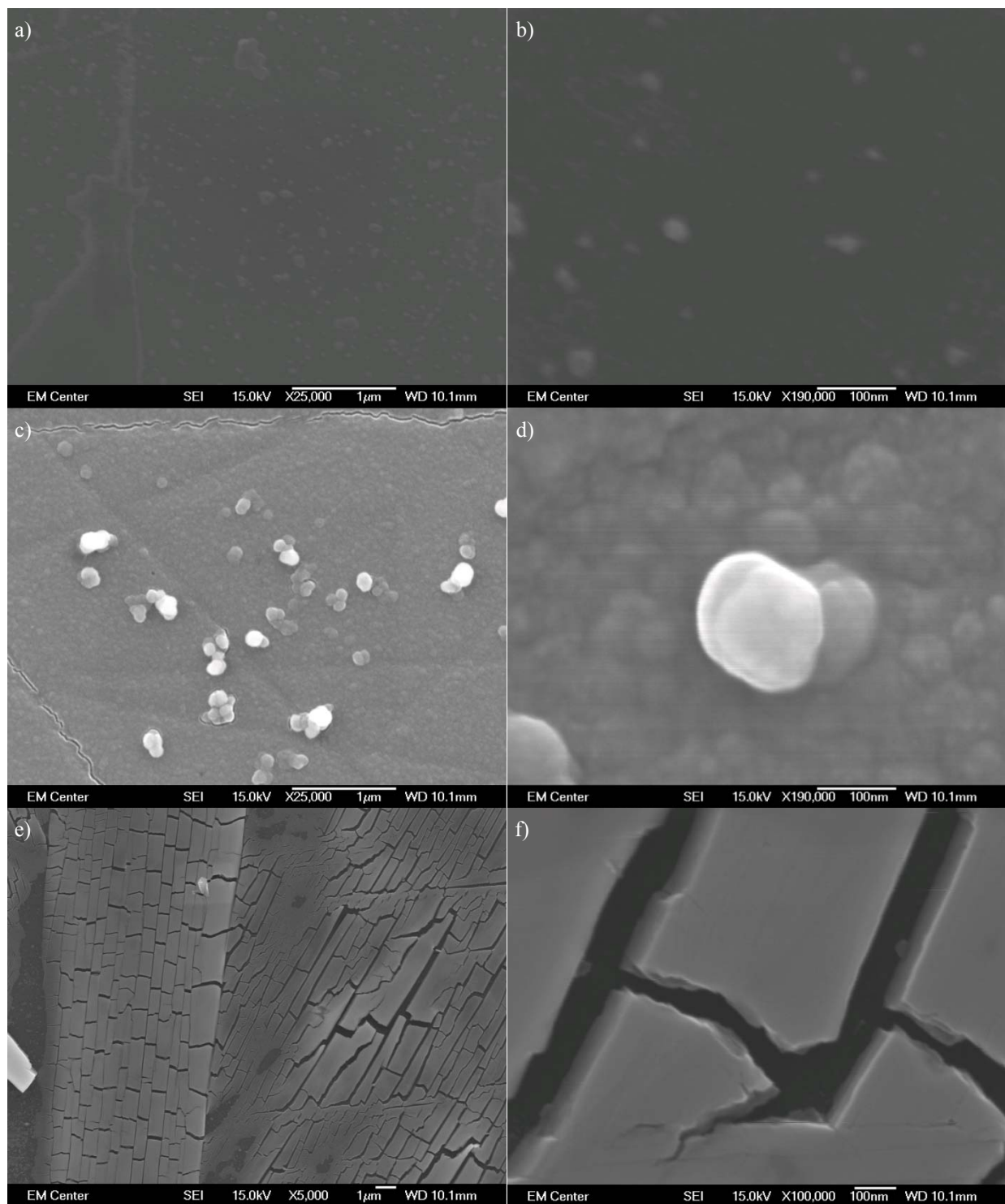


Figure S3.2. SEM images of: a) and b) clean glassy carbon substrate; c) and d) CoO_x film and nodules deposited at 1.1V vs Ag/AgCl onto glassy carbon from a 500 μM [Co₄(H₂O)₂(PW₉O₃₄)₂]¹⁰⁻ solution; e) and f) Na₁₀[Co₄(H₂O)₂(PW₉O₃₄)₂] film drop coated from a 500 μM polyoxometalate solution onto glassy carbon. The results demonstrate a clear difference between the CoO_x (c and d) and Na₁₀[Co₄(H₂O)₂(PW₉O₃₄)₂] (e and f) films.

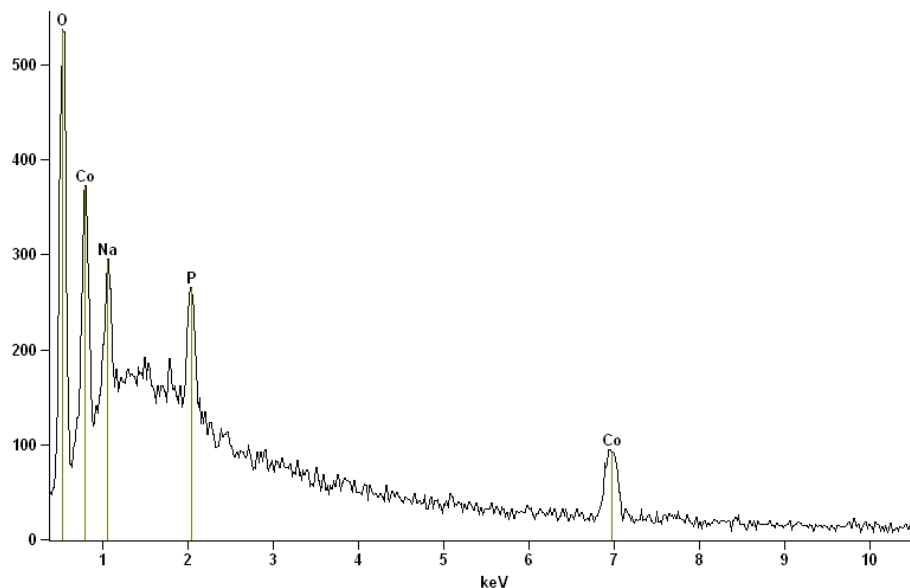


Figure S3.3. EDX analysis of a CoO_x film deposited for 1 hour at 1.1 V vs Ag/AgCl on a glassy carbon plate from a $500 \mu\text{M Na}_{10}[\text{Co}_4(\text{H}_2\text{O})_2(\text{PW}_9\text{O}_{34})_2]$ solution. Three separate analyses gave the following average atom % values and apparent 3σ standard deviation: oxygen = $87.0 \pm 4.5\%$; cobalt = $7.8 \pm 3.3\%$; sodium = $3.0 \pm 0.9\%$; phosphorus = $2.2 \pm 1.2\%$. The actual errors are likely even larger due to the non-ideal geometry of the material and well-established need for the use of standards for more accurate EDX values (which, however, were not necessary for the purposes and use of EDX as part of this work).²²

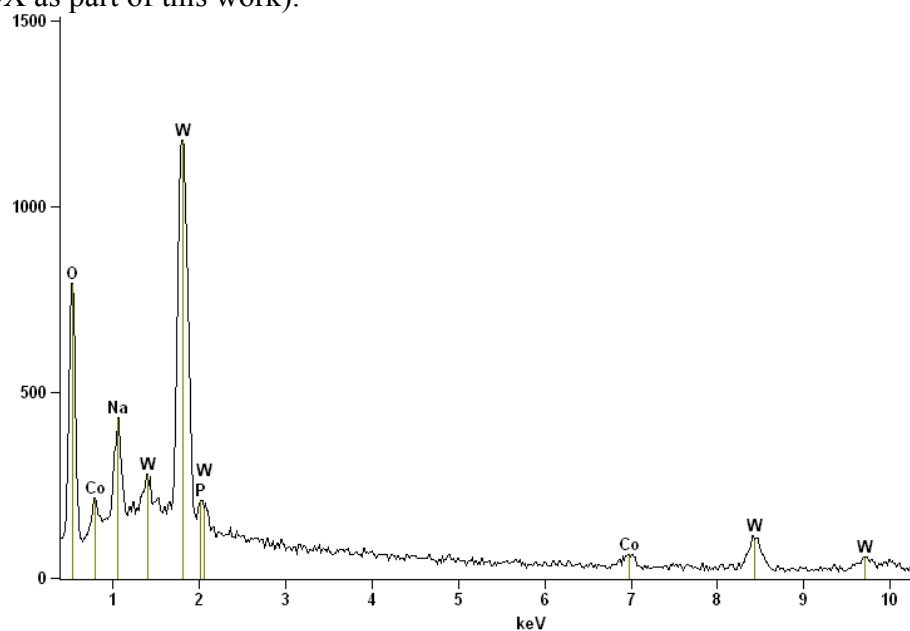


Figure S3.4. EDX analysis of a drop coated $\text{Na}_{10}[\text{Co}_4(\text{H}_2\text{O})_2(\text{PW}_9\text{O}_{34})_2]$ film on a glassy carbon substrate. Three separate analyses gave the following average atom % values and 3σ standard deviation: oxygen = $89.6 \pm 1.8\%$; tungsten = $5.3 \pm 1.2\%$; sodium = $3.7 \pm 2.1\%$; cobalt = $1.4 \pm 0.9\%$. Again, the actual error is likely even larger (as noted in Figure S3.3).²² Note that the overlap of the W $M\gamma$ line with the P $K\alpha, \beta$ lines at ~ 2 KeV prohibits determination of phosphorus, as was noted in the main text.

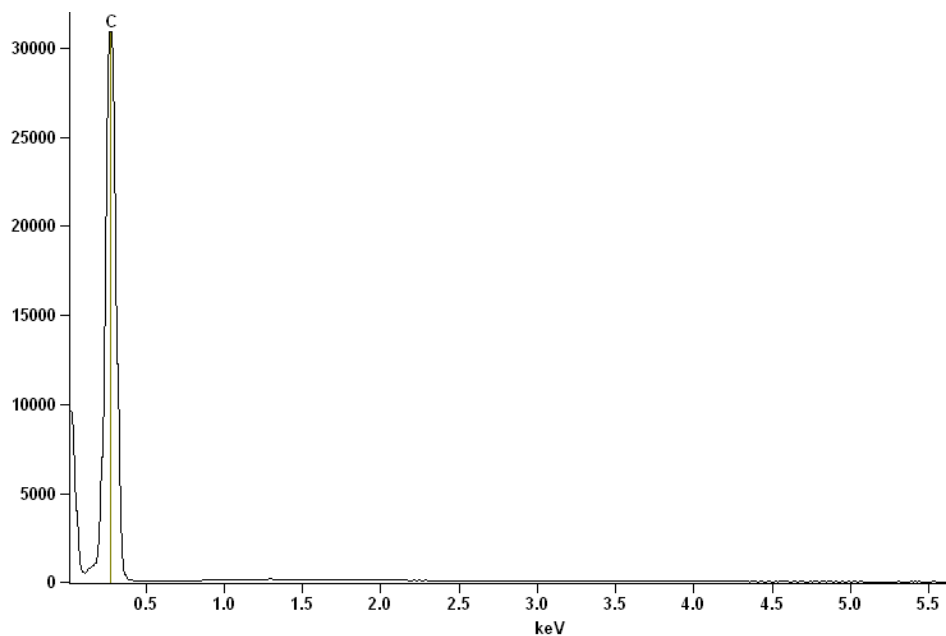


Figure S3.5. EDX analysis of a clean glassy carbon substrate, performed as a control experiment.

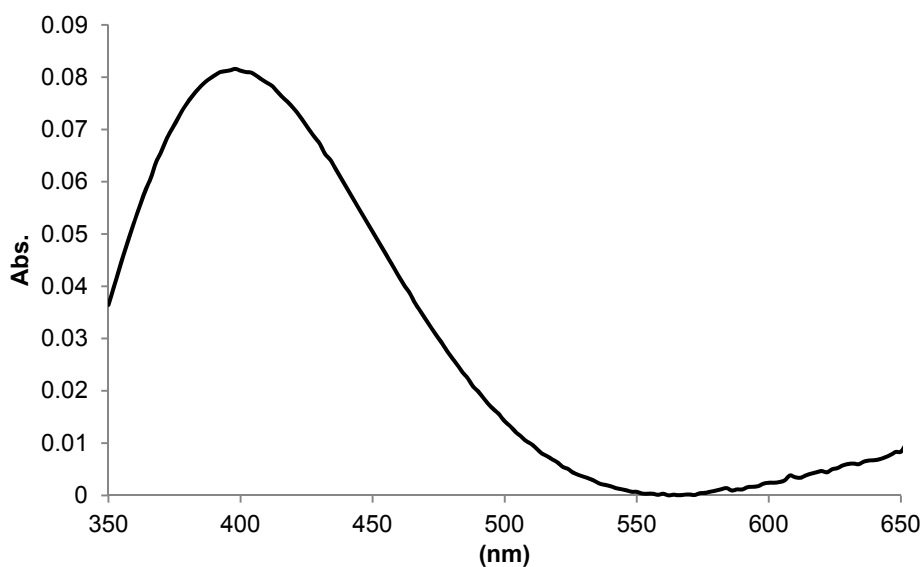


Figure S3.6. Absorption spectrum of a CoO_x film electrodeposited onto an ITO electrode from a $500 \mu\text{M} [\text{Co}_4(\text{H}_2\text{O})_2(\text{PW}_9\text{O}_{34})_2]^{10-}$ solution at 1.1 V vs Ag/AgCl for 1 hour. Note that the absorbance of the green film is approximately zero over the range which the cobalt polyoxometalate absorbs strongest (550-600 nm) as shown in Figure 3.3 (inset) of the main text, so that the cobalt polyoxometalate should have been observable if it had been present in the deposited film.

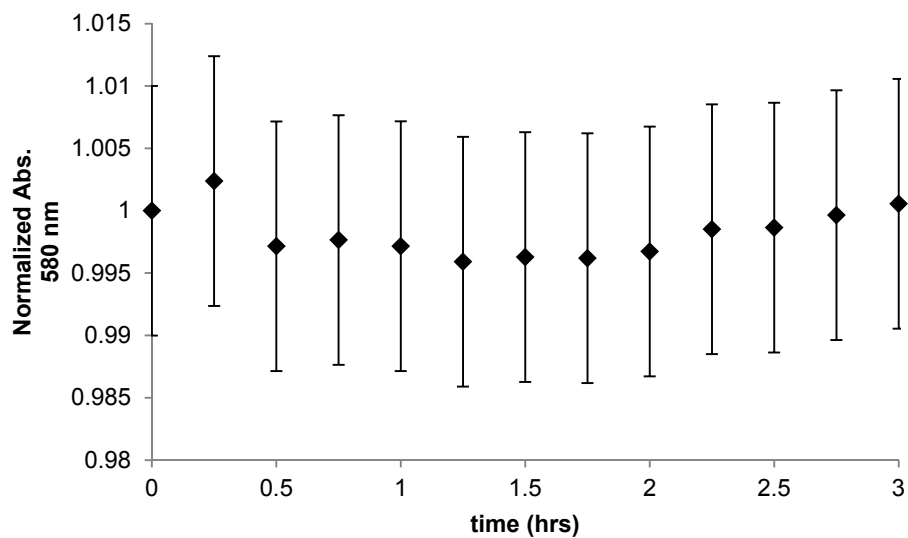


Figure S3.7. Normalized peak absorbance at 580 nm of a 500 μM $[\text{Co}_4(\text{H}_2\text{O})_2(\text{PW}_9\text{O}_{34})_2]^{10-}$ plus 0.1 LiClO_4 solution over a three hour period. There is no detectable decrease within the 1.0% experimental error.

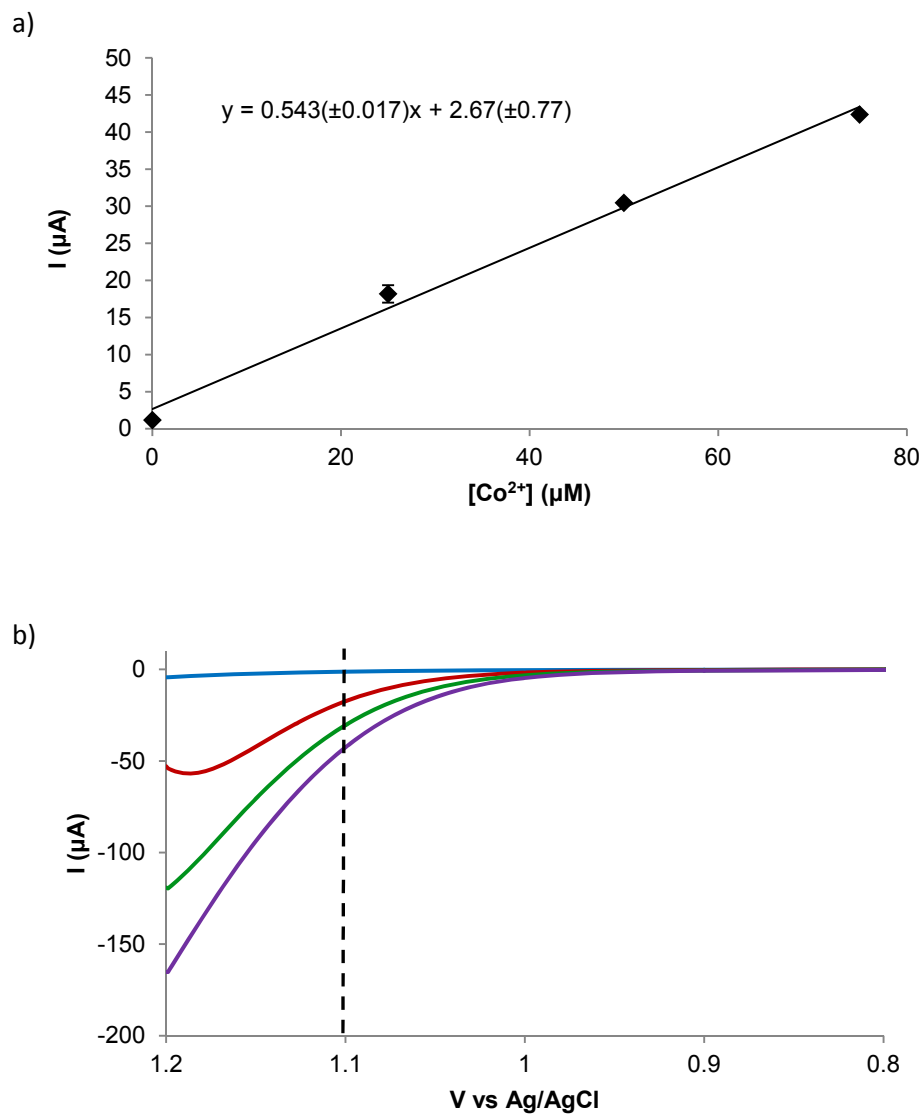


Figure S3.8. (a) Calibration curve for aqueous cobalt(II) generated from the anodic current at 1.1V and the $[\text{Co}^{2+}]$ in (b); the linear least squares fit gives: $I = 0.54[\text{Co}^{2+}] + 2.67$. (b) Linear sweep voltammetry of $\text{Co}(\text{NO}_3)_2$ in pH 8.0 sodium phosphate buffer: $[\text{Co}^{2+}] = 0$ (blue), 25 (red), 50 (green), 75 (purple) μM . The dashed line indicates the potential used for generating the cobalt(II) calibration curve. The supporting electrolyte is sodium phosphate (0.1 M, pH 8.0).

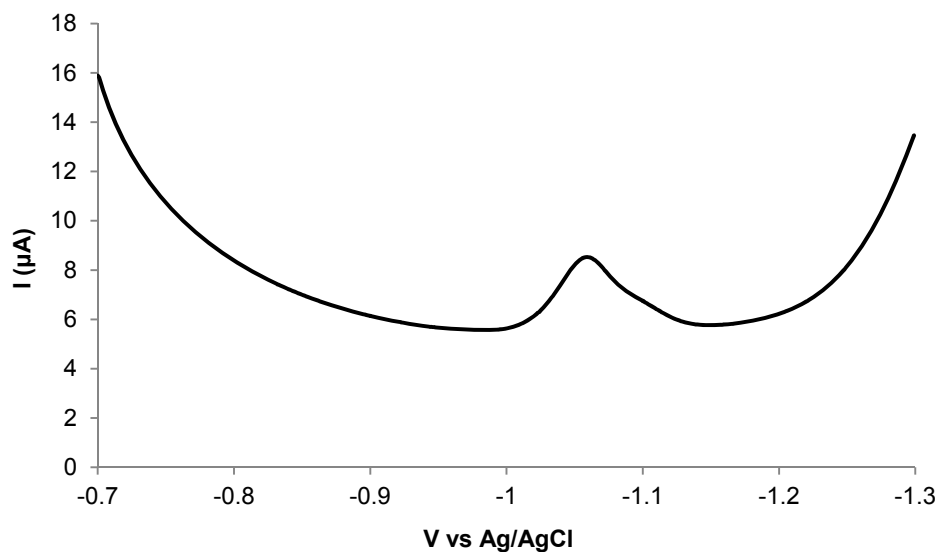


Figure S3.9. Sample linear sweep voltammogram for adsorptive stripping analysis; [cobalt(II) nitrate] = 5 μM , [dimethylglyoxime] = 100 μM , [sodium phosphate buffer] = 0.1 M. The scan rate was 10 mV/s in the negative direction.

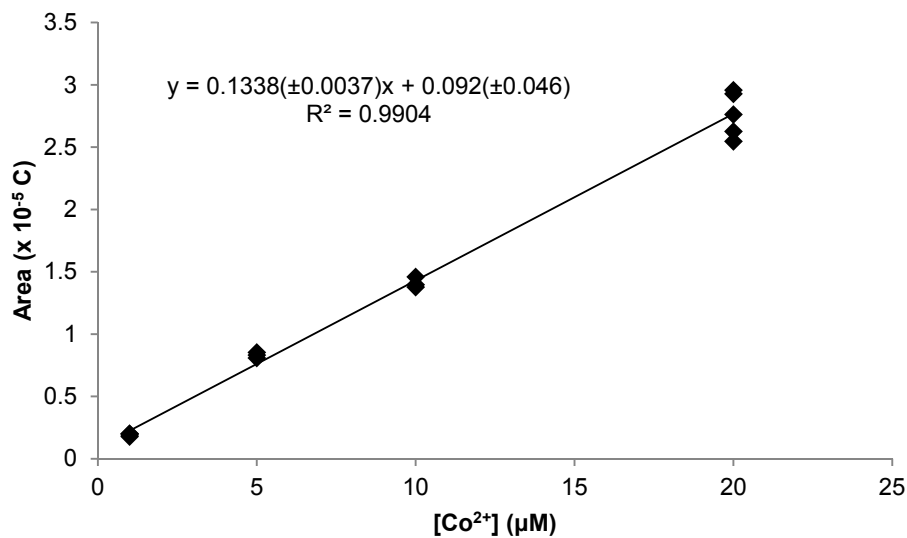


Figure S3.10. [Co²⁺] calibration curve for cathodic adsorptive stripping analysis using the cathodic peak area at ~ 1.05 V vs Ag/AgCl. Co(NO₃)₂ was used as the cobalt(II) standard.

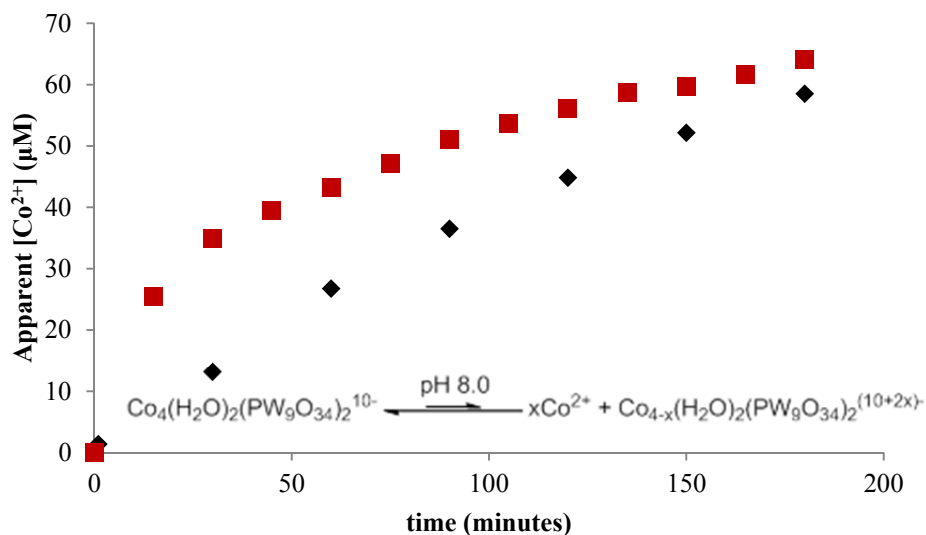


Figure S3.11. Overlaid *apparent* $[Co^{2+}]$ vs *time* curve of a $500 \mu M [Co_4(H_2O)_2(PW_9O_{34})_2]^{10-}$ plus $0.1 M$ sodium phosphate solution based on electrochemical detection and as shown in the main text (◆, Figure 3.4) and the calculated *apparent* $[Co^{2+}]$ vs *time* curve (■) based on UV-vis measurements at $580 nm$ in $0.1 M$ sodium phosphate buffer (Figure 3.3 in the main text) and for the tentative value $x = 3$ where x is the stoichiometric factor as shown in the equilibrium (above) and in Scheme 3.1 of the main text. The predicted $[Co^{2+}]$ was calculated by: $(1 - \text{Normalized Abs.}) \cdot (500 \mu M) \cdot x$. While the two curves are in qualitative agreement, their difference quantitatively indicates that (a) either all the species absorbing at $580 nm$ are not accounted for, and/or (b) the degradation of the cobalt polyoxometalate is not fully understood. Worth mentioning here is a study by Hill and co-workers which synthesized $[Co_2Li_2(PW_9O_{34})_2]^{12-}$ and observed it to be unstable in $1 M LiCl$,²³ forming $[Co_4(H_2O)_2(PW_9O_{34})_2]^{10-}$ plus other decomposition products. In other words, that study does support the notion that $x \geq 3$ since the $x = 2$ complex $[Co_2Li_2(PW_9O_{34})_2]^{12-}$ is unstable, at least under their $1M LiCl$ condition.

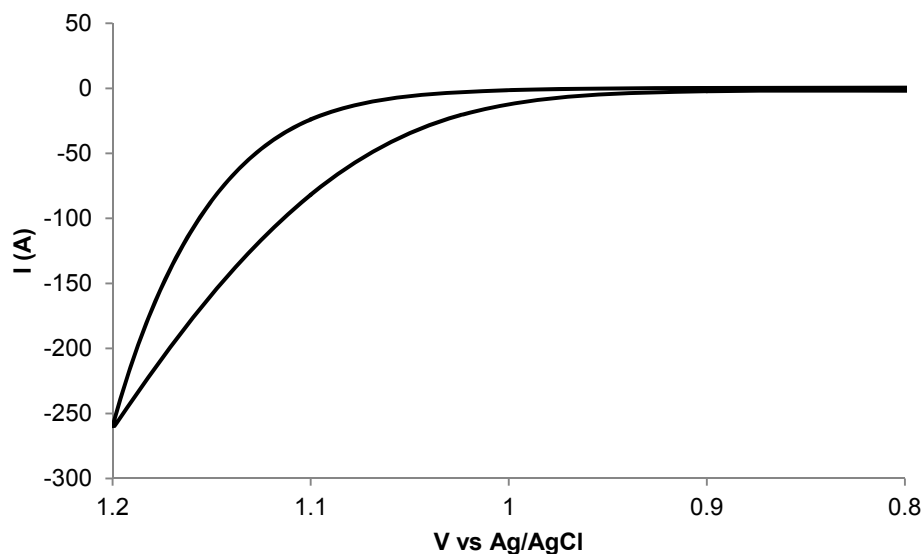


Figure S3.12. An additional aging experiment which shows the cyclic voltammogram of a 500 μM $[\text{Co}_4(\text{H}_2\text{O})_2(\text{PW}_9\text{O}_{34})_2]^{10-}$ in 0.1 M, pH 8.0 sodium phosphate buffer solution after 24 hours of aging in air. The *apparent* $[\text{Co(II)}]$ was not calculated from the anodic catalytic wave for this experiment since the current is outside of the linear portion of the calibration curve, Figure S3.8.

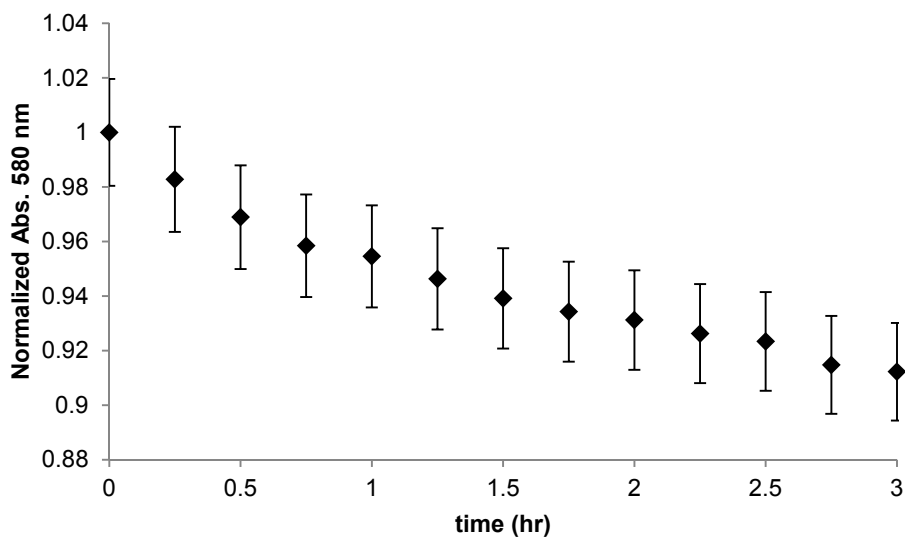


Figure S3.13. The under argon (i.e. air-free) normalized peak absorbance at 580 nm of a 500 μM $[\text{Co}_4(\text{H}_2\text{O})_2(\text{PW}_9\text{O}_{34})_2]^{10-}$ plus 0.1 M sodium phosphate solution (pH 8.0). The decrease over 3 hours is $8.8(\pm 2.0)\%$.

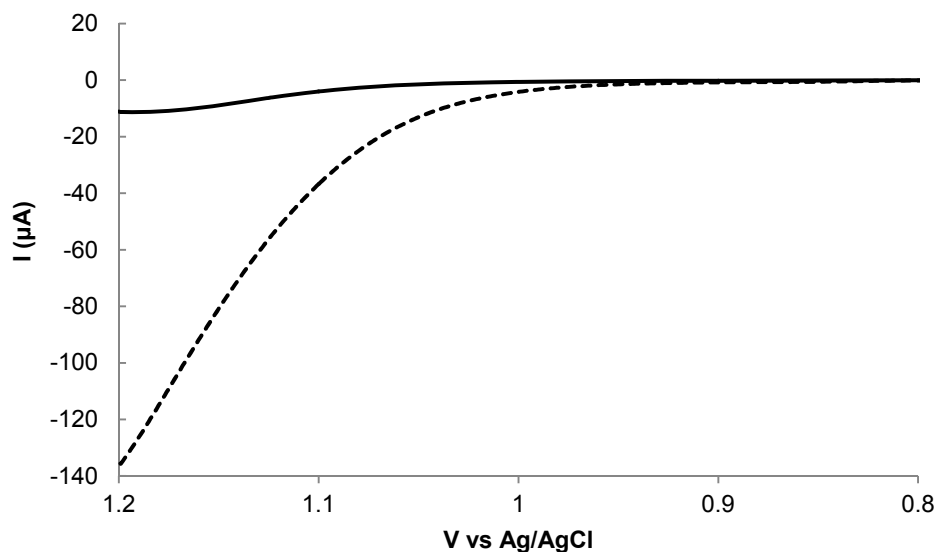


Figure S3.14. The under argon (i.e. air-free), linear sweep voltammetry of 500 μM $[\text{Co}_4(\text{H}_2\text{O})_2(\text{PW}_9\text{O}_{34})_2]^{10-}$ in pH 8.0 sodium phosphate buffer \sim 1 minute after dissolving (solid line) and after 3 hours of aging (dashed line). The *apparent* $[\text{Co(II)}]$, which was calculated from the anodic current of the linear sweep voltammogram at 1.1 V (vs Ag/AgCl) and the calibration curve Figure S3.8, was found to be 2.5 (\pm 1.4) and 62.8 (\pm 2.4) μM at time = 1 min. and time = 3 hr., respectively. Importantly, the calculated apparent $[\text{Co(II)}]$ is the same within experimental error when the linear sweep voltammetry experiment was conducted either under an argon (this control experiment) or under an air atmosphere (Figure 3.1).

REFERENCES

¹ a) Lewis, N. S.; Nocera, D. G. *Proc. Natl. Acad. Sci. USA* **2006**, *103*, 15729. b) Lewis, N. S. *MRS Bulletin* **2007**, *32*, 808. c) Cook, T. R.; Dogutan, D. K.; Reece, S. Y.; Surendranath, Y.; Teets, T. S.; Nocera, D. G. *Chem. Rev.* **2010**, *110*, 6474.

² a) Balzani, V.; Moggi, L.; Manfrin, M. F.; Bolletta, F.; Gleria, M. *Science* **1975**, *189*, 852. b) Bard, A. J.; Fox, M. A. *Acc. Chem. Res.* **1995**, *28*, 141. c) McDaniel, N. D.; Bernhard, S. *Dalton Trans.* **2010**, *39*, 10021. d) Walter, M. G.; Warren, E. L.; McKone, J. R.; Boettcher, S. W.; Mi, Q.; Santori, E. A.; Lewis, N. S. *Chem. Rev.* **2010**, *110*, 6446.

³ a) Ruttinger, W.; Dismukes, G. C. *Chem. Rev.* **1997**, *97*, 1. b) Betley, T. A.; Wu, Q.; Van Voorhis, T.; Nocera, D. G. *Inorg. Chem.* **2008**, *47*, 1849. c) Liu, F.; Concepcion, J. J.; Jurss, J. W.; Cardolaccia, T.; Templeton, J. L.; Meyer, T. J. *Inorg. Chem.* **2008**, *47*, 1727. d) Dau, H.; Limberg, C.; Reier, T.; Risch, M.; Roggan, S.; Strasser, P. *ChemCatChem*, **2010**, *2*, 724.

⁴ a) Kanan, M. W.; Nocera, D. G. *Science* **2008**, *321*, 1072. b) Suzuki, O.; Takahashi, M.; Fukunaga, T.; Kuboyama, J.; U.S. Patent 3,399,966, September 3, 1968. c) Chen, Y-W. D.; Noufi, R. N. *J Electrochem. Soc.* **1984**, *131*, 1447. d) Schmidt, T.; Wendt, H. *Electrochim. Acta* **1994**, *39*, 1763. e) Vittal, R.; Gommathi, H.; Rao, G. P. *J. Electroanal. Chem.* **2001**, *497*, 47. f) Kanan, M. W.; Surendranath, Y.; Nocera, D. G. *Chem. Soc. Rev.* **2009**, *38*, 109. g) Lutterman, D. A.; Surendranath, Y.; Nocera, D. G. *J. Am. Chem. Soc.* **2009**, *131*, 3838. h) Risch, M.; Khare, V.; Zaharieva, I.; Gerencser, L.; Chernev, P.; Dau, H. *J. Am. Chem. Soc.* **2009**, *131*, 6936. i) Steinmiller, E. M. P.; Choi, K.-S. *Proc. Natl. Acad. Sci. USA* **2009**, *106*, 20633. j) Surendranath, Y.; Dinca, M.; Nocera, D. G. *J. Am. Chem. Soc.* **2009**, *131*, 2615. k) Gerken, J. B.; Landis, E. C.; Hamers, R. J.; Stahl, S. S. *ChemSusChem* **2010**, *3*, 1176. l) Kanan, M. W.; Yano, J.; Surendranath, Y.; Dinca, M.; Yachandra, V. K.; Nocera, D. G. *J. Am. Chem. Soc.* **2010**, *132*, 13692. m) McAlpin, J. G.; Surendranath, Y.; Dinca, M.; Stich, T. A.; Stoian, S. A.; Casey, W. H.; Nocera, D. G.; Britt, R. D. *J. Am. Chem. Soc.* **2010**, *132*, 6882. n) Surendranath, Y.; Kanan, M. W.; Nocera, D. G. *J. Am. Chem. Soc.* **2010**, *132*, 16501. o) Shevchenko, D.; Anderlund, M. F.; Thapper, A.; Styring, S. *Energy Environ. Sci.* **2011**, *4*, 1284. (p) Gerken, J. B.; McAlpin, J. G.; Chen, J. Y. C.; Rigsby, M. L.; Casey, W. H.; Britt, R. D.; Stahl, S. S. *J. Am. Chem. Soc.* [Just Accepted], DOI: 10.1021/ja205647m. Published online: Aug., 1, 2011.

⁵ Using Co(II) salts as water oxidation catalyst precursors in conjunction with tris(2,2'-bipyridyl)ruthenium(III) as an oxidant was reported by Creutz and Sutin in 1983; interestingly, these authors note that at neutral pH and when [Ru(III)] and [Co(II)] are approximately equal, a heterogeneous CoO_x material precipitated from solution. However, determination of whether the active catalyst is heterogeneous was not performed as part of that classic study: Brunschwig, B. S.; Chou, M. H.; Creutz, C.; Ghosh, P.; Sutin, N. *J. Am. Chem. Soc.* **1983**, *105*, 4832. b) Ghosh, P. K.; Brunschwig, B. S.; Chou, M.; Creutz, C.; Sutin, N. *J. Am. Chem. Soc.* **1984**, *106*, 4772.

⁶ The 2010 *Science* paper reported that when [Co₄(H₂O)₂(PW₉O₃₄)₂]¹⁰⁻ was combined with the sacrificial oxidant tris(2,2'-bipyridyl)ruthenium(III) in pH 8.0 sodium phosphate solution (0.03 M), rapid water oxidation to oxygen was observed at rates of up to 5 s⁻¹ (moles O₂ • moles catalyst⁻¹ • seconds⁻¹) and turn over numbers of ~10³ (total moles O₂/moles POM) were reported.

Yin, Q.; Tan, J. M.; Besson, C.; Geletii, Y. V.; Musaev, D. G.; Kuznetsov, A. E.; Luo, Z.; Hardcastle, K. I.; Hill, C. L. *Science* **2010**, 328, 342.

⁷ A photo-driven system using $[\text{Co}_4(\text{H}_2\text{O})_2(\text{PW}_9\text{O}_{34})_2]^{10-}$ was reported in the following 2011 *JACS* paper; when a solution containing the cobalt POM, tris(2,2'-bipyridyl)ruthenium(II) as a photosensitizer, and sodium persulfate as a sacrificial oxidant was illuminated (420-450 nm), water oxidation occurred with (internal) quantum efficiencies of up to 30% (2•moles O_2 /einsteins absorbed) and turn over numbers of 220 (moles O_2 /moles POM). Huang, Z.; Luo, Z.; Geletii, Y. V.; Vickers, J. W.; Yin, Q.; Wu, D.; Hou, Y.; Ding, Y.; Song, J.; Musaev, D. G.; Hill, C. L.; Lian, T. *J. Am. Chem. Soc.* **2011**, 133, 2068.

⁸ Gao, S.; Li, T.; Li, X.; Cao, R. *Mater. Lett.* **2006**, 60, 3622. These authors reported that $[\text{Co}_4(\text{H}_2\text{O})_2(\text{PW}_9\text{O}_{34})_2]^{10-}$ did not show any electrochemical activity at positive potentials (the potential range was not specified) in 0.2-0.3 M sodium acetate buffer (pH 4.4 or 5.8) at a glassy carbon electrode.

⁹ In contrast to the studies of Gao et al.,⁸ Balula et al. found that $[(\text{C}_4\text{H}_9\text{N})_7\text{H}_3[\text{Co}_4(\text{H}_2\text{O})_2(\text{PW}_9\text{O}_{34})_2]$ in acetonitrile showed sequential one-electron oxidation waves at 0.811 V and 1.123 V (versus Ag/Ag^+) at a Pt electrode with 0.1 M $[\text{N}(\text{C}_4\text{H}_9)_4]\text{ClO}_4$ electrolyte. Balula, M. S.; Gamelas, J. A.; Carapuca, H. M.; Cavaleiro, A. M. V.; Schlindwein, W. *Eur. J. Inorg. Chem.* **2004**, 619.

¹⁰ Weakley, T. J. R.; Evans, H. T.; Showell, J. S.; Tourne, G. F.; Tourne, C. M. *J. Chem. Soc., Chem. Commun.* **1973**, 139.

¹¹ a) Contant, R. *J. Chem. Res. Synop.* **1982**, 50. b) Contant, R. *J. Chem. Res. Synop.* **1984**, 120.

¹² Hamlaoui, M.-L.; Vlassenko, K.; Messadi, D. *Comptes Rendus Acad. Sci. Paris* **1990**, 311, 795.

¹³ The time-dependent absorbance was also measured for $[\text{Co}_4(\text{H}_2\text{O})_2(\text{PW}_9\text{O}_{34})_2]^{10-}$ dissolved in aqueous 0.1 M lithium perchlorate; the absorbance at 580nm in LiClO_4 did not decrease over the 3 hour time scale of the experiment (Figure S7), an important result which demonstrates an electrolyte dependence on the solution stability of $[\text{Co}_4(\text{H}_2\text{O})_2(\text{PW}_9\text{O}_{34})_2]^{10-}$.

¹⁴ Ohlin, C. A.; Harley, S. J.; McAlpin, J. G.; Hocking, R. K.; Mercado, B. Q.; Johnson, R. L.; Villa, E. M.; Fidler, M. K.; Olmstead, M. M.; Spiccia, L.; Britt, R. D.; Casey, W. H. *Chem. Eur. J.* **2011**, 17, 4408.

¹⁵ Pope, M. T. *Heteropoly and Isopoly Oxometalates*; Springer-Verlag: Berlin, 1983.

¹⁶ The following references provide the first, rational and higher yield syntheses for this class of POMs as well as discovery of the related $[\text{M}^{\text{II}}_4(\text{H}_2\text{O})_2(\text{P}_2\text{W}_{15}\text{O}_{56})_2]^{16-}$ series: a) Finke, R. G.; Droege, M.; Hutchinson, J. R.; Gansow, O. *J. Am. Chem. Soc.* **1981**, 103, 1587. b) Finke, R. G.; Droege, M. W. *Inorg. Chem.* **1983**, 22, 1006.

¹⁷ Krolicka, A.; Brobrowski, A.; Kalcher, K.; Mocak, J.; Svancara, I.; Vytras, K. *Electroanalysis* **2003**, *15*, 1859.

¹⁸ We emphasize that the present studies have not examined the system, nor the precise conditions, utilized in the 2010 *Science* paper (i.e. water oxidation beginning with 3.2 μM $[\text{Co}_4(\text{H}_2\text{O})_2(\text{PW}_9\text{O}_{34})_2]^{10-}$ using tris(2,2'-bipyridyl)ruthenium(III) as an oxidant in 0.03 M, pH = 8 sodium phosphate).⁶ In addition, further study is needed of the (slightly) different conditions in the present and prior study before one could have any firm basis for believing that the instability of the cobalt POM observed herein discredits the central claim made elsewhere⁶ of the POM stability at pH = 8 under their⁶ specific conditions.

¹⁹ a) Hocking, R. K.; Brimblecombe, R.; Chang, L.-Y.; Singh, A.; Cheah, M. H.; Glover, C.; Casey, W. H.; Spiccia, L. *Nature Chem.* **2011**, *3*, 461. b) Blakemore, J. D.; Schley, N. D.; Olack, G. W.; Incarvito, C. D.; Brudvig, G. W.; Crabtree, R. H. *Chem. Sci.* **2011**, *2*, 94. c) Schley, N. D.; Blakemore, J. D.; Subbaiyan, N. K.; Incarvito, C. D.; D'Souza, F.; Crabtree, R. H.; Brudvig, G. W. *J. Am. Chem. Soc.* **2011**, *133*, 10473.

²⁰ Widegren, J. A.; Finke, R. G. *J. Mol. Cat. A* **2003**, *198*, 317.

²¹ a) Evans, J. F.; Kuwana, T. *Anal. Chem.* **1979**, *51*, 358. b) Zak, J.; Kuwana, T. *J. Am. Chem. Soc.* **1982**, *104*, 5514. c) Kamau, G. N.; Willis, W. S.; Rusling, J. F. *Anal. Chem.* **1985**, *57*, 545.

²² Goldstein, J. I.; Newbury, D. E.; Joy, D. C.; Lyman, C. E.; Echlin, P.; Lifshin, E.; Sawyer, L.; Michael, J. R. *Scanning Electron Microscopy and X-Ray Microanalysis*, 3rd ed.; Kluwer: New York, 2003.

²³ Hou, Y.; Cichon, M. J.; Lense, S.; Hardcastle, K. I.; Hill, C. L. *Inorg. Chem.* **2010**, *49*, 4125.

IV. WATER OXIDATION CATALYSIS BEGINNING WITH 2.5 μM
[Co₄(H₂O)₂(PW₉O₃₄)₂]¹⁰⁻: INVESTIGATION OF THE TRUE ELECTROCHEMICALLY
DRIVEN CATALYST AT ≥ 600 mV OVERPOTENTIAL AT A GLASSY CARBON
ELECTRODEⁱ

Overview

Evidence for the true water oxidation catalyst (WOC) when beginning with the cobalt polyoxometalate [Co₄(H₂O)₂(PW₉O₃₄)₂]¹⁰⁻ (Co₄-POM) is investigated at deliberately chosen low polyoxometalate concentrations (2.5 μM) and high electrochemical potentials (≥ 1.3 V vs Ag/AgCl) in pH 5.8 and 8.0 sodium phosphate electrolyte at a glassy carbon working electrode—conditions which ostensibly favor Co₄-POM catalysis if present. Multiple experiments argue against the dominant catalyst being CoO_x formed exclusively from Co²⁺ dissociated from the parent POM. Measurement of [Co²⁺] in the Co₄-POM solution and catalytic controls with the corresponding amount of Co(NO₃)₂ cannot account for the O₂ generated from 2.5 μM [Co₄(H₂O)₂(PW₉O₃₄)₂]¹⁰⁻ solutions. This result contrasts with our prior investigation of Co₄-POM under higher concentration and lower potential conditions (i.e., 500 μM [Co₄(H₂O)₂(PW₉O₃₄)₂]¹⁰⁻, 1.1 V vs Ag/AgCl, as described in Stracke, J. J.; Finke, R. G. *J. Am. Chem. Soc.* **2011**, *133*, 14872) and *highlights the importance of reaction conditions in governing the identity of the true, active WOC*. Although electrochemical studies are consistent with

ⁱ The prior chapter (III) provides significant evidence that the cobalt POM [Co₄(H₂O)₂(PW₉O₃₄)₂]¹⁰⁻ can transform into a heterogeneous WOC under the conditions therein (0.5 mM [Co₄(H₂O)₂(PW₉O₃₄)₂]¹⁰⁻, pH 8, 0.1 M sodium phosphate buffer, 1.1 V vs Ag/AgCl at a glassy carbon electrode). Since a discrete POM WOC is of fundamental interest to the field of water oxidation catalysis, this dissertation chapter addresses the question of whether [Co₄(H₂O)₂(PW₉O₃₄)₂]¹⁰⁻ could be a homogeneous WOC under different conditions of lower concentration (2.5 μM) and a larger electrochemical driving force (≥ 1.3 V vs Ag/AgCl). This work was published in *ACS Catalysis* (Stracke, J. J.; Finke, R. G. *ACS Catal.* **2013**, *3*, 1209).

Co₄-POM being oxidized at the glassy carbon electrode, it is not yet possible to distinguish a Co₄-POM catalyst from a CoO_x catalyst formed via decomposition of Co₄-POM. Controls with authentic CoO_x indicate conversion of only 3.4% or 8.3% (at pH 8.0 and 5.8) of Co₄-POM into a CoO_x catalyst could account for the O₂-generating activity, and HPLC quantification of the Co₄-POM stability shows the post-reaction Co₄-POM concentration decreases by 2.7±7.6% and 9.4±5.1% at pH 8.0 and 5.8. Additionally, the [Co²⁺] in a 2.5 μM Co₄-POM solution increases by 0.55 μM during 3 min of electrolysis—further evidence of the *Co₄-POM instability under oxidizing conditions*. Overall, this study demonstrates the challenges of identifying the true WOC when examining micromolar amounts of a partially stable material and when *nanomolar* heterogeneous metal-oxide will account for the observed O₂-generating activity.

Introduction

Catalytic oxidation of water to oxygen and protons is a central reaction to many sustainable energy storage schemes including water splitting or direct conversion of carbon dioxide into methanol.^{1,2,3,4,5,6,7,8,9,10,11,12} Ideally, water oxidation catalysts (WOCs) should be efficient, long-lived (i.e., stable under the reaction conditions), highly active, and composed of earth-abundant elements.^{13,14,15,16,17,18,19,20,21}

Polyoxometalates (POMs) are of particular interest as WOCs since these discrete metal-oxo compounds can self-assemble (typically at neutral to acidic pHs), are composed primarily of high-valent metals such as tungsten, vanadium, or molybdenum, and can incorporate a variety of redox active transition metal centers including cobalt, ruthenium, or iridium.²² In addition, since the POM backbone contains metals in their highest accessible oxidation state, they are resistant to oxidative damage. A caveat here is that the POM-incorporated transition metals are still subject to ligand exchange reactions^{23,24,25,26} and possibly oxidative transformations.

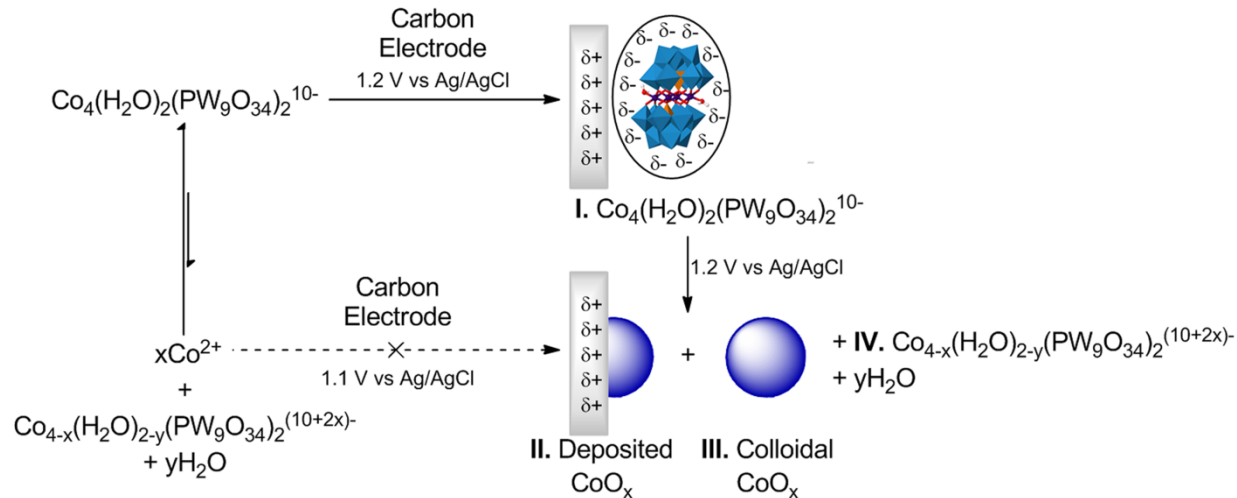
The practical advantages listed above have led to a number of publications describing polyoxometalate WOCs.^{27,28,29,30,31,32,33,34,35,36,37,38,39,40,41,42,43,44,45,46} Of particular relevance to the present work is a 2010 *Science* paper which reported the cobalt POM $\text{Co}_4(\text{H}_2\text{O})_2(\text{PW}_9\text{O}_{34})_2^{10-}$ ($\text{Co}_4\text{-POM}$) as a highly active WOC when $\text{Ru}(\text{bpy})_3^{3+}$ is used as the chemical oxidant.⁴⁶ Under the specific conditions of 3.2 μM $\text{Co}_4\text{-POM}$, 1.5 mM $\text{Ru}(\text{bpy})_3^{3+}$ oxidant, and pH 8, turnover frequencies of up to 5 ($\text{mol O}_2 \cdot \text{s}^{-1} \cdot \text{mol Co}_4\text{-POM}^{-1}$) and total turnovers of >1000 ($\text{mol O}_2 \cdot \text{mol Co}_4\text{-POM}^{-1}$) were reported.

Subsequently, we reported that under the *different conditions* of 500 μM $\text{Co}_4(\text{H}_2\text{O})_2(\text{PW}_9\text{O}_{34})_2^{10-}$, pH 8, and electrochemically driven oxidation at 1.1 V vs Ag/AgCl, the true catalyst is heterogeneous, electrode-bound CoO_x generated from micromolar aqueous Co^{2+} which had dissociated from the parent $\text{Co}_4\text{-POM}$.⁴⁷ This conclusion is strongly supported by (1) the isolation and testing of a CoO_x film formed during bulk electrolysis at 1.1 V, (2) the decomposition of $4.3 \pm 0.6\%$ $\text{Co}_4\text{-POM}$ measured by UV-vis over a 3 h period, (3) the concomitant increase of $[\text{Co}^{2+}]$ to $58 \pm 2 \mu\text{M}$ during that same 3 h period, and importantly, (4) control experiments which showed *identical* water oxidation activity for solutions containing either 58 μM $\text{Co}(\text{NO}_3)_2$ or 500 μM $\text{Co}_4\text{-POM}$ during bulk electrolysis at 1.1 V vs Ag/AgCl. Noteworthy here is that CoO_x type⁴⁸ materials have been studied extensively and form under operating conditions while oxidizing water with moderate overpotentials.^{49,50,51,52,53,54,55} However, the key question remained whether the $\text{Co}_4(\text{H}_2\text{O})_2(\text{PW}_9\text{O}_{34})_2^{10-}$ POM could be a catalyst under conditions specifically chosen to favor a discrete $\text{Co}_4\text{-POM}$ WOC including higher electrochemical potential, lower concentration, and more acidic pH conditions where the POM should be more stable.

As depicted in Scheme 4.1, four hypotheses are considered in the current study under low Co₄-POM concentrations, which are closer to those used in the 2010 *Science* paper,⁴⁶ and high electrochemical potentials, since that is where O₂ generation is observed (i.e., 2.5 μM Co₄(H₂O)₂(PW₉O₃₄)₂¹⁰⁻ and 1.1 to 1.4 V vs Ag/AgCl at pH 5.8 or 8.0). The four hypotheses considered herein for the true WOC are as follows: (1) That the starting Co₄(H₂O)₂(PW₉O₃₄)₂¹⁰⁻ polyoxometalate is an active WOC; (2) That the starting polyoxometalate is converted into an active CoO_x colloidal (soluble) or deposited (insoluble, electrode-bound) WOC at highly oxidizing potentials (i.e., ≥1.3 V vs Ag/AgCl); (3) That the polyoxometalate releases cobalt(II) from its core and the dissociated cobalt is then oxidatively converted into a CoO_x (colloidal or deposited) WOC (Scheme 4.1); or (4) That an unknown polyoxometalate or discrete cobalt-oxo(hydroxo) fragment is the true WOC.

Herein, we report Co₄(H₂O)₂(PW₉O₃₄)₂¹⁰⁻ electrochemical activity and stability measurements in conjunction with Co(NO₃)₂ control experiments which rule out hypothesis (3)—CoO_x formed from dissociated Co²⁺. However, comparison of the Co₄-POM stability, O₂ evolution activity, and XPS surface analysis with authentic electrodeposited CoO_x is consistent with either homogeneous Co₄-POM or heterogeneous colloidal CoO_x formed from direct oxidative decomposition of the Co₄-POM. Indeed, this remaining ambiguity (i) highlights the difficulty in effectively answering the “who is the true catalyst?” question for water oxidation catalysts when beginning with micromolar concentrations of a metastable material that can lead to nanomolar concentrations of possible catalytic species, and (ii) emphasizes the need for the synthesis, characterization and study of CoO_x colloidal WOCs under the precise conditions of a given WOC system such as that examined herein.

Scheme 4.1. Plausible WOCs and Their Formation Pathways That Underlie the 4 Hypotheses Tested Herein^a



^a Possible catalysts include I. $\text{Co}_4(\text{H}_2\text{O})_2(\text{PW}_9\text{O}_{34})_2^{10-}$, II. deposited (i.e., not soluble) CoO_x , III. colloidal (i.e., soluble) CoO_x , and/or IV. a discrete POM fragment (e.g. $\text{Co}_3(\text{H}_2\text{O})(\text{PW}_9\text{O}_{34})^{12-}$). The aqueous Co^{2+} to CoO_x pathway will be shown to be insignificant under the conditions herein, vide infra.

Experimental Section

Materials

$\text{Na}_{10}[\text{Co}_4(\text{H}_2\text{O})_2(\text{PW}_9\text{O}_{34})_2]$ was synthesized according to published procedures,^{46,56} recrystallized, and confirmed via ³¹P NMR, UV-vis, and IR spectroscopies which reproduced literature values.^{46,47} Other chemicals and solvents were obtained from Sigma-Aldrich or Fisher Scientific and used without further purification. Ultrapure water (resistivity = 18 MΩ-cm) was used to prepare all aqueous solutions and to clean and rinse electrodes.

Electrochemical Measurements

A CHI630D potentiostat (CH Instruments), Ag/AgCl (1 M KCl) reference electrode (CH Instruments), and platinum wire counter electrode were used for all electrochemical measurements. Working electrodes were 3 mm diameter glassy carbon disk (CH Instruments), 1 cm² glassy carbon plate (Alfa Aesar), boron-doped diamond 3 mm diameter disk (CCL Diamond), or indium tin oxide (ITO) coated glass slides (Delta Technologies). Glassy carbon

electrodes were cleaned by polishing with 0.05 μm alumina for 1 min, rinsing with water, sonicating for 30 s, rinsing with water, and drying under air. No attempt was made to remove oxygen from the solutions since O_2 is produced in most of the electrochemical experiments.

Cyclic Voltammetry

The $\text{Na}_{10}[\text{Co}_4(\text{H}_2\text{O})_2(\text{PW}_9\text{O}_{34})_2]$ and 0.1 M sodium phosphate buffer solution was prepared by diluting the appropriate amount of a 500 μM $\text{Na}_{10}[\text{Co}_4(\text{H}_2\text{O})_2(\text{PW}_9\text{O}_{34})_2]$ solution (e.g., 0.010 mL for a final $[\text{Co}_4\text{-POM}] = 2.5 \mu\text{M}$) to 2.00 mL using 0.1 M sodium phosphate buffer. A clean glassy carbon working electrode (3 mm diameter disk) was then pretreated by holding at 1.2 V (vs Ag/AgCl) for 30 s in a pure 0.1 M sodium phosphate electrolyte. The electrodes were then moved to the polyoxometalate solution where cyclic voltammetry was performed; typical scans had a potential range = 0.5 to 1.6 V (vs Ag/AgCl) and a scan rate = 20 mV/s. $\text{Co}_4\text{-POM}$ solutions were aged 15-60 min prior to recording the voltammogram, aging which did not appear to significantly change the observed CV.

Determination of $[\text{Co}^{2+}]_{\text{apparent}}$ by Differential Pulse Cathodic Adsorptive Stripping

Voltammetry

Bismuth Plating and Stripping Voltammetry Conditions. Stripping voltammetry was based upon a previously published procedure.⁵⁷ Briefly, bismuth was plated onto a clean glassy carbon electrode (3mm diameter disk) at -0.25 V (vs Ag/AgCl) for 45 s from a solution containing 0.02 $\text{Bi}(\text{NO}_3)_2$, 0.5 M LiBr, 1 M HCl. The electrodes were then rinsed and placed into the analyte solution. The potential was then held at 1.3 V for 15 s, followed by magnetic stirring for 2 s, and then differential pulse voltammetry. Parameters for the voltammogram were as follows: potential range = -0.7 to -1.3 V (vs Ag/AgCl), potential increments = 0.004 V, step

amplitude = 0.05 V, pulse width = 0.1 s, pulse period = 0.2 s, quiet time before initiating scan = 10 s.

A standard curve was generated using $\text{Co}(\text{NO}_3)_2$ solutions at known concentrations of 0, 50, 250, and 500 nM; the standard solutions also contained 0.10 M sodium phosphate buffer at pH 8.0, and 20 μM dimethylglyoxime.

Determination of $[\text{Co}^{2+}]$ in $\text{Na}_{10}[\text{Co}_4(\text{H}_2\text{O})_2(\text{PW}_9\text{O}_{34})_2]$ Solutions under Noncatalytic Conditions. Polyoxometalate solutions used to determine the $[\text{Co}^{2+}]_{\text{apparent}}$ initially contained 2.63 μM $\text{Na}_{10}[\text{Co}_4(\text{H}_2\text{O})_2(\text{PW}_9\text{O}_{34})_2]$ and 0.105 M sodium phosphate buffer at pH 8.0. Then, 0.10 mL of 400 μM dimethylglyoxime was added to make a 2.50 μM $\text{Na}_{10}[\text{Co}_4(\text{H}_2\text{O})_2(\text{PW}_9\text{O}_{34})_2]$, 0.100 M sodium phosphate, and 20 μM dimethylglyoxime solution. Dimethylglyoxime was added to either the $\text{Na}_{10}[\text{Co}_4(\text{H}_2\text{O})_2(\text{PW}_9\text{O}_{34})_2]$ or $\text{Co}(\text{NO}_3)_2$ standards just 5 min before starting the differential pulse voltammogram to minimize any kinetic acceleration effects of dimethylglyoxime binding of Co^{2+} on the final amount of $[\text{Co}^{2+}]_{\text{apparent}}$.

Comparison of $[\text{Co}^{2+}]$ in $\text{Na}_{10}[\text{Co}_4(\text{H}_2\text{O})_2(\text{PW}_9\text{O}_{34})_2]$ solutions before and after bulk electrolysis. A 2.50 μM $\text{Na}_{10}[\text{Co}_4(\text{H}_2\text{O})_2(\text{PW}_9\text{O}_{34})_2]$ solution in pH 8.0, 0.1 M sodium phosphate was prepared. 1.50 mL of that solution was subjected to a 1.4 V vs Ag/AgCl bulk electrolysis as described below in the section “Bulk electrolysis and Dissolved O_2 Measurements”. After the electrolysis, 1.00 mL of the solution was transferred to a vial and 5.0 μL of an aqueous 4.0 mM dimethylglyoxime solution was added to the $\text{Na}_{10}[\text{Co}_4(\text{H}_2\text{O})_2(\text{PW}_9\text{O}_{34})_2]$ solution. After 5 min, the cathodic stripping voltammogram was recorded as described above in the “Bismuth plating and stripping voltammetry conditions” section. Next, 1.00 mL of the original 2.50 μM $\text{Na}_{10}[\text{Co}_4(\text{H}_2\text{O})_2(\text{PW}_9\text{O}_{34})_2]$ solution in pH 8.0, 0.1 M sodium phosphate (i.e., a portion of the original solution which had not been subjected to bulk electrolysis) was transferred to a vial, and

5.0 μL of an the 4.0 mM dimethylglyoxime solution was added to the polyoxometalate solution. The solution was aged 5 min and then the cathodic stripping voltammogram was recorded using the “Bismuth plating and stripping voltammetry conditions” described above. The total aging time of the $\text{Na}_{10}[\text{Co}_4(\text{H}_2\text{O})_2(\text{PW}_9\text{O}_{34})_2]$ solution was 24 min for the electrolyzed sample and 33 min for the unelectrolyzed sample.

In a variation of the above experiment, a 2.50 μM $\text{Na}_{10}[\text{Co}_4(\text{H}_2\text{O})_2(\text{PW}_9\text{O}_{34})_2]$ solution was subjected to three consecutive 60 s bulk electrolysis experiments at 1.4V vs Ag/AgCl. The 1.0 cm^2 glassy carbon electrode was polished and cleaned between each electrolysis experiment as described in the “Electrochemical Measurements” section above. After the three electrolysis experiments were completed, 1.00 mL of both the electrolyzed and nonelectrolyzed $\text{Na}_{10}[\text{Co}_4(\text{H}_2\text{O})_2(\text{PW}_9\text{O}_{34})_2]$ solution were subjected to the cathodic stripping voltammetry procedure described in the previous paragraph. Total aging times for the electrolyzed and unelectrolyzed sample were 41 and 50 min, respectively.

Bulk Electrolysis and Dissolved O_2 Measurements

Bulk water electrolysis was conducted using a two compartment electrochemical cell where the working compartment contained the glassy carbon plate working electrode ($A = 1.0 \text{ cm}^2$), the Ag/AgCl reference electrode, the O_2 measurement probe, a stir bar, and 1.50 mL of analyte solution. The other compartment contained the platinum wire counter electrode. The oxygen was measured using an Ocean Optics FOXY-R probe connected to a Neofox system. The probe was calibrated using 0% and 20.9% (i.e., air saturated) O_2 solutions, that is, using 0 and 236 μM O_2 at 20 $^\circ\text{C}$ and correcting for the lower air pressure in Fort Collins, Colorado (pressure values ranged from 0.83 to 0.86 bar during the periods of data collection). The dissolved [O_2] was measured beginning 20 s before initiation of the bulk electrolysis. The solution was stirred at

400 rpm throughout the experiment. Between each electrolysis experiment, the solutions were changed and the electrodes were cleaned as described in the “electrochemical measurements” section above. POM solutions were aged for 15-60 min prior to electrolysis; this aging did not result in a measurable change in the O₂ producing activity of the Co₄-POM solutions, *vide infra*.

Deposited CoO_x Controls. Prior to bulk electrolysis and O₂ measurements, CoO_x was deposited onto the glassy carbon working electrode by placing the working, reference, and counter electrodes into a 0.1 mM Co(NO₃)₂ plus 0.1 M, pH 8.0 sodium phosphate solution and holding the potential at 0.79 V vs (Ag/AgCl) for a predetermined amount of time. Electrodes were then rinsed with water, dried by wicking away excess water with a kim-wipe, and placed into their respective electrochemical compartments as described in the previous paragraph. The amount of deposited CoO_x was estimated by subtracting the current passed during a blank electrolysis (i.e., containing only 0.1 M sodium phosphate buffer) from the current passed during the Co(NO₃)₂ plus sodium phosphate electrolysis while assuming 1 e⁻ was passed per deposited cobalt.

HPLC

A Hewlett-Packard 1050 system fitted with a Kromasil C18 column (100 x 4.6 cm, 3.5 μm particles) was used for all HPLC analyses. Mobile phase composition, similar to a previously published procedure for polyoxometalate separations,⁵⁸ was 80% water, 20% acetonitrile, 30 mM *n*-butyl ammonium, 10 mM sodium citrate, pH 6.5. The ammonium and citrate portion of the eluent was prepared by dissolving the appropriate amounts of *n*-butyl amine and sodium citrate in water and adjusting the pH with concentrated HCl. The injection volume was 50 μL and the flow rate was 1.25 mL/minute. Samples were monitored at 240 and 580 nm.

For comparing electrolyzed and unelectrolyzed polyoxometalate samples, the post-electrolysis solution was analyzed immediately after stopping [O₂] data collection (see above), and was followed by HPLC analysis of the otherwise identical, unelectrolyzed sample.

XPS

X-ray photoelectron spectra were obtained using a Physical Instruments PHI-5800 spectrometer. Samples were prepared by rinsing with water after completion of a bulk electrolysis experiment, followed by drying under vacuum. Data was collected using a 7 mm aluminum anode during a 15 minute measurement time.

SEM/EDX

Scanning electron microscopy and energy dispersive X-ray spectroscopy was conducted using a JEOL JSM-6500F microscope and a Thermo Scientific NORAN system. Sample preparation was the same as for XPS.

Results and Discussion

Electrochemical Studies of Co₄(H₂O)₂(PW₉O₃₄)₂¹⁰⁻ Solutions

Consistent with our prior investigation,⁴⁷ cyclic voltammetry of freshly dissolved Co₄(H₂O)₂(PW₉O₃₄)₂¹⁰⁻ in aqueous 0.1 M sodium phosphate buffer yields almost no anodic response up to 1.1 V vs Ag/AgCl (e.g., 578 mV of overpotential for the water-to-oxygen oxidation reaction at pH 8).⁵⁹ However, at larger overpotentials, one (or two) oxidative wave(s) is observed for the 2.5 μM Co₄(H₂O)₂(PW₉O₃₄)₂¹⁰⁻ solutions (Figure 4.1A) at a glassy carbon electrode.⁶⁰ These waves are chemically irreversible regardless of pH, switching potential (see the Supporting Information, Figure S4.1A), or scan rate (Supporting Information, Figure S4.1B). Additionally, the first oxidation wave exhibits current saturation at concentrations greater than 5 μM Co₄(H₂O)₂(PW₉O₃₄)₂¹⁰⁻ (Figure 4.1B), which is consistent with adsorption of Co₄-POM (or

a different active species) to the glassy carbon electrode. This behavior is not surprising given the precedent of POM adsorption to electrodes,⁶¹ as well as the expected Coulombic attraction of a highly positively polarized electrode in conjunction with the large, 10⁻ negative charge on Co₄-POM. Although indium tin oxide and boron doped diamond electrodes were also tested, neither of these materials showed measurable activity in 2.5 μM Co₄(H₂O)₂(PW₉O₃₄)₂¹⁰⁻ solutions relative to blank experiments (Supporting Information, Figure S4.2). Therefore, a glassy carbon electrode was used herein for all electrochemical studies of the Co₄-POM solutions.

As shown in Figure 4.2, the anodic wave in the Co₄-POM solution shifts by -36 mV/pH unit with increasing pH and -93±3 mV/decade in the Tafel plots. The combination of these data indicates a fractional dependence of the anodic current on pH. However, these parameters might include contributions from noncatalytic processes, as has been reported previously for cobalt oxide WOCs.⁶² For example, Gerken et al. observed that up to 30 min of equilibration time at a given potential is sometimes necessary to make reproducible Tafel plots using CoO_x catalysts.⁵⁴ Unfortunately, the oxidation currents for the Co₄-POM decay rapidly to background levels within minutes, *vide infra*, which prevents study of the present Co₄-POM system at long equilibration times. Hence, it follows that the current system is being studied under nonequilibrium conditions.

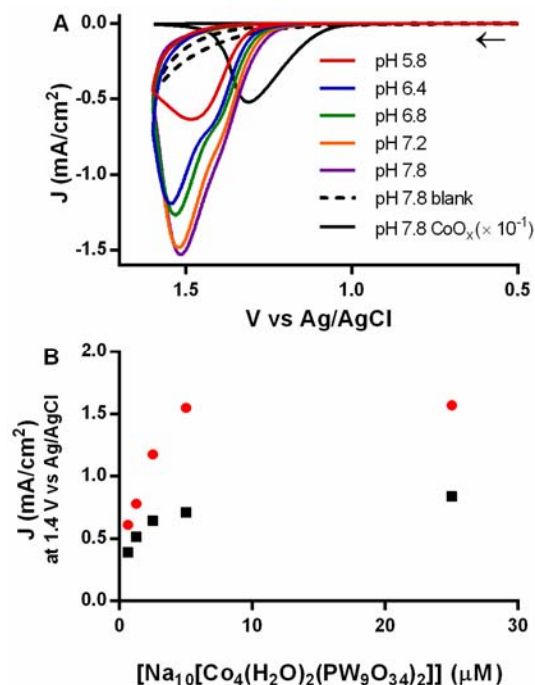


Figure 4.1. (A) Cyclic voltammetry of $2.5 \mu\text{M Co}_4(\text{H}_2\text{O})_2(\text{PW}_9\text{O}_{34})_2^{10-}$ as a function of pH after subtraction of the background current at the indicated pH. For comparison, the uncorrected background current at pH 7.8 is shown as a dotted line and a CoO_x catalytic film—*at $1/10^{\text{th}}$ of its measured intensity*—is shown as a solid black line. The CoO_x was deposited from $100 \mu\text{M Co}(\text{NO}_3)_2$ plus $0.1 \text{ M, pH } 8.0$ sodium phosphate buffer at 0.79 V for 39 s (i.e., conditions which correspond to passage of $1.0 \times 10^{-4} \text{ coulombs/cm}^2$, vide infra). An arrow indicates the initial scan direction. (B) Saturation of the measured cyclic voltammetry current at 1.4 V with increasing polyoxometalate concentration at pH 5.8 (black squares) and pH 8.0 (red circles). Supporting electrolyte is 0.1 M sodium phosphate buffer. Working, reference, and counter electrodes are glassy carbon (3 mm diameter disk), Ag/AgCl , and Pt , respectively. The scan rate is 20 mV/s .

Cyclic voltammetry and the corresponding current-pH and current-overpotential dependences were used to compare empirically the Co_4 -POM solutions with heterogeneous CoO_x . Authentic CoO_x samples were deposited from $100 \mu\text{M Co}(\text{NO}_3)_2$ plus $0.1 \text{ M, pH } 8.0$ sodium phosphate buffer using a procedure similar to that reported by Surendranath et al.⁵³ where it was assumed that one electron oxidation corresponds to the deposition of one cobalt(III) atom. Using this treatment, the prepared CoO_x films in Figures 4.1 and 4.2 contain approximately $10 \text{ nmols of cobalt}$.

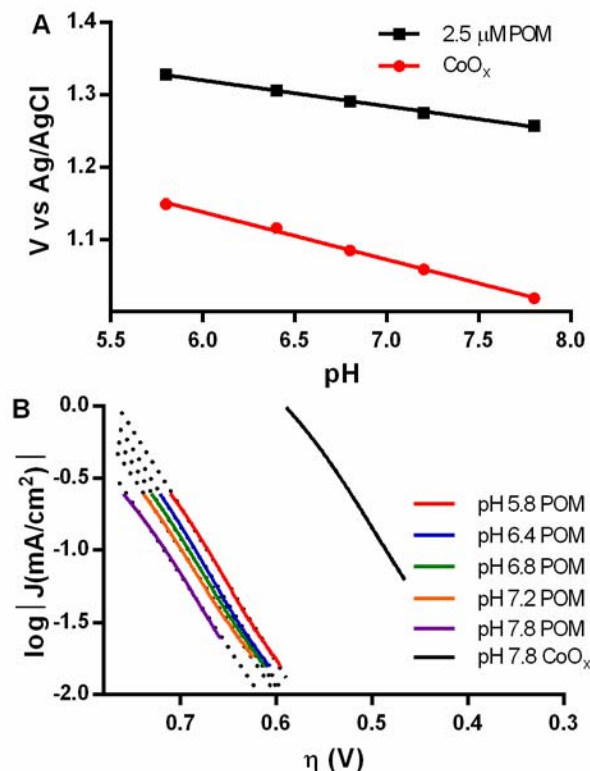


Figure 4.2. (A) $\text{Co}_4(\text{H}_2\text{O})_2(\text{PW}_9\text{O}_{34})_2^{10-}$ (POM) and CoO_x pH dependence of the potential measured at a constant current of 0.1 mA/cm^2 using the cyclic voltammetry data in Figure 4.1 and Supporting Information, Figure S4.3. The slopes of the POM and CoO_x curves are -36 and -66 mV/pH unit. (B) Tafel plots for $\text{Co}_4(\text{H}_2\text{O})_2(\text{PW}_9\text{O}_{34})_2^{10-}$ (POM) and CoO_x derived from the cyclic voltammetry data in Figure 4.1. Dotted lines indicate the linear fit to the data and where $1/\text{slope}$ (i.e., the current-overpotential relationship) of the Co_4 -POM fits varies between -93 and -100 mV/decade and the CoO_x fit is a similar -101 mV/decade . The overpotential was calculated using the equation: $\eta = E - (1.23 - 0.059 \cdot \text{pH}) + 0.236 \text{ V}$, where E is the potential versus Ag/AgCl, $(1.23 - 0.059 \cdot \text{pH})$ is the reversible potential for water oxidation versus NHE, and 0.236 is the voltage addition needed to convert the measured potential from Ag/AgCl to NHE.

The resultant electrochemical data when beginning with $\text{Co}_4(\text{H}_2\text{O})_2(\text{PW}_9\text{O}_{34})_2^{10-}$ differs from heterogeneous, deposited CoO_x in at least two significant ways. First, the onset for water oxidation by CoO_x occurs a few hundred millivolts less positive than the Co_4 -POM anodic wave (e.g. $\sim 240 \text{ mV}$ less oxidizing potentials at pH 7.8 as shown in Figure 4.1). Second, the pH and Tafel dependences for a CoO_x catalyst exhibit slopes of -66 mV/pH unit and $-104 \pm 7 \text{ mV/decade}$ (Supporting Information, Figure S4.3), respectively. Cumulatively, these differences offer strong

evidence *against* the hypothesis that the true catalyst is heterogeneous CoO_x *formed from aqueous* Co^{2+} (either insidious or dissociated from Co_4 -POM) while under the reaction conditions here.

Additionally, repeated cycling of the Co_4 -POM voltammogram shows no evidence of any CoO_x peaks growing in (Supporting Information, Figure S4.4). Moreover, cyclic voltammetry of the glassy carbon electrodes show only background activity levels after bulk electrolysis of a $2.5 \mu\text{M}$ $\text{Co}_4(\text{H}_2\text{O})_2(\text{PW}_9\text{O}_{34})_2^{10-}$ at 1.4 V vs Ag/AgCl and then rinsing of the electrodes (Supporting Information, Figure S4.5). These results contrast our previous study of $\text{Co}_4(\text{H}_2\text{O})_2(\text{PW}_9\text{O}_{34})_2^{10-}$ at $500 \mu\text{M}$ concentration and 1.1 V vs Ag/AgCl which showed clearly that the dominant catalyst is, under those different concentration and electrochemical potential conditions, heterogeneous CoO_x formed from Co^{2+} which had been released by the parent Co_4 -POM.

To confirm O_2 as a reaction product and to determine the faradaic efficiency of the system, bulk electrolysis of Co_4 -POM solutions was performed at several potentials. Similar to the cyclic voltammetry above, significant water oxidation activity was not observed until 1.3 V vs Ag/AgCl . At a potential of 1.4 V , quantifiable water oxidation activity was observed where 15.6 ± 1.2 and $28.4 \pm 1.8 \text{ nmol O}_2$ were produced at $\text{pH } 5.8$ and 8.0 , respectively (Figure 4.3A). If the POM is *assumed* to be a WOC, then conversion of this O_2 generation data into an average turnover frequency when beginning with the Co_4 -POM yields an approximate $\text{TOF} = 0.54$ and $0.98 \text{ mol O}_2 \cdot \text{s}^{-1} \cdot \text{mol cobalt}^{-1}$ at $\text{pH } 5.8$ and 8.0 . This calculation assumes the only active portion of the POM solution is a monolayer in contact with the 1 cm^2 electrode and where the area coverage of one Co_4 -POM is 1.38 nm^2 —which is the area of the the smallest crystallographically determined face.⁴⁶ Note, the assumption that only the Co_4 -POM molecules which are in a monolayer contribute to the catalysis will overestimate the TOF since it is likely that exchange

between solution and adsorbed Co₄-POMs occurs during the reaction. Further details of this TOF calculation can be found in the Supporting Information. This TOF estimation is provided primarily for comparison to the TOF for CoO_x, *vide infra*.

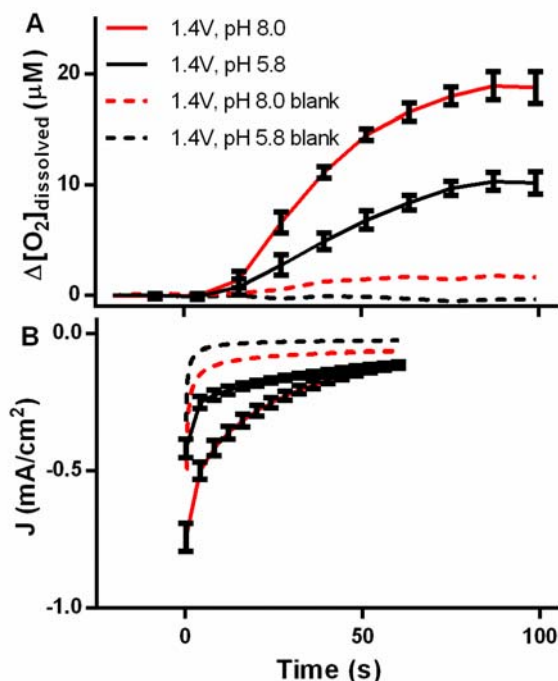


Figure 4.3. Bulk electrolysis dissolved O₂ and current density measurements for a 2.5 μM Co₄(H₂O)₂(PW₉O₃₄)₂¹⁰⁻ solution (volume = 1.50 mL) in 0.1 M sodium phosphate buffer (pH 8.0 or 5.8) at 1.4 V vs Ag/AgCl on a glassy carbon electrode (A = 1.0 cm²). The O₂ was measured using a fluorescence based detection system (FOXY-R probe from Ocean Optics). Electrolysis was started at t = 0 s. The lag between the start of electrolysis and the detection of oxygen is primarily due to a slow response time of the probe. Error bars indicate the standard deviation of three experiments.

Additionally, the calculated TOF for the putative Co₄-POM based catalyst is underestimated since the current densities decayed to 15-25% of their initial values during the 60 s electrolysis, as shown in Figure 4.3B. Decomposition of activity for glassy carbon is not unexpected at these large, 1.4 V positive potentials. Decay in oxidation current likely corresponds primarily to electrode surface changes and not significant decomposition in the

Co₄-POM solution since oxidation activity of the system is restored upon polishing/cleaning the glassy carbon electrode (Supporting Information, Figure S4.6).

Despite the oxidative fouling of the glassy carbon electrode, the faradaic efficiency (i.e., the current to O₂ efficiency) of the Co₄-POM solution was found to be 75.0 ± 2.2% and 88.8 ± 1.4% at pH 5.8 and 8.0. This efficiency is important since it indicates most of the current corresponds to the catalyzed O₂ producing reaction and not to oxidative catalyst decomposition pathways. In comparison the control bulk electrolysis experiments, where no Co₄-POM is present in solution, no O₂ increase is seen at pH 5.8 and only 2.0 nmol of O₂ are produced at pH 8.0.

In short, these electrochemical studies show that (i) significant water oxidation activity is present in Co₄(H₂O)₂(PW₉O₃₄)₂¹⁰⁻ solutions at applied potentials greater than 1.25 V vs Ag/AgCl, (ii) this activity saturates at low (~5 μM) Co₄-POM concentrations, and (iii) this activity occurs at approximately 200 mV more overpotential than heterogeneous CoO_x catalysts—three lines of evidence which demonstrates that CoO_x formed from dissociated Co²⁺ is *not* the active catalyst under the specific conditions of 2.5 μM Co₄(H₂O)₂(PW₉O₃₄)₂¹⁰⁻ at ≥1.3 V vs Ag/AgCl.

Determination of [Co²⁺] in Co₄-POM Solutions

To investigate the hydrolytic stability under nonoxidizing conditions, the aqueous [Co²⁺]_{apparent} was determined by cathodic stripping voltammetry at pH 8.^{57,63} This electrochemical method was used by us previously⁴⁷ to determine the [Co²⁺]_{apparent} in 500 μM Co₄(H₂O)₂(PW₉O₃₄)₂¹⁰⁻ solution and found to accurately report the apparent aqueous cobalt(II) concentration determined by an alternative, independent electrochemical method. (Specifically, the [Co²⁺]_{apparent} was determined to be 56 ± 2 μM using the cathodic stripping technique and 58 ±

2 μM using the alternative method which relies on the measurement of an anodic current- $[\text{Co}^{2+}]$ relationship.)⁴⁷ However, it should be noted that the observed $[\text{Co}^{2+}]$ is likely an upper limit to the true aqueous $[\text{Co}^{2+}]$ since complexation of cobalt(II) by the additive dimethylglyoxime (DMG) can shift the equilibrium in (eq 1) to the right. To minimize this effect, the dimethylglyoxime was added only 5 min before the measurement was taken as detailed in the Experimental Section.



As shown in Figure 4.4, about 100 nM Co^{2+} is present in the $2.5 \mu\text{M Co}_4(\text{H}_2\text{O})_2(\text{PW}_9\text{O}_{34})_2^{10-}$ solution after 15 min of aging which increases to 250 nM ($0.25 \pm 0.06 \mu\text{M}$) Co^{2+} after 1 h. That is, 10% of the $\text{Co}_4\text{-POM}$ has released a cobalt atom from their core or, alternatively, 2.5% of the $\text{Co}_4\text{-POM}$ has released all four core cobalts after 1 h in 0.1 M phosphate buffer solution. This result confirms our prior observation that, in general, $\text{Co}_4(\text{H}_2\text{O})_2(\text{PW}_9\text{O}_{34})_2^{10-}$ is not 100% stable in aqueous pH 8.0, 0.1 M sodium phosphate buffer.

Controls with $\text{Co}(\text{NO}_3)_2$

With the degree of Co^{2+} dissociated from the parent $\text{Co}_4(\text{H}_2\text{O})_2(\text{PW}_9\text{O}_{34})_2^{10-}$ established, it is then possible to conduct the proper control experiments comparing the activity observed in $\text{Co}_4\text{-POM}$ solutions to the above measured amount of $[\text{Co}^{2+}]_{\text{apparent}}$. In Figure 4.5 the O_2 yields for both $2.5 \mu\text{M Co}_4(\text{H}_2\text{O})_2(\text{PW}_9\text{O}_{34})_2^{10-}$ and $0.2 \mu\text{M Co}(\text{NO}_3)_2$ are shown. Interestingly, these $0.2 \mu\text{M Co}(\text{NO}_3)_2$ controls *do not account for the observed O_2 generating catalysis*. This result contrasts starkly with our prior results at higher polyoxometalate concentrations and lower electrochemical potentials (i.e., at $500 \mu\text{M Co}_4\text{-POM}$ and 1.1 V vs Ag/AgCl) where the $58 \pm 2 \mu\text{M Co}^{2+}$ dissociated from the parent POM accounted quantitatively ($101 \pm 12\%$) for the observed O_2 production.⁴⁷

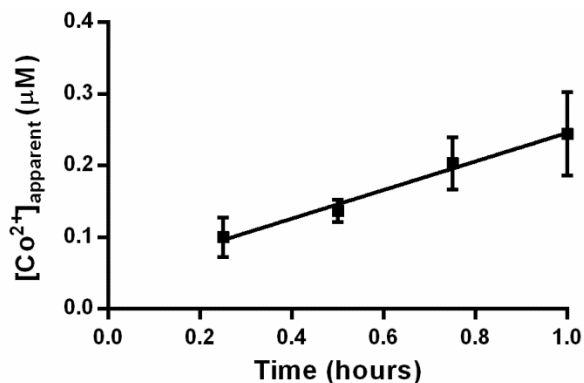


Figure 4.4. Apparent Co^{2+} concentration, determined using cathodic stripping voltammetry in $2.5 \mu\text{M Co}_4(\text{H}_2\text{O})_2(\text{PW}_9\text{O}_{34})_2^{10-}$ plus $20 \mu\text{M}$ dimethylglyoxime in 0.1 M , $\text{pH } 8.0$ sodium phosphate buffer, taken at 15 minute aging intervals. The concentrations were calculated using a standard curve generated from $\text{Co}(\text{NO}_3)_2$ solutions (Supporting Information, Figure S4.7). Error bars indicate the standard deviation of three experiments.

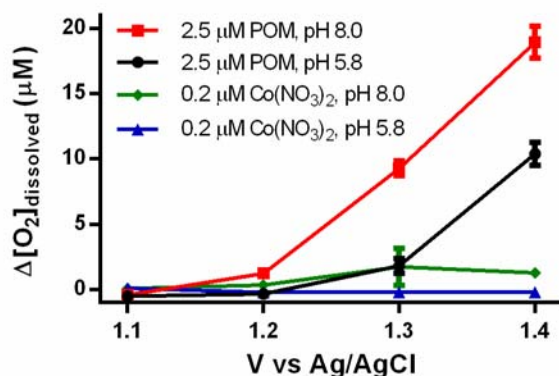


Figure 4.5. Dissolved oxygen production (μM) during catalytic water oxidation at a glassy carbon electrode and the given $\text{Co}_4(\text{H}_2\text{O})_2(\text{PW}_9\text{O}_{34})_2^{10-}$ (POM) or $\text{Co}(\text{NO}_3)_2$ concentrations, pH , and potential during a 60 s bulk electrolysis. Oxygen was measured using a FOXY-R O_2 detection probe. The plotted lines are meant solely to guide the eye. Error bars indicate the standard deviation of three experiments.

Although the above evidence indicates a Co^{2+} to CoO_x catalyst formation mechanism is *not* a dominant O_2 production pathway under the specific conditions investigated herein (i.e., when using the $[\text{Co}^{2+}]$ present after approximately 1 h of aging), it does not rule out the possibility that a small portion of the current could correspond to direct transformation of the electrode-adsorbed Co_4 -POM into highly active CoO_x (Scheme 4.1, *vide supra*). Therefore it is crucial (i) to determine how much authentic CoO_x is needed to carry the water oxidation activity

observed in the $\text{Co}_4(\text{H}_2\text{O})_2(\text{PW}_9\text{O}_{34})_2^{10-}$ solution, and then (ii) determine whether this amount of Co_4 -POM decomposition can be observed.

Controls with Authentic CoO_x

To address the question whether direct oxidative decomposition of the cobalt POM into CoO_x could account for the catalytic water oxidation activity observed in Co_4 -POM solutions, a series of CoO_x coated electrodes were prepared by electro-deposition of the CoO_x material from cobalt(II) nitrate solutions at pH 8.0, and then tested in pure sodium phosphate electrolyte for their ability to generate O_2 at 1.4 V vs Ag/AgCl (Figure 4.6). By dividing the slopes of these curves by the reaction time (i.e., 60 s), an approximate, average turnover frequency for the CoO_x catalyst is found to be $\text{TOF} = 1.0$ and $0.27 \text{ mol O}_2 \cdot \text{s}^{-1} \cdot \text{mol cobalt}^{-1}$ at pH 8.0 and 5.8, respectively. Additional details of this calculation can be found in the Supporting Information. This estimate is likely an underestimate of the true activity since the deposited CoO_x -glassy carbon catalyst is not stable under the reaction conditions (vide infra). In comparison, Surendranath et al. reported a CoO_x $\text{TOF} = 0.0026 \text{ mol O}_2 \cdot \text{s}^{-1} \cdot \text{mol cobalt}^{-1}$ in pH 7.0 potassium phosphate and at 410 mV of overpotential. That is, they observed TOF values which would be 1.2×10^5 and $9.0 \times 10^3 \text{ mol O}_2 \cdot \text{s}^{-1} \cdot \text{mol cobalt}^{-1}$ if their observed current-overpotential relationship of 61 mV/decade is extrapolated to our working overpotentials of 878 mV and 748 mV at pH 8.0 or 5.8 and at 1.4V vs Ag/AgCl. Again, these TOF estimates and ranges are, admittedly, crude, but are provided herein as initial estimates from which to base the needed future studies. Once one has the true, per-active-site, TOFs for CoO_x , Co_4 -POM, and other POMs, metal oxides, and WOCs of interest, then the problem of determining the true catalyst, as well as which type of WOC merits future emphasis, will become much easier and clearer.

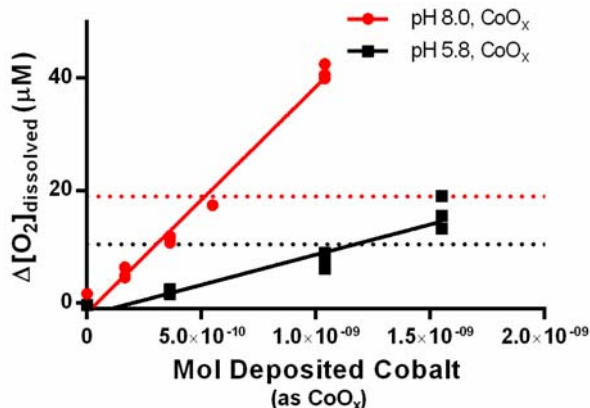


Figure 4.6. Calibration curve of oxygen yielded during a 60 s, 1.4 V electrolysis of predeposited CoO_x catalysts containing the approximate mols of cobalt indicated. The CoO_x catalysts were prepared in 0.1 mM Co(NO₃)₂ plus pH 8.0, 0.1 M sodium phosphate at 0.79 V for predetermined amounts of time (as described in the main text). The dashed lines indicate the observed O₂ yield in a 2.5 μM Co₄(H₂O)₂(PW₉O₃₄)₂¹⁰⁻ bulk electrolysis at 1.4 V for 60 s at pH 5.8 (black) and 8.0 (red) (i.e., the same conditions as in Figure 4.3); that is, the amounts of deposited CoO_x at (or above) the dashed lines are equivalent to (or more active than) the 2.5 μM Co₄-POM solutions under identical reaction conditions.

When the O₂ yields of these CoO_x coated electrodes were compared to the yields observed for Co₄-POM solutions, it was found that *0.45-0.58 nmols* (at pH 8.0) and *1.0-1.5 nmols* (at pH 5.8) of cobalt in the form of deposited CoO_x can account for the total amount of oxygen generated at 1.4 V during a 60 s bulk electrolysis experiment. Restated, as little as 4 to 8% transformation of the starting POM into CoO_x could carry the observed O₂ production of the Co₄-POM solutions at pH 8 or 5.8, assuming all four cobalts from Co₄-POM are converted into CoO_x. Therefore, it is necessary to determine the oxidative stability of the initially 2.5 μM Co₄-POM under the oxidizing reaction conditions (i.e., the postreaction level of decomposition of Co₄-POM).

Polyoxometalate Stability Measured by HPLC

Stability of Co₄-POM under the highly oxidizing reaction conditions was quantified by HPLC with absorbance detection. The HPLC separation used herein is based upon an ion-pair chromatography method developed previously by our group (Figure 4.7).⁵⁸ In these experiments,

the 2.5 μM $\text{Co}_4(\text{H}_2\text{O})_2(\text{PW}_9\text{O}_{34})_2^{10-}$ pre- and post-bulk electrolysis solutions were compared to determine whether any loss of $\text{Co}_4\text{-POM}$ could be detected (Figure S4.8). Evidence that the HPLC measurement is faithfully reporting the $[\text{Co}_4\text{-POM}]$ includes: (i) the background subtracted chromatograms show a single peak at pH 5.8, which (ii) increases in area linearly with $\text{Co}_4\text{-POM}$ concentration (Supporting Information, Figure S4.9), and (iii) collection of the eluent from $t = 2.5\text{-}3.0$ min with subsequent visible spectroscopy shows that the eluted sample has the expected visible absorption spectrum when compared to a non-chromatographed $\text{Co}_4(\text{H}_2\text{O})_2(\text{PW}_9\text{O}_{34})_2^{10-}$ sample (Supporting Information, Figure S4.10). When the $\text{Co}_4\text{-POM}$ sample in pH 8.0 sodium phosphate buffer is tested by HPLC, a shoulder is observed immediately next to the primary peak; this may be due to partial conversion of the $\text{Co}_4(\text{H}_2\text{O})_2(\text{PW}_9\text{O}_{34})_2^{10-}$ to one of the related POMs where one or two of the cobalt atoms have dissociated from the core and have been replaced by sodium (e.g., $\text{NaCo}_3(\text{H}_2\text{O})(\text{PW}_9\text{O}_{34})_2^{11-}$ or $\text{Na}_2\text{Co}_2(\text{PW}_9\text{O}_{34})_2^{12-}$).⁶⁴ Note that the dissociation of cobalt from $\text{Co}_4\text{-POM}$ is supported by the independent determination of $[\text{Co}^{2+}]_{\text{apparent}}$ above (Figure 4.4).

At pH 5.8 or 8.0 and electrochemical potentials ranging from 1.1 to 1.4 V vs Ag/AgCl the relative stability of $\text{Co}_4\text{-POM}$ is listed in Table 4.1, data which indicate that the starting polyoxometalate is somewhat, but not absolutely, stable under the oxidizing environment encountered in this study. HPLC measured $\text{Co}_4\text{-POM}$ stability at *lower electrochemical potentials* is consistent with $\text{Co}_4(\text{H}_2\text{O})_2(\text{PW}_9\text{O}_{34})_2^{10-}$ being hydrolytically stable over the approximately 15 min duration of the experiment, plus or minus the 2-12% error of the method. Significantly, at pH 5.8 and pH 8.0 the change in $[\text{Co}_4\text{-POM}]$ after a 1.4 V electrolysis (Table 4.1) corresponds to the loss of 1.41 ± 0.76 and 0.4 ± 1.1 nmols of cobalt during electrolysis while the CoO_x electrolysis controls (Figure 4.6) indicate that 1.2 ± 0.3 and 0.51 ± 0.07 nmols of CoO_x

are capable of carrying the observed WOC activity under these conditions. These closely matched values indicate that deposited and/or soluble, colloidal CoO_x cannot be ruled out as a WOC when beginning with $\text{Co}_4(\text{H}_2\text{O})_2(\text{PW}_9\text{O}_{34})_2^{10-}$ under the specific conditions of this study.

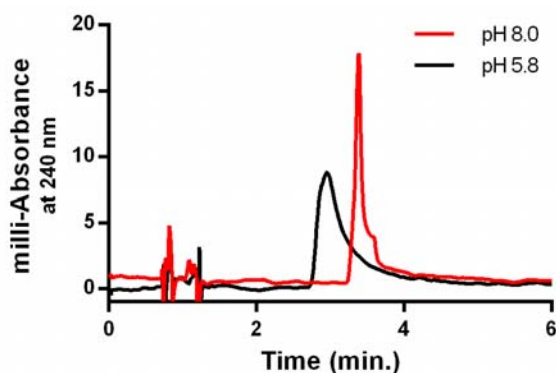


Figure 4.7. HPLC traces of Co_4 -POM solutions with $2.5 \mu\text{M Co}_4(\text{H}_2\text{O})_2(\text{PW}_9\text{O}_{34})_2^{10-}$ in 0.1 M sodium phosphate buffer at the indicated pH; the chromatograms are corrected by subtracting a blank HPLC trace which contained only 0.1 M sodium phosphate at the same pH as the sample. Chromatograms were monitored using the 240 nm absorbance of the sample. HPLC conditions are 80% water, 20% acetonitrile, 30 mM butylammonium chloride, 10 mM sodium citrate, pH 6.5, 1.25 mL flow rate, and room temperature.

Table 4.1. Stability of $2.5 \mu\text{M Co}_4(\text{H}_2\text{O})_2(\text{PW}_9\text{O}_{34})_2^{10-}$ Solutions During Bulk Electrolysis Determined by HPLC^a

pH	Potential vs Ag/AgCl	Electrolysis Time (s)	Co_4 -POM Stability ^{b,c}
5.8	1.1	60	97.4% ± 6.4
5.8	1.2	60	99.0% ± 2.1
5.8	1.3	60	90.1% ± 8.9
5.8	1.4	60	90.6% ± 5.1
8	1.1	60	93.7% ± 2.5
8	1.2	60	100.8% ± 5.5
8	1.3	60	100.8% ± 12.3
8	1.4	60	97.3% ± 7.6

^aElectrolysis conditions are the same as described in Figure 4.3. ^bStability is calculated by dividing the area of the electrolyzed Co_4 -POM HPLC peak (at $t = 3\text{-}4$ min in Figure 4.7) by the unelectrolyzed Co_4 -POM HPLC peak: $\text{Co}_4\text{-POM Stability} = \text{Area}_{\text{electrolyzed}} / \text{Area}_{\text{unelectrolyzed}} \cdot 100\%$. ^cError bars are the standard deviation of three experiments.

Determination of [Co²⁺] in Post-Catalysis Co₄-POM Solutions

To further support the hypothesis of Co₄-POM instability under the oxidizing reaction conditions, the postelectrolysis cobalt(II) concentrations were determined via cathodic stripping voltammetry. In these experiments, a standard solution of 2.5 μM Co₄(H₂O)₂(PW₉O₃₄)₂¹⁰⁻ plus pH 8.0, 0.1 M sodium phosphate was subjected to a 60 s bulk electrolysis at 1.4 V vs Ag/AgCl. Then, using cathodic stripping voltammetry, the [Co²⁺] in the Co₄-POM solution was found to be 250 ± 27 nM. In comparison, a Co₄(H₂O)₂(PW₉O₃₄)₂¹⁰⁻ solution which was not subjected to bulk electrolysis had [Co²⁺] = 200 ± 22 nM, even though this solution was aged an additional 9 min compared to the electrolyzed sample. That is, bulk electrolysis of the Co₄-POM results in 50 (± 34) nM higher aqueous cobalt(II) concentrations—evidence which is consistent with the oxidative instability of the starting polyoxometalate.

Additionally, if a 2.5 μM Co₄(H₂O)₂(PW₉O₃₄)₂¹⁰⁻ plus pH 8.0, 0.1 M sodium phosphate solution is subjected to *three consecutive 1.4 V vs Ag/AgCl bulk electrolysis experiments* for 60 s each, the resultant [Co²⁺] is significantly higher, [Co²⁺] = 825 nM. The corresponding unelectrolyzed Co₄-POM solution, examined as a control, contained only [Co²⁺] = 273 nM. This substantial increase in [Co²⁺] during only 3 min of electrolysis is consistent with at least 5.5% of the starting polyoxometalate being transformed into aqueous Co²⁺ during the electrolysis (in addition to the 2.7% which appears to be hydrolytically unstable), assuming all four of the core cobalt atoms are removed from the parent Co₄-POM. This calculation is only a lower limit on the stability since we do not know the amounts of other possible Co₄-POM decomposition products including both colloidal and deposited CoO_x. In summary of the Co²⁺ determinations post water oxidation reactions, the data corroborate the HPLC results by showing increasing Co₄-POM decomposition with increasing electrolysis time. This, in turn, provides a very important insight:

even if Co₄-POM is initially a WOC, it is not stable in a thermodynamic sense under at least the reaction conditions employed herein.

Surface Characterization of the Glassy Carbon Electrode

Additional evidence concerning the identity of any deposited catalyst was collected via XPS of the postelectrolysis glassy carbon electrode. Figure 4.8 shows the cobalt 2p_{3/2} portion of the spectrum for glassy carbon electrodes treated with either the Co₄-POM solutions or a CoO_x control which showed the same O₂ producing activity within experimental error as the Co₄-POM. At pH 8, it was found that trace cobalt was observable in the film for both the Co₄-POM and the CoO_x control, while at pH 5.8 only the CoO_x control showed detectable amounts of cobalt. The low surface cobalt coverage was also consistent with SEM/EDX imaging and spectroscopy which showed no discernible difference between blank glassy carbon and the samples (Supporting Information, Figure S4.11); the lack of cobalt detection by EDX is somewhat expected in this case since this method is much less sensitive to surface composition.⁶⁵

In contrast to the low cobalt coverages observed in postcatalysis electrodes, the pre-electrolysis CoO_x controls showed significantly higher amounts of surface cobalt (Figure 4.8). *This indicates that even the deposited heterogeneous CoO_x is not stable at the oxidizing 1.4 V conditions herein.* That is, care must be taken when attempting to distinguish homogeneous and heterogeneous electrocatalysis based solely on the presence or absence of an ex-situ catalytic film on the electrode at the end of the electrolysis. Multiple, complementary methods should always be used to confirm or refute initial observations when attempting to answer the question of whether a catalyst is homogeneous or heterogeneous.^{66,67}

In the present case, surface characterization of the glassy carbon electrodes is ultimately inconclusive since minimal (if any) CoO_x is deposited during electrolysis of

$\text{Co}_4(\text{H}_2\text{O})_2(\text{PW}_9\text{O}_{34})_2^{10-}$ and since controls with authentic deposited CoO_x show dissolution of the heterogeneous catalyst during electrolysis at 1.4 V vs Ag/AgCl. *In operando* nanobalance experiments⁶⁸ may be useful for this system, but even there the oxidative instability of the CoO_x films and the large positive potential of the electrode promise to prove problematic.

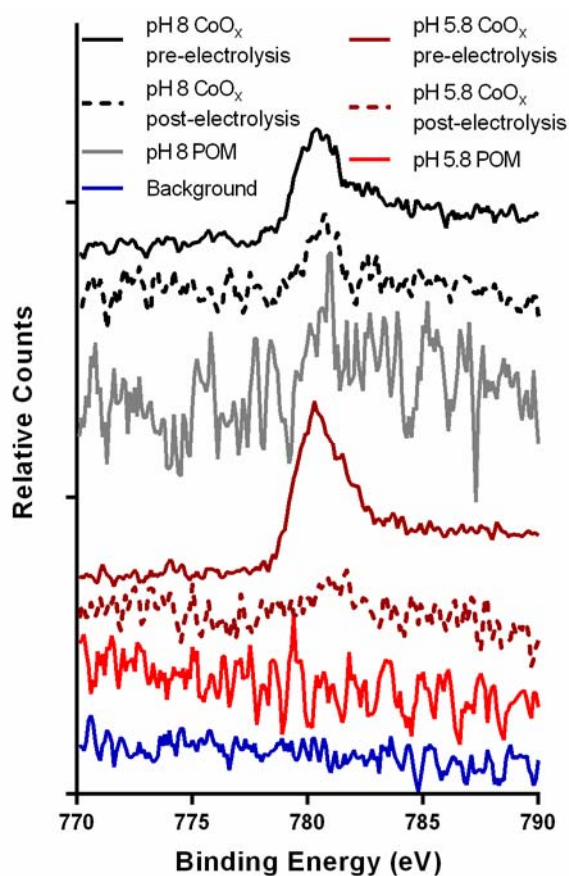


Figure 4.8. XPS data for the Co 2p_{3/2} region using 2.5 μM Co_4 -POM treated electrodes after bulk electrolysis and CoO_x coated electrodes both before and after electrolysis. Conditions for the electrolysis were 1.4 V vs Ag/AgCl for 60 s in 0.1 M sodium phosphate buffer at the pH given in the legend. Also shown is a blank glassy carbon electrode. The CoO_x covered electrodes were prepared by controlled potential electrolysis of 0.1 mM $\text{Co}(\text{NO}_3)_2$ plus pH 8.0, 0.1 M sodium phosphate at 0.79 V for 15 and 42 s for the pH 8.0 and pH 5.8 experiments, respectively.

Conclusions

In summary, one conclusion from this study is that heterogeneous, deposited CoO_x is not formed in catalytically significant amounts from aqueous Co^{2+} dissociated from the parent 2.5 μM $\text{Co}_4(\text{H}_2\text{O})_2(\text{PW}_9\text{O}_{34})_2^{10-}$ when using a glassy carbon working electrode, at applied potentials

≥ 1.3 V vs Ag/AgCl, and pH 5.8 or 8.0 sodium phosphate buffer. The specific results which lead directly to this conclusion are as follows: (1) The apparent concentration of aqueous Co^{2+} in the $\text{Co}_4\text{-POM}$ solution prior to the reaction is found to be $0.17 \mu\text{M}$ (average during a 1 h aging period at pH 8.0), and (2) testing an equivalent amount of $\text{Co}(\text{NO}_3)_2$ (i.e., $0.2 \mu\text{M}$) in bulk electrolysis experiments at 1.4 V demonstrates that the 2.0 nmols of O_2 produced in these controls is significantly lower relative to the 28.4 nmols O_2 produced under equivalent conditions using $2.5 \mu\text{M Co}_4(\text{H}_2\text{O})_2(\text{PW}_9\text{O}_{34})_2^{10-}$. Additional electrochemical evidence which is inconsistent with a Co^{2+} -to- CoO_x WOC formation mechanism includes (3) cyclic voltammetry of the $\text{Co}_4\text{-POM}$ solutions show an oxidative wave onset of 1.25 V (compared to 1.10 V for a CoO_x catalyst); (4) repeated CV scans show no evidence of a CoO_x type catalyst growing in (i.e., negative evidence for CoO_x); (5) rinsing of the glassy carbon electrode used in $\text{Co}_4\text{-POM}$ bulk electrolysis followed by electro-catalytic testing in pure sodium phosphate electrolyte (i.e., no added $\text{Co}_4\text{-POM}$) shows currents comparable to background levels (additional negative evidence for a deposited catalyst); and (6) the pH dependence of -36 mV/pH unit for $\text{Co}_4\text{-POM}$ solutions versus -64 mV/pH unit for CoO_x is considerably different (i.e., consistent with a substoichiometric proton transfer versus a single proton transfer involved in, or prior to, the rate determining step starting from $\text{Co}_4\text{-POM}$ vs CoO_x). This finding, that a Co^{2+} to electrodeposited CoO_x catalyst is not the kinetically dominant catalyst when starting in $2.5 \mu\text{M Co}_4(\text{H}_2\text{O})_2(\text{PW}_9\text{O}_{34})_2^{10-}$ and at ≥ 1.3 V vs Ag/AgCl, contrasts with our prior investigation at higher $\text{Co}_4\text{-POM}$ concentrations and lower potentials (i.e., $500 \mu\text{M Co}_4(\text{H}_2\text{O})_2(\text{PW}_9\text{O}_{34})_2^{10-}$ and 1.1 V vs Ag/AgCl) where heterogeneous CoO_x deposited from aqueous Co^{2+} is clearly the dominant catalyst.⁴⁷ That is, the precise conditions can have a profound effect on the dominant, observed water oxidation reaction pathway and catalyst.⁶⁹

A second primary conclusion—backed by the electrochemical, HPLC, and surface characterization methods applied herein—is that we are unable to definitively distinguish between homogeneous polyoxometalate and heterogeneous CoO_x (either electrode-bound or soluble, colloidal) formed *via direct oxidation of $\text{Co}_4\text{-POM}$* . This conclusion is supported by the following observations: (7) bulk electrocatalytic testing of $\text{Co}_4\text{-POM}$ gives 28.4 ± 1.8 and 15.6 ± 1.2 nmol O_2 at 2.5 μM (3.8 nmol of catalyst) at 1.4 V and pH 8.0 and 5.8, respectively; and, (8) controls using pre-deposited CoO_x indicate that transformation of only $3.9\% \pm 0.4$ and $8.2\% \pm 1.1$ of $\text{Co}_4\text{-POM}$ into a CoO_x type catalyst would account for the observed amount of O_2 generation during a 60 s electrolysis under the same 1.4 V potential and at pH 8.0 or 5.8 conditions. In addition, (9) comparison of the electrolyzed and unelectrolyzed $\text{Co}_4\text{-POM}$ solutions by HPLC indicate the loss of $2.7\% \pm 7.6$ (at pH 8.0) to $9.5\% \pm 5.1$ (at pH 5.8) of $\text{Co}_4\text{-POM}$ during electrolysis described in point (8) above; that is, *if the lost $[\text{Co}_4\text{-POM}]$ is transformed completely into a CoO_x type catalyst, then all of the O_2 generating activity of the $\text{Co}_4\text{-POM}$ solution could be accounted for by CoO_x* . (10) Furthermore, determination of the $[\text{Co}^{2+}]$ in the post-bulk electrolysis $\text{Co}_4\text{-POM}$ solutions is consistent with the instability of the starting polyoxometalate under the oxidizing reaction conditions. But, even with all of the quantitative evidence and controls, *often at the nmol level*, we are unable to definitively distinguish a CoO_x catalyst from a $\text{Co}_4(\text{H}_2\text{O})_2(\text{PW}_9\text{O}_{34})_2^{10-}$ based catalyst (or from a combination of the two).⁷⁰

A third, major—and perhaps most important—conclusion of these studies is that increasing amounts of $\text{Co}_4\text{-POM}$ decomposition, as detected by $[\text{Co}_4\text{-POM}]$ decreases in HPLC and increasing $[\text{Co}^{2+}]$ in post catalysis reactions, is seen with increasing reaction times. From this

it seems inescapable that $\text{Co}_4\text{-POM}$ is not stable in a thermodynamic sense to the conditions examined herein.

Overall, our studies highlight the challenges of distinguishing homogeneous and heterogeneous water oxidation catalysis when beginning with micromolar molecular cobalt precursors (other than aqueous cobalt(II) salts) and where nanomolar heterogeneous metal-oxide will account for the observed O_2 generation—a finding consistent with the efforts of other researchers in the area.^{71,72,73,74} Ultimately, a successful approach to answering the “who is the true WOC?” question in a given system will rely on identifying and characterizing all hypothesized forms of the catalyst, determining the possible (or actual) amounts of those materials formed during the reaction, and then conducting control experiments comparing the catalytic activity of each species present en route to determining the true catalyst. Our own efforts in the area of “who is the true WOC?” are continuing.

Supporting Information

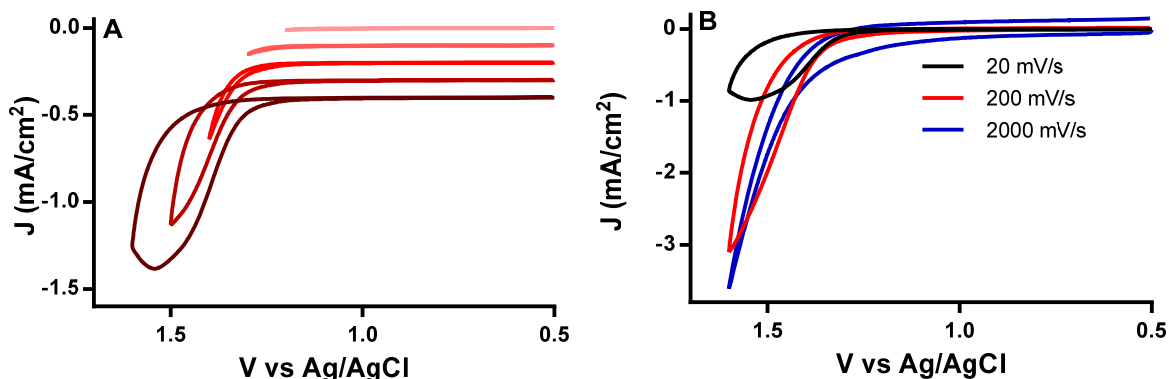


Figure S4.1. Cyclic voltammograms for $2.5 \mu\text{M Co}_4(\text{H}_2\text{O})_2(\text{PW}_9\text{O}_{34})_2^{10-}$ while varying (A) the potential at which the scan is reversed, and (B) the scan rate. All CVs were taken in pH 5.8 sodium phosphate electrolyte. The voltammograms in (A) are offset by 0.1 mA/cm^2 for clarity. The main result to be noted is the irreversibility of the anodic wave regardless of switching potential or scan rate—evidence suggestive of a fast, chemically irreversible process which does not lead to measurable deposition of a catalytic CoO_x film.

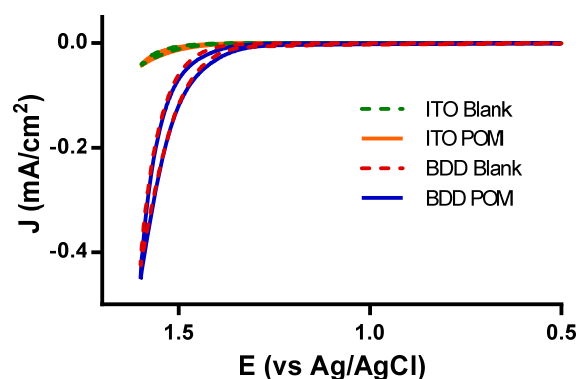


Figure S4.2. Cyclic voltammograms using either a boron doped diamond (BDD) or indium tin oxide (ITO) working electrode in pH 5.8, 0.1 M sodium phosphate electrolyte in pure electrolyte (Blank) or in the presence of $2.5 \mu\text{M Co}_4(\text{H}_2\text{O})_2(\text{PW}_9\text{O}_{34})_2^{10-}$ ($\text{Co}_4\text{-POM}$). The scan rate is 20 mV/s. The nearly identical electrochemical response of the electrodes in both the presence and absence of the $\text{Co}_4\text{-POM}$ suggests this polyoxometalate is not electrochemically active under these conditions at either ITO or BDD working electrodes.

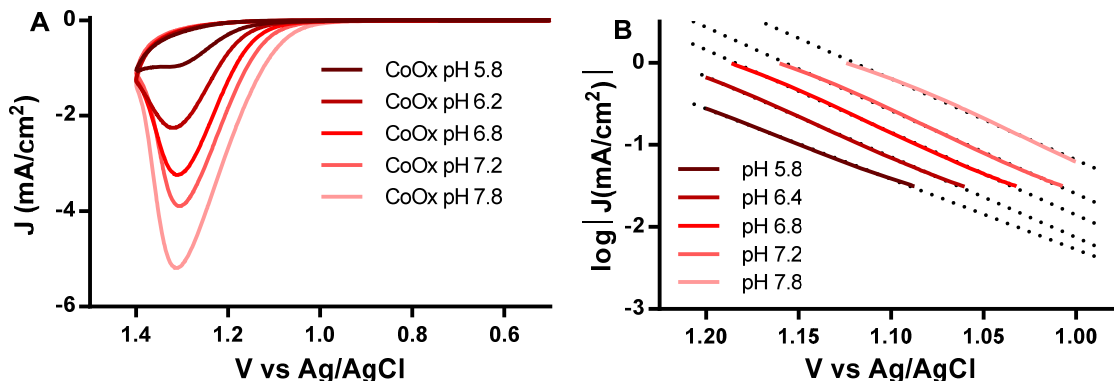


Figure S4.3. (A) Cyclic voltammetry of pre-deposited CoO_x on glassy carbon in 0.1M sodium phosphate buffer at the pH values indicated in the legend, and (B) the corresponding Tafel plots. The dotted lines in (B) are the linear fits to the data where $1/\text{slope}$ varies from -99 to -117 mV/decade. As described in detail in the main text, the CoO_x was deposited from $100 \mu\text{M Co}(\text{NO}_3)_2$ in sodium phosphate buffer at pH 8.0 where $1.0 \times 10^{-4} \text{ C/cm}^2$ charge was passed during electrodeposition after subtraction of the background current. Noteworthy in these experiments is the onset of the anodic wave at approximately 1.01 V at pH 7.8 and 1.14 V at pH 5.8 which is 0.18 to 0.24 V negative of the oxidation wave onset for $2.5 \mu\text{M Co}_4(\text{H}_2\text{O})_2(\text{PW}_9\text{O}_{34})_2^{10-}$ solutions. Also, and as noted in the main text, the Tafel plots probably do not reflect the true current-overpotential relationship for catalytic water oxidation since the system is not at equilibrium.^{53,54,62}

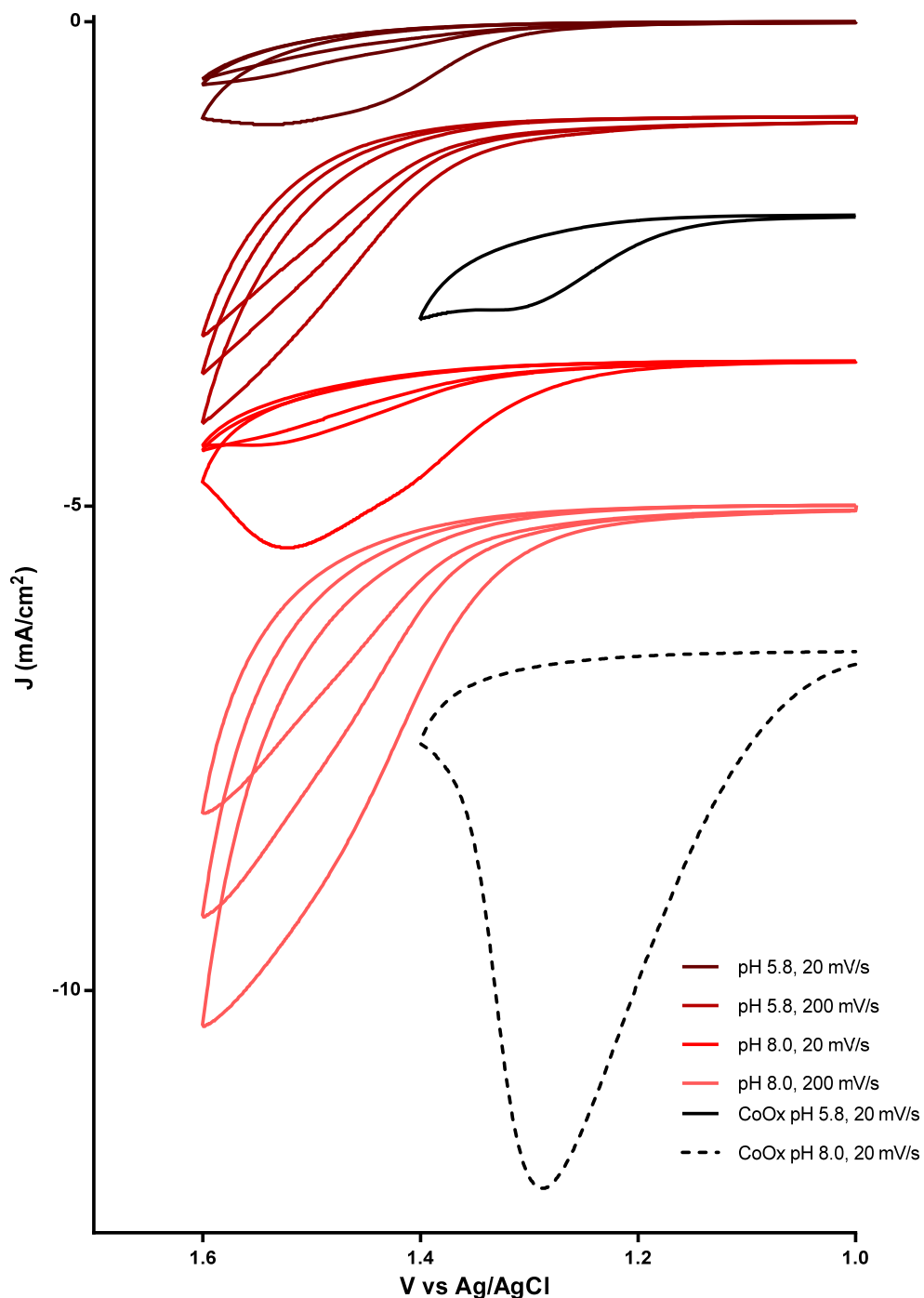


Figure S4.4. Repeated cyclic voltammetry scans of $2.5 \mu\text{M Co}_4(\text{H}_2\text{O})_2(\text{PW}_9\text{O}_{34})_2^{10-}$ solutions in pH 5.8 and 8.0 sodium phosphate electrolyte using 20 or 200 mV/s scan rates. CoO_x samples are also plotted for comparison and were prepared as described below in Figure S4.5. Of importance here is the absence of any CoO_x peaks growing in during the experiment. Note also and however, that CoO_x is unstable under these high potential conditions, as detailed further in the main text.

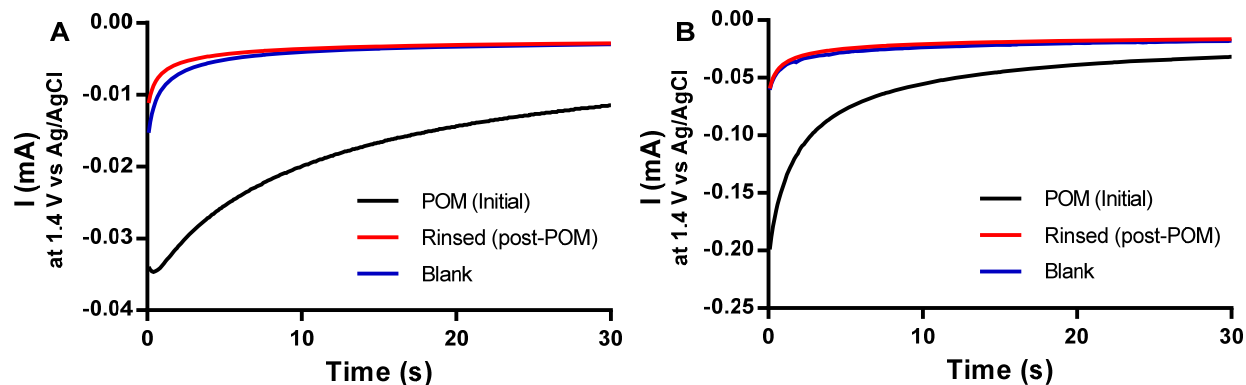


Figure S4.5. Bulk electrolysis experiments conducted at 1.4 V which test for deposited CoO_x catalysts (or other insoluble, active materials) at pH 5.8 (A) and pH 8.0 (B). Initially a $2.5 \mu\text{M Co}_4(\text{H}_2\text{O})_2(\text{PW}_9\text{O}_{34})_2^{10-}$ solution was electrolyzed using a glassy carbon electrode (3mm diameter) at 1.4 V vs Ag/AgCl (black line). At the end of electrolysis the electrodes were rinsed with water and placed into a Co_4 -POM -free (i.e., no added $\text{Co}_4(\text{H}_2\text{O})_2(\text{PW}_9\text{O}_{34})_2^{10-}$), 0.1 M sodium phosphate electrolyte at the same pH as the original Co_4 -POM solution followed by electrolysis at 1.4 V again (red line). For comparison, a blank controlled potential electrolysis curve was also recorded in 0.1 M sodium phosphate electrolyte (i.e., the glassy carbon electrode was held at 1.4 V vs Ag/AgCl in 0.1 M sodium phosphate electrolyte for 30 seconds, the solution was stirred and the electrode was held at 1.4 V vs Ag/AgCl for another 30 seconds—the blue line represents the second bulk electrolysis run). A Ag/AgCl reference and platinum wire counter electrode were used for all experiments. Solutions were not stirred during the electrolysis.

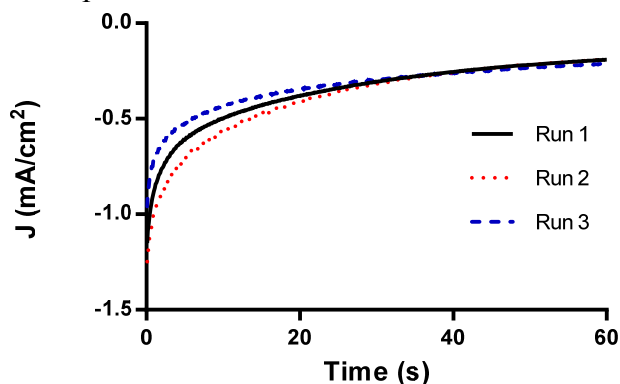


Figure S4.6. Bulk electrolysis currents for $2.5 \mu\text{M Co}_4(\text{H}_2\text{O})_2(\text{PW}_9\text{O}_{34})_2^{10-}$ at 1.4 V vs Ag/AgCl in pH 8.0, 0.1 M sodium phosphate electrolyte. The same solution was used for 3 consecutive experiments where the glassy carbon working electrode ($A = 1 \text{ cm}^2$) was polished for 60s and sonicated for 30 s between the experiments. No significant decrease in the currents was observed between runs, which indicates the oxidation activity lost during the bulk electrolysis is due primarily to deactivation of the electrode, not the Co_4 -POM. However, these data do not rule out the possibility of Co_4 -POM decomposition since saturation of the anodic current is observed at low (μM) concentrations of Co_4 -POM (as shown in Figure 4.1B of the main text). That is, the oxidation current is relatively insensitive to the Co_4 -POM concentration. In fact, HPLC and post-catalysis Co^{2+} stripping voltammetry provide compelling evidence for Co_4 -POM instability under the water oxidation reaction conditions employed.

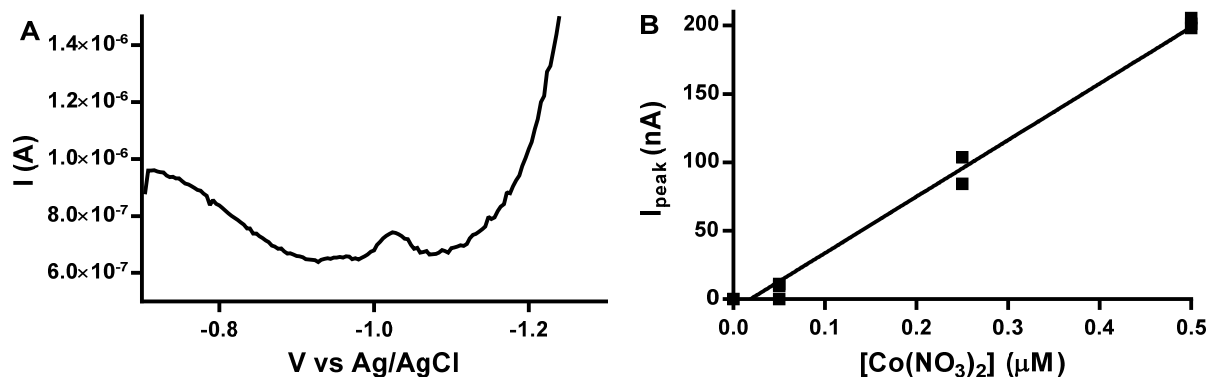


Figure S4.7. (A) Sample differential pulse cathodic stripping voltammogram for a 0.25 μM $\text{Co}(\text{NO}_3)_2$ solution plus 20 μM dimethylglyoxime in pH 8.0, 0.10 M sodium phosphate buffer. The glassy carbon electrode (3 mm diameter) was plated with bismuth immediately prior to analysis, as described in the literature.⁵⁷ Additional experimental details are given in the Experimental section of the main text. (B) Calibration curve for aqueous cobalt(II) analyzed by cathodic stripping voltammetry where I_{peak} indicates the maximum current of the -1.02 V peak minus the background current.

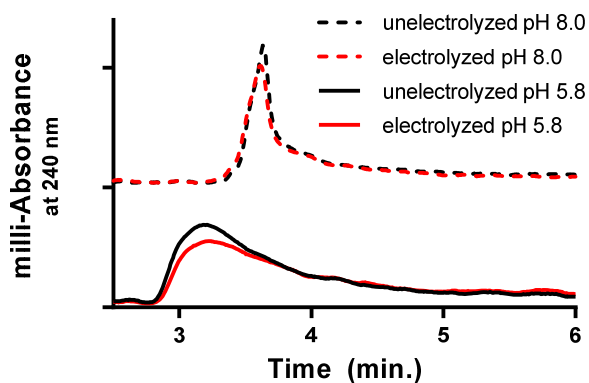


Figure S4.8. HPLC with 240 nm absorbance detection for $\text{Co}_4(\text{H}_2\text{O})_2(\text{PW}_9\text{O}_{34})_2^{10-}$ samples in 0.1 M sodium phosphate buffer at the indicated pH. The electrolyzed samples were subjected to bulk electrolysis at 1.4 V vs Ag/AgCl for 60 s immediately prior to injection onto the column. The chromatograms are offset for clarity, are an average of 3 samples each, and are corrected by subtracting the blank chromatograms which contained only 0.1 M sodium phosphate buffer at either pH 5.8 or 8.0.

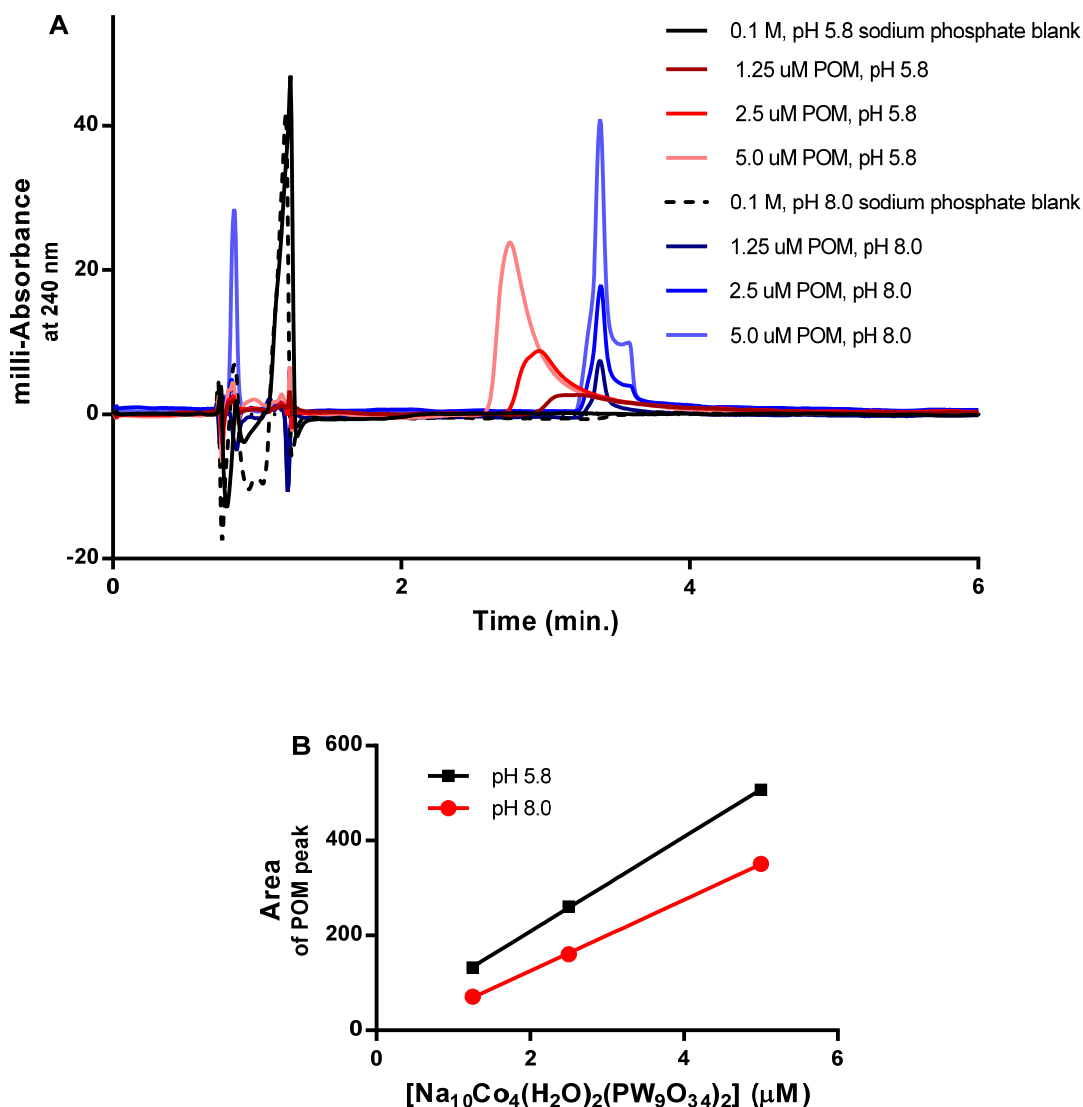


Figure S4.9. (A) HPLC with 240 nm absorbance detection for $\text{Co}_4(\text{H}_2\text{O})_2(\text{PW}_9\text{O}_{34})_2^{10-}$ samples in 0.1 M sodium phosphate buffer at the indicated Co_4 -POM concentration and pH; the Co_4 -POM chromatograms were corrected by subtracting the blank chromatograms which contained only 0.1 M sodium phosphate buffer at either pH 5.8 or 8.0 (solid and dashed black lines). (B) The area of the Co_4 -POM peak (i.e., the peak between 2.5 and 4 minutes) is plotted versus concentration and fit with a linear regression. HPLC conditions are 80% water, 20% acetonitrile, 30 mM butylammonium chloride, 10 mM sodium citrate, pH 6.5, 1.25 mL flow rate, room temperature.

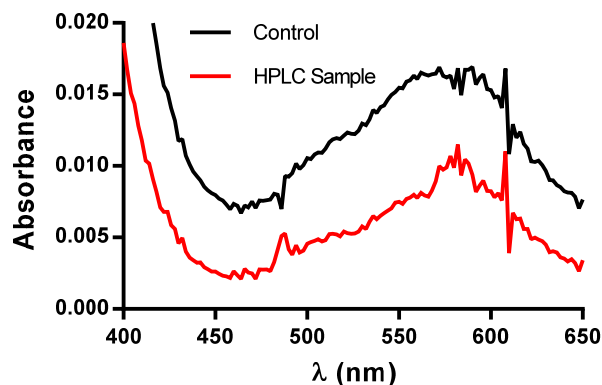


Figure S4.10. Visible absorption spectrum for $\sim 50 \mu\text{M Co}_4(\text{H}_2\text{O})_2(\text{PW}_9\text{O}_{34})_2^{10-}$ dissolved in an 80% water, 20% acetonitrile, 30 mM butylammonium chloride, 10 mM sodium citrate, pH 6.5 solution (Control, black line). The “HPLC Sample” (red line) spectrum contains the eluent from an HPLC separation of a $\text{Co}_4(\text{H}_2\text{O})_2(\text{PW}_9\text{O}_{34})_2^{10-}$ sample which was collected between 2.5 and 3.0 minutes (i.e., when the peak identified as $\text{Co}_4(\text{H}_2\text{O})_2(\text{PW}_9\text{O}_{34})_2^{10-}$ is eluting). The Co_4 -POM sample (prior to injection onto the HPLC column) contained 1 mM $\text{Co}_4(\text{H}_2\text{O})_2(\text{PW}_9\text{O}_{34})_2^{10-}$ and 0.1 M, pH 5.8 sodium phosphate electrolyte. HPLC conditions are the same as in Figure S4.6 above. Both visible spectra were corrected by subtracting the background absorbance of an 80% water, 20% acetonitrile, 30 mM butylammonium chloride, 10 mM sodium citrate, pH 6.5 solution. The close match between the control and HPLC sample spectra supports the assignment of the HPLC peak at $t \sim 2.5$ minutes as $\text{Co}_4(\text{H}_2\text{O})_2(\text{PW}_9\text{O}_{34})_2^{10-}$.

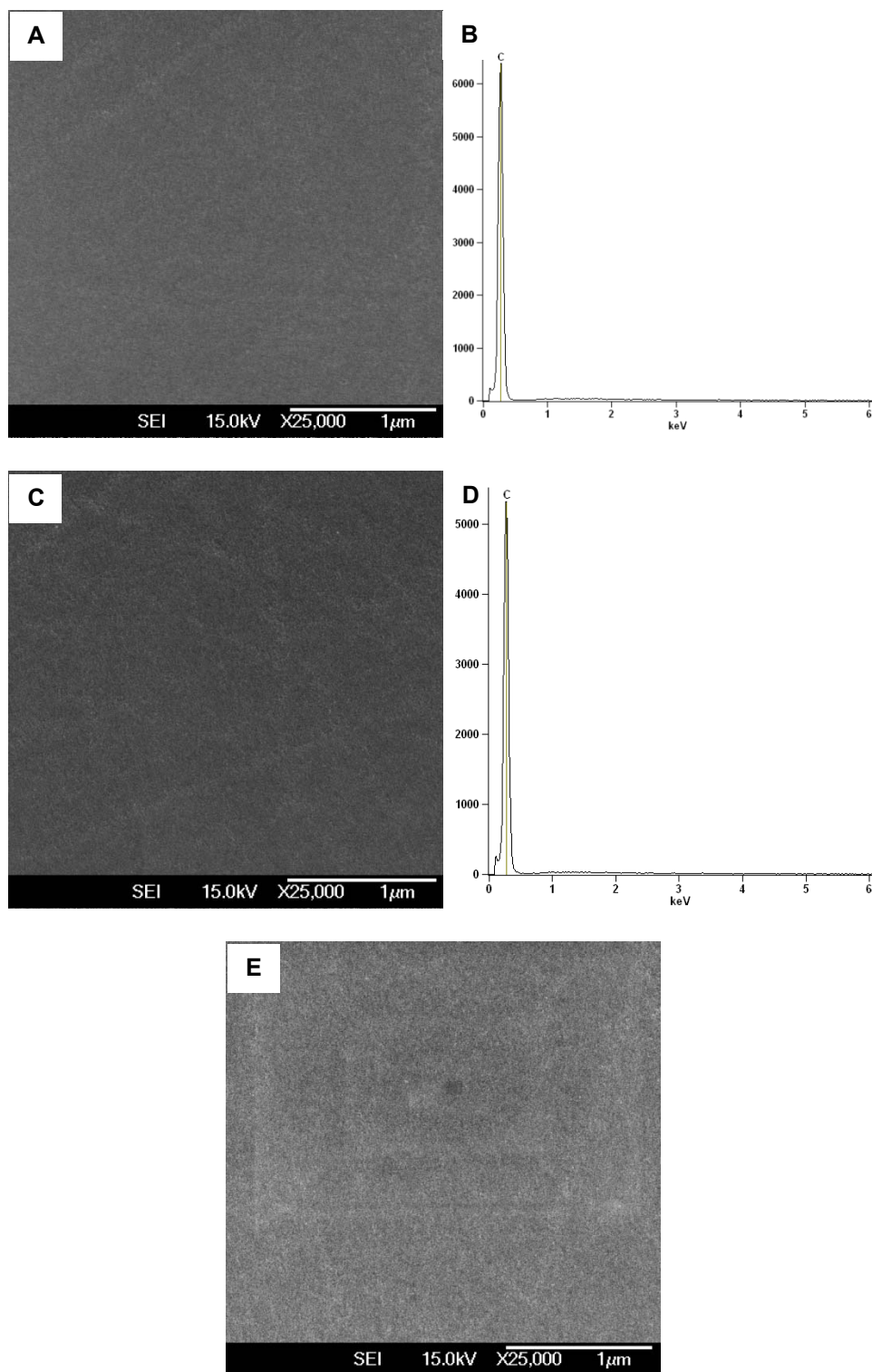


Figure S4.11. Scanning electron microscopy and energy dispersive x-ray spectra of the glassy carbon electrode after bulk electrolysis of a $2.5 \mu\text{M Co}_4(\text{H}_2\text{O})_2(\text{PW}_9\text{O}_{34})_2^{10-}$ at 1.4 V vs Ag/AgCl in 0.1 M sodium phosphate electrolyte at pH 5.8 (A and B) or pH 8.0 (C and D). SEM control of untreated glassy carbon (E) is also shown for comparison. The SEM and EDX spectra for all samples show no apparent features other than residual alumina from electrode polishing.

Turnover Frequency Calculations

The *average, estimated* turnover frequency calculations for $\text{Co}_4(\text{H}_2\text{O})_2(\text{PW}_9\text{O}_{34})_2^{10-}$, under conditions described in Figure 4.3 of the main text, are given below in equations (S1) and (S2) for pH 5.8 and pH 8.0, respectively.

$$\begin{aligned} \text{Average } TOF_{\text{per cobalt}} \text{ pH } 5.8, \text{ POM} &= \frac{1.38 \text{ nm}^2}{1 \text{ POM}} \cdot \frac{1.0 \text{ cm}^2 \text{ electrode}}{1 \times 10^{14} \text{ nm}^2} \cdot \frac{6.022 \times 10^{23} \text{ POM}}{\text{mol POM}} \cdot \frac{1 \text{ mol POM}}{4 \text{ mol cobalt}} \cdot \\ \frac{1.56 \times 10^{-8} \text{ mol O}_2}{60 \text{ s}} &= 0.54 \text{ mol O}_2 \cdot \text{s}^{-1} \cdot \text{mol cobalt}^{-1} \quad (\text{S1}) \end{aligned}$$

$$\begin{aligned} \text{Average } TOF_{\text{per cobalt}} \text{ pH } 8, \text{ POM} &= \frac{1.38 \text{ nm}^2}{1 \text{ POM}} \cdot \frac{1.0 \text{ cm}^2 \text{ electrode}}{1 \times 10^{14} \text{ nm}^2} \cdot \frac{6.022 \times 10^{23} \text{ POM}}{\text{mol POM}} \cdot \frac{1 \text{ mol POM}}{4 \text{ mol cobalt}} \cdot \\ \frac{2.84 \times 10^{-8} \text{ mol O}_2}{60 \text{ s}} &= 0.98 \text{ mol O}_2 \cdot \text{s}^{-1} \cdot \text{mol cobalt}^{-1} \quad (\text{S2}) \end{aligned}$$

This calculation makes the following assumptions: (i) the only active catalyst is a monolayer coverage of polyoxometalate on the working electrode; (ii) the area per polyoxometalate is 1.38 nm^2 ; (iii) the glassy carbon working electrode has both a geometrical and electrochemically active area of 1.0 cm^2 ; (iv) the O_2 produced is the amount measured in Figure 4.3 of the main text. Note, these calculations assume $\text{Co}_4(\text{H}_2\text{O})_2(\text{PW}_9\text{O}_{34})_2^{10-}$ is the dominant WOC even though we cannot rule out the possibility that CoO_x is the active WOC in Co_4 -POM solutions.

The average, estimated turnover frequency calculations for a CoO_x WOC are shown in equations (S3) and (S4) at pH 5.8 and 8.0, under conditions described in Figure 4.6 of the main text:

$$\text{Average } TOF_{\text{per cobalt}} \text{ pH } 5.8, \text{ CoO}_x = \frac{16 \text{ mol O}_2}{1 \text{ mol cobalt}} \cdot \frac{1}{60 \text{ s}} = 0.27 \text{ mol O}_2 \cdot \text{s}^{-1} \cdot \text{mol cobalt}^{-1}$$

$$\text{Average } TOF_{\text{per cobalt}} \text{ pH } 8, \text{ CoO}_x = \frac{60 \text{ mol O}_2}{1 \text{ mol cobalt}} \cdot \frac{1}{60 \text{ s}} = 1.0 \text{ mol O}_2 \cdot \text{s}^{-1} \cdot \text{mol cobalt}^{-1}$$

where the first term is the slope of the lines in Figure 4.6 of the main text (i.e., the amount of O_2 produced during a 60 s bulk water electrolysis when using different amounts of CoO_x catalyst).

As noted in the main text, this TOF is likely a significant underestimate of the true activity since the CoO_x material is not stable during the electrolysis.

We emphasize, as also noted in the main text, that the purpose of these admittedly crude TOF estimates is that they are intended to provide just a start—really, hypotheses for future research—on the desired, badly needed, true TOFs for $\text{Co}_4\text{-POM}$ versus CoO_x , and other molecular and their corresponding possible MO_x (i.e., heterogeneous metal oxo type) WOCs. Only when those true TOFs are in hand, and under a range of relevant operating conditions, will it be more readily apparent (i) what the true, WOC probably is, and (ii) which class or classes of WOC merit the greatest future emphasis.

REFERENCES

- ¹ Walter, M. G.; Warren, E. L.; McKone, J. R.; Boettcher, S. W.; Mi, Q.; Santori, E. A.; Lewis, N. S. *Chem. Rev.* **2010**, *110*, 6446.
- ² Cook, T. R.; Dogutan, D. K.; Reece, S. Y.; Surendranath, Y.; Teets, T. S.; Nocera, D. G. *Chem. Rev.* **2010**, *110*, 6474.
- ³ McDaniel, N. D.; Bernhard, S. *Dalton Trans.* **2010**, *39*, 10021.
- ⁴ Andreiadis, E. S.; Chavarot-Kerlidou, M.; Fontecave, M.; Artero, V. *Photochem. Photobiol.* **2011**, *87*, 946.
- ⁵ Herrero, C.; Quaranta, A.; Leibl, W.; Rutherford, A. W.; Aukauloo, A. *Energy Environ. Sci.* **2011**, *4*, 2353.
- ⁶ Artero, V.; Chavarot-Kerlidou, M.; Fontecave, M. *Ang. Chem., Int. Ed.* **2011**, *50*, 7238.
- ⁷ Gust, D.; Moore, T. A.; Moore, A. L. *Faraday Discuss.* **2012**, *155*, 9.
- ⁸ Hou, H. J. M. *J. Int. Plant Biol.* **2010**, *52*, 704.
- ⁹ Young, K. J.; Martini, L. A.; Milot, R. L.; Snoeberger, R. C., III; Batista, V. S.; Schmuttenmaer, C. A.; Crabtree, R. H.; Brudvig, G. W. *Coord. Chem. Rev.* **2012**, *256*, 2503.
- ¹⁰ Swierk, J. R.; Mallouk, T. E. *Chem. Soc. Rev.* **2013**, *42*, 2357-2387.
- ¹¹ Tran, P. D.; Artero, V.; Fontecave, M. *Energy Environ. Sci.* **2010**, *3*, 727.
- ¹² Artero, V.; Fontecave, M. *Chem. Soc. Rev.* **2013**, *42*, 2338-2356.
- ¹³ Dau, H.; Limberg, C.; Reier, T.; Risch, M.; Roggan, S.; Strasser, P. *ChemCatChem*, **2010**, *2*, 724.
- ¹⁴ Du, P.; Eisenberg, R. *Energy Environ. Sci.* **2012**, *5*, 6012.
- ¹⁵ Geletii, Y. V.; Yin, Q.; Hou, Y.; Huang, Z.; Ma, H.; Song, J.; Besson, C.; Luo, Z.; Cao, R.; O'Halloran, K. P.; Zhu, G.; Zhao, C.; Vickers, J. W.; Ding, Y.; Mohebbi, S.; Kuznetsov, A. E.; Musaev, D. G.; Lian, T.; Hill, C. L. *Isr. J. Chem.* **2011**, *51*, 238.
- ¹⁶ Han, Z. G.; Bond, A. M.; Chuan, Z. *Sci. China, Ser. B: Chem.* **2011**, *54*, 1877.
- ¹⁷ Liu, X.; Wang, F. *Coord. Chem. Rev.* **2012**, *256*, 1115.
- ¹⁸ Limburg, B.; Bouwman, E.; Bonnet, S. *Coord. Chem. Rev.* **2012**, *256*, 1451.
- ¹⁹ Lv, H.; Geletii, Y. V.; Zhao, C.; Vickers, J. W.; Zhu, G.; Luo, Z.; Song, J.; Lian, T.; Musaev, D. G.; Hill, C. L. *Chem. Soc. Rev.* **2012**, *41*, 7572.

- ²⁰ Sartorel, A.; Bonchio, M.; Campagna, S.; Scandola, F. *Chem. Soc. Rev.* **2013**, *42*, 22652-2280.
- ²¹ Joya, K. S.; Vallés-Pardo, J. L.; Joya, Y. F.; Eisenmayer, T.; Thomas, B.; Buda, F.; de Groot, H. J. M. *ChemPlusChem* **2013**, *78*, 35.
- ²² Pope, M. T. *Heteropoly and Isopoly Oxometalates*; Springer-Verlag: Berlin, 1983.
- ²³ Contant, R.; Ciabrini, J.P. *J. Chem. Res. Synop.* **1982**, 50.
- ²⁴ Contant, R. *J. Chem. Res. Synop.* **1984**, 120.
- ²⁵ Hamlaoui, M.-L.; Vlassenko, K.; Messadi, D. *C. R. Acad. Sci. Paris* **1990**, *311*, 795.
- ²⁶ Ruhlmann, L.; Schaming, D.; Ahmed, I.; Courville, A.; Canny, J.; Thouvenot, R. *Inorg. Chem.* **2012**, *51*, 8202.
- ²⁷ Howells, A. R.; Sankarraj, A.; Shannon, C. J. *Am. Chem. Soc.* **2004**, *126*, 12258.
- ²⁸ Sartorel, A.; Carraro, M.; Scorrano, G.; De Zorzi, R.; Geremia, S.; McDaniel, N. D.; Bernhard, S.; Bonchio, M. *J. Am. Chem. Soc.* **2008**, *130*, 5006.
- ²⁹ Geletii, Y. V.; Botar, B.; Kögerler, P.; Hillesheim, D. A.; Musaev, D. G.; Hill, C. L. *Angew. Chem., Int. Ed.* **2008**, *47*, 3896.
- ³⁰ Sartorel, A.; Miro, P.; Salvadori, E.; Romain, S.; Carraro, M.; Scorrano, G.; Di Valentin, M.; Llobet, A.; Bo, C.; Bonchio, M. *J. Am. Chem. Soc.* **2009**, *131*, 16051.
- ³¹ Geletii, Y. V.; Besson, C.; Hou, Y.; Yin, Q.; Musaev, D. G.; Quiñonero, D.; Cao, R.; Hardcastle, K. I.; Proust, A.; Kögerler, P.; Hill, C. L. *J. Am. Chem. Soc.* **2009**, *131*, 17360.
- ³² Geletii, Y. V.; Huang, Z.; Hou, Y.; Musaev, D. G.; Lian, T.; Hill, C. L. *J. Am. Chem. Soc.* **2009**, *131*, 7522.
- ³³ Besson, C.; Huang, Z.; Geletii, Y. V.; Lense, S.; Hardcastle, K. I.; Musaev, D. G.; Lian, T.; Proust, A.; Hill, C. L. *Chem. Commun.* **2010**, *46*, 2784.
- ³⁴ Orlandi, M.; Argazzi, R.; Sartorel, A.; Carraro, M.; Scorrano, G.; Bonchio, M.; Scandola, F. *Chem. Commun.* **2010**, *46*, 3152.
- ³⁵ Puntoriero, F.; La Ganga, G.; Sartorel, A.; Carraro, M.; Scorrano, G.; Bonchio, M.; Campagna, S. *Chem. Commun.* **2010**, *46*, 4725.
- ³⁶ Murakami, M.; Hong, D.; Suenobu, T.; Yamaguchi, S.; Ogura, T.; Fukuzumi, S. *J. Am. Chem. Soc.* **2011**, *133*, 11605.
- ³⁷ Natali, M.; Orlandi, M.; Berardi, S.; Campagna, S.; Bonchio, M.; Sartorel, A.; Scandola, F. *Inorg. Chem.* **2012**, *51*, 7324.

- ³⁸ Ogo, S.; Miyamoto, M.; Ide, Y.; Sano, T.; Sadakane, M. *Dalton Trans.* **2012**, *41*, 9901.
- ³⁹ Wang, H.; You, W.; Meng, B.; Sun, X.; Cheng, H.; Shan, W. *J. Cluster Sci.* **2010**, *21*, 857.
- ⁴⁰ Tanaka, S.; Annaka, M.; Sakai, K. *Chem. Commun.* **2012**, *48*, 1653.
- ⁴¹ Zhu, G.; Geletii, Y. V.; Kögerler, P.; Schilder, H.; Song, J.; Lense, S.; Zhao, C.; Hardcastle, K. I.; Musaev, D. G.; Hill, C. L. *Dalton Trans.* **2012**, *41*, 2084.
- ⁴² Car, P.-E.; Guttentag, M.; Baldridge, K. K.; Alberto, R.; Patzke, G. R. *Green Chem.* **2012**, *14*, 1680.
- ⁴³ Huang, Z.; Luo, Z.; Geletii, Y. V.; Vickers, J. W.; Yin, Q.; Wu, D.; Hou, Y.; Ding, Y.; Song, J.; Musaev, D. G.; Hill, C. L.; Lian, T. *J. Am. Chem. Soc.* **2011**, *133*, 2068.
- ⁴⁴ Goberna-Ferrón, S.; Vígara, L.; Soriano-López, J.; Ramón, J.; Galán-Mascarós, J. R. *Inorg. Chem.* **2012**, *51*, 11707.
- ⁴⁵ Natali, M.; Berardi, S.; Sartorel, A.; Bonchio, M.; Campagna, S.; Scandola, F. *Chem. Commun.* **2012**, *48*, 8808.
- ⁴⁶ Yin, Q.; Tan, J. M.; Besson, C.; Geletii, Y. V.; Musaev, D. G.; Kuznetsov, A. E.; Luo, Z.; Hardcastle, K. I.; Hill, C. L. *Science* **2010**, *328*, 342.
- ⁴⁷ Stracke, J. J.; Finke, R. G. *J. Am. Chem. Soc.* **2011**, *133*, 14872.
- ⁴⁸ The term CoO_x indicates a heterogeneous material which contains cobalt and oxygen (e.g., oxo or hydroxo groups) in addition to other cations or anions from the catalytic solution such as Na⁺ or HPO₄²⁻; overall, these materials have the general stoichiometry Co_aO_bH_cNa_dP_e. See for example references 49-55 and citations therein for more information. Also note, we use the terms homogeneous and heterogeneous to indicate the type of active site and not necessarily the solubility/insolubility of the material—a convention which was originally proposed by Schwartz: Schwartz, J. *Acc. Chem. Res.* **1985**, *18*, 302.
- ⁴⁹ Suzuki, O.; Takahashi, M.; Fukunaga, T.; Kuboyama, J.; U.S. Patent 3,399,966, September 3, 1968.
- ⁵⁰ Shafirovich, V. Ya.; Strelets, V. V. *New J. Chem.* **1978**, *2*, 199.
- ⁵¹ Kanan, M. W.; Nocera, D. G. *Science* **2008**, *321*, 1072.
- ⁵² Kanan, M. W.; Surendranath, Y.; Nocera, D. G. *Chem. Soc. Rev.* **2009**, *38*, 109.
- ⁵³ Surendranath, Y.; Kanan, M. W.; Nocera, D. G. *J. Am. Chem. Soc.* **2010**, *132*, 16501.
- ⁵⁴ Gerken, J. B.; McAlpin, J. G.; Chen, J. Y. C.; Rigsby, M. L.; Casey, W. H.; Britt, R. D.; Stahl, S. S. *J. Am. Chem. Soc.* **2011**, *133*, 14431.

- ⁵⁵ Du, P.; Kokhan, O.; Chapman, K. W.; Chupas, P. J.; Tiede, D. M. *J. Am. Chem. Soc.* **2012**, *134*, 11096.
- ⁵⁶ Weakley, T. J. R.; Evans, H. T.; Showell, J. S.; Tourne, G. F.; Tourne, C. M. *J. Chem. Soc., Chem. Commun.* **1973**, 139.
- ⁵⁷ Krolicka, A.; Bobrowski, A.; Kalcher, K.; Mocak, J.; Svancara, I.; Vytras, K. *Electroanalysis* **2003**, *15*, 1859.
- ⁵⁸ Kirk, A. D.; Riske, W.; Lyon, D. K.; Rapko, B.; Finke, R. G. *Inorg. Chem.* **1989**, *28*, 792.
- ⁵⁹ Overpotential for the water oxidation reaction is calculated using the equation: $\eta = E - (1.23 - 0.059 \cdot \text{pH}) + 0.236 \text{ V}$, where E is the measured working electrode potential versus Ag/AgCl, (1.23 – 0.059·pH) is the reversible potential for water oxidation versus NHE, and 0.236 is the voltage correction needed to convert the measured potential from Ag/AgCl (1 M KCl) to NHE.
- ⁶⁰ Also of relevance here is the study of Balula et al. which reported reversible oxidation waves for [(C₄H₉N)₇H₃[Co₄(H₂O)₂(PW₉O₃₄)₂]] at 0.811 and 1.123 V (versus Ag/Ag⁺) in acetonitrile: Balula, M. S.; Gamelas, J. A.; Carapuca, H. M.; Cavaleiro, A. M. V.; Schlindwein, W. *Eur. J. Inorg. Chem.* **2004**, 619. In contrast, Gao et al. reported no electrochemical oxidation activity for Co₄(H₂O)₂(PW₉O₃₄)₂¹⁰⁻ in pH 4.4 or 5.8 acetate buffer, although no potential range was given: Gao, S.; Li, T.; Li, X.; Cao, R. *Mater. Lett.* **2006**, *60*, 3622.
- ⁶¹ Rong, C.; Anson, F. C. *Anal. Chem.* **1994**, *66*, 3124.
- ⁶² Lyons, M. E. G.; Brandon, M. P. *J. Electroanal. Chem.* **2009**, *631*, 62.
- ⁶³ The term [Co²⁺]_{apparent} is used herein since the species measured by stripping voltammetry behaves the same as the cobalt(II) nitrate control, but we cannot rule out some other cobalt or cobalt-polyoxometalate fragment which might behave similarly.
- ⁶⁴ Hou, Y.; Xu, L.; Cichon, M. J.; Lense, S.; Hardcastle, K. I.; Hill, C. L. *Inorg. Chem.* **2010**, *49*, 4125-4132.
- ⁶⁵ Goldstein, J. I.; Newbury, D. E.; Joy, D. C.; Lyman, C. E.; Echlin, P.; Lifshin, E.; Sawyer, L.; Michael, J. R. *Scanning Electron Microscopy and X-Ray Microanalysis*, 3rd ed.; Kluwer: New York, 2003.
- ⁶⁶ Widegren, J. A.; Finke, R. G. *J. Mol. Catal. A: Chem.* **2003**, *198*, 317-341.
- ⁶⁷ Crabtree, R. H. *Chem. Rev.* **2012**, *112*, 1536-1554.
- ⁶⁸ Schley, N. D.; Blakemore, J. D.; Subbaiyan, N. K.; Incarvito, C. D.; D'Souza, F.; Crabtree, R. H.; Brudvig, G. W. *J. Am. Chem. Soc.* **2011**, *133*, 10473-10481.
- ⁶⁹ We have noted this point previously in our prior study (ref 47). Specifically, we “emphasize that the present studies [ref 47 herein] have not examined either the system or the precise

conditions utilized in the 2010 *Science* paper [and ...] further study of the (slightly) different conditions in the present [ref 47 herein] and prior [ref 46 herein] study is needed before one could have any firm basis for believing [...] the central claim made in ref 6” is incorrect. Although ref 12 agrees that conditions can be significant in determining the true catalyst, and good evidence for that conclusion is an important part of the valuable review in ref 12, the review’s authors do misinterpret our conclusions in ref 47 by stating incorrectly that “a report by Finke following Hill’s papers [...] suggested that the catalysis [in ref 46 herein] is in fact heterogeneous”. As our conclusion quoted above clearly states, one cannot directly extrapolate our results to those of Hill and co-workers because of the different conditions involved.

⁷⁰ Other electrochemical evidence—described in points (3) to (6) in the conclusion, especially the different current-pH relationship and potential of catalytic O₂ production onset when beginning with the Co₄-POM versus CoO_x—is consistent with the possibility of a polyoxometalate (or polyoxometalate derived) WOC. Additionally, (11) the absence of significant amounts of cobalt observed in XPS, SEM, and EDX electrode characterization, is also consistent with Co₄-POM being a true WOC. However, and despite the negative evidence for deposited CoO_x given in experiments (3)-(5) in the conclusion and (11) above, care must be taken in interpreting these results since (12) control cyclic voltammetry and XPS experiments indicate that *predeposited CoO_x is unstable at 1.4 V*. Restated, the absence of a catalytic film on the electrode at the end of the electrolysis does not in itself rule out heterogeneous catalysis. Needed at this point are authentic examples of CoO_x colloids (i.e., stabilized by whatever ligands and other stabilization mechanisms are present under the reaction conditions) and *in operando* methods capable of detecting nanomolar amounts of CoO_x.

⁷¹ Hong, D.; Jung, J.; Park, J.; Yamada, Y.; Suenobu, T.; Lee, Y.-M.; Nam, W.; Fukuzumi, S. *Energy Environ. Sci.* **2012**, *5*, 7606-7616.

⁷² Wasylenko, D. J.; Palmer, R. D.; Schott, E.; Berlinguette, C. P. *Chem. Commun.* **2012**, *48*, 2107-2109.

⁷³ Fukuzumi, S.; Yamada, Y. *J. Mater. Chem.* **2012**, *22*, 24284.

⁷⁴ McCool, N. S.; Robinson, D. M.; Sheats, J. E.; Dismukes, G. C. *J. Am. Chem. Soc.* **2011**, *133*, 11446-11449.

V. WATER OXIDATION CATALYSIS BEGINNING WITH $[\text{Co}_4(\text{H}_2\text{O})_2(\text{PW}_9\text{O}_{34})_2]^{10-}$ WHEN DRIVEN BY THE CHEMICAL OXIDANT RUTHENIUM(III)TRIS(2,2'-BIPYRIDINE): STOICHIOMETRY, KINETIC, AND MECHANISTIC STUDIES EN ROUTE TO IDENTIFYING THE TRUE CATALYSTⁱ

Overview

Stoichiometry and kinetics are reported for catalytic water oxidation to O_2 beginning with the cobalt polyoxometalate $\text{Co}_4(\text{H}_2\text{O})_2(\text{PW}_9\text{O}_{34})_2^{10-}$ (Co_4POM) and the chemical oxidant ruthenium(III)tris(2,2'-bipyridine) ($\text{Ru(III)(bpy)}_3^{3+}$). This specific water oxidation system was first reported in a 2010 *Science* Paper (Yin et al. *Science* **2010**, 328, 342). Under Standard Conditions employed herein of 1.0 μM Co_4POM , 500 μM $\text{Ru(III)(bpy)}_3^{3+}$, 100 μM $\text{Ru(II)(bpy)}_3^{2+}$, pH 7.2, and 0.03 M sodium phosphate buffer, the highest O_2 yields observed herein of 22% are seen when $\text{Ru(II)(bpy)}_3^{2+}$ is added prior to the $\text{Ru(III)(bpy)}_3^{3+}$ oxidant; hence, those conditions are employed in the present study. Measurement of the initial O_2 evolution and $\text{Ru(III)(bpy)}_3^{3+}$ reduction rates while varying the initial pH, $[\text{Ru(III)(bpy)}_3^{3+}]$, $[\text{Ru(II)(bpy)}_3^{2+}]$, and $[\text{Co}_4\text{POM}]$ indicate that the reaction follows the empirical rate law: $-\text{d}[\text{Ru(III)(bpy)}_3^{3+}]/\text{dt} = (k_1 + k_2)[\text{Co}_4\text{POM}][\text{Ru(III)(bpy)}_3^{3+}]/[\text{H}^+]$, where rate constants $k_1 \sim 0.0014 \text{ s}^{-1}$ and $k_2 \sim 0.0044 \text{ s}^{-1}$ correspond to the water oxidation and ligand oxidation reactions while for O_2 evolution $\text{d}[\text{O}_2]/\text{dt} = (k_1/4)[\text{Co}_4\text{POM}][\text{Ru(III)(bpy)}_3^{3+}]/[\text{H}^+]$. Overall, at least seven important insights result from

ⁱ The previous chapters (III and IV) found that conditions matter in determining the true WOC when beginning with $[\text{Co}_4(\text{H}_2\text{O})_2(\text{PW}_9\text{O}_{34})_2]^{10-}$ and when using electrochemical oxidation methods. Another important question is what influence the oxidant source has on the dominant WOC. Therefore, the current dissertation chapter investigates the stoichiometry, kinetics, and mechanism of catalytic water oxidation when using $[\text{Co}_4(\text{H}_2\text{O})_2(\text{PW}_9\text{O}_{34})_2]^{10-}$ and a ruthenium(III)tris(2,2'-bipyridine) oxidant. These results are then compared to kinetic controls using $\text{Co}(\text{NO}_3)_2$ in order to help determine the true WOC when using the $[\text{Co}_4(\text{H}_2\text{O})_2(\text{PW}_9\text{O}_{34})_2]^{10-}$ precursor. This manuscript has been submitted to *ACS Catalysis*.

the present studies: (i) parallel WOC and Ru(III)(bpy)₃³⁺-self-oxidation reactions well documented in the prior literature limit the desired WOC and selectivity to O₂ in the present system to ≤28%; (ii) the formation of a precipitate from ~2 Ru(II)(bpy)₃²⁺ : 3 Co₄(H₂O)₂(PW₉O₃₄)₂¹⁰⁻ with a K_{sp} = (8±7)×10⁻²⁵ (M⁵) greatly complicates the reaction and interpretation of the observed kinetics, but (iii) the best O₂ yields are still when Ru(II)(bpy)₃²⁺ is pre-added; (iv) CoO_x is 2-11 times more active than Co₄POM under the reaction conditions; but, (v) Co₄POM is still the dominant WOC under the Co₄POM / Ru(III)(bpy)₃³⁺ and other reaction conditions employed. The present studies also (vi) confirm that the specific conditions matter greatly in determining the true WOC, and (vii) allow one to begin to construct a plausible WOC mechanism for the Co₄POM / Ru(III)(bpy)₃³⁺ system.

Introduction

Catalysts capable of efficiently transforming abundant materials such as water and carbon dioxide into fuel and oxygen are of great interest for the advancement of renewable energy storage.^{1,2,3,4,5} Water oxidation catalysts (WOCs) with stability, selectivity, affordability, and high activity at low driving forces (i.e., low overpotentials) are critical to the implementation of the desired energy storage, solar fuels, and other technology.^{6,7,8,9,10,11,12,13,14} In order to understand and rationally improve these WOCs, it is necessary to study the mechanism by which they oxidize water to O₂.^{15,16}

Polyoxometalates are of interest as WOCs since these metal-oxide compounds are discrete, contain no oxidizable organic ligands, can be synthetically altered, and can be models for heterogeneous metal-oxide catalysts^{17,18}—properties which make them good candidates for mechanistic water oxidation studies.^{19,20,21,22} Despite these apparent advantages of POM-based

WOCs, only a few studies have examined the kinetics and mechanism of reported polyoxometalate WOCs.^{23,24,25,26,27}

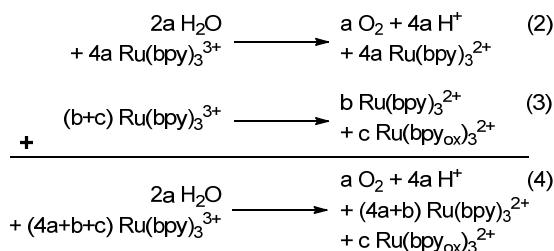
Co₄POM is of particular interest, and hence the focus of the current investigation, since it incorporates the moderately earth abundant element cobalt. Water oxidation catalysis by this POM was first reported by Hill and co-workers in a 2010 *Science*²⁸ and 2011 *JACS* papers²⁹, and subsequent studies have investigated the identity of the true water oxidation catalyst.^{30,31,32} In the *Science* paper, ruthenium(III)tris(2,2'-bipyridine) (Ru(III)(bpy)₃³⁺) was used as a chemical oxidant to drive the oxidation of water to oxygen with a reported TOF of up to 5 s⁻¹ under the specific conditions of 3.2 μM Co₄POM, 1500 μM Ru(III)(bpy)₃³⁺, pH 8.0, and 0.03 M sodium phosphate buffer.²⁸ However, the prior studies of Co₄POM using Ru(III)(bpy)₃³⁺ as an oxidant do not include kinetic studies en route to establishing the water oxidation mechanism—studies which are of importance for comparing the activity, selectivity, and stability of different catalyst species, as well as for assisting in identifying the true active catalyst.³³

As studied by Creutz and Sutin et al.,^{34,35,36} and as noted in the 2010 *Science* paper, when Ru(III)(bpy)₃³⁺ is used as an oxidant, bipyridine ligand oxidation occurs in parallel with water oxidation; this results in oxygen yields which are always less than 100% and concomitant non-optimal selectivity to O₂. Creutz and Sutin et al. also thoroughly investigated the kinetics and mechanism of both the cobalt(II) catalyzed and uncatalyzed reduction of the Ru(III)(bpy)₃³⁺ species.^{34,35,36} That classic work showed that the uncatalyzed reduction of Ru(III)(bpy)₃³⁺ into Ru(II)(bpy)₃²⁺ plus Ru(bpy_{ox})₃²⁺ is dependent on the [Ru(III)(bpy)₃³⁺] in *two parallel paths* which are dependent on [OH⁻] and [OH⁻]², under their conditions of pH ≥ 12 and initial [Ru(III)(bpy)₃³⁺] of 30-170 μM.³⁶

In the presence of a cobalt(II) precatalyst, Creutz and Sutin observed oxygen generation and Ru(III)(bpy)₃³⁺ loss followed the rate law:^{35,36}

$$-d[\text{Ru(III)(bpy)}_3^{3+}] = \frac{k_{\text{Co}}[\text{Ru(bpy)}_3^{3+}]^2[\text{Co}]}{[\text{Ru(bpy)}_3^{2+}][\text{H}^+]^2} \quad (1)$$

The combination of the water oxidation (equation 2) and ligand oxidation (equation 3) parallel pathways results in an overall generalized reaction stoichiometry given in equation 4, where Ru(bpy_{ox})₃²⁺ encompasses all the possible products formed when a ruthenium(II)tris(bipyridine) species undergoes one or more bipyridine ligand oxidation reactions.



Although classic work of Creutz and Sutin did not identify the true active catalyst in their reactions, other studies have identified CoO_x colloids to be the active WOC when beginning with Co(II) salts and Ru(III)(bpy)₃³⁺.^{37,38,39} Styring and co-workers have also shown a correlation between decreased CoO_x colloid size and increased activity (i.e., presumably between increasing number of surface sites and increasing activity).³⁷ Hence, studies which contain cobalt precursors should attempt to rule out the possibility that the starting material is transformed into a heterogeneous, colloidal CoO_x catalyst under the reaction conditions.

Prior studies have investigated this possibility of in-situ CoO_x formation when beginning with Co₄POM. In *electrochemical* studies of Co₄POM, we found that when a glassy carbon electrode at 1.1 V vs Ag/AgCl was used as the oxidant source in 500 uM Co₄POM solutions, the dominant WOC is actually a heterogeneous CoO_x material and not the starting Co₄POM.³⁰ More

recently, in a deliberate attempt to try to favor water oxidation catalysis by the cobalt polyoxometalate, we reported that when the Co₄POM concentration is lowered to 2.5 μ M and the electrode potential is increased to >1.3 V vs Ag/AgCl—again, in an attempt to favor a discrete Co₄POM-based WOC—we were unable to distinguish between a true POM catalyst and CoO_x-based catalysis.³² Specifically and in that study, key controls revealed that if even 8.2% of the POM was converted into CoO_x, then that amount of CoO_x catalyst would account for all of the O₂ produced during a 60 s electrolysis at 1.4 V. Additionally, we measured the [Co₄POM] by HPLC after the electrolysis and found that $9.4 \pm 5.1\%$ of the Co₄POM was absent at the end of the electrolysis experiment. In the end, and under those conditions designed to favor a Co₄POM-based WOC, we were unable to unambiguously identify the true WOC. Those studies demonstrate the difficulty of determining the identity of the true water oxidation catalyst when the alternative heterogeneous decomposition material is extremely active, as is typically observed for CoO_x.³²

In another study, Sartorel and Scandola used flash photolysis experiments which indicated that neither Co²⁺ (i.e. CoO_x) or Co₄POM were the active catalyst.³¹ Instead, they favored a Co₄POM decomposition product (i.e., a different but as yet unknown POM) as the true WOC when using, now, a photochemically derived Ru(III) oxidant. However, and as pointed out by Hill and co-workers,⁴⁰ Sartorel and Scandola did not quantify O₂ generation in their experiments³¹ and, therefore, the precise reaction that they were studying remains unclear.

Most recently, Hill and co-workers have addressed the question of homogeneous vs heterogeneous catalysis when beginning with Co₄POM.⁴⁰ They reported pre-catalysis stability and dissociation to [Co²⁺]_{apparent,aqueous} measurements using cathodic stripping voltammetry, clever extraction experiments of anionic species using tetra-heptylammonium nitrate,

$\text{Ru(III)(bpy)}_3^{3+}$ loss measurements comparing Co_4POM and $\text{Co(NO}_3)_2$ controls, and pH variation plus O_2 quantification experiments.⁴⁰ Although an amount of CoO_x equivalent to the 4 cobalts in Co_4POM was shown to be the superior catalyst in terms of total turnovers or rate of O_2 formation (Table 2 therein⁴⁰), overall the results support the authors' previous conclusion²⁸ that the observed WOC derives from Co_4POM and not heterogeneous CoO_x under the conditions studied and when $\text{Ru(III)(bpy)}_3^{3+}$ is used as the chemical oxidant. However, the precise identity of the true, active WOC was not the focus of that work, so that the detailed kinetic studies and full rate law—necessary to begin to answer the challenging question of the precise identity of the true catalyst—were not reported therein⁴⁰ nor previously^{28,29}—as, again, that was not the focus of their studies.

Herein we report the stoichiometry and kinetics of water oxidation when beginning with Co_4POM and the $\text{Ru(III)(bpy)}_3^{3+}$ oxidant under conditions when excess $\text{Ru(II)(bpy)}_3^{2+}$ is added prior to $\text{Ru(III)(bpy)}_3^{3+}$ —conditions which give the best O_2 yields, which are also relevant to literature photochemically-driven oxidations which employ $\text{Ru(II)(bpy)}_3^{2+}$, and are useful in understanding the influence of the Ru(bpy)_3^{2+} byproduct.^{29, 31,40} The Co_4POM results are then compared to those for an in-situ formed CoO_x WOC to provide further insight into the true WOC when beginning with Co_4POM and $\text{Ru(III)(bpy)}_3^{3+}$. In this comparison we find differing trends in the selectivity and activity of the Co_4POM and CoO_x —kinetic and mechanistic evidence which strongly suggests the active catalysts in these two systems are, indeed, distinguishable and as Professor Hill and his co-workers have argued.^{28,29,40} We also discuss, briefly, the drawbacks of the $\text{Ru(III)(bpy)}_3^{3+}$ -based chemical oxidant system and what is, and is not, known about the true catalyst in both the Co_4POM and CoO_x cases. Lastly, we propose a water oxidation

mechanism consistent with our evidence in the case of catalysis beginning with Co₄POM, a mechanism that has some unexpected features.

Experimental Section

Materials

Na₁₀Co₄(H₂O)₂(PW₉O₃₄)₂ was synthesized and recrystallized according to the method of Weakley et al.⁴¹ with modifications reported by Yin et al.²⁸ Its identity was verified by ³¹P-NMR, IR, and UV-vis spectroscopies which matched published characterization data.²⁸ Co(NO₃)₂, Na₂HPO₄, and NaH₂PO₄ were obtained from Sigma-Aldrich or Fisher and used without further purification.

Ruthenium(III)tris(2,2'-bipyridine) triperchlorate (Ru(III)(bpy)₃³⁺) and ruthenium(II)tris(2,2'-bipyridine) diperchlorate were synthesized from ruthenium(II)tris(2,2'-bipyridine) dichloride according to the method of Creutz and Sutin.³⁵ The ruthenium(III)tris(2,2'-bipyridine)triperchlorate matched the published molar absorptivity ($\epsilon_{675\text{ nm}} = 440\text{ M}^{-1}\cdot\text{cm}^{-1}$).³⁵ The ruthenium(II)tris(2,2'-bipyridine)diperchlorate was recrystallized by dissolving in a minimum amount of water at room temperature with crystallization occurring at 5 °C over one day.

Clark Electrode Calibration

The Clark electrode was calibrated prior to O₂ evolution experiments using a 0% and 20.9% (air) standard solutions. These values correspond to typical O₂ concentrations of 0 and 236 μM after correcting for temperature and air pressure.

O₂ evolution and yield quantification

In a 1 dram vial with a stir bar, a solution was prepared using stock solutions of 0.2 M sodium phosphate buffer (pH 6.8-7.8), 0.2 mM Co₄POM (or Co(NO₃)₂), and 0.5 mM

$\text{Ru(II)(bpy)}_3(\text{ClO}_4)_2$. A calibrated Clark electrode (Microelectrodes Inc.) was immersed in the solution. For example, a reaction run under Standard Conditions contained 1.1 mL water, 0.4 mL $\text{Ru(II)(bpy)}_3^{2+}$ stock solution, and 10 μL of Co_4POM solution. The $\text{Ru(II)(bpy)}_3^{2+}$ and Co_4POM solutions were combined 42 ± 9 s before addition of $\text{Ru(III)(bpy)}_3^{3+}$ unless otherwise specified; this aging time was needed to ensure the Clark electrode reading was stable prior to initiation of the reaction. The solution was stirred at 600 rpm. Next, a solution of $\text{Ru(III)(bpy)}_3(\text{ClO}_4)_3$ was prepared by dissolving the solid in water—for example a 5 mM $\text{Ru(III)(bpy)}_3^{3+}$ solution was prepared by dissolving 8.68 mg $\text{Ru(III)(bpy)}_3^{3+}$ in 2.00 mL H_2O with sonication ($\sim 10\text{-}30$ s). The dissolved O_2 concentration was recorded before adding the $\text{Ru(III)(bpy)}_3^{3+}$ solution to the Co_4POM (or $\text{Co}(\text{NO}_3)_2$) solution via auto-pipette to ensure a stable base-line response of the Clark electrode. A reaction under Standard Conditions used 0.20 mL of the stock $\text{Ru(III)(bpy)}_3^{3+}$ solution; reactions which contained $[\text{Ru(III)(bpy)}_3^{3+}] \geq 0.5$ mM used stock solution of 5.0 mM $\text{Ru(III)(bpy)}_3^{3+}$, while reactions which had lower oxidant concentrations used 1.0 mM $\text{Ru(III)(bpy)}_3^{3+}$ stock solutions. Immediately after addition of the $\text{Ru(III)(bpy)}_3^{3+}$ solution, stirring was stopped and the reaction was allowed to proceed until the electrode-response plateaued at which time stirring was resumed and the final O_2 concentration reading was taken. Reactions were typically 2-5 minutes in length. This procedure was followed in order to minimize the solution-to-gas transfer of O_2 generated during the reaction, so the O_2 yield could be measured in solution.

Kinetics of O_2 evolution

Oxygen evolution rates were measured using a custom-built Clark electrode which was made according to the method of Bard and co-workers,⁴² except a 368 μm diameter platinum wire (Alfa Aesar, 99.95% purity) was used and the reference solution contained 0.2 M NaCl plus

0.2 M, pH 8.0 sodium phosphate. This electrode has a faster response time than the Microelectrodes O₂ electrode and is therefore better suited to the kinetic experiments herein (i.e., the 95% response time is ~2-3 seconds going from 236 to 0 μM O₂ solution). The electrode was polarized at -800 mV and was allowed to equilibrate with the solution before starting the experiment; typical equilibration times were 3-5 minutes. The current was recorded every 0.1 s using a CHI630D potentiostat and software (CH Instruments Inc.).

Reactions were run using the procedure described in the “O₂ evolution and yield quantification” section above except the reaction was stirred throughout the reaction and the electrode was recalibrated at the end of each reaction. The initial O₂ evolution rate, $\{d[O_2]/dt\}_i$, was measured by linearly fitting the first 5-10 s of the electrode response where the fitted slope corresponds to the initial rate. See Figure S5.1 for sample data.

Kinetics of Ru(III)(bpy)₃³⁺ loss

The water oxidation reaction was run as described in the “O₂ evolution and yield quantification” section with the following alterations: (1) the reaction was run in a plastic cuvette (Spectronic, 1 cm pathlength); and (2) the reaction was not stirred during the reaction, but was mixed when the reactants were combined by quickly removing and re-injecting a portion of the solution using an auto-pipette. The concentration of Ru(III)(bpy)₃³⁺ was monitored by the absorbance at 675 nm using the known molar absorptivity, $\epsilon_{675\text{ nm}} = 440\text{ M}^{-1}\cdot\text{cm}^{-1}$. Data points were collected every 1.0 s for 60 s on an HP 8452A diode array spectrometer. The initial ruthenium(III) reduction rate, $\{-d[\text{Ru(III)(bpy)}_3^{3+}]/dt\}_i$, was measured by linearly fitting the first ~10% of the reaction (i.e., typically the first 5-10 s of the reaction). Sample data are given in Figure S5.1.

K_{sp} Measurement of the Co₄POM-Ru(II)(bpy)₃ Precipitate

Four solutions were prepared in 0.03 M, pH 7.2 sodium phosphate buffer and contained 100 μM Ru(II)(bpy)₃²⁺ plus 0, 5.0, 10.0, or 20.0 μM Co₄POM. After 8 hours, the solutions were filtered through 0.22 μm nylon syringe filters into plastic cuvettes and the absorbance spectra recorded and analyzed to determine the equivalents of Ru(II)(bpy)₃²⁺ per Co₄POM in the precipitate (found ~2 : 3 Co₄POM:Ru(II)(bpy)₃²⁺). Three solutions were prepared in 0.03 M, pH 7.2 sodium phosphate buffer containing the Co₄POM and Ru(II)(bpy)₃²⁺ in the predetermined 1:1.5 ratio: (1) 10.0 : 15.0 μM; (2) 20.0 : 30.0 μM; (3) 50.0 : 75.0 μM. After 8 hours these solutions were filtered through 0.22 μm nylon syringe filters, and the absorbance spectra measured to determine the remaining [Ru(II)(bpy)₃²⁺] which was used to calculate the K_{sp} value.

Results and Discussion

Stoichiometry of the oxidation reaction

As discussed in the introduction, the catalytic oxidation of water into oxygen using the terminal oxidant Ru(III)(bpy)₃³⁺ nearly always results in sub-stoichiometric production of O₂ due to the parallel oxidation of the 2,2'-bipyridine ligands. The net observed stoichiometry of these reactions (equation 4) is therefore a measurement of the catalyst selectivity *and* the relative activity of the water oxidation reaction vs ligand oxidation. Restated, the ratio of ligand versus water oxidation is a measure of the net relative production of these two parallel pathways.

We therefore began our investigation of the Co₄POM by determining the stoichiometry of the POM catalyzed water oxidation reaction. Throughout the current investigation, a standard reaction is run by making a solution of the Co₄POM in 0.30 M sodium phosphate buffer, adding a 0.50 mM Ru(II)(bpy)₃²⁺ solution (except in controls or other experiments where it was intentionally omitted) and then adding a Ru(III)(bpy)₃³⁺ solution to initiate the reaction. The

dissolved oxygen concentration was then measured using a Clark electrode immersed in the reaction solution.

The O₂ yields for a series of experiments are shown in Table 5.1. The data reveal several interesting insights, including: (i) the O₂ yields are considerably higher when Ru(II)(bpy)₃²⁺ is added prior to Ru(III)(bpy)₃³⁺ (entries 6 and 8 versus 14 and 15); (ii) the ligand oxidation path is always favored by at least 3-fold under the various conditions examined herein; and (iii) the O₂ yields increase with increasing pH (entries 6, 11-13) and increasing [Ru(III)(bpy)₃³⁺] (entries 4-8). These results indicate the active catalyst(s) in Co₄POM solutions show poor selectivity for water oxidation relative to ligand oxidation.

Table 5.1. O₂ yields for Ru(III)(bpy)₃³⁺ plus Co₄POM reactions.^a

Entry	[Co ₄ POM] (μM)	[Ru(III)] (μM)	[Ru(II)] (μM)	pH	O ₂ yield (μM)	% yield
1	0.5	100	100	7.2	5	20
2	1.0	100	100	7.2	3	12
3	2.0	100	100	7.2	4	16
4	1.0	50	100	7.2	1	8
5	1.0	200	100	7.2	9	18
6	1.0	500	100	7.2	27	22
7	1.0	750	100	7.2	40	21
8	1.0	1000	100	7.2	47	19
9	1.0	500	50	7.2	26	21
10	1.0	500	200	7.2	12	10
11	1.0	500	100	6.8	8	6
12	1.0	500	100	7.5	31	25
13	1.0	500	100	7.8	35	28
14 ^b	1.0	500	100	7.2	9	7
15 ^b	1.0	1000	100	7.2	20	8
16	1.0	500	0	7.2	13	10
17	0	500	100	7.2	2	2

^a The order of experiments in this table are organized by listing entries in sets which vary the concentration of [POM] (entries 1-3), [Ru(III)(bpy)₃³⁺] (4-8), [Ru(II)(bpy)₃²⁺] (9-10), and pH (11-13). ^b Ru(III)(bpy)₃³⁺ and Ru(II)(bpy)₃²⁺ were added simultaneously; for all other experiments, Ru(II)(bpy)₃²⁺ was combined with the Co₄POM solution 42 ± 9 seconds before addition of the Ru(III)(bpy)₃³⁺.

Kinetics of O₂ Formation

Kinetics of oxygen evolution were measured directly by a Clark electrode to gain further insight into the water oxidation mechanism. Since addition of Ru(II)(bpy)₃²⁺ to the Co₄POM solution yields larger amounts of O₂, all kinetic experiments include pre-added Ru(II)(bpy)₃²⁺. The O₂ evolution rates displayed a complex dependence on the Co₄POM, Ru(III)(bpy)₃³⁺, Ru(II)(bpy)₃²⁺, and H⁺ concentrations. Therefore, the method of initial rates was used to derive an empirical rate law for the Co₄POM precatalyst.

Figure 5.1 shows the initial rate data for O₂ evolution with variation in the initial concentration for each of [Co₄POM], [Ru(III)(bpy)₃³⁺], [Ru(II)(bpy)₃²⁺], and [H⁺] while holding the other three concentrations constant. Note, for all initial rate data ($\{d[O_2]/dt\}_i$ and $\{d[Ru(III)(bpy)_3^{3+}]/dt\}_i$) the given concentrations and pH values are the initial conditions for the reaction. When using a Co₄POM precatalyst, these initial rate plots are consistent with a first-order dependence on the [Ru(III)(bpy)₃³⁺] oxidant and inverse-first-order dependences on [Ru(II)(bpy)₃²⁺] and [H⁺]. The fits to other reaction orders are worse (Table S5.1 and S5.2).

Interestingly, Figure 5.1C reveals only a small dependence of the initial O₂ evolution rate on the initial Co₄POM concentration *suggesting that the actual water oxidation catalyst concentration changes little between these experiments*. Indeed, this curve is fit well by either first-order saturation kinetics or a 0.25-order fit (which makes little physical sense). This observation suggests two possible hypotheses: (i) precipitation of a Ru(II)(bpy)₃²⁺-Co₄POM¹⁰⁻ complex, where only a relatively constant amount of Co₄POM remains in solution, or (ii) decomposition of the Co₄POM into a different, possibly heterogeneous, catalyst in which the number of active sites does not scale linearly with precursor concentration.

Evidence for a Precipitate Formed With a ~2 : 3 Co₄POM : Ru(II)(bpy)₃²⁺ Ratio, Its K_{sp} and Its Effect on the Kinetics

To investigate this sub-stoichiometric precatalyst dependence phenomenon further, the Co₄POM plus Ru(II)(bpy)₃²⁺ solution was aged prior to addition of Ru(III)(bpy)₃³⁺. Consistent with the precipitation hypothesis, the initial O₂ evolution rate *decreases* from 0.34 to 0.22 to 0.12 μM/s for 30, 60, or 120 s aging times (Figure S5.2). *Additionally, when Co₄POM is combined with Ru(II)(bpy)₃²⁺ a precipitate forms in a ~2 : 3 Co₄POM : Ru(II)(bpy)₃²⁺ ratio and this precipitate has a K_{sp} = (8±7) × 10⁻²⁵ (M⁵)* (Tables S3 and S4). These observations are in-line with precedents for ion-pairing and aggregation between Ru(II)(bpy)₃²⁺ and polyoxometalates; [Ru₄O₄(μ-OH)₂(H₂O)₄(γ-SiW₁₀O₃₆)₂]¹⁰⁻, [PW₁₂O₄₀]³⁻, and [PW₁₁O₃₉]⁷⁻ have been reported to form POM:Ru(II)(bpy)₃²⁺ complexes with ~1:4,²⁷ 1:1,⁴³ and 1:1⁴³ ratios. This literature precedent and low observed K_{sp} value observed herein demonstrate the importance of considering Co₄(H₂O)₂(PW₉O₃₄)₂¹⁰⁻-Ru(II)(bpy)₃²⁺ solution/precipitate equilibria in the study of O₂ evolution kinetics of highly negatively charged polyoxometalates.

Since addition of Ru(II) to the Co₄POM solution appears to induce precipitation, we addressed next whether the inverse, [Ru(II)(bpy)₃²⁺]⁻¹ dependence in Figure 5.1C derives from precipitation (i.e., from the removal of the POM from the catalytic cycle), or from a reversible electron-transfer step within the catalytic cycle. Comparison of {d[O₂]/dt}_i when Ru(II)(bpy)₃²⁺ is added at the same time as Ru(III)(bpy)₃³⁺, or when no Ru(II)(bpy)₃²⁺ is added, reveals no significant difference in the initial rates ({d[O₂]/dt}_i = 2.5 μM/s and 2.3 μM/s, respectively); that is, the initial O₂ evolution rate does not depend on initial [Ru(II)(bpy)₃²⁺] when it is added at the same time as Ru(III)(bpy)₃³⁺. This strongly suggests that the inverse, [Ru(II)(bpy)₃²⁺]⁻¹ dependence observed in Figure 5.1C is the result of the Co₄POM interacting with the

$\text{Ru(II)(bpy)}_3^{2+}$ prior to addition of oxidant. Overall, these order-of-addition experiments, the Co_4POM plus $\text{Ru(II)(bpy)}_3^{2+}$ aging tests and the K_{sp} determination all strongly suggest *precipitation plays a significant, complicating role in the O_2 evolution reaction, the observed kinetics and the underlying mechanism for polyoxometalate/ $\text{Ru(III)(bpy)}_3^{3+}$ systems.*

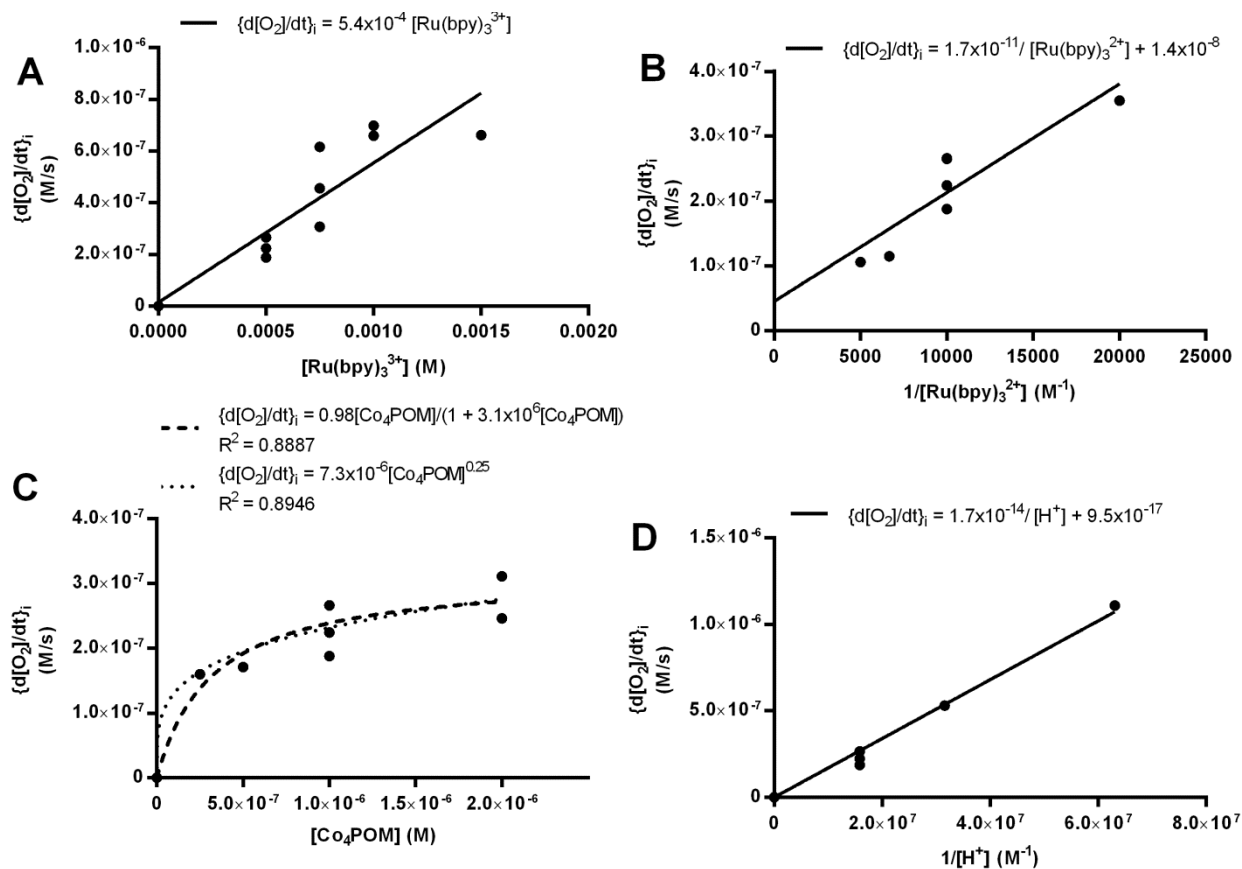


Figure 5.1. Initial O_2 evolution rate data measured by a custom-built Clark electrode⁴² with variation in the initial (A) $[\text{Ru(III)(bpy)}_3^{3+}]$, (B) $[\text{Ru(II)(bpy)}_3^{2+}]$, (C) $[\text{Co}_4\text{POM}]$, and (D) pH. For each of the plots, all other initial concentrations were held constant where the Standard Conditions are $1.0 \mu\text{M}$ Co_4POM , $500 \mu\text{M}$ $\text{Ru(III)(bpy)}_3^{3+}$, $100 \mu\text{M}$ $\text{Ru(II)(bpy)}_3^{2+}$, pH 7.2, and 0.03 M sodium phosphate buffer. Solid lines are linear fits. The dotted line is fit assuming a reaction order of 0.25 ($Y = aX^{0.25} + b$, where a and b are fitting parameters). Since the 0.25-order fit to the Co_4POM data (C) is physically unreasonable, plot (C) was also fit to a first-order reaction with saturation kinetics (dashed line) ($Y = aX/(1 + bX)$ where a and b are fitting parameters). The y intercept for all plots was constrained to values ≥ 0 . R^2 values and fits to other reaction orders can be found in the SI.

Kinetics of Ru(III)(bpy)₃³⁺ oxidant loss

The kinetics of Ru(III)(bpy)₃³⁺ loss were investigated next in order to extract the ligand oxidation kinetics and to allow comparison of the relative rates of the water and ligand oxidation reactions. Specifically, the oxidation of the bipyridine ligand was studied in greater detail by measuring the decrease in the 675 nm absorbance band of Ru(III)(bpy)₃³⁺ while in the presence of Co₄POM. As before, the dependence of the initial rate, $\{-d[\text{Ru(III)(bpy)}_3^{3+}]/dt\}_i$, was measured while varying the initial reaction parameters; for these experiments, the initial concentrations of [Ru(III)(bpy)₃³⁺], [Ru(II)(bpy)₃²⁺], [Co₄POM], and [H⁺] were each changed while keeping the other three initial variables constant. The obtained initial rates were then corrected by subtracting the initial Ru(III)(bpy)₃³⁺ loss due to water oxidation (using the data fits in Figure 5.1) so that the resultant corrected rates, $\{-d[\text{Ru(III)(bpy)}_3^{3+}]_{\text{ligand ox.}}/dt\}_i$, *reflect only the ligand oxidation path*:

$$\left\{ \frac{-d[\text{Ru(bpy)}_3^{3+}]_{\text{ligand ox.}}}{dt} \right\}_i = \left\{ \frac{-d[\text{Ru(bpy)}_3^{3+}]_{\text{total}}}{dt} \right\}_i - 4 \left\{ \frac{d[\text{O}_2]}{dt} \right\}_i \quad (5)$$

Plotting this ligand-oxidation-only initial rate data shows a first-order dependence on [Ru(III)(bpy)₃³⁺], an inverse-first-order dependence on [Ru(II)(bpy)₃²⁺] with a non-zero intercept and an initial inverse-first-order dependence on [H⁺], which then flattens some at increasing pH values (Figure 5.2). The kinetic data also reveal an initial first-order dependence in [Co₄POM] with flattening towards a lower-order dependence at increasing concentrations. Other tested fits to the data proved inferior and are provided in Table S5.2 and S5.3.

The non-zero intercepts for both the Co₄POM and Ru(II)(bpy)₃²⁺ plots are consistent with a background reaction of Ru(III)(bpy)₃³⁺ undergoing an uncatalyzed ligand-oxidation reaction with itself (i.e., a self-oxidation)—a process which has precedent in the previously cited, classic studies by Creutz and Sutin et al.^{34,35} Indeed, the data in Figure 5.2B can be corrected by

subtracting the background, uncatalyzed ligand-oxidation rate in Figure 5.S3A; the 90% confidence interval for the corrected intercept is -6.9×10^{-7} to 1.7×10^{-6} (Figure 5.S3B), which is within experimental error of zero.

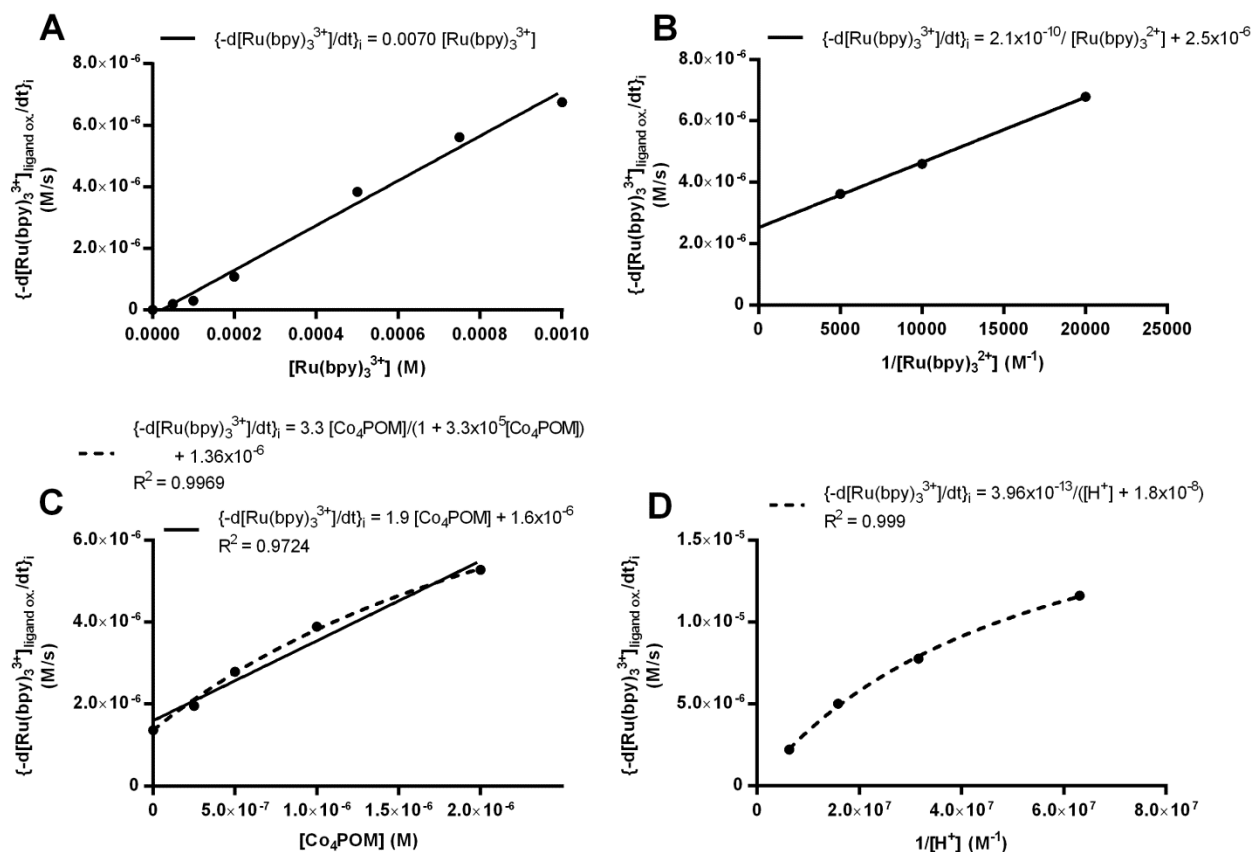


Figure 5.2. Initial bipyrindine ligand oxidation rate data with variation in the initial (A) $[\text{Ru}(\text{III})(\text{bpy})_3^{3+}]$, (B) $[\text{Ru}(\text{II})(\text{bpy})_3^{2+}]$, (C) $[\text{Co}_4\text{POM}]$, and (D) pH. For each of the plots, all other initial concentrations were held constant where the Standard Conditions are $1.0 \mu\text{M}$ Co_4POM , $500 \mu\text{M}$ $\text{Ru}(\text{III})(\text{bpy})_3^{3+}$, $100 \mu\text{M}$ $\text{Ru}(\text{II})(\text{bpy})_3^{2+}$, pH 7.2, and 0.03 M sodium phosphate buffer. The $\{-d[\text{Ru}(\text{III})(\text{bpy})_3^{3+}]/dt\}_i$ is derived from the loss in absorbance at 675 nm and after correcting for the amount of $\text{Ru}(\text{III})(\text{bpy})_3^{3+}$ which corresponds to O_2 evolution, as shown in equation (5). Solid lines indicate linear fits. Dashed lines are fits assuming a first-order reaction with saturation kinetics: $Y = aX/(1 + bX) + \text{intercept}$, where a and b are fitting parameters and the intercept was set to zero for plot (C) and set to the experimentally measured intercept of 1.36×10^{-6} for plot (D). The y intercept for all plots was constrained to values ≥ 0 for all other plots. R^2 values and fits to other reaction orders can be found in the SI over this range). Interestingly, the lack of a similar flattening of the $1/[\text{H}^+]$ kinetics is not observed in the O_2 evolution kinetics, Figure 5.1D. It is unclear at present whether this modest difference in the pH dependence of the water and ligand-oxidation kinetics is real or due to experimental error in the O_2 kinetic measurements.

The $1/[H^+]$ saturation kinetics are interesting since they imply either a reversible proton-transfer prior to the turnover limiting step in the reaction, or that the rate changes with the concentration of base (e.g., the $[HPO_4^{2-}]$ increases with the pH).

An additional complicating factor when interpreting the kinetics, as discussed in the O_2 evolution kinetics section above, concerns the origin of the observed inverse $Ru(II)(bpy)_3^{2+}$ dependence. Specifically, is the only role of $Ru(II)(bpy)_3^{2+}$ to bind/precipitate the Co_4POM^{10-} polyanion, thereby removing the Co_4POM polyoxometalate from the catalytic cycle, or is it perhaps involved as a product of a *reversible*, $Ru(III)(bpy)_3^{3+}$ -to- $Ru(II)(bpy)_3^{2+}$ electron-transfer reaction within the catalytic cycle? Consistent with the O_2 evolution kinetics, the $\{-d[Ru(III)(bpy)_3^{3+}]/dt\}$ is the same (42 and 41 $\mu M/s$) when 1.0 μM Co_4POM is combined with either 500 μM $Ru(III)(bpy)_3^{3+}$ or 500 μM $Ru(III)(bpy)_3^{3+}$ plus 100 μM $Ru(II)(bpy)_3^{2+}$ (where the $Ru(II)(bpy)_3^{2+}$ is added at the same time as the $Ru(III)(bpy)_3^{3+}$) in 0.03 M, pH 7.2 sodium phosphate buffer. This result suggests both the inverse $Ru(II)(bpy)_3^{2+}$, and the slight flattening of the $[Co_4POM]$ vs $\{-d[Ru(III)(bpy)_3^{3+}]_{ligand\ ox.}/dt\}_i$ curve, are due primarily to the precipitation reaction between the Co_4POM and the $Ru(II)(bpy)_3^{2+}$, thereby removing Co_4POM from within the catalytic cycle. Importantly, given that we have shown that $Ru(II)(bpy)_3^{2+}$ can precipitate the Co_4POM^{10-} , an added implication here from the above control—as well as from simple chemical intuition—is the suggestion that $Ru(III)(bpy)_3^{3+}$ might also form an ion pair with or precipitate Co_4POM^{10-} . This will be important later when interpreting the rate law for O_2 formation. But first, studies aimed at providing evidence for or against a heterogeneous CoO_x colloidal catalyst needs to be presented.

Stoichiometric and Kinetic Contrasts of Co₄POM and Co(NO₃)₂ WOC precursors

One recurring question when beginning with homogeneous water oxidation catalysts is whether the starting material is the true catalyst or whether the initially homogeneous complex is transformed into a heterogeneous catalyst under the reaction conditions.^{44,45} To provide independent, kinetic-based evidence for the nature of the true catalyst above that already available,^{28,29,40} we have collected data on the stoichiometry, oxygen evolution kinetics, and Ru(III)(bpy)₃³⁺ reduction kinetics *for a heterogeneous CoO_x type catalyst under the otherwise identical conditions* used to study the Co₄POM. In these studies, Co(NO₃)₂ was used as the precursor for the heterogeneous CoO_x catalyst—a transformation which has been studied by others under similar, but primarily photochemical, conditions of 10-50 μM Co(NO₃)₂, 100-500 μM Ru(II)(bpy)₃²⁺, 1.0-10.0 mM Na₂S₂O₈, hv, and in pH 7.0 or 8.0 sodium phosphate buffer.^{37,39,40} That is, if the Co₄POM is actually transformed into a CoO_x catalyst under the reaction conditions, then the two systems should show similar—if not identical—reaction stoichiometry and kinetics. Alternatively, and as is observed, different stoichiometries and kinetics would be the expected fingerprints of different catalysts.

Controls starting with cobalt(II) nitrate in Table 5.2 show O₂ yields of 18 to 56% which decrease with increasing [Ru(III)(bpy)₃³⁺] and which are greater than or equal to those of Co₄POM under identical conditions; the differences between these precursors is even greater when considering that Co₄POM has four equivalents of cobalt per POM. These results are similar to other studies of cobalt WOCs beginning with cobalt(II) salts or heterogeneous Co(OH)₂ colloids since these precedents show higher selectivity for water oxidation of up to 90% under conditions of pH 9.4 and [Co(OH)₂] = 1 μM and [Ru] = 240-340 μM.⁴⁶ Both the prior and current studies of Co²⁺ derived catalysts indicate the O₂ yield depends on the ratio of oxidant

to pre-catalyst and where the optimal ratio is between 10 and 100.^{35,36,47} In contrast, the Co₄POM system shows optimal O₂ yields when greater than 125 equivalents of oxidant per cobalt is used (Table 5.1, entry 6)—an observation which distinguishes the reaction stoichiometry when beginning with Co₄POM versus Co(NO₃)₂ but does not definitively identify the true catalyst.

Differences between Co₄POM and CoO_x derived from Co(NO₃)₂ are also observed in the oxygen evolution kinetics and are the primary evidence for different WOCs in the current study. As seen in Figure 5.3A, O₂ evolution rates when beginning with Co(NO₃)₂ show a first-order dependence on [precatalyst] and are 2-11 times faster than identical reactions which have Co₄POM. Furthermore, the {d[O₂]/dt}_i does not increase significantly with increasing initial [Ru(III)(bpy)₃³⁺] when 1.0 μM Co(NO₃)₂ is used (Figure 5.3B) which opposes the observed first-order [Ru(III)(bpy)₃³⁺] dependence when beginning with Co₄POM. This comparison argues that Co²⁺ dissociated from the polyoxometalate core is *not* forming a significant amount of CoO_x in-situ. That is, because the Co(NO₃)₂ precatalyst shows first-order and zero-order O₂ evolution kinetics on [precatalyst] and [Ru(III)(bpy)₃³⁺], it cannot be the same catalyst as in Co₄POM solutions which shows first-order dependences on both [precatalyst] and [Ru(bpy)₃³⁺].

Table 5.2. O₂ yields for Ru(III)(bpy)₃³⁺ plus Co(NO₃)₂ reactions.

Entry	[Co(NO ₃) ₂] (μM)	[Ru(III)] (μM)	[Ru(II)] (μM)	pH	O ₂ yield (μM)	% yield
1	0.5	500	100	7.2	22	18
2	1.0	500	100	7.2	41	33
3	2.0	500	100	7.2	57	46
4	1	50	100	7.2	7	56
5	1	100	100	7.2	12	48
6	1	200	100	7.2	23	46
7	1	750	100	7.2	52	28
8	1	1000	100	7.2	45	18
9	1	500	50	7.2	39	32
10	1	500	200	7.2	30	24
11	1	500	100	6.8	20	16
12	1	500	100	7.5	42	34
13	1	500	100	7.8	50	40

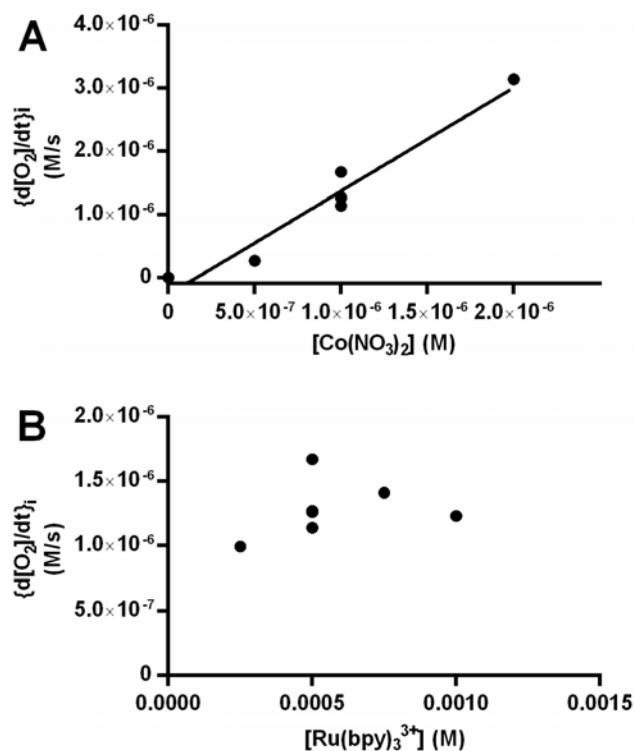


Figure 5.3. Initial water oxidation rates during controls with variation in the (A) starting $[\text{Co}(\text{NO}_3)_2]$ and (B) starting $[\text{Ru}(\text{III})(\text{bpy})_3^{3+}]$. Standard conditions are $1.0 \mu\text{M Co}(\text{NO}_3)_2$, $500 \mu\text{M Ru}(\text{III})(\text{bpy})_3^{3+}$, $100 \mu\text{M Ru}(\text{II})(\text{bpy})_3^{2+}$ at pH 7.2 in 0.03 M sodium phosphate buffer. The O_2 was measured using a Clark electrode described in the experimental section.⁴² The solid line is a linear fit to the initial O_2 evolution rate data.

This finding, that CoO_x derived from aqueous Co^{2+} is *not* the dominant catalyst in the current Co_4POM plus $\text{Ru}(\text{III})(\text{bpy})_3^{3+}$ system, fortifies Hill and co-workers' investigations,^{28,29,40} and Ohlin et al.'s observation of enhanced Co_4POM stability in neutral to mildly acidic solutions.⁴⁸ Moreover, our prior electrochemical studies,³² the present study, and those of Hill⁴⁰ demonstrate rather clearly that the conditions, and notably the form of the oxidant, *can play an important role in determining the kinetically dominant form of WOCs*—as we had hinted at in an important footnote (#18) in our initial publication in this area.³⁰ Worth noting here is that our electrochemical oxidation studies employing Co_4POM at higher concentrations (0.5 mM) and pH 8.0 revealed $101 \pm 12\%$ of the observed water oxidation catalysis corresponds to CoO_x derived

from $58 \pm 2 \mu\text{M Co}^{2+}$ dissociated from the parent polyoxometalate.³⁰ *The specific conditions, including the oxidant source, do matter in determining the true WOC!*

Investigation of the ligand-oxidation kinetics provides additional insight into the differences between oxidation catalysts derived from $\text{Co}(\text{NO}_3)_2$ and Co_4POM . As shown in Figure S5.4, CoO_x shows ligand oxidation rates which are comparable to Co_4POM reactions. This observation of faster water oxidation, but comparable ligand oxidation, for CoO_x relative to Co_4POM solutions are consistent with the *observed higher selectivity for water oxidation for CoO_x vs Co_4POM* . Cumulatively, the differences in ligand oxidation and oxygen evolution kinetics strongly support the conclusion herein and elsewhere^{28,29,40} that different catalysts are present in the CoO_x and Co_4POM systems when a $\text{Ru}(\text{bpy})_3^{3+}$ oxidant is used.

Efforts Towards Constructing a Water Oxidation/Ligand Oxidation Working Mechanistic Hypothesis When Beginning with Co_4POM and $\text{Ru}(\text{III})(\text{bpy})_3^{3+}$

In addition to helping distinguish the Co_4POM and $\text{Co}(\text{NO}_3)_2$ derived catalysts, the kinetics of oxygen evolution and ligand oxidation are invaluable in helping one start to construct a plausible reaction mechanism—that is, a working mechanistic hypothesis—when starting with Co_4POM and $\text{Ru}(\text{III})(\text{bpy})_3^{3+}$. Greatly hindering that effort, however, is that the precise composition of the water-oxidation catalyst has not been fully addressed for the Co_4POM system herein nor previously^{28,29,40}—nor for the CoO_x system, for that matter (although others have examined similar WOCs^{35,36,37,38,46,47}). Significantly, for the present $\text{Co}_4\text{POM}^{10-}$ system, neither we nor others know the exact extent and composition of the ion-pairing by $\text{Ru}(\text{II})(\text{bpy})_3^{2+}$ and $\text{Ru}(\text{III})(\text{bpy})_3^{3+}$ in either the catalytically most active species, nor in the catalyst resting state.⁴⁹ What this means is that any interpretation of the rate law—and especially the *apparent* $[\text{Ru}(\text{II})(\text{bpy})_3^{2+}]$ and $[\text{Ru}(\text{III})(\text{bpy})_3^{3+}]$ concentration dependencies, needs to be made with great

caution. And, again, the presence of a precipitate quantitated herein complicates interpretation of the kinetics even further.

Below, we start our construction of a working mechanistic hypothesis with the assumption that the catalytically active species is soluble (since that, and the presence of a precipitate, allowed us to rationalize the observed $\{d[\text{O}_2]/dt\}_1 \propto [\text{Co}_4\text{POM}]^{1-0}$ dependence of the O_2 kinetics, *vide supra*). Interestingly, and as seen in Figures 5.1 and 5.2, the general trends in the oxygen evolution kinetics mirror those seen in the ligand oxidation kinetics and when beginning with Co_4POM . This similarity suggest that the same intermediate(s) is (are) active in both the water oxidation and ligand oxidation reactions; the matching rate trends are also consistent with the constant reaction stoichiometry over a range of initial $\text{Ru(III)(bpy)}_3^{3+}$ concentrations.

Combination of the oxygen evolution and ligand oxidation rate data yields the empirical rate law in equation 6:

$$\frac{-d[\text{Ru(III)(bpy)}_3^{3+}]}{dt} = (k_1 + k_2) \frac{[\text{Ru(III)(bpy)}_3^{3+}][\text{Co}_4\text{POM}]^{-1}}{[\text{H}^+]} \quad (6)$$

In eq. (6), the working hypothesis is that the $[\text{Co}_4\text{POM}]$ is largely determined by the solubility product equilibrium $[\text{Co}_4\text{POM}] = \{K_{\text{sp}}/[\text{Ru(II)(bpy)}_3^{2+}]^3\}^{0.5}$. The constants $k_1 + k_2$ are, then, the apparent rate constants for the parallel paths of O_2 generation and ligand oxidation (and correspond to rate constants for the sum of multiple elementary steps). Note that the given rate law is a simplification since it incorporates the uncatalyzed ligand oxidation reaction rate into k_2 ; a discussion of this simplification is given in eq. (S1-S6), which also shows the dependence of $\{-d[\text{Ru(III)(bpy)}_3^{3+}]_{\text{ligand ox.}}/dt\}_i$ on the initial $[\text{Ru(III)(bpy)}_3^{3+}]$ in the absence of a catalyst precursor (Figure S5.5). The rate of oxygen evolution shows a similar empirical rate law,

equation (7). A discussion of how this rate law relates to the stoichiometry in eq. (3-5) is given in eq. (S7-S9).

$$\frac{d[\text{O}_2]}{dt} = \frac{k_1}{4} \frac{[\text{Ru(III)(bpy)}_3^{3+}][\text{Co}_4\text{POM}]^{\sim 1}}{[\text{H}^+]} \quad (7)$$

Due to the complication of precipitation, the precise values of k_1 and k_2 apparent rate constants can only be estimated. Since the observed initial O_2 evolution and $\text{Ru(III)(bpy)}_3^{3+}$ loss rates decrease by approximately an order of magnitude when $\text{Ru(II)(bpy)}_3^{2+}$ is pre-mixed with the Co_4POM (Figure S5.2), a zeroth-order approximation is that the $[\text{Co}_4\text{POM}]$ has also decreased by the same magnitude. That is, using the assumption that the initial $[\text{Co}_4\text{POM}]$ is 0.1 μM , along with the observed rate law, and the slope from Figures 5.1A and 5.2A, results in the estimated rate constant values of $k_1 \sim 1.4 \times 10^{-3} \text{ s}^{-1}$ and $k_2 \sim 4.4 \times 10^{-3} \text{ s}^{-1}$.

To check the validity of these constants, the predicted O_2 yield was determined by dividing the O_2 rate constant (k_1) by the sum of the two rate constants ($k_1 + k_2$); a derivation of this calculation is given in eq. (S7). This calculation results in a predicted O_2 yield of 24%, *which is within experimental error of the observed yield of 22% under Standard Conditions*—support for at least the consistency, and arguably the validity, of the separately produced experiments, the resultant data, data analyses, and any underlying approximations/assumptions made.

Returning to the construction of a working hypothesis for the proposed WOC mechanism, the resting state of the catalyst at pH 7.2 is most likely $\text{Co}^{\text{II}}_4(\text{H}_2\text{O})_2(\text{PW}_9\text{O}_{34})_2^{10-}$ (neglecting any ion-pairing to $\text{Ru(II)(bpy)}_3^{2+}$ or $\text{Ru(III)(bpy)}_3^{3+}$ for the moment) since (i) this species is observed at the end of the reaction by ^{31}P -NMR according to Yin et al.,²⁸ (ii) the $\text{Ru(bpy)}_3^{3+/2+}$ couple occurs at 1.26 V vs NHE compared to the oxidation wave onset of the Co_4POM solution $E \sim 1.4$ V vs NHE at pH 7.2 (i.e., which implies the majority of the Co_4POM should be in the starting $\text{Co}^{\text{II}}_4(\text{H}_2\text{O})_2(\text{PW}_9\text{O}_{34})_2^{10-}$ oxidation state),³² and (iii) Ohlin et al.

estimated the pKa of the Co₄POM to be ~8 and the Co₄POM should, therefore, have two aquo ligands coordinated to its two outermost cobalts at pH 7.2.⁴⁸

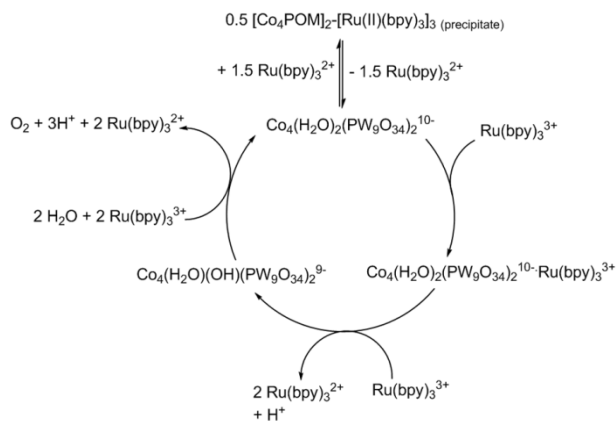
If one interprets the non-first order, [Co₄POM]¹⁻⁰ and the 1/[Ru(II)(bpy)₃²⁺] dependencies in eq. (7) in terms of the (demonstrated) precipitate, then one is left with the remaining terms in eq (7) of $d[\text{O}_2]/dt \propto \{[\text{Co}_4\text{POM}]^{-1}[\text{Ru(III)(bpy)}_3^{3+}]^1\} / [\text{H}^+]^1$. The simplest interpretation of the remaining terms of that rate law, eq (7), is that a one-electron-, one-proton-transfer occurs at or before the turnover limiting step (TLS) of the catalytic cycle, Schemes S5.1-S5.2. The observation that the inverse Ru(II)(bpy)₃²⁺ dependence requires pre-mixing of the Co₄POM and Ru(II)(bpy)₃²⁺ suggests the electron-transfer step is not reversible and precipitate formation is not significant within the time needed to take the initial rate measurement (5-10 s). Although consistent with the empirical rate law, this mechanism would require all subsequent (three) electron/proton transfers and O-O bond formation steps to be relatively fast—a requirement which contrasts with the majority of other single-site WOCs where O-O bond formation is typically turnover limiting.

Alternatively, it is possible that two equivalents of Ru(III)(bpy)₃³⁺ react with Co₄POM at or prior to the TLS. This hypothetical two electron transfer would be consistent with the empirical rate law (eq. 7) if either the resting state of the catalyst is a {[Co₄POM][Ru(III)(bpy)₃³⁺]} ion-pair which is “on-path” (shown in Scheme 5.1 and S5.3), or (ii) a catalytically inactive {[Co₄POM][Ru(III)(bpy)₃³⁺]} precipitate forms and equilibrates quickly with the solution (Scheme S5.4). The latter hypothesis seems less likely than the former since the related {[Co₄POM]₂[Ru(II)(bpy)₃²⁺]}₃ precipitation reaction is slow compared to catalyst turnover, *vide supra*. Therefore, a two-electron/one-proton transfer occurring prior to the TLS is a mechanism which is supported by both prior literature of cobalt-WOCs and the

observed kinetics. Additional discussion and kinetic derivations of possible water oxidation mechanisms are found in the Supporting Information.

However, we note once more that, due to the complications of ion-pairing and precipitation of polyanionic polyoxoanions such as $\text{Co}_4\text{POM}^{10-}$ with polycations such as $\text{Ru(II/III)(bpy)}_3^{2/3+}$, the mechanism in Scheme 5.1 is at best *an equivocal, working hypothesis*. What, however, is unequivocal is that use of polycations such as $\text{Ru(II/III)(bpy)}_3^{2/3+}$ as the oxidant with polyanionic precatalysts makes the resultant WOC systems *much more complicated*, effectively removing many of the reasons and intrinsic advantages for mechanistic understanding of such molecular (pre)catalysts.

Scheme 5.1. One working mechanistic hypothesis for water oxidation when beginning with Co_4POM .^a



^a $\text{Co}_4(\text{H}_2\text{O})_2(\text{PW}_9\text{O}_{34})_2^{10-} \cdot \text{Ru(bpy)}_3^{3+}$ is the catalyst resting state in this scheme. Discussion of four detailed mechanisms consistent with the observed kinetics are provided in the SI for the interested reader.

Conclusions

Investigation of catalytic water oxidation beginning with $\text{Co}_4(\text{H}_2\text{O})_2(\text{PW}_9\text{O}_{34})_2^{10-}$ and $\text{Ru(III)(bpy)}_3^{3+}$ has revealed the complexity and non-ideal nature of this otherwise interesting, state-of-the-art WOC system. Although Co_4POM is a discrete pre-catalyst, the use of the $\text{Ru(II/III)(bpy)}_3^{2+/3+}$ reagent induces ion-pairing and precipitation of the $\text{POM-Ru(II)(bpy)}_3^{2+}$.

Undesired oxidative decomposition of the bipyridine ligands is another very much undesired feature of the system—indeed, O₂ is the *minor product* in the reaction, corresponding to *at most a 28% yield* under the conditions herein (and based on the initial [Ru(III)(bpy)₃³⁺]). In order to more efficiently study Co₄POM (and other such) precatalysts, a more robust one-electron oxidant is badly needed⁵⁰—ideally one less highly charged or anionic. As a corollary, it appears the present Co₄POM precatalyst would be a poor choice for incorporation into a photo-driven water oxidation system containing organic or organometallic photosensitizers due to the Co₄POM-based catalyst's propensity to oxidize organics relative to the desired substrate, water.

In contrast with the Co₄POM, controls beginning with Co(NO₃)₂, which forms heterogeneous CoO_x in-situ,^{37,39} show a broad range of O₂ yields ranging from 18-54%, overall higher maximum O₂ yields than Co₄POM (as Hill and co-workers also report⁴⁰). These Co(NO₃)₂ controls also show initial O₂ evolution rates which are 2 to 11 times *greater per mol of Co(NO₃)₂ than per mol of Co₄POM* under otherwise identical conditions—again showing that CoO_x, and not Co₄POM, is the superior WOC.

However and although the above data indicate that just 20% of CoO_x *could* account for the observed water oxidation activity (i.e., ~0.2 μM CoO_x when starting with 1.0 μM Co₄POM and under the Standard Conditions herein), the opposing trends in ligand oxidation and differences in the water oxidation rate laws when comparing the Co(NO₃)₂ and Co₄POM starting materials argues that CoO_x—at least alone, and made from aqueous Co²⁺—is *not* the true catalyst in this Co₄POM system. Analysis of the O₂ evolution and Ru(III)(bpy)₃³⁺ reduction initial rates indicate that a one-electron-, one-proton-transfer is involved before the turnover limiting step in the catalytic cycle, but the ion-pairing and precipitations induced by the Ru(II/III)(bpy)₃^{2+/3+} reagents complicates the system considerably and its kinetics—*possibly* masking the true

underlying rate law and turnover-limiting step, Scheme 5.1, *vide supra*. However, the kinetic data do indicate that the same reactive intermediate is formed in both the water and ligand-oxidation reactions. This in turn means that the selectivity of the catalyst is primarily limited by the catalytic species present and their mechanism, not by the reaction conditions. This finding has important implications for the limitations of future applications of a Co₄POM-based WOC in artificial photosynthetic schemes—poor selectivity for water oxidation can be anticipated if organics (such as organic photovoltaics or organometallic-based dye-sensitized solar cells) are present.

The present studies issue a caution for comparing TOFs between different systems—and especially between any two systems *where the full rate law is not first established for each system*. Comparisons of even closely related system and TOFs based on their “ k_{cat} ” values could, then, often be an unintended comparison of *different mechanisms*. Moreover, comparison of different systems based on “ k_{obsd} ” values are likely to also have an *unintended comparison of conditions* (i.e., concentration terms in the rate law) in that comparison as well. This message is timely, the use and comparison of TOFs being a controversial topic at present.⁵¹ Reflection teaches that comparisons of TOFs should be made *only* when the full rate law for each system being compared is first in hand.⁵¹

Overall, the present studies make very apparent that there is a pressing need to find a chemical oxidant other than Ru(III)(bpy)₃³⁺ which is not prone to self-oxidation and that is less highly charged to uncharged, for applications with polyanionic precatalysts such as polyometalates. There is also a need for more extensive studies of other Co-POMs to see what are the exceptions, vs the rules, for other Co-POMs in comparison to the extant literature of others,^{28,29,40} our prior work (i.e., of electrode-bound CoOx catalysis)³⁰, and compared to the

kinetics and implied mechanism uncovered herein. That said, kinetic and mechanistic studies at or beyond the present level might best be reserved for other systems where the system is not plagued by precipitation phenomena and where the primary product of the oxidizing equivalents is the desired O_2 .

Supporting Information

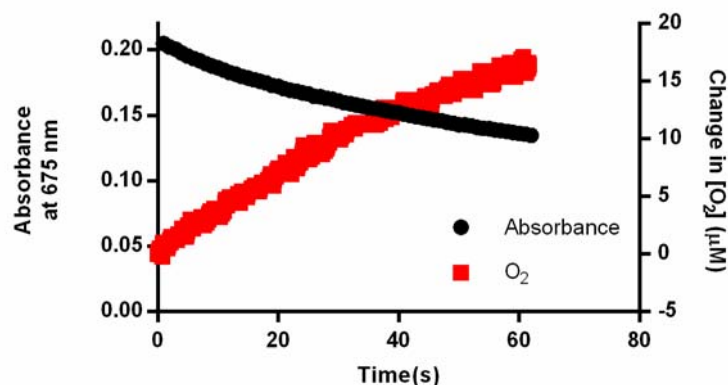


Figure S5.1. Sample absorbance decay and oxygen evolution data under initial Standard Conditions of $500 \mu M$ $Ru(III)(bpy)_3^{3+}$, $100 \mu M$ $Ru(II)(bpy)_3^{2+}$, $1.0 \mu M$ Co_4POM , pH 7.2, and $0.03 M$ sodium phosphate buffer and where the $Ru(II)(bpy)_3^{2+}$ was combined with the Co_4POM solution ~ 30 s before the $Ru(III)(bpy)_3^{3+}$ solution. The absorbance loss at 675 nm corresponds to the decrease in $[Ru(III)(bpy)_3^{3+}]$. The O_2 evolution was measured in solution using a custom-built Clark electrode, as detailed in the main text, which was calibrated with 20.9% (air saturated) and 0% standards. Note that these experiments were performed and recorded separately.

Table S5.1. Comparison of different fits to the oxygen evolution kinetic data. Each entry represents the non-linear least squares fit to the equation $Y = \text{Coefficient} * X^{\text{Order}} + \text{Intercept}$. Where “Coefficient” and “Intercept” are fitted parameters, “Order” is set to the indicated value in the table, Y is the $\{d[\text{O}_2]/dt\}_i$, and X is the concentration of the species of interest (indicated by the “Variable” column). The entry which corresponds to the best fit (i.e., highest R^2 value) for a given variable is highlighted for clarity.

Entry	Variable	Order	Coefficient	Intercept	R^2
1	$\text{Ru(III)(bpy)}_3^{3+}$	0.5	1.644E-05	$\sim 1.188\text{e-}016$	0.6873
2	$\text{Ru(III)(bpy)}_3^{3+}$	1	0.0005397	1.438E-08	0.7757
3	$\text{Ru(III)(bpy)}_3^{3+}$	2	0.2882	2.129E-07	0.582
4	$1/\text{Ru(II)(bpy)}_3^{2+}$	0.5	2.252E-09	$\sim 1.534\text{e-}016$	0.7139
5	$1/\text{Ru(II)(bpy)}_3^{2+}$	1	1.676E-11	4.536E-08	0.8051
6	$1/\text{Ru(II)(bpy)}_3^{2+}$	2	5.855E-16	1.443E-07	0.6846
7	Co_4POM	0.25	7.329E-06	$\sim 1.368\text{e-}016$	0.8946
8	Co_4POM	0.5	0.0001884	3.523E-08	0.8465
9	Co_4POM	1	0.1057	1.007E-07	0.6439
10	$1/\text{H}^+$	0.5	9.836E-11	$\sim 1.490\text{e-}016$	0.7331
11	$1/\text{H}^+$	1	1.7E-14	9.502E-17	0.9871
12	$1/\text{H}^+$	2	2.484E-22	1.565E-07	0.9406

Table S5.2. Additional fits of oxygen evolution and $\text{Ru(III)(bpy)}_3^{3+}$ loss kinetic data to first-order saturation kinetics. Each entry represents the non-linear least squares fit to the equation: $Y = aX/(1+bX) + \text{Intercept}$ where a and b are fitted variables, Intercept is a constant, Y is the initial rate of either O_2 evolution or $\text{Ru(III)(bpy)}_3^{3+}$ loss (as defined in the “Rate” column), and X is the concentration of the species of interest (“Variable” column).

Entry	Rate	Variable	a	b	Intercept	R^2
1	$\{-d[\text{Ru(III)(bpy)}_3^{3+}]_{\text{ligand ox.}}/dt\}_i$	$1/\text{H}^+$	3.96E-13	1.842E-08	0	0.999
2	$\{-d[\text{Ru(III)(bpy)}_3^{3+}]_{\text{ligand ox.}}/dt\}_i$	Co_4POM	3.258	325587	$1.36\text{E-}6^a$	0.9969
3	$\{d[\text{O}_2]/dt\}_i$	Co_4POM	0.9784	3100000	0	0.8887

^a The intercept for this plot was determined experimentally by measuring the $\text{Ru(III)(bpy)}_3^{3+}$ loss in a reaction under Standard Conditions but without Co_4POM where the initial concentrations of the reactants were: 500 μM $\text{Ru(III)(bpy)}_3^{3+}$, 100 μM $\text{Ru(II)(bpy)}_3^{2+}$, pH 7.2, and 0.03 M sodium phosphate.

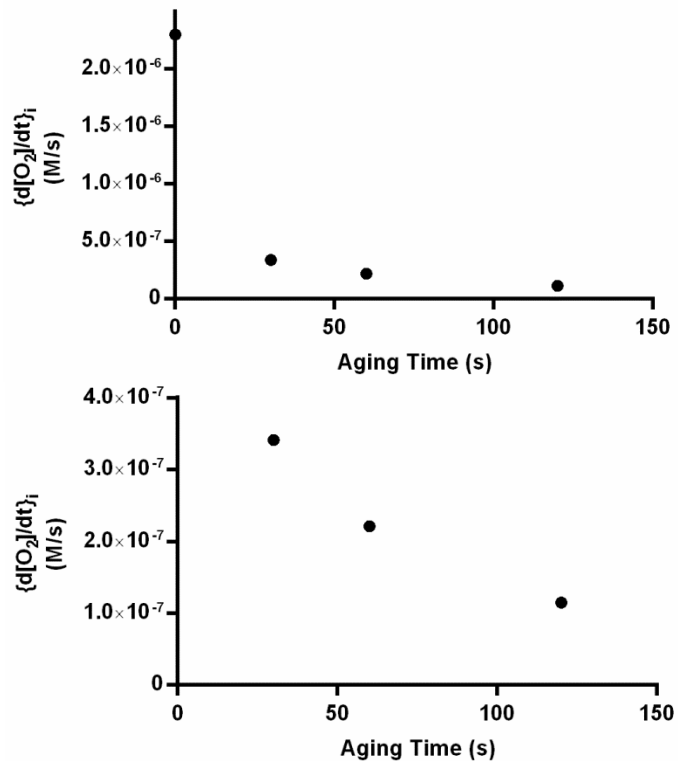


Figure S5.2. Plots of initial O₂ evolution rate as a function of aging time. The aging time is the duration between when the Co₄POM and Ru(II)(bpy)₃²⁺ solutions were combined and when the Ru(III)(bpy)₃³⁺ solution was added. The plot on the bottom is a zoomed-in view of the 30, 60, and 120 s aging experiments. The 0 s aging experiment was accomplished by adding the Ru(III)(bpy)₃³⁺ and Ru(II)(bpy)₃²⁺ solutions simultaneously. Note, most kinetic experiments in the main text are aged 30-60 s. Reaction conditions were the standard 500 μM Ru(III)(bpy)₃³⁺, 100 μM Ru(II)(bpy)₃²⁺, 1.0 μM Co₄POM, pH 7.2, and 0.03 M sodium phosphate buffer.

Table S5.3. Determination of the $\text{Co}_4\text{POM} : \text{Ru(II)(bpy)}_3^{2+}$ ratio formed in their precipitate.^a

Entry	$[\text{Co}_4(\text{H}_2\text{O})_2(\text{PW}_9\text{O}_{34})_2^{10-}]_{\text{initial}}$ (M)	$[\text{Ru(II)(bpy)}_3^{2+}]_{\text{initial}}$ (M)	$[\text{Ru(II)(bpy)}_3^{2+}]_{\text{final}}$ (M)	$\text{Co}_4(\text{H}_2\text{O})_2(\text{PW}_9\text{O}_{34})_2^{10-} : \text{Ru(II)(bpy)}_3^{2+}$
1	5.00E-06	1.00E-04	9.29853E-05	1.40
2	1.00E-05	1.00E-04	8.36868E-05	1.63
3	2.00E-05	1.00E-04	6.73736E-05	1.63

^aAs described in the Experimental section of the main text, four solutions were prepared in 0.03 M sodium phosphate buffer which contained 100 μM $\text{Ru(II)(bpy)}_3^{2+}$ plus (1) 0 μM Co_4POM , (2) 5.0 μM Co_4POM , (3) 10.0 μM Co_4POM , and (4) 20.0 μM Co_4POM . These solutions were allowed to stand, unstirred, for 8 hours at which time they were filtered through 0.22 μm syringe filters and their absorbance at 450 nm taken. In the following analysis, it was assumed that K_{sp} is relatively small—an assumption which will prove to be valid, *vide infra*, and which means that the $\text{Co}_4(\text{H}_2\text{O})_2(\text{PW}_9\text{O}_{34})_2^{10-}$ will act as the limiting reagent in these experiments (i.e., all of it will be assumed to wind up in the precipitate, within a very small error). By assuming nearly all of the $\text{Co}_4(\text{H}_2\text{O})_2(\text{PW}_9\text{O}_{34})_2^{10-}$ has precipitated from the solution the ratio of $\text{Co}_4(\text{H}_2\text{O})_2(\text{PW}_9\text{O}_{34})_2^{10-} : \text{Ru(II)(bpy)}_3^{2+}$ in the precipitate was calculated by: (1) measuring the change in $[\text{Ru(II)(bpy)}_3^{2+}]$ relative to the 0 μM $\text{Co}_4(\text{H}_2\text{O})_2(\text{PW}_9\text{O}_{34})_2^{10-}$ control, and then (2) dividing the change in $[\text{Ru(II)(bpy)}_3^{2+}]$ by the initial $[\text{Co}_4(\text{H}_2\text{O})_2(\text{PW}_9\text{O}_{34})_2^{10-}]$. This resulted in the calculated ratio of 1.55 ± 0.13 for $\text{Ru(II)(bpy)}_3^{2+} / \text{Co}_4(\text{H}_2\text{O})_2(\text{PW}_9\text{O}_{34})_2^{10-}$.

Table S5.4. Determination of the K_{sp} for the $(\text{Co}_4(\text{H}_2\text{O})_2(\text{PW}_9\text{O}_{34})_2^{10-})_2(\text{Ru(II)(bpy)}_3^{2+})_3$ complex.^a

Entry	$[\text{Co}_4(\text{H}_2\text{O})_2(\text{PW}_9\text{O}_{34})_2^{10-}]_{\text{initial}}$ (M)	$[\text{Ru(II)(bpy)}_3^{2+}]_{\text{initial}}$ (M)	$[\text{Co}_4(\text{H}_2\text{O})_2(\text{PW}_9\text{O}_{34})_2^{10-}]_{\text{final}}$ (M)	$[\text{Ru(II)(bpy)}_3^{2+}]_{\text{final}}$ (M)	K_{sp} ($\text{M}^{2.5}$)
1	1.00E-05	1.50E-05	9.93E-06	1.49E-05	3.25E-25
2	2.00E-05	3.00E-05	1.34E-05	2.00E-05	1.44E-24
3	5.00E-05	7.50E-05	1.16E-05	1.74E-05	7.01E-25

^aThree solutions were prepared in 0.03 M, pH 7.2 sodium phosphate buffer containing: (1) 10 μM Co_4POM and 15 μM $\text{Ru(II)(bpy)}_3^{2+}$, (2) 20 μM Co_4POM and 30 μM $\text{Ru(II)(bpy)}_3^{2+}$, and (3) 50 μM Co_4POM and 75 μM $\text{Ru(II)(bpy)}_3^{2+}$. These solutions were filter through a 0.22 μm syringe filter after aging for 8 hours. By measuring the final concentration of $\text{Ru(II)(bpy)}_3^{2+}$ (via the 450 nm absorbance), the K_{sp} was calculated for each of the samples using the equation: $K_{\text{sp}} = [\text{Co}_4\text{POM}]_{\text{final}}^2 [\text{Ru(II)(bpy)}_3^{2+}]_{\text{final}}^3$, where the $[\text{Co}_4\text{POM}]_{\text{final}} = [\text{Co}_4\text{POM}]_{\text{initial}} - \Delta[\text{Ru(II)(bpy)}_3^{2+}] / 1.5$ and the exponents of 2 and 3 are derived from the 2 : 3 ratio of the $\text{Co}_4\text{POM} : \text{Ru(II)(bpy)}_3^{2+}$. The calculated average $K_{\text{sp}} = 8 \pm 7 \times 10^{-25} \text{ M}^5$. As discussed above in Table S5.3, this K_{sp} value reinforces the assumption that nearly all the Co_4POM should have precipitated in the experiments in Table S5.3; for example, using the determined K_{sp} and the initial conditions from Table S5.3, entry 2, the final $[\text{Co}_4\text{POM}] = (K_{\text{sp}} / [\text{Ru(II)(bpy)}_3^{2+}]_{\text{final}}^3)^{0.5} = 1 \text{ } \mu\text{M}$ (i.e., about 90% of the Co_4POM has precipitated).

Table S5.5. Comparison of different fits to the ligand oxidation kinetic data. Each entry represents the non-linear least-squares fit to the equation $Y = \text{Coefficient} * X^{\text{Order}} + \text{Intercept}$. Where “Coefficient” and “Intercept” are fitted parameters, “Order” is set to the indicated value in the table, Y is the initial $-d[\text{Ru(III)(bpy)}_3^{3+}]_{\text{ligand oxidation}}/dt$, and X is the concentration of the species of interest (indicated by the “Variable” column). The entry which corresponds to the best fit (i.e. highest R^2 value) for a given variable is highlighted for clarity.

Entry	Variable	Order	Coefficient	Intercept	R^2
1	$\text{Ru(III)(bpy)}_3^{3+}$	0.5	0.000182	$\sim 1.624\text{e-}016$	0.8224
2	$\text{Ru(III)(bpy)}_3^{3+}$	1	0.007042	$\sim 2.174\text{e-}016$	0.9876
3	$\text{Ru(III)(bpy)}_3^{3+}$	2	6.991	6.758E-07	0.9004
4	$1/\text{Ru(II)(bpy)}_3^{2+}$	0.5	4.54E-08	2.835E-07	0.9861
5	$1/\text{Ru(II)(bpy)}_3^{2+}$	1	2.12E-10	2.525E-06	0.9993
6	$1/\text{Ru(II)(bpy)}_3^{2+}$	2	8.12E-15	3.582E-06	0.9865
7	Co_4POM	0.25	8.52E-07	9.358E-05	0.751
8	Co_4POM	0.5	0.002851	9.988E-07	0.9492
9	Co_4POM	1	1.938	1.611E-06	0.9724
10	$1/\text{H}^+$	0.5	1.38E-09	$\sim 1.385\text{e-}016$	0.9539
11	$1/\text{H}^+$	1	1.58E-13	2.019E-06	0.9669
12	$1/\text{H}^+$	2	2.03E-21	3.966E-06	0.8552

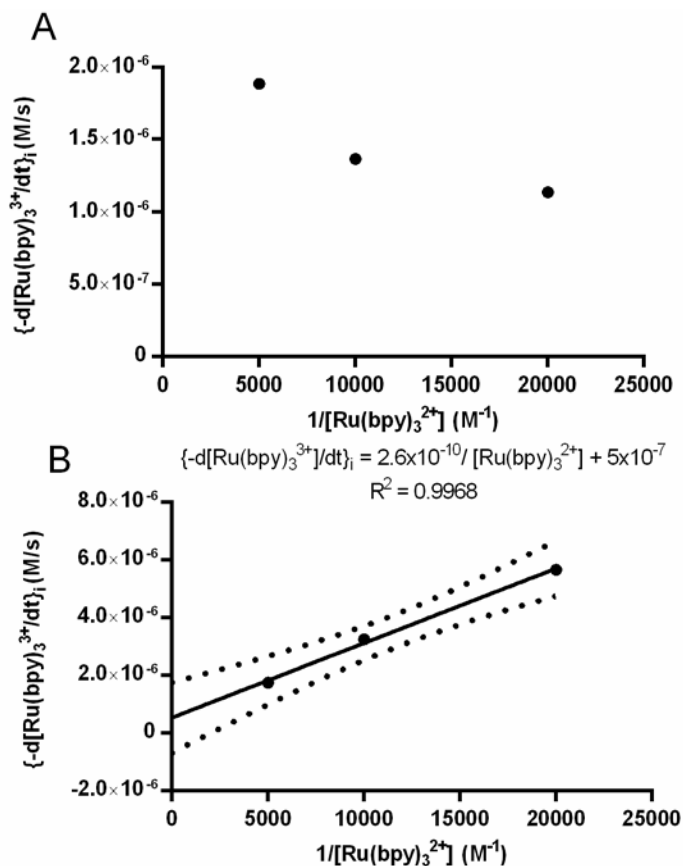


Figure S5.3. (A) Control experiments showing the initial rate of Ru(III)(bpy)₃³⁺ loss as a function of $1/[\text{Ru}(\text{II})(\text{bpy})_3^{2+}]$ in solutions containing no added Co₄POM. Other conditions are the same as in Figure 5.2B, specifically: 500 μM Ru(III)(bpy)₃³⁺, pH 7.2, and 0.03 M sodium phosphate buffer. These data show an increasing rate for the uncatalyzed ligand oxidation reaction as the initial concentration of Ru(II)(bpy)₃²⁺ increases. (B) The background corrected $\{-d[\text{Ru}(\text{III})(\text{bpy})_3^{3+}]_{\text{ligand ox.}}/dt\}_i$ for the Co₄POM solutions as a function of $1/[\text{Ru}(\text{III})(\text{bpy})_3^{2+}]$ which was calculated by subtracting the uncatalyzed ligand oxidation rate (in graph (A), above) from the ligand oxidation rate in Figure 5.2B. The dotted line indicates the 90% confidence interval of the linear fit. Of importance here, is that the 90% confidence interval for the intercept is -6.9×10^{-7} to 1.7×10^{-6} ; that is, the intercept in Figure S5.3B is within experimental error of zero, which indicates the non-zero intercept in Figure 5.2B is due primarily to the non-catalyzed ligand oxidation pathway).

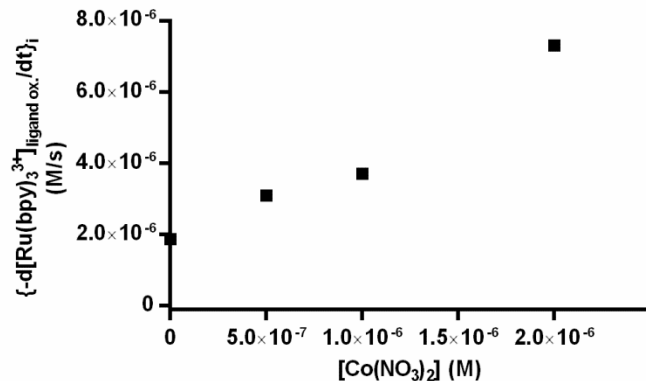


Figure S5.4. Control experiments showing the initial rate of ligand oxidation in solutions under initial conditions of $\text{Co}(\text{NO}_3)_2$ at the given concentration, $500 \mu\text{M}$ $\text{Ru}(\text{III})(\text{bpy})_3^{3+}$, $100 \mu\text{M}$ $\text{Ru}(\text{II})(\text{bpy})_3^{2+}$, $1.0 \mu\text{M}$, $\text{pH } 7.2$, and 0.03 M sodium phosphate buffer. Initial ligand oxidation rate data was determined by measuring the initial rate of total $\text{Ru}(\text{III})(\text{bpy})_3^{3+}$ loss at 675 nm , $\{-d[\text{Ru}(\text{III})(\text{bpy})_3^{3+}]_{\text{total}}/dt\}_i$, and then calculating the $\{-d[\text{Ru}(\text{III})(\text{bpy})_3^{3+}]_{\text{ligand ox.}}/dt\}_I$ using equation (5). These ligand oxidation rates are comparable to when a Co_4POM precursor is used (as shown in Figure 5.2). However, because the O_2 evolution rate is higher for a $\text{Co}(\text{NO}_3)_2$ precatalyst compared to a Co_4POM precursor, the resulting O_2 yield (i.e., reaction selectivity) is higher for the $\text{Co}(\text{NO}_3)_2$ -containing reaction.

Discussion of the Uncatalyzed Ligand Oxidation Pathway

As noted in the main text there is an uncatalyzed ligand oxidation reaction which is incorporated into the $\text{Ru}(\text{III})(\text{bpy})_3^{3+}$ loss rate law in eq. (6) of the main text. That is, the total ligand oxidation rate includes both catalyzed and uncatalyzed ligand oxidation pathways, eq (S1).

$$\begin{aligned} \frac{-d[\text{Ru}(\text{bpy})_3^{3+}]_{\text{ligand ox.,total}}}{dt} &= \frac{-d[\text{Ru}(\text{bpy})_3^{3+}]_{\text{ligand ox.,cat.}}}{dt} + \frac{-d[\text{Ru}(\text{bpy})_3^{3+}]_{\text{ligand ox.,uncat.}}}{dt} \quad (\text{S1}) \end{aligned}$$

As defined in the main text (eq. (6)), the total ligand oxidation rate is given by equation S2,

$$\frac{-d[\text{Ru}(\text{bpy})_3^{3+}]_{\text{ligand ox.,total}}}{dt} = \frac{k_2[\text{Co}_4\text{POM}][\text{Ru}(\text{III})(\text{bpy})_3^{3+}]}{[\text{H}^+]} \quad (\text{S2})$$

and the catalyzed and uncatalyzed ligand oxidation reaction rates are defined by S3 and S4.

$$\frac{-d[\text{Ru}(\text{bpy})_3^{3+}]_{\text{ligand ox.,cat.}}}{dt} = \frac{k_{2,\text{true}}[\text{Co}_4\text{POM}][\text{Ru}(\text{III})(\text{bpy})_3^{3+}]}{[\text{H}^+]} \quad (\text{S3})$$

$$\frac{-d[\text{Ru}(\text{bpy})_3^{3+}]_{\text{ligand ox.,uncat.}}}{dt} = k_{3,\text{obs.}}[\text{Ru}(\text{III})(\text{bpy})_3^{3+}] \quad (\text{S4})$$

In these equations k_2 is the apparent, overall rate constant for the ligand oxidation reaction, $k_{2,\text{true}}$, is the rate constant for the catalyzed ligand oxidation path, and $k_{3,\text{obs.}}$ is the observed rate constant for the uncatalyzed ligand oxidation pathway. Note, $k_{3,\text{obs.}}$ likely masks other terms such as pH and $[\text{Ru}(\text{II})(\text{bpy})_3^{2+}]$ dependences, but is simplified herein since $k_{3,\text{obs.}}$ is calculated from Figure S5.5, where the only variable is $[\text{Ru}(\text{III})(\text{bpy})_3^{3+}]$. A more complete treatment of uncatalyzed ligand oxidation reactions is given by Creutz and Sutin et al.^{35,36}

Substituting equations S2, S3, and S4, into eq. S1 results in eq. S5.

$$\begin{aligned} & \frac{k_2[\text{Co}_4\text{POM}][\text{Ru}(\text{III})(\text{bpy})_3^{3+}]}{[\text{H}^+]} \\ &= \frac{k_{2,\text{true}}[\text{Co}_4\text{POM}][\text{Ru}(\text{III})(\text{bpy})_3^{3+}]}{[\text{H}^+]} + k_{3,\text{obs.}}[\text{Ru}(\text{III})(\text{bpy})_3^{3+}] \quad (\text{S5}) \end{aligned}$$

Rearrangement reveals the relationship between k_2 , $k_{2,\text{true}}$, and $k_{3,\text{obs.}}$.

$$k_{2,\text{true}} = k_2 - \frac{k_{3,\text{obs.}}[\text{H}^+]}{[\text{Co}_4\text{POM}]} \quad (\text{S6})$$

Using this equation, the k_2 determined in the main text, the $k_{3,\text{obs.}}$ in Figure S5.5 below, and Standard Conditions of pH 7.2 and an approximate initial $[\text{Co}_4\text{POM}] \sim 0.1 \mu\text{M}$, results in $k_{2,\text{true}} \sim 2.5 \times 10^{-3} \text{ s}^{-1}$. That is, even after correcting for the uncatalyzed ligand oxidation pathway, the catalyze ligand oxidation reaction still dominates over the desired water oxidation path where $k_1 \sim 1.4 \times 10^{-3} \text{ s}^{-1}$.

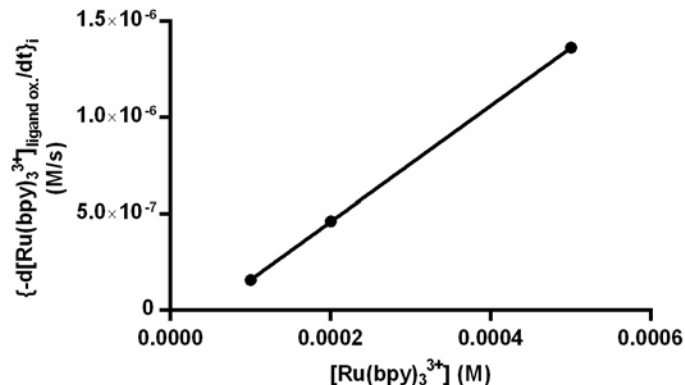


Figure S5.5. The initial, uncatalyzed ligand oxidation rate shows a linear dependence on the initial concentration of Ru(III)(bpy)₃³⁺. The other starting conditions are 100 μM Ru(II)(bpy)₃²⁺, pH 7.2, and 0.3 M sodium phosphate buffer. As defined in eq. (S4), the slope of this line equals the observed rate constant for uncatalyzed ligand oxidation, $k_{3,obs.} = (3.00 \pm 0.01) \times 10^{-3} \text{ s}^{-1}$. Initial ligand oxidation rates were determined by measuring the loss in Ru(III)(bpy)₃³⁺ absorbance at 675 nm.

Additional kinetic definitions and derivations

$$\begin{aligned} \text{Fractional O}_2 \text{ yield} &= \frac{\int_0^\infty -d [\text{Ru(III)(bpy)}_3^{3+}]_{\text{water oxidation}}}{\int_0^\infty -d [\text{Ru(III)(bpy)}_3^{3+}]_{\text{total}}} \\ &= \frac{\int_0^\infty k_1 [\text{Co}_4\text{POM}] [\text{Ru(III)(bpy)}_3^{3+}] / [\text{H}^+] dt}{\int_0^\infty (k_1 + k_2) [\text{Co}_4\text{POM}] [\text{Ru(III)(bpy)}_3^{3+}] / [\text{H}^+] dt} = \frac{k_1}{k_1 + k_2} \quad (\text{S7}) \end{aligned}$$

Where $-d [\text{Ru(III)(bpy)}_3^{3+}]_{\text{water oxidation}}/dt$ is the rate of Ru(III)(bpy)₃³⁺ loss which corresponds only to the water oxidation pathway. That is:

$$\frac{-d [\text{Ru(III)(bpy)}_3^{3+}]_{\text{water oxidation}}}{dt} = \frac{d[\text{O}_2]}{dt} \quad (\text{S8})$$

Comparison of the fractional O₂ yield calculation above and the fractional O₂ yield derived from the stoichiometry in equations 2-4 in the main text reveals the relationship between the two:

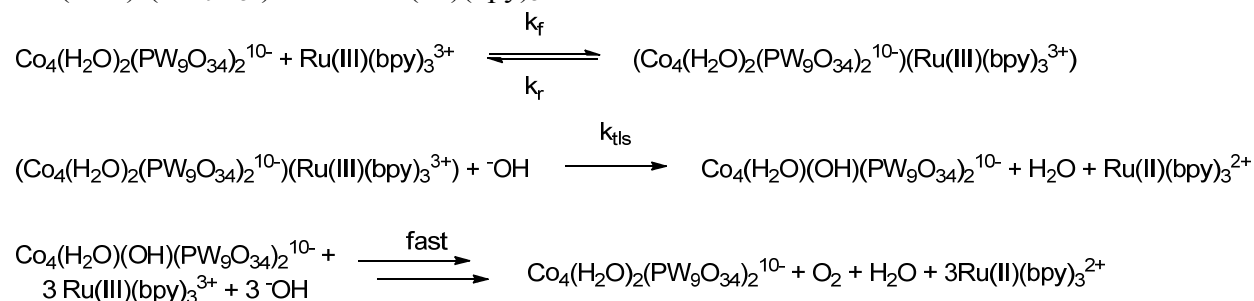
$$\frac{k_1}{k_1 + k_2} = \frac{4a}{4a + b + c} \quad (\text{S9})$$

It is apparent from eq. S9 that 4a is equivalent to k₁, and (b + c) is equivalent to k₂.

Four possible, more detailed, water oxidation mechanisms consistent with the data

Due to the expected strong electrostatic association of the $\text{Co}_4(\text{H}_2\text{O})_2(\text{PW}_9\text{O}_{34})_2^{10-}$ with the $\text{Ru}(\text{III})(\text{bpy})_3^{3+}$ oxidant, one possible mechanism involves association of these two species followed by turnover-limiting proton-transfer (Scheme S5.1).

Scheme S5.1. A possible proton-coupled electron-transfer pathway for water oxidation using Co_4POM and $\text{Ru}(\text{III})(\text{bpy})_3^{3+}$. All species are soluble and a 1 : 1 complex between $\text{Co}_4(\text{H}_2\text{O})_2(\text{PW}_9\text{O}_{34})_2^{10-}$ and $\text{Ru}(\text{III})(\text{bpy})_3^{3+}$ is assumed.



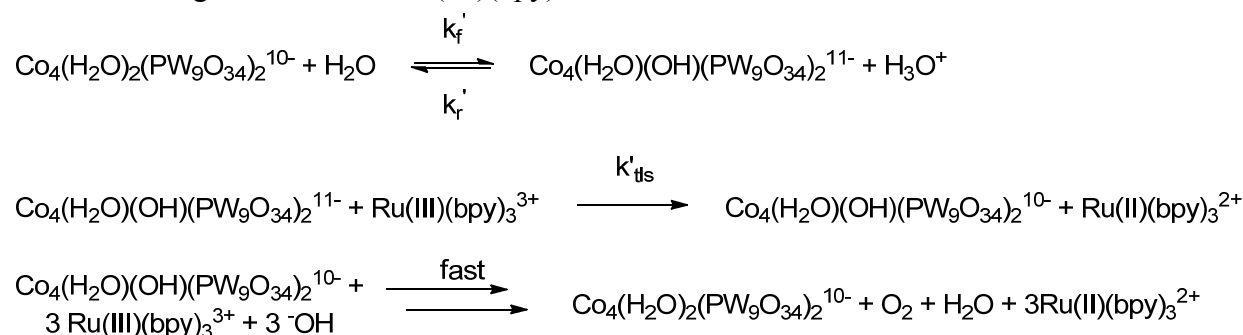
Which results in the rate law:

$$\frac{-d [\text{Ru}(\text{III})(\text{bpy})_3^{3+}]_{\text{water oxidation}}}{dt} = \frac{4k_f k_{\text{tls}} K_w [\text{Co}_4\text{POM}] [\text{Ru}(\text{III})(\text{bpy})_3^{3+}]}{k_r [\text{H}^+] + k_{\text{tls}} K_w} \quad (\text{S10})$$

Where k_{tls} is the rate constant for the turnover limiting step, hydroxide is assumed to be the proton accepting species and K_w is the ion product constant for water. In this case, k_1 (defined in the main text) would equal $(4k_f k_{\text{tls}} K_w / k_r)$.

Alternatively, the first step could be reversible deprotonation of the Co_4POM followed by turnover limiting electron transfer shown in Scheme S5.2.

Scheme S5.2. A possible, proton transfer followed by electron transfer, pathway for water oxidation using Co_4POM and $\text{Ru}(\text{III})(\text{bpy})_3^{3+}$.

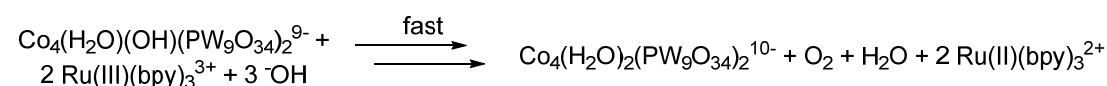
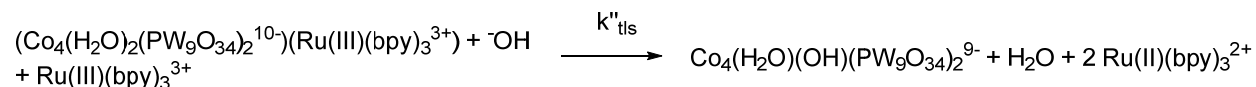


Which leads to the rate law for Ru(III)(bpy)₃³⁺ loss:

$$\frac{-d [\text{Ru(III)(bpy)}_3^{3+}]_{\text{water oxidation}}}{dt} = \frac{4k'_f k'_{\text{tls}} [\text{Co}_4\text{POM}] [\text{Ru(III)(bpy)}_3^{3+}]}{k'_r [\text{H}^+] + k'_{\text{tls}} [\text{Ru(III)(bpy)}_3^{3+}]} \quad (\text{S11})$$

Where k_1 , as defined in the main text, corresponds to $(4k'_f k'_{\text{tls}}/k'_r)$.

Scheme S5.3. A possible WOC mechanism containing a two-electron, one-proton transfer at or prior to the turnover limiting step. This scheme is similar to that shown in Scheme 5.1 in the main text.

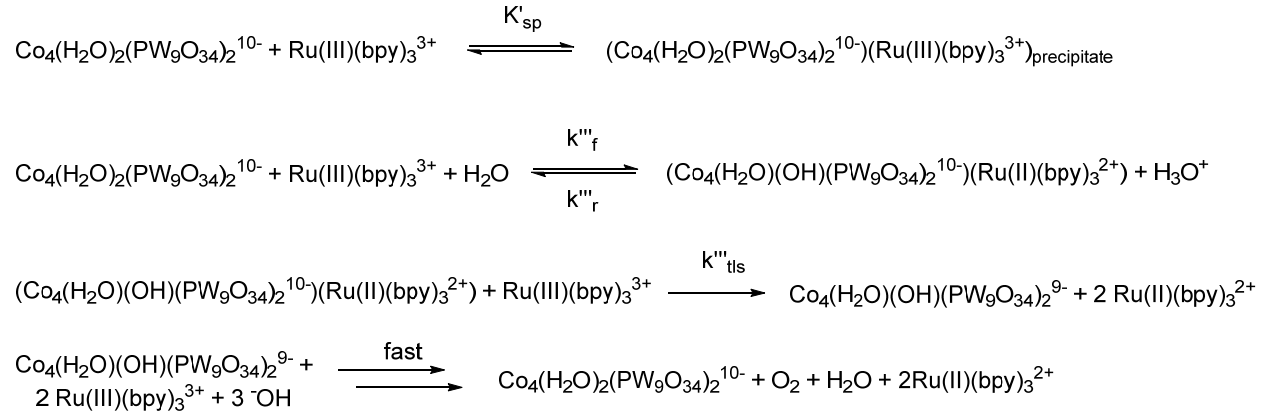


This scheme assumes fast formation of a Co₄POM-Ru(III)(bpy)₃³⁺ ion pair within the catalytic cycle, and results in the following rate law:

$$\frac{-d [\text{Ru(III)(bpy)}_3^{3+}]_{\text{water oxidation}}}{dt} = \frac{4k''_{\text{tls}} K_w [(\text{Co}_4\text{POM})(\text{Ru(III)(bpy)}_3^{3+})] [\text{Ru(III)(bpy)}_3^{3+}]}{[\text{H}^+]} \quad (\text{S12})$$

Where $[(\text{Co}_4\text{POM})(\text{Ru(III)(bpy)}_3^{3+})] = [\text{Co}_4\text{POM}]_{\text{total, soluble}}$ (i.e., all of the soluble Co₄POM is in the ion-paired form) assuming the ion-pair formation is fast relative to the turnover limiting step, hydroxide is assumed to be the proton accepting species and K_w is the ion product constant for water. In this mechanism, $4k''_{\text{tls}} K_w$ equals k_1 in eq. (7) of the main text.

Scheme S5.4. A fourth water oxidation mechanism consistent with the observed, empirical rate law (eq. 7 of the main text).



Where $[(\text{Co}_4\text{POM})(\text{Ru}(\text{III})(\text{bpy})_3^{3+})]_{\text{precipitate}}$ is a non-catalytically active species, and $(\text{Co}_4(\text{H}_2\text{O})(\text{OH})(\text{PW}_9\text{O}_{34})_2^{10-})(\text{Ru}(\text{II})(\text{bpy})_3^{2+})$ is a catalytic intermediate. The resulting rate law for this mechanism is given eq. (S13):

$$\begin{aligned} \frac{-d [\text{Ru}(\text{III})(\text{bpy})_3^{3+}]_{\text{water oxidation}}}{dt} &= \frac{4k'''_{\text{tls}}k''_f[\text{Co}_4\text{POM}][\text{Ru}(\text{III})(\text{bpy})_3^{3+}]^2}{k''_r[\text{H}^+]} \\ &= \frac{4k'''_{\text{tls}}k''_fK'_{\text{sp}}[\text{Ru}(\text{III})(\text{bpy})_3^{3+}]^1}{k''_r[\text{H}^+]} \quad (\text{S13}) \end{aligned}$$

Where K'_{sp} is a fast equilibrium between an inactive precipitate and an active, soluble Co_4POM species. This rate law contains an alternative explanation for the $[\text{Co}_4\text{POM}]^{1 \rightarrow 0}$ saturation kinetics where this observed precatalyst dependence is a result of the Co_4POM - $\text{Ru}(\text{III})(\text{bpy})_3^{3+}$ precipitation reaction.

REFERENCES

- ¹ Walter, M. G.; Warren, E. L.; McKone, J. R.; Boettcher, S. W.; Mi, Q.; Santori, E. A.; Lewis, N. S. *Chem. Rev.* **2010**, *110*, 6446.
- ² Cook, T. R.; Dogutan, D. K.; Reece, S. Y.; Surendranath, Y.; Teets, T. S.; Nocera, D. G. *Chem. Rev.* **2010**, *110*, 6474.
- ³ McDaniel, N. D.; Bernhard, S. *Dalton Trans.* **2010**, *39*, 10021.
- ⁴ Artero, V.; Chavarot-Kerlidou, M.; Fontecave, M. *Ang. Chem. Int. Ed.* **2011**, *50*, 7238.
- ⁵ Tran, P. D.; Artero, V.; Fontecave, M. *Energy Environ. Sci.* **2010**, *3*, 727.
- ⁶ Andreiadis, E. S.; Chavarot-Kerlidou, M.; Fontecave, M.; Artero, V. *Photochem. Photobiol.* **2011**, *87*, 946.
- ⁷ Herrero, C.; Quaranta, A.; Leibl, W.; Rutherford, A. W.; Aukauloo, A. *Energy Environ. Sci.* **2011**, *4*, 2353.
- ⁸ Artero, V.; Chavarot-Kerlidou, M.; Fontecave, M. *Ang. Chem. Int. Ed.* **2011**, *50*, 7238.
- ⁹ Gust, D.; Moore, T. A.; Moore, A. L. *Faraday Discuss.* **2012**, *155*, 9.
- ¹⁰ Young, K. J.; Martini, L. A.; Milot, R. L.; Snoeberger, R. C., III; Batista, V. S.; Schmuttenmaer, C. A.; Crabtree, R. H.; Brudvig, G. W. *Coord. Chem. Rev.* **2012**, *256*, 2503.
- ¹¹ Du, P.; Eisenberg, R. *Energy Environ. Sci.* **2012**, *5*, 6012.
- ¹² Swierk, J. R.; Mallouk, T. E. *Chem. Soc. Rev.* **2013**, *42*, 2357.
- ¹³ Liu, X.; Wang, F. *Coord. Chem. Rev.* **2012**, *256*, 1115.
- ¹⁴ Sartorel, A.; Bonchio, M.; Campagna, S.; Scandola, F. *Chem. Soc. Rev.* **2013**, *42*, 2262.
- ¹⁵ Wasylenko, D. J.; Palmer, R. D.; Berlinguette, C. P. *Chem. Commun.* **2013**, *49*, 218.
- ¹⁶ Dau, H.; Limberg, C.; Reier, T.; Risch, M.; Roggan, S.; Strasser, P. *ChemCatChem*, **2010**, *2*, 724.
- ¹⁷ Droege, M. W.; Finke, R. G. *J. Am. Chem. Soc.* **1984**, *106*, 7274.
- ¹⁸ Finke, R. G.; Rapko, B.; Saxton, R. J.; Domaille, P. J. *J. Am. Chem. Soc.* **1986**, *108*, 2947.
- ¹⁹ Geletii, Y. V.; Yin, Q.; Hou, Y.; Huang, Z.; Ma, H.; Song, J.; Besson, C.; Luo, Z.; Cao, R.; O'Halloran, K. P.; Zhu, G.; Zhao, C.; Vickers, J. W.; Ding, Y.; Mohebbi, S.; Kuznetsov, A. E.; Musaev, D. G.; Lian, T.; Hill, C. L. *Isr. J. Chem.* **2011**, *51*, 238.
- ²⁰ Han, Z. G.; Bond, A. M.; Chuan, Z. *Sci. China Chem.* **2011**, *54*, 1877.

- ²¹ Lv, H.; Geletii, Y. V.; Zhao, C.; Vickers, J. W.; Zhu, G.; Luo, Z.; Song, J.; Lian, T.; Musaev, D. G.; Hill, C. L. *Chem. Soc. Rev.* **2012**, *41*, 7572.
- ²² Sartorel, A.; Carraro, M.; Scorrano, G.; Bonchio, M. *Energy Procedia* **2012**, *22*, 78.
- ²³ Murakami, M.; Hong, D.; Suenobu, T.; Yamaguchi, S.; Ogura, T.; Fukuzumi, S. *J. Am. Chem. Soc.* **2011**, *133*, 11605.
- ²⁴ Geletii, Y. V.; Besson, C.; Hou, Y.; Yin, Q.; Musaev, D. G.; Quinonero, D.; Cao, R.; Hardcastle, K. I.; Proust, A.; Koegerler, P.; Hill, C. L. *J. Am. Chem. Soc.* **2009**, *131*, 17360.
- ²⁵ Besson, C.; Huang, Z.; Geletii, Y. V.; Lense, S.; Hardcastle, K. I.; Musaev, D. G.; Lian, T.; Proust, A.; Hill, C. L. *Chem. Commun.* **2010**, *46*, 2784.
- ²⁶ Sartorel, A.; Miro, P.; Salvadori, E.; Romain, S.; Carraro, M.; Scorrano, G.; Di Valentin, M.; Llobet, A.; Bo, C.; Bonchio, M. *J. Am. Chem. Soc.* **2009**, *131*, 16051.
- ²⁷ Natali, M.; Orlandi, M.; Berardi, S.; Campagna, S.; Bonchio, M.; Sartorel, A.; Scandola, F. *Inorg. Chem.* **2012**, *51*, 7324.
- ²⁸ Yin, Q.; Tan, J. M.; Besson, C.; Geletii, Y. V.; Musaev, D. G.; Kuznetsov, A. E.; Luo, Z.; Hardcastle, K. I.; Hill, C. L. *Science* **2010**, *328*, 342.
- ²⁹ Huang, Z.; Luo, Z.; Geletii, Y. V.; Vickers, J. W.; Yin, Q.; Wu, D.; Hou, Y.; Ding, Y.; Song, J.; Musaev, D. G.; Hill, C. L.; Lian, T. *J. Am. Chem. Soc.* **2011**, *133*, 2068.
- ³⁰ Stracke, J. J.; Finke, R. G. *J. Am. Chem. Soc.* **2011**, *133*, 14872.
- ³¹ Natali, M.; Berardi, S.; Sartorel, A.; Bonchio, M.; Campagna, S.; Scandola, F. *Chem. Commun.* **2012**, *48*, 8808.
- ³² Stracke, J. J.; Finke, R. G. *ACS Catal.* **2013**, *3*, 1209.
- ³³ Widegren, J. A.; Finke, R. G. *J. Mol. Cat. A* **2003**, *198*, 317-341.
- ³⁴ Creutz, C.; Sutin, N. *Proc. Nat. Acad. Sci.* **1975**, *72*, 2858.
- ³⁵ Brunschwig, B. S.; Chou, M. H.; Creutz, C.; Ghosh, P.; Sutin, N. *J. Am. Chem. Soc.* **1983**, *105*, 4832.
- ³⁶ Ghosh, P.; Brunschwig, B. S.; Chou, M.; Creutz, C.; Sutin, N. *J. Am. Chem. Soc.* **1984**, *106*, 4772.
- ³⁷ Shevchenko, D.; Anderlund, M. F.; Thapper, A.; Styring, S. *Energy Environ. Sci.* **2011**, *4*, 1284.
- ³⁸ Risch, M.; Shevchenko, D.; Anderlund, M. F.; Styring, S.; Heidkamp, J.; Lange, K. M.; Thapper, A.; Zaharieva, I. *Int. J. Hydrogen Energy* **2012**, *37*, 8878.

- ³⁹ Hong, D.; Jung, J.; Park, J.; Yamada, Y.; Suenobu, T.; Lee, Y.-M.; Nam, W.; Fukuzumi, S. *Energy Environ. Sci.* **2012**, *5*, 7606-7616.
- ⁴⁰ Vickers, J. W.; Lv, H.; Sumliner, J. M.; Fielden, J.; Zhu, G.; Luo, Z.; Musaev, D. G.; Geletii, Y. V.; Hill, C. L. *J. Am. Chem. Soc., In Press*.
- ⁴¹ Weakley, T. J. R.; Evans, H. T.; Showell, J. S.; Tourne, G. F.; Tourne, C. M. *J. Chem. Soc., Chem. Commun.* **1973**, 139.
- ⁴² Carano, M.; Holt, K. B.; Bard, A. J. *Anal. Chem.* **2003**, *75*, 5071.
- ⁴³ Song, J.; Luo, Z.; Zhu, H.; Huang, Z.; Lian, T.; Kaledin, A. L.; Musaev, D. G.; Lense, S.; Hardcastle, K. I.; Hill, C. L. *Inorg. Chim. Acta* **2010**, *363*, 4381.
- ⁴⁴ Crabtree, R. H. *Chem. Rev.* **2012**, *112*, 1536-1554.
- ⁴⁵ Artero, V.; Fontecave, M. *Chem. Soc. Rev.* **2013**, *42*, 2338
- ⁴⁶ Zidki, T.; Zhang, L.; Shafirovich, V.; Lyman, S. V. *J. Am. Chem. Soc.* **2012**, *134*, 14275.
- ⁴⁷ Pestunova, O. P.; Elizarova, G. L.; Parmon, V. N. *Kinetics and Catalysis* **2000**, *41*, 340 and references therein.
- ⁴⁸ Ohlin, C. A.; Harley, S. J.; McAlpin, J. G.; Hocking, R. K.; Mercado, B. Q.; Johnson, R. L.; Villa, E. M.; Fidler, M. K.; Olmstead, M. M.; Spiccia, L.; Britt, R. D.; Casey, W. H. *Chem. Eur. J.* **2011**, *17*, 4408.
- ⁴⁹ (a) Answering the question of the precise composition of the Co₄POM derived WOC requires knowing the precise speciation of the Co₄POM *under the catalytic conditions*—that is, any and all forms present *in operando*.^{49b} Then, to determine the true catalyst, the precise, quantitative kinetic contribution of *each* of those species must be known—so that, then, the kinetically dominant form(s) can be determined.
- (b) Weckhuysen, B. M. *Chem. Commun.* **2002**, 97.
- ⁵⁰ A discussion of various oxidants used in water oxidation catalyst testing is given in: Parent, A. R.; Crabtree, R. H.; Brudvig, G. W. *Chem. Soc. Rev.* **2013**, *42*, 2247.
- ⁵¹ (a) Kozuch, S.; Martin, J. M. *ACS Catal.* **2012**, *2*, 2787-2794. (b) Lente, G. *ACS Catal.* **2013**, *3*, 381-382. (c) For a classic contribution on the definition and proper use of TOF in catalysis, see: Boudart, M.; *Chem. Rev.* **1995**, *95*, 661-666.

VI. SUMMARY

This dissertation has addressed the problem of distinguishing homogeneous and heterogeneous water oxidation catalysts when starting with polyoxometalate precatalysts. An overview of this problem was provided through a comprehensive review of the literature and methods needed to distinguish homogeneous POM from heterogeneous metal-oxide WOCs. The methodology to identify the true WOC ultimately relies on multiple stability, characterization, kinetic, and control experiments. Due to the complexity of this problem, only a handful of reports extensively address the identity of the true WOC when POM precursors are used. In order to advance catalyst identification efforts, development and application of methods capable of determining the POM speciation under reaction conditions are needed.

The methodology for distinguishing catalytic materials was in part developed via our specific investigations of $[\text{Co}_4(\text{H}_2\text{O})_2(\text{PW}_9\text{O}_{34})_2]^{10-}$ (Co_4POM) described in Chapters III through V. These investigations revealed that when Co_4POM is dissolved in pH 8 sodium phosphate buffer, it is unstable and releases aqueous $\text{Co}(\text{II})$. In electrochemical studies described in Chapters III and IV, the specific Co_4POM concentration and electrode potential are key variables in determining whether this $\text{Co}(\text{II})$ is converted into a dominant, heterogeneous CoO_x WOC; higher Co_4POM concentrations and lower electrode potentials favor a CoO_x catalyst whereas lower Co_4POM concentrations and higher electrode potentials are consistent with a POM WOC—although CoO_x cannot be definitively ruled out in this latter case.

Lastly, kinetic and mechanistic studies of Co_4POM plus $\text{Ru}(\text{bpy})_3^{3+}$ have been used to determine an empirical rate law for the parallel water oxidation and bpy ligand oxidation reactions and provide evidence for $\{[\text{Co}_4(\text{H}_2\text{O})_2(\text{PW}_9\text{O}_{34})_2]^{10-}\}_2:[\text{Ru}(\text{bpy})_3^{2+}]_3$ precipitation. This

analysis reveals that the undesired bpy ligand oxidation reaction is the favored pathway when using the Co₄POM precatalyst under all reaction conditions examined therein. Controls with Co(NO₃)₂ show higher selectivity and activity for O₂ evolution. Comparison of the reaction kinetics and stoichiometry for Co₄POM and Co(NO₃)₂ starting materials suggest that the true WOC is significantly different when using these two precatalysts—further evidence that the oxidant can play an important role in determining the true WOC.

The studies included in this dissertation demonstrate the importance of understanding the precatalyst stability, conducting kinetic controls, and measuring the reaction stoichiometry and kinetics when attempting to distinguish homogeneous and heterogeneous WOCs. In addition to developing the methods needed to identify the dominant WOC, this work has also pointed out the general need for more quantitative investigation of homogeneous WOC precursors under the reaction conditions. Ultimately, advancement of the water oxidation catalysis field will rely on a fundamental understanding of the precise active sites for these scientifically interesting and societally relevant materials.